Characterisation of Surface and Sub-surface Discontinuities in Metals Using Pulsed Eddy Current Sensors

A thesis submitted to the University of Huddersfield
in partial fulfilment of the requirements
for the degree of Doctor of Philosophy

by
Ali Sophian B.Eng (Hons)

School of Computing and Engineering
The University of Huddersfield

in collaboration with

The TWI Ltd, Cambridge, UK

October 2003

Abstract

Due primarily to today's rigorous safety standards the focus of non-destructive testing (NDT) has shifted from flaw detection to quantitative NDT, where characterisation of flaws is the objective. This means information such as the type of flaw and its size is desired. The Pulsed Eddy Current (PEC) technique has been acknowledged as one of the potential contenders for providing this additional functionality, due to the potential richness of the information that it provides. The parameters mainly used to obtain information about the detected flaws are the signal's peak height and arrival time. However, it has been recognised that these features are not sufficient for defect classification. In this research, based on a comprehensive literature survey, the design of PEC systems and the interpretation of PEC signals, mainly for flaw classification, are studied.

A PEC system consisting of both hardware and software components has been designed and constructed to facilitate the research work on PEC signal interpretation. After a comparative study of several magnetic sensing devices, probes using Hall device magnetic sensors have also been constructed. Some aspects related to probe design, such as coil dimensions and the use of ferrite core and shielding have also been studied.

A new interpretation technique that uses the whole part of PEC responses and is able to produce more features has been proposed. The technique uses Principal Component Analysis (PCA) and Wavelet Transforms, and attempts to find the best features for discrimination from extracted time and frequency domain data. The simultaneous use of both temporal and spectral data is a logically promising extension to the use of time domain only with the signal-peak-based technique. Experiments show that the new

technique is promising as it performs significantly better than the conventional technique using peak value and peak time of PEC signals in the classification of flaws. A hierarchical structure for defect classification and quantification has been presented.

Experiments in the project have also shown that the signal-peak-based technique cannot be used for flaw detection and characterisation in steels, both with and without magnetisation. The new proposed technique has shown to have potential for this purpose when magnetisation is used. The new technique proposed in the report has been successfully used for ferromagnetic and non-ferromagnetic materials. It has also been demonstrated that the new proposed technique performs better in dynamic behaviour tests, which shows its better potential for on-line dynamic NDT inspection which is required in many industrial applications. In addition to testing calibrated samples with different discontinuities, a study case using an aircraft lap-joint sample from industry has further supported the statement regarding the potential of the new technique.

Acknowledgements

I would like to express my sincere gratitude to my director of studies, Dr. G.Y. Tian, who has guided and supported me through every stage in the project. My gratitude also goes to my supervisors, Prof. D. Taylor and Dr. J. Rudlin who have helped and supported me in the project.

I would like also to thank all the technicians in the School of Computing and Engineering for all the helpful assistance.

I dedicate this as a token of appreciation to my late father who used to teach me the foundation of maths and engineering and encourage me to study hard, and to my mother for her sincere and continuous prayers and moral support. My appreciation is also offered to my wife and children for their understanding, support and patience during the last three years.

Finally yet importantly, I would like to thank the School of Computing and Engineering, University of Huddersfield for granting me the opportunity to carry out this project. I would also thank TWI ltd. and the HEFCE for co-funding the project.

Related Publications

1. Tian GY, Sophian A, Taylor D and Rudlin J, Dynamic Behaviour Investigation of Pulsed Eddy Current for Flaw Characterisation, Proceedings of NDT 2003 Conference, British Institute of NDT, pp. 145, 16-18 September 2003

2. Sophian A, Tian GY, Taylor D and Rudlin J, Flaw Detection and Quantification for Ferromagnetic Steel Materials using Magnetisation Based Pulsed Eddy Current sensors, Proceedings of the Lamdamap International Conference 2003, pp. 381-390, 1-4 July 2003

3. Tian GY, Sophian A, Taylor D and Rudlin J, Wavelet-based PCA Defect Classification and Quantification for Pulsed Eddy Current NDT, submitted to IEEE Sensors Journal, 2002

4. Sophian A, Tian GY, Taylor D and Rudlin J, A Feature Extraction Technique based on Principal Component Analysis for Pulsed Eddy Current NDT, NDT&E International Journal, vol. 36, no.1, pp. 37-41, January 2003

5. Sophian A, Tian GY, Taylor D and Rudlin J, Feature Extraction Techniques for Pulsed Eddy Current NDT, Proceedings of NDT 2002 Conference, British Institute of NDT, pp. 187-192, September 2002

6. Sophian A, Tian GY, Taylor D and Rudlin J, Design of a Pulsed Eddy Current Sensor for Detection of Defects in Aircraft Lap-Joints, Sensors and Actuators A Journal, vol. 101, no. 1-2, pp. 92-98, September 2002

7. Sophian A, Tian GY, Taylor D and Rudlin J, Electromagnetic and Eddy Current NDT: A Review, Insight, British Institute of NDT Journal, vol. 43, no. 5, pp. 308-313, May 2001

Table of Contents

List of Figures

List of Tables

List of Abbreviations

ADC	Analogue-to-Digital Conversion
DAQ	Data Acquisition
DC	Direct Current
ECT	Eddy Current Technique
EMAT	Electromagnetic Acoustic Transducer
FIFO	First In First Out
HAZ	Heat Affected Zone
MFL	Magnetic Flux Leakage
FEM	Finite Element Modelling
GMR	Giant Magnetoresistive
MOSFET	Metal-Oxide-Silicon Field Effect Transistor
NDT	Non-destructive Testing
PC	Personal Computer
PCA	Principal Component Analysis
PCI	Peripheral Component Interconnect
PEC	Pulsed Eddy Current
QNDT	Quantitative Non-destructive Testing
RDS	Resistance of Drain-Source channel
SNR	Signal-to-Noise Ratio

SQUID	Superconducting Quantum Interference Devices
TWI	It used to be standing for The Welding Institute. Now, it is a name on its own

Chapter 1. Introduction

1.1 Background

Non-destructive testing (NDT) technologies are essential in various types of industries, including the transportation, aerospace, automotive, manufacturing, petrochemical, and defence industries (Sophian, Tian et al. 2001). They are employed to detect and characterise flaws, as well as to measure material and structural properties. In many cases NDT is so safety critical that malpractice of NDT can end up with tragic human loss. Current safety standards have required NDT not just to provide information about whether a flaw is present, but also to provide quantitative information about the flaw. This new branch of NDT is frequently referred as Quantitative NDT (QNDT). Despite significant advancements being achieved, accurate characterisation of surface and sub-surface flaws still poses a major challenge (Bar-Cohen 2000).

In NDT applications, the eddy current technique (ECT) is one of the most commonly performed techniques and has been used for more than four decades for metal inspection. There are many advantages that make ECTs so popular (Shull 2002). The technique is sensitive to various magnetic and structural properties of conductive samples. This leads to diverse applications of eddy current techniques, such as flaw detection, proximity measurement, metal thickness measurement, non-conductive coating thickness measurement, conductivity measurement and metal sorting. Compared to many systems of other NDT techniques, eddy current systems are of relatively low cost. Surface preparation prior to inspection is generally not necessary or very minimum, therefore preparation time

and cost is minimised. No safety hazards and high portability are other reasons for its popularity.

One of the recent developments in eddy current NDT techniques is the emergence of pulsed eddy current (PEC) techniques (Bar-Cohen 2000). These techniques, in contrast to the conventional techniques that use a single frequency sinusoidal excitation, use a pulsed coil excitation. The pulsed excitation is naturally comprised of a spectrum of frequencies, which allows simultaneous inspection to different depths of the sample. This enables the detection and characterisation of flaws at both surface and sub-surface levels. Interpretation techniques are required to translate the transient response from pulsed eddy current sensors into useful information. The PEC techniques have the potential advantages of greater penetration, the ability to locate discontinuities from time-of-flight determinations and a ready means of multi-frequency measurement. However, current feature extraction and signal interpretation algorithms are not good enough to provide rich information in line with its potential. The lack of interpretation techniques is one of the main reasons why PEC sensing is not widely used by the NDT community (Giguere and Dubois 2000). This drawback can potentially be overcome by using the recent advances in computing power and signal processing techniques, and already a number of different approaches on interpreting the eddy current sensor response using advanced signal processing techniques have been proposed (Udpa and Udpa 1997; Morabito 2000).

The study of PEC techniques has become essential because of two main reasons. Firstly, some NDT problems faced by a few industries need new approaches, and secondly, the promising potentials of PEC techniques. With the purpose of studying and getting more understanding of the techniques, this project has been initiated and carried out collaboratively between the University of Huddersfield and TWI Ltd.

The university has an extensive research record in Eddy current sensors for high precision displacement measurement and advanced signal processing for pattern recognition and image processing. A very sensitive Eddy current system with high precision has been developed and used in industry (Tian, Zhao et al. 1996; Tian, Zhao et al. 1997; Tian, Zhao et al. 1998; Finlayson and Tian 1999; Tian, Zhao et al. 1999; Tian, Zhao et al. 1999; Tian 2001; Gledhill, Tian et al. 2003; Tian, Gledhill et al. 2003).

TWI has expertise in all forms of welding, surfacing, cutting and other joining methods for various materials and is one of the world leaders in this area (TWI 2003). Under the organisation, the Structural Integrity Department performs research and services in NDT, with foremost techniques being Ultrasonic, Electromagnetic, and Thermography. Dr. J. Rudlin has a long record of academic and industrial research in NDT and enjoys a distinguished reputation in NDT research in the UK. Some of his publications: (Rudlin and Wolstenholme 1992; Rudlin 1996; Rudlin 1997; Patel and Rudlin 2000).

1.2 Objectives

The objective of this project is to develop a pulsed eddy current system, which is able to detect and identify surface and sub-surface flaws in metal specimens with the help of advanced signal processing techniques. The objectives can be broken down as follows:

- To undertake a literature review on recent research work on eddy current NDT techniques, particularly pulsed eddy current techniques, and other NDT techniques. Both academic and industrial research and development work on PEC will be surveyed
- To design a new pulsed eddy current system, this includes selection of a suitable magnetic sensor, the design of electronic hardware, software and the probes
- To apply advanced signal processing techniques for analysing eddy current signals in identification of flaws
- To evaluate the feature extraction of the sensor signals and their interpretation
- To identify the key features of the pulsed eddy current systems for applications in surface and sub-surface flaw inspection

1.3 Scope of the Work

This research is multi-disciplinary and includes the fields of physics, electronics, computing, material science, and instrumentation. The scope of the work can be summarised as follows:

- design and construction of a PEC system, which includes hardware and software

- investigation on PEC feature extraction techniques and flaw classification and quantification
- development and evaluation of an effective feature extraction algorithm for flaw classification
- identification of capabilities of the PEC system on non-ferromagnetic and ferromagnetic materials

1.4 Main Achievements

The main achievements of the research work include:

- Literature survey that brought understanding and familiarity with electromagnetic NDT techniques, PEC research work and the use of signal processing in ECTs. Part of the review was published.
- The new design of a PEC system that allows research work to be carried out and also becomes a basis for further development. Probe layouts and coil dimensions have been investigated through simulation and the results have been discussed.
- Design and development of a PCA or Wavelet-based PCA as a feature extraction method, which effectively extracts features from PEC signals for flaw classification. The PCA based features, which may be integrated with conventional peak time and peak value, can also be used for quantification. A hierarchical structure for defect classification and quantification has been introduced.
- Investigation on the performance of the proposed Wavelet-based PCA technique for dynamic measurements compared to the technique using peak time and peak height features.
- Magnetisation that minimises the effective permeability and its variations to enhance effective ferromagnetic material inspection results using a PEC system.

- Publications of the work through refereed journals and conferences.
- Two prototype systems have been established in the University of Huddersfield and TWI in Cambridge for demonstration of NDE applications.

1.5 Thesis Layout

Chapter 1 outlines the background, objectives and scope of the project.

Chapter 2 reports the findings of the literature survey undertaken on the recent research work carried out in eddy current NDT techniques, with emphasis on PEC. Reviews on the use of advanced signal processing techniques in NDT and electromagnetic NDT techniques for steel inspection are also reported. Problems with PEC signal analysis are highlighted.

Chapter 3 reports the design and implementation of a new PEC system, which is comprised of electronics hardware, software and a probe. Issues, such as selection of magnetic sensors, noise reduction and signal pre-processing are also discussed.

Chapter 4 discusses why a new feature extraction technique is needed. Based on the discussion, a new feature extraction technique using Wavelet Transforms and Principal Component Analysis is proposed to make improvements over the current most widely used technique using peak value and time.

Chapter 5 introduces the experiments on the performance of the built system and the newly proposed feature extraction technique on aluminium samples. Comparative results between the conventional and the new techniques on flaw classification and quantification are presented. Significant improvement is achieved using the newly proposed feature extraction technique.

Chapter 6 runs through the experiments on the performance of the built system and the newly proposed feature extraction technique on ferromagnetic steel samples. Improvement of the ability of the PEC system for steel inspection by means of magnetic saturation is discussed and proven by experiments. Comparative results using the conventional and the new techniques on flaw classification and quantification are presented.

Chapter 7 demonstrates the use of the system and the proposed feature extraction technique on an aircraft lap joint sample from industry. The sample consists of two layers and defects are manufactured on both layers with different lengths. A good classification of the flaws has been achieved.

Chapter 8 presents dynamic behaviour investigations on the PEC system and compares the performances of the conventional and the newly proposed technique in terms of their dynamic behaviour. This is essential to anticipate the use of the system in on-line dynamic inspection such as in railway manufacturing and maintenance. The new technique shows higher potential than the conventional technique for on-line dynamic inspection.

Chapter 9 sets out recommendations for further work

Chapter 10 outlines the conclusions drawn from the research work

Chapter 2. Literature survey

2.1 Non-destructive Testing (NDT)

Non-destructive Testing (NDT) is commonly practised to examine structures in a manner, which will not impair their future usefulness. Any manufactured structure develops flaws during manufacture or/and in service. Even worse, the materials used for the construction of the structure might have already contained flaws. Load conditions, material properties and the flaw characteristics will determine whether the serviceability of the structure is affected (Bray and Stanley 1997). Failure in detecting and characterising flaws early and accurately might lead the structure to fail early, and even worse, tragic human loss may also result. Good practice of NDT is expected to prevent these from happening. NDT is required to detect and characterise flaws of appropriate severity before the undesirable failures happened. In addition, effective use of NDT can lead to longer life of systems without compromising the safety factors, and in turn, this will offer economic profits.

NDT has shifted from flaw detection to flaw characterisation that attempts to acquire more information about a detected flaw. This transition has partially been driven by the advancement in the field of fracture mechanics that has made more reliable prediction of flaw growth possible. Using the fracture mechanics analysis, the size of critical defects in a given structure can be calculated. Consequently, capabilities in flaw quantification or characterisation have become more important and demanded to allow the utilisation of the figures produced by the fracture mechanics analysis. This, in turn, forces the advancement of NDT techniques and equipment. Conveniently, the realisation has been made possible by the fast advancement of microprocessors with higher speed and vast computing power.

Further more, with the computer power advancement, implementation of automatic signal interpretation has also been possible. This feature is very useful in reducing the possibility of misdetection of flaws due to human error, which is one of the main factors in drawing a wrong decision in an NDT inspection. It has been shown that human decisions are affected by so many external factors, including the inspection environment (Bray and Stanley 1997).

There are various techniques employed in NDT. The most commonly used are ultrasonics, radiography, liquid penetrant, visual inspection and eddy current. Each of these methods complements the others in various applications, while in many cases they overlap in function.

Visual inspection is the least expensive method and the one that finds more defects because it is widely used (Bray and Stanley 1997). A thorough visual inspection of a component should be done first, whenever possible. Only defects on the specimen surface can be detected using this method, and even these can be missed (e.g. small fatigue cracks are invisible to the naked eye). The success of this inspection technique relies entirely on the skill and judgement of the performing NDT engineers. This type of inspection can be performed by naked eye or and with optical aids, such as magnifying glasses and boroscopes. Advanced visual techniques are also available. These techniques use laser and interferometry techniques. The family includes electronic speckle pattern interferometry (ESPI), holographic interferometry, speckle interferometry and speckle shearography (Richardson, Zhang et al. 1998). They can be very accurate in measuring surface displacement, however the general advantages of visual inspection techniques of being straight forward and inexpensive may no longer hold. Careful surface cleaning and preparation is required with visual inspection.

Ultrasonic testing is probably the most widely used in NDT after visual inspection. The technique works on various solid materials. It is used to detect a wide variety of defects buried below the surface. The most common technique of ultrasonic is the traditional pulse-echo. In this technique, piezoelectric transducers generate ultrasonic pulses, which are transmitted into the specimen to check for cracks and other defects (Zahran, Shihab et al. 2002). Flaws in the specimen will reflect the signals back to be detected by the transducers. The amplitude and size of reflected pulses indicate the size and location of the flaw. Ultrasonics is limited in its capability to characterise near surface defects because of

the interference between transmitted and received pulses in this area. A couplant is required for this technique and for most ultrasonic techniques, and this becomes a disadvantage of using ultrasonic techniques in certain applications.

Recently, a new ultrasonic technique that requires no couplant and no contacts has emerged. The technique, called Electromagnetic Acoustic Transducer (EMAT), uses the Lorenz force and the magnetostrictive effect to generate and receive acoustic signals for ultrasonic inspection. The non-contacting nature of EMAT offers advantages, such as capability of inspecting high temperature samples (Dixon, Edwards et al. 1999). The drawback of the method is the relatively low transmitted energy into the sample and this requires more robust signal processing than that of conventional ultrasonic techniques. As opposed to the conventional ultrasonic techniques that can inspect a great variety of materials, EMAT can only be applied on electrically conductive or magnetic materials. This drawback is not shared by another non-contact ultrasonic technique referred to as laser ultrasonic (Gao, Glorieux et al. 2003).

The underlying principle of radiographic NDT is the change in intensity of the transmitted radiation. Different material densities will absorb the radiation differently. Radiographic NDT provides high spatial resolution in two dimensions and can be very sensitive to deeply buried flaws. The technique requires both sides of the sample to be accessible, which is often not possible. It does not provide through-thickness crack dimension (Ditchburn, Burke et al. 1996) and has limited ability in detection of planar defects. In addition, the technique has rigorous safety legislation, and often requires screening or evacuation from the surrounding area. The safety issue has made this technique less preferred in many circumstances. For instance, in welding inspection there has been a shift from radiography towards ultrasonic NDT.

Penetrant liquid is used only for surface breaking defect detection. It is based on application of a film of liquid on the surface of the sample. The liquid will penetrate through any surface-breaking cracks due to the capillary effect. Following this, the excess liquid on the surface is carefully removed leaving the liquid in the cracks. Then, a developer applied on the surface will draw out this penetrant liquid and stains will mark over the cracks. For enhanced visibility, different types of lighting, such as visible light with a specific spectrum, ultraviolet and laser lights, might be used depending on the penetrant materials used. One of the limitations of the technique is that it can not be

applied on highly porous materials (NDTA 2002), due to the tendency of fluid to fill in the surface opening pores. It is essential that the material is carefully cleaned prior to inspection, which might include grinding in some cases, otherwise the penetrant will not be able to get into the defect. Detection limits of penetrant testing depend upon the surface roughness of the area being inspected. Defects smaller than about three times the surface roughness are unlikely to be reliably detected. Smallest detectable defect dimensions under optimal conditions are in the order of about 1.0 to 3.0 mm long x 0.05 to 0.1 mm deep. Generally, this technique is inexpensive and easy to perform, even on irregular shaped parts that can be difficult for other techniques.

Eddy current techniques are reviewed in more detail in the following section. Electromagnetic techniques used in ferromagnetic steel inspection are reviewed in Section 2.5.

2.2 Eddy Current NDT

The use of eddy current for NDT was pioneered by Friedrich Forster in the 1940s (Deutsch 2000). Eddy current sensors exploit the phenomenon of electromagnetic induction. As illustrated in Figure 2-1, a time-varying current passing through an excitation coil will create a varying electromagnetic field. If an electrically conductive material is in the proximity of this electromagnetic field, an eddy current will be induced in the material, as predicted by Faraday's Law (Kriezis, Tsiboukis et al. 1992). The induced eddy current will generate an electromagnetic field that will be in opposition to the primary magnetic field generated by the coil. The interaction between these fields causes a back EMF in the coil and therefore results in an apparent change in the impedance of the coil. This change of the impedance depends on the distance between the coil and the material, the surface and subsurface geometry, the conductivity and the permeability of the material. The presence of a material flaw will disturb or impede the induced eddy-current and in turn will also change the apparent impedance of the coil, which is generally measured as an indicator of the presence of a flaw (Tian, Zhao et al. 1998).

To measure the characteristics of the metal target, pick-up coils or other magnetic sensing devices such as Hall device transducers and magnetoresistive devices, are used to sense the net magnetic field. In general, the response signal Z, as indicated in equation 2.1, is a complex function of the target material parameters, such as permeability ρ and

conductivity σ, the distance x between the metal target and the sensor probe, the excitation signal frequency ω, the target surface geometry, the material thickness etc.

$$Z = f(\mu, \sigma, x, \varpi, ...) \tag{2-1}$$

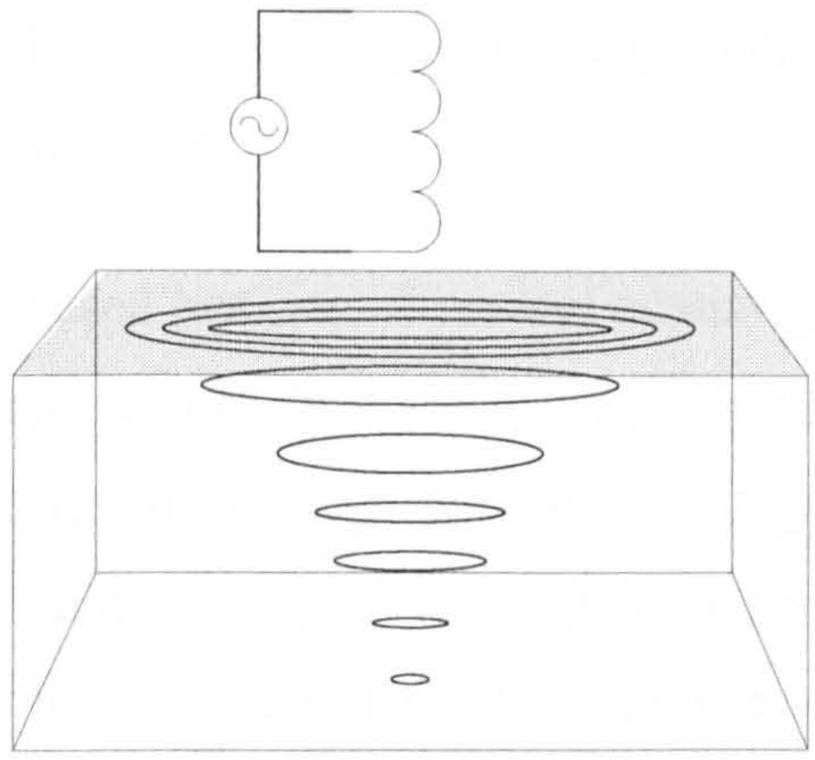

Figure 2-1 Eddy Current Induction

One of the important issues in eddy current testing is surface penetration. The penetration depth of eddy currents is limited due to the skin effect. This effect dictates that alternating currents will concentrate near the surface due to mutual interactions between them. The factors that determine the skin depth, i.e. the depth where the magnitude of the current is reduced by a factor of 1/e, are the oscillating frequency, the magnetic permeability of the material and the conductivity of the material. As frequency increases, the eddy currents are increasingly concentrated near the surface into which energy flows from the excitation source. The skin depth is defined by:

$$\delta = \sqrt{\frac{2}{\varpi \mu \sigma}} \tag{2-2}$$

Where δ is skin depth (m), μ is magnetic permeability (H/m), σ is electrical conductivity (S/m) and ω is frequency (Hz). The effective penetration depth of the eddy current has been proposed as 3δ and if the material under test has thickness less than the effective depth, it will affect the measurement significantly.

The important relationships for eddy current sensor design are derived from Maxwell's equations, which involve non-linear, three dimensional, partial differential equations with involved boundary conditions. Maxwell's Equations are defined as follows:

$$\nabla \times E = -\frac{dB}{dt} \tag{2-3}$$

$$\nabla \times H = J \tag{2-4}$$

$$\nabla . B = 0 \tag{2-5}$$

The equations can be solved using analytical methods and numerical methods. However, analytical solutions are limited to simple geometries, whereas numerical solutions can solve any geometrical configurations.

Eddy current NDT is widely used because of several advantages. Eddy current techniques are non-contact, which means minimum surface preparation, and they are even able to penetrate through non-conductive coatings. Other advantages include high sensitivity, relatively low development and running costs, and high operation speed. On the other hand, the disadvantages include limitation to electrically conductive materials, required response interpretation skills, and sensitivity to lift-off x, i.e. the space distance between the coil and the test specimen. This sensitivity is indicated in equation 2.1. The variation of lift-off is an important challenge in eddy current sensor design. Sensitivity to irregularities in the material surface, and sub-surface, often bury the desired signal in noise, and therefore flaws are not clearly indicated. It is desirable to control as many variables in equation 2.1 as possible to produce reliable measurements.

Eddy current NDT has been applied on different materials and structures, namely aircraft structures (Buckley and Calvert 1995; Lepine, Wallace et al. 1998; Moulder and Bieber 1998; Clauzon, Thollon et al. 1999; Lepine, Giguere et al. 2001; Smith and Hugo 2001), railway tracks (Oukhellou, Aknin et al. 1999), pressure vessels (D'Annucci, Baro et al. 1995; Hulsey and Goolsby 1996; Attaar and Davis 1997), welds (McNab and Thomson 1995; Goldberg 1998; Koyama, Hiroshikawa et al. 2000; Theodoulidis and Kotouzas 2000) and steam generator tubes among others. Besides crack detection, other applications of eddy current techniques include displacement measurement (Tian, Zhao et al. 1996; Tian, Zhao et al. 1999; Tian, Zhao et al. 1999; Tian 2001), proximity sensing (Sadler and Ahn 2001), material stress measurement (Ricken, Liu et al. 2001), coating thickness measurement (Beamish 2000), materials separation (Rem, Leest et al. 1997), material thickness measurement (de Halleux, de Limburg Stirum et al. 1996) and conductivity measurement (de Halleux, de Limburg Stirum et al. 1996).

2.2.1 Single Frequency Eddy Current NDT

Conventional eddy current sensors use single frequency coil excitation. To date single frequency technique has been the most widely used among NDT eddy current techniques, especially for surface and near-surface crack detection. The oscillation is sinusoidal (Bray and Stanley 1997), and may range from a few Hz up to a few MHz. The excitation frequency is selected based on the test material and the depths of the defects to be detected. To obtain the best sensor response, the sensor must induce the greatest eddy current density around the defect (Thollon and Burais 1994; Thollon and Burais 1995). The deeper the flaw is, the lower the excitation frequency needs to be. The induced current density depends on the excitation frequency, the electrical conductivity and the magnetic permeability of the material, the geometry of the structure and on the dimensions of the excitation coil (Mottl 1990) and its driving current (Lebrun, Jayet et al. 1997).

Single frequency eddy current systems usually consist of an oscillator, an excitation coil, one or more sensing coils, signal processing circuitry, and a phasor diagram display for result presentation. The field excitation and sensing devices can be implemented in either a single coil or separated coils and the coil design is adapted to suit the application. In general the designs incorporate an impedance bridge circuit, which converts the impedance variation into the amplitude modulation. Then, the variations in the amplitude and the phase give an indication of the characteristic variations of the test conditions.

There are different types of coils used in ECT. The shape is adapted to the sample. For flat surfaced samples, pancake coils are generally used. Encircling coils are used for inspection of rod-shaped samples. Specific types of coils have also been developed for specific applications, for example for ferromagnetic welds inspection, which are normally characterised by significant undesirable variations of magnetic characteristics, a uniform eddy current probe illustrated in Figure 2-2 has been proposed (Hoshikawa and Koyama 1998; Hoshikawa and Koyama 1998; Hoshikawa and Koyama 1998; Koyama, Hiroshikawa et al. 2000). The probe consists of a large, wide, tangential exciting coil that induces a uniform eddy current in the test material and differential detector coils located inside the exciting coil. The differential coils reduce the noise from the weld zone and detect any flaw signal that is due to local variation of the eddy current around the flaw. In this way, the design manages to increase the signal-to-noise ratio, however the technique requires two different types of probe. Because flaws that are parallel to the eddy current

flow will not be detected, two probes are used to detect flaws in each orientation; one is used for flaws parallel to the weld line, the other is used for flaws perpendicular to the weld line.

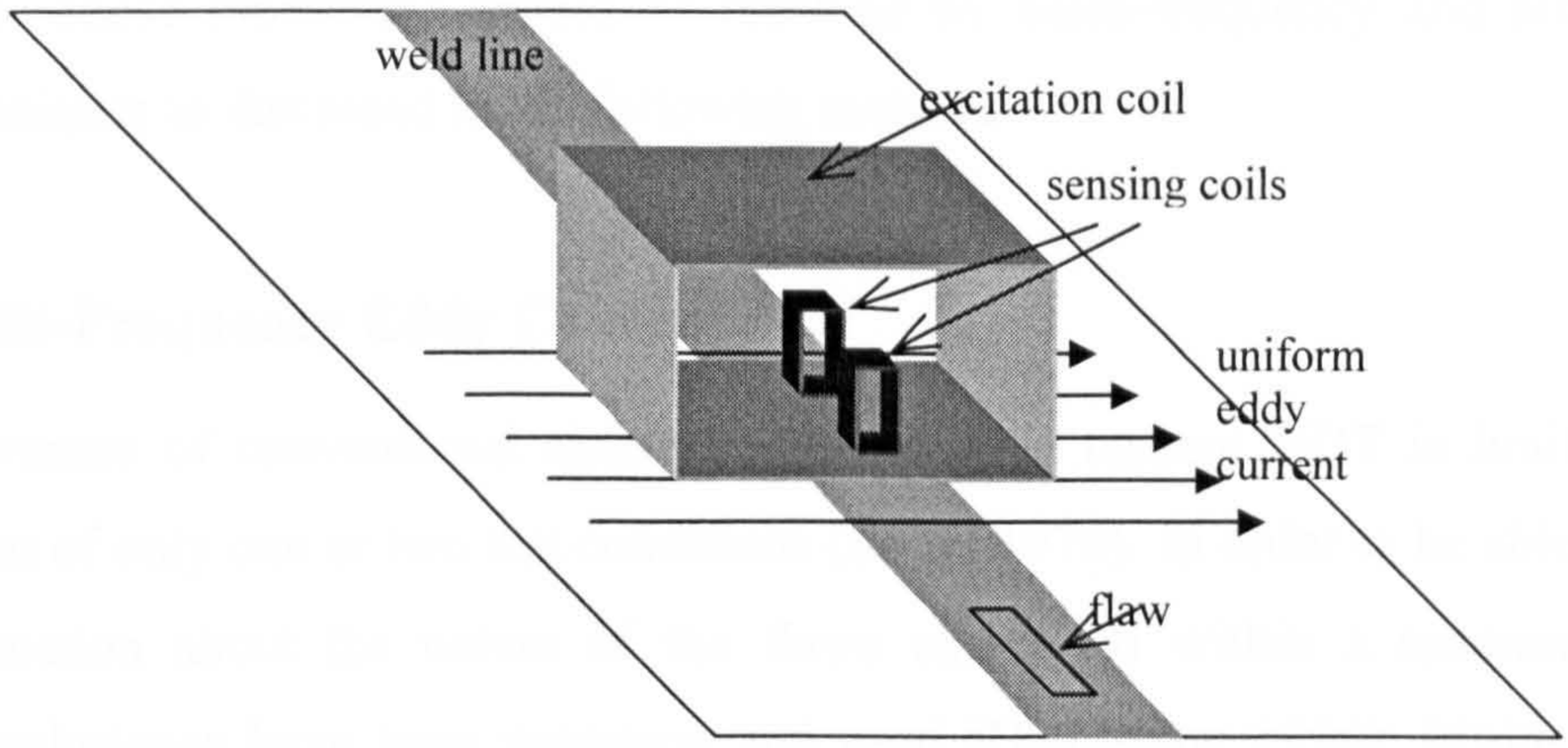

Figure 2-2 The Uniform Eddy Current Probe

Another type of eddy current probe, designed and used for welding inspection, has been mass-produced by Hocking Ltd. The probe is called a cross axis bridge differential weld probe (Tehodoulidis and Kotouzas 2000). The probe employs two differentially wound, 90 degree opposed coils, as shown in Figure 2-3, that minimise lack of detection due to flaw orientation. If only one detection coil is used, flaws that are predominantly perpendicular to the coil plane will hardly be detected. Due to its differential nature, any noise detected by both coils will cancel out and therefore, the noise level will be reduced and the signal-to-noise ratio increased. In this way, the probe is relatively immune to variations in conductivity, permeability and lift-off in the weld and heat affected zone (HAZ).

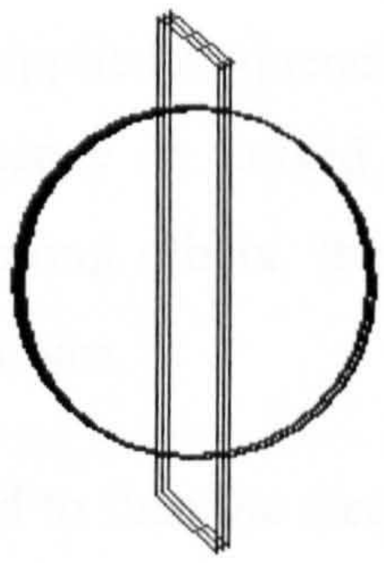

Figure 2-3 The Cross Axis Bridge Differential Coils

Both probes have the ability to detect surface flaws, but they are not meant to be used for detection of sub-surface flaws. The use of a single frequency gives some indication of the

depth size of the detected flaws, however it is not possible to give accurate information. The information obtained is also relatively prone to noise with no remedy as limited information obtained from a single frequency. Another problem is the difficulty in producing a single frequency sinusoidal waveform with low harmonic frequency components. These limitations should be resolved by multi-frequency and pulsed eddy current techniques as discussed in the following sections.

2.2.2 Multi-Frequency Eddy Current NDT

The effectiveness of conventional single frequency eddy current NDT is limited to the identification of only one or two test conditions (Libby 1970). In order to be able to obtain more information about the nature of the flaws embedded within a specimen, multi-frequency techniques have been proposed and used (Halmshaw 1996). Multi-frequency eddy current sensors have also been used for testing ferromagnetic materials, with improved results over single frequency eddy current sensors (Blitz and Peat 1981). This technique is particularly useful when the defects have complex shapes and in resolving the acquired data when it is affected by a large number of variables, including conductivity, permeability, geometry and probe lift-off (Liu, Tsukada et al. 1998).

The various excitation frequencies can be applied either simultaneously or sequentially. If they are applied sequentially, the system must be given sufficient time to allow it to reach a steady state before applying the next frequency excitation. Obviously simultaneous excitation results in a shorter testing time, however if sensitivity is lost, such as in unsaturated ferromagnetic materials testing, the sequential technique may be preferred (Blitz and Peat 1981). The loss of sensitivity in testing unsaturated ferromagnetic materials is caused by cross modulation of the applied frequencies. The complexity of the electronics is greater compared to single frequency or pulsed eddy current discussed in the next section. The complexity includes, among others, the generation of the excitation signals that should have low amplitude harmonics.

Data fusion techniques can be applied to fuse the frequency responses in order to improve the signal-to-noise ratio (Liu, Tsukada et al. 1998). Research on the use of data fusion in NDT started in 1993 and has gained a lot of attention from researchers in recent years. Recent years have also seen other proposed approaches that use neural networks to invert the multi-frequency signals in order to find the profiles of the test material (Chady and

Enokizono 1999; Katragadda, Lewis et al. 2000; Udpa 2000). The use of artificial intelligence solutions is a way to get round the analytical and numerical solutions that require enormous computation power and reduce the complex inversion problems into classification tasks.

A system design employing the multi-frequency excitation technique has generated promising results (Chady and Enokizono 2000). The system produces a 2D crack image, presented using spectrograms, which allow easy interpretation of the structure. The spectrogram is a two-dimensional display of the relative amplitude of the frequency components of a signal from the single sensing coil, corresponding to the sensor position. This system is able to provide a good approximation of the flaw size, and its location, whether on the same side as the probe or on the opposite side. The features exploited in classifying are the response maximum amplitude and the frequency at which this maximum amplitude occurred. The probe used in this system consists of a single exciting coil and a set of sensing coils mounted on a ferrite core. The block diagram of the system is shown in Figure 2-4. The design in (Chady and Enokizono 1999), by the same authors, is very similar, but it uses a different probe design and exploits neural networks in classification of the flaws. The multiple frequency approach has also been used for other inspection applications such as tomography (Binns 2003)

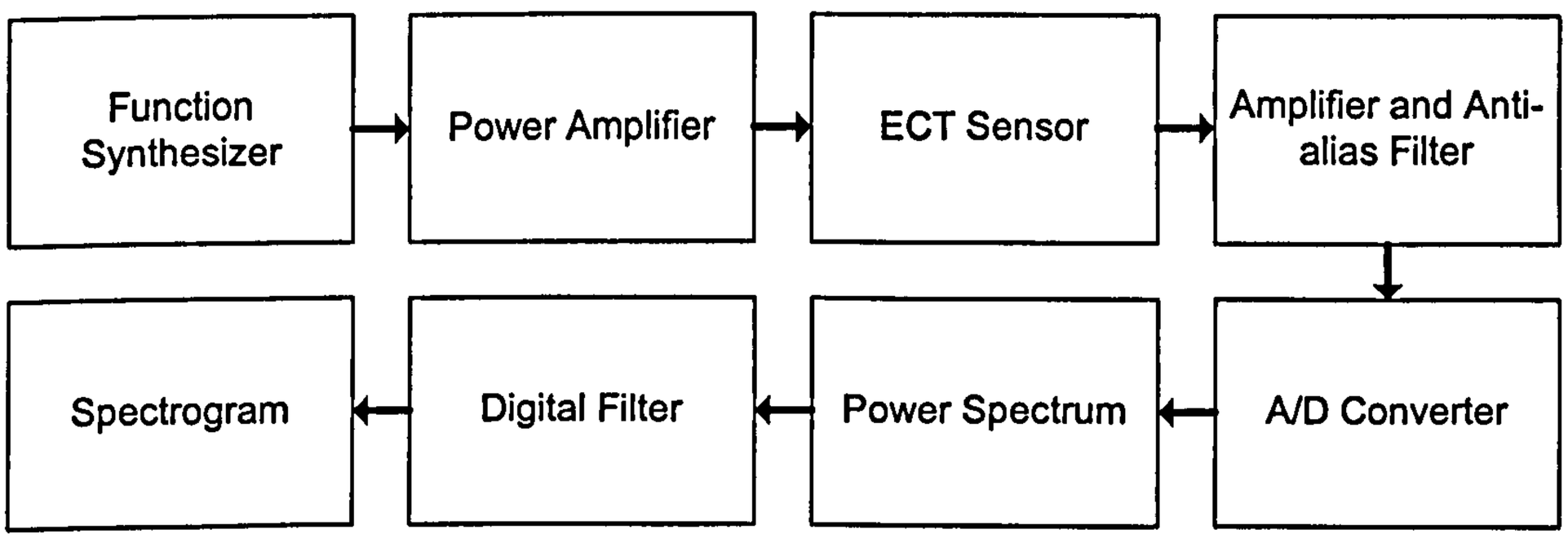

Figure 2-4 Block Diagram of A Spectrogram-based Multi-frequency Eddy Current System

Despite the achievements of this technique, another technique that employs pulsed eddy currents has been introduced, which gives better inspection speed and employs a more simple driving circuit. Multi-frequency methods are limited by their inability to perform quantitative measurements, and it is difficult to generate visualisations of the data in an

intuitive manner (Lepine, Wallace et al. 1999). The preferred technique is discussed in the next section.

2.3 Pulsed Eddy Current (PEC) NDT

Pulsed eddy current (PEC) is a new emerging technology in eddy current NDT. It is considered as a leading candidate in quantitative NDT (Lepine, Giguere et al. 2002). In recent years, it has gained attention in QNDE (Achenbach 2000) and intensive research has been carried out in the area thanks to its wideband spectrum excitation that is an improvement to the multi-frequency techniques. The pulsed excitation which contains the wide spectrum of frequencies is also easier to produce, and a simpler driving circuit can be expected. The emergence of pulsed eddy current techniques is strongly supported by parallel advances in computing power and signal processing capability. However, currently PEC is not widely used by the engineering community, principally because the interpretation of its transient response is still in its infancy (Giguere and Dubois 2000). Presently, PEC is not as precise as conventional methods. PEC has mainly been investigated for flaw detection and characterisation for layered materials.

PEC technology has the potential to identify a large number of parameters, such as flaw size, location and probe lift-off during inspection, which is standing side-by-side with the current requirement of quantitative NDT. The pulsed eddy current technique shares all the advantages possessed by the multi-frequency technique over the single frequency techniques but also shows promising performance in very conductive materials testing, where single frequency techniques generally fail (Lebrun, Jayet et al. 1997). This approach also permits the detection of flaws, near the surface and at depth, simultaneously, without the need to change the probe and operating frequency.

PEC systems drive a large pulsed current into the excitation coil. The transient changes, at rising and trailing edges, induce an eddy current in the test specimen. As the pulse propagates into the specimen, it is broadened by dispersion and scattered back to the surface by discontinuities in the conductivity and permeability of the conductor. The induction does not happen at any other times, hence PEC is also called transient eddy current. A long duration pulse consists of a continuum of frequencies, and is especially rich in low frequency components, which are essential for sub-surface flaw detection.

The frequency components of a pulse or a step voltage can be demonstrated using Fourier Series. If the step excitation is defined as

$$f(t) = \begin{cases} A, t \geq 0 \\ 0, t < 0 \end{cases} \tag{2-6}$$

then using the Fourier Series theorem the excitation can be represented as

$$f(t) \approx \frac{2A}{\pi}\sin\varpi t + \frac{2A}{3\pi}\sin 3\varpi t + \frac{2A}{5\pi}\sin 5\varpi t + \ldots \tag{2-7}$$

The series show that the excitation has a range of frequency components. This derivation is achieved by using the discrete Fourier transform formula:

$$V_k = \sum_{r=0}^{N-1} v_r e^{i(2\pi kr/N)} \tag{2-8}$$

A typical base PEC response measured using a Hall device is shown in Figure 2-5. The base signal is of exponential rise type. The transient starts with fast rise and gradually changes to a slower rise and eventually reaches a stable state. This establishes that the initial part of the signal contains high frequencies and the latter parts contain lower frequencies. The high frequencies are suitable for near surface inspection and the lower frequencies for deep penetration. Therefore, it can be expected that the time shift is relevant to the depth, e.g. surface cracks will be represented by changes in the early parts of the signal and buried defects will be shown later in the signal.

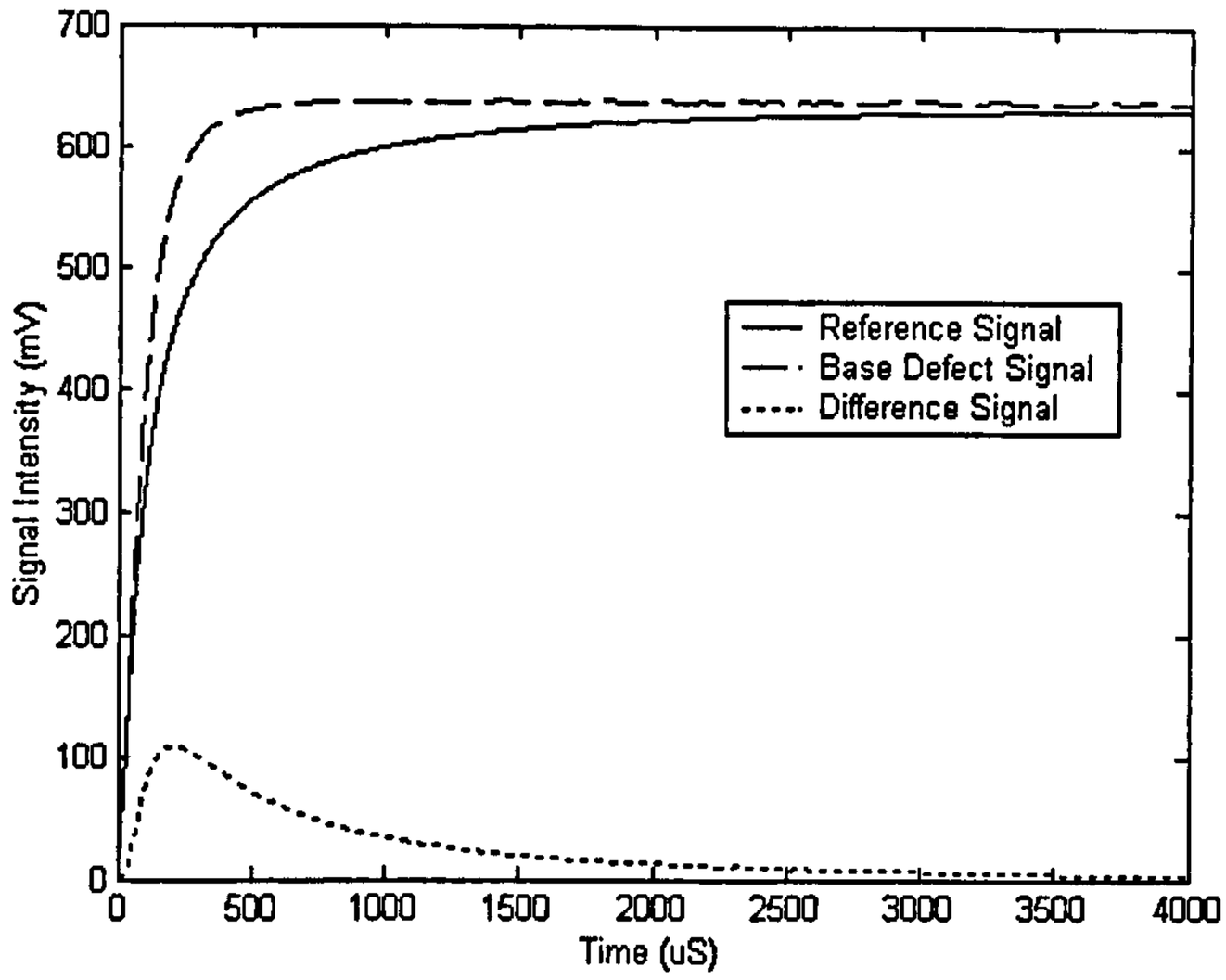

Figure 2-5 Typical PEC Responses Using A Hall Sensor

The pulse eddy current response data can be analysed in either the time domain (Bowler and Harrison 1992; Lebrun, Jayet et al. 1995; Bowler 1997; Moulder and Bieber 1998) or in the frequency domain (Patel and Rodger 1996) or both (Lebrun, Jayet et al. 1997). Figure 2-5 shows an example of a pulsed eddy current response in the time domain. In time domain analysis the peak amplitude is used to determine the size and location of the defect and the time to the peak is used to determine the location of the defect. The deeper the defect is located inside the test material, the longer the time to zero crossing is. This has been implemented for corrosion and crack characterisation in aircraft structures (Moulder and Bieber 1998) and Clauzon T. et al use time to zero crossing and phases at two different frequencies to determine the depth, length and height of flaws under rivets (Clauzon, Thollon et al. 1999).

Lepine et al constructed the specimens from 1mm thick 2024-T3 aluminium alloy sheets, commonly used for aircraft fuselage skin structures (Lepine, Wallace et al. 1999). The signals are not averaged because of the fast scanning movement.

Safizadeh et al carried out an investigation on time-frequency analysis of PEC signals (Safizadeh, Lepine et al. 2001). The study shows that the time-frequency analysis of PEC signals provides specific visual patterns that can be related to the interlayer gap, lift-off, and material loss.

Peak height and arrival time are the most common features used with PEC (Sophian, Tian et al. 2001). The peak arrival time generally gives an indication of the depth of the defect and the peak height indicates the size of defects. In addition to these features, researchers in France introduced another feature called characteristic frequency when they investigated the quantification of flaws under fastener in aircraft structure (Lebrun, Jayet et al. 1997). More recently, researchers in Canada introduced Gap Feature points to resolve the noise problem caused by interlayer gap variation (Lepine, Giguere et al. 2001). They also introduced the use of Half-power Width (HPW) to predict the location of corrosion in multilayer structures. This feature works with some limitations. Without these innovative features, the flaw signals can be obscured by noise, and hence render PEC ineffective. Another reported work is (Sophian, Tian et al. 2002) presenting the use of FFT and relevant frequency components to improve defect signals based on their location.

PEC has special requirements in terms of excitation and detection (Bowler and Harrison 1992). For detection, an induction coil is not suitable as it is not sensitive to the slow rate of change of a magnetic field. A better solution is to use magnetic field transducers, such as magnetoresistive (Lebrun, Jayet et al. 1995) and Hall effect devices (Clauzon, Thollon et al. 1999).

The potential advantages of a PEC system as suggested by Smith and Hugo (Smith and Hugo 2001) are:

- The ease of scanning large areas of a complex structure without the need to change any set-up parameters
- The ability to compensate during post-processing for lift-off and edge effects
- The speed of acquisition
- Instrumentation costs may potentially be lower than for multi-frequency eddy currents

In addition to the potential advantages above, in aircraft lap-splices inspection, PEC is also expected to provide better discrimination against interfering signals from fasteners and subsurface structures (Rose, Uzal et al. 1999).

2.3.1 Recent Main Research and Development Work on PEC

2.3.1.1 QinetiQ Ltd, UK and AMRL, Australia

QinetiQ Ltd, or formerly known as The Defence Evaluation and Research Agency (DERA), has developed a PEC system called TRECSCAN in the UK (Burke, Hugo et al. 1997; Smith and Hugo 2001; Smith and Hugo 2001; Smith and Hugo 2001). In the research and development work, they co-operated with an Australia-based partner called the Aeronautical and Maritime Research Laboratory (AMRL). One of the features of their system is that they use Hall-effect sensors to measure the magnetic field directly, as illustrated in Figure 2-6 that shows their probe layout (Smith and Hugo 2001). Hall-effect sensors offer an advantage over a coil for depth penetration structure and for spatial resolution. The ferrite core is useful to amplify and concentrate the magnetic field. The ferrite increases the inductivity of the sensor and consequently slows down the transient excitation current change and limits the high frequency contents.

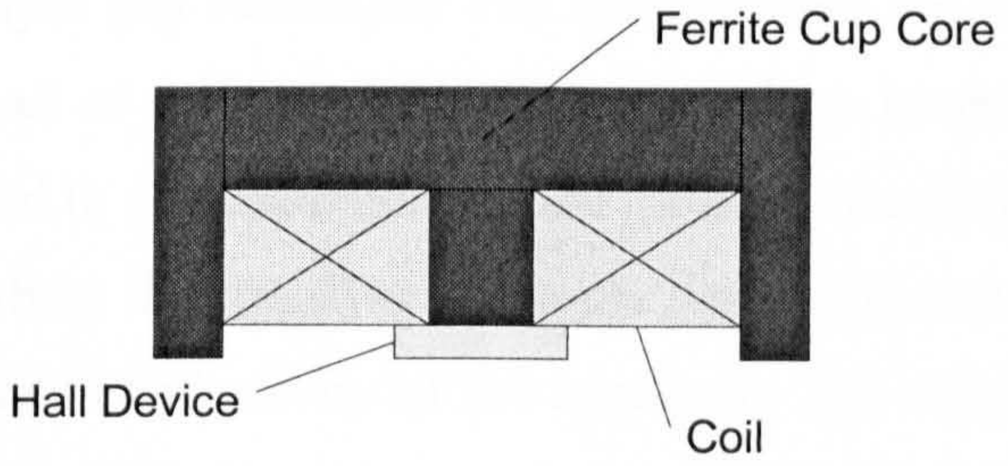

Figure 2-6 The Layout of DERA's Probe

2.3.1.2 Canada

National Research Council of Canada, National Defence Headquarters, Royal Military College of Canada, and Tektrend International Inc. are involved in research and development work in Canada (Lepine, Wallace et al. 1998; Giguere and Dubois 2000; Giguere, Lepine et al. 2001; Lepine, Giguere et al. 2001; Lepine, Giguere et al. 2002). The research is focused on the use of PEC for detection and characterisation of corrosion in multi-layered aircraft structures. Their system diagram is as illustrated in Figure 2-7.

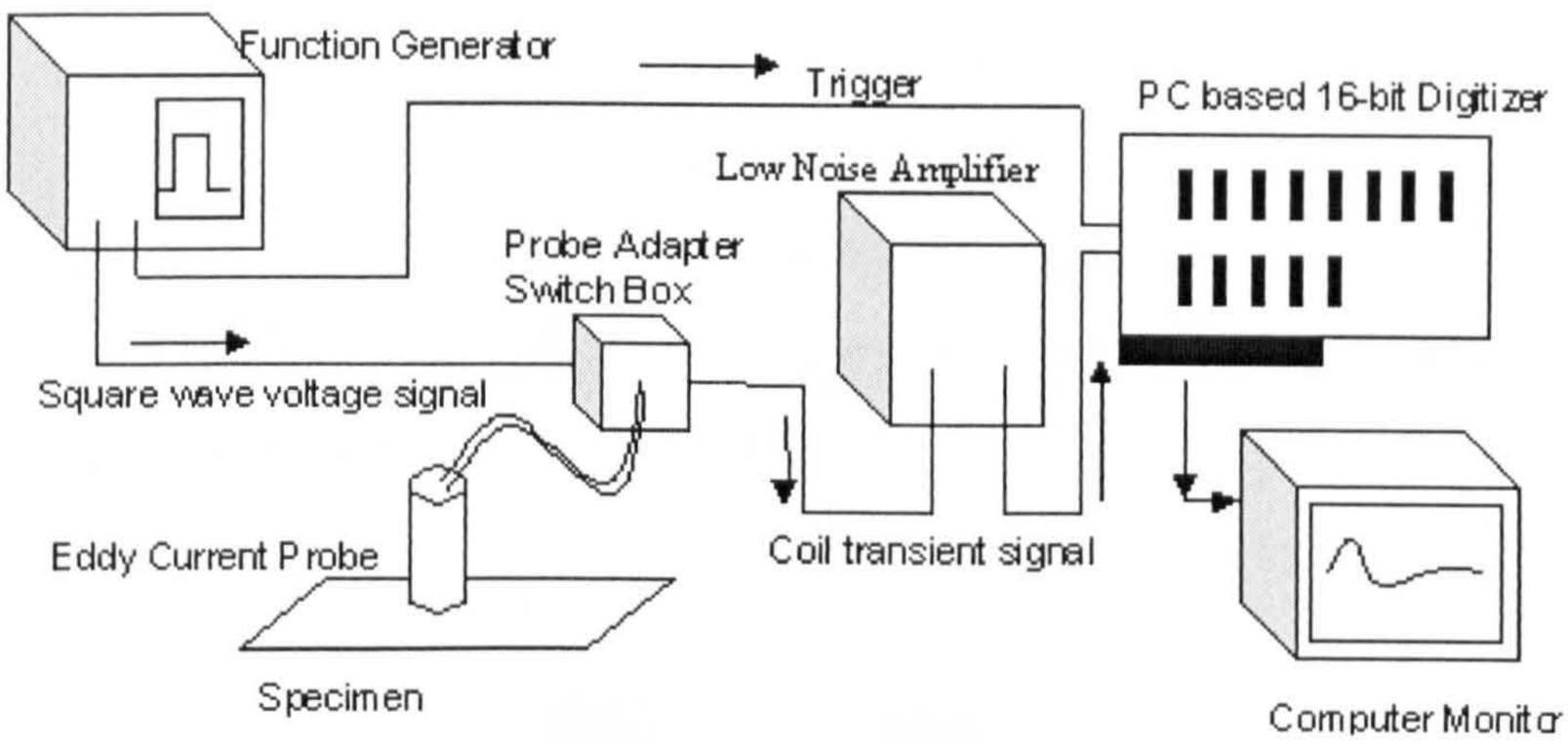

Figure 2-7 The Canadian PEC System Diagram

They investigate the use of PEC in multi-layered structures, where the main noise comes in the form of lift-off effect and interlayer gap separation. In contrast to QinetiQ who use a Hall device, the Canadian researchers use a coil for picking-up the magnetic field signals. Pick-up coils can be employed effectively when the specimen is relatively thin.

They exploit unique signal characteristics of the pick-up coil for overcoming problems with lift-off and interlayer gap variations. The features used are not obtainable when Hall devices are used instead of sensing coils. The researchers invented Lift-off intersection point (LOI) that is useful to eliminate most of the lift-off noise (Giguere and Dubois 2000). The LOI is the time where the transient is insensitive to common lift-off variations. LOI depends on the probe and conductivity of the specimen. The signal magnitude at the LOI point will change when a flaw is encountered. By this method, they have eliminated the effect of lift-off from the flaw detection process.

Later, they introduced Gap Point feature to eliminate interlayer gap variation noise (Lepine, Giguere et al. 2002). This is a small range in time where the gap effect is minimised. As the variation happens deep in the structure, the gap point occurs later in time than LOI.

2.3.1.3 Centre de Génie Electrique de Lyon (CEGELY), France

In 1993, it was reported that Lebrun et al in France developed a system using a pair of magnetoresistive devices. The layout of the system is illustrated in Figure 2-8. A differential mode is applied to increase the sensitivity of the system. By using cross

relation between defect signals, the depth of the crack can be approximated successfully. One of the defects used in the experiment has a depth of 20 mm (Lebrun, Jayet et al. 1995). In 1997, they reported a similar system, but now with additional features. The features used are peak height, zero crossing of the impulse response, and characteristic frequency. Characteristic frequency is the frequency component of the impulse response that has the maximum amplitude (Lebrun, Jayet et al. 1997).

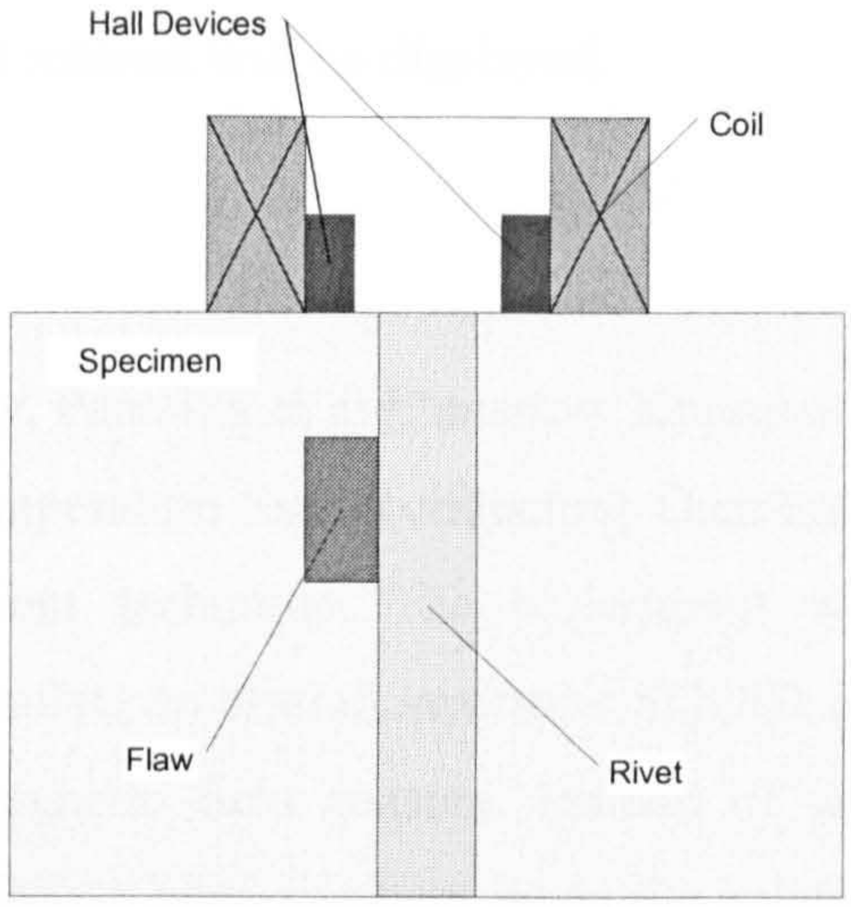

Figure 2-8 The Thollon's Probe and Experimental Setup

In 1999, Thollon et al reported a new system they designed. The system is designed for aircraft inspection, specifically for detection of cracks emanating from rivets. Two Hall devices are incorporated. The system works on the assumption that one Hall device will be sensing on a flawed region, and the other on a flawless. When both devices are sensing flawed regions, the measurement results will be affected. The measurement quantity is the difference between signals output by the two Hall devices. Three best features are chosen based on some experiments. The first feature is the time corresponding to the maximum of the impulse response. The second and third features are the phase values at frequencies 500 and 800Hz respectively. Using the system, the depth, length and height of the flaw can be approximated satisfactorily (Clauzon, Thollon et al. 1999).

2.3.1.4 Iowa State University, USA

The focus of the PEC research and development work at Iowa State University has been on defect detection and characterisation for multi-layered structures (Bieber, Shaligram et al. 1997; Moulder and Bieber 1998). They obtained a patent for their work on PEC (Moulder,

Shaligram et al. 2000). They use an air-cored pancake coil for excitation and the same coil or another coil for sensing. The main features used are peak height and zero-crossing time. The peak height is proportional to the metal loss and the zero-crossing time contains information about the depth of the flaw in the structure. They introduced a time-gating method to determine the location of defects and reduce unwanted interferences (Bieber, Shaligram et al. 1997). Using time-gating, a time range of interest is specified, any peak that occurs outside this time range is neglected. As peak-arrival time corresponds to defect depth, only depth range of interest will be displayed.

2.3.1.5 Others

Very recently, in Germany, Panaitov et al (Panaitov, Krause et al. 2002) ran an experiment using High Transient Temperature Superconducting Quantum Interference Device (HTS SQUID) for PEC transient technique. The experiment was done on multi layered aluminium samples to simulate an aircraft structure. SQUID magnetometers are known to be the most sensitive magnetic field sensors. Instead of using the rising edge of the excitation, they used the falling edge transient when the excitation current is switched off. Having measured magnetic field transient, they applied an equation taken from Geophysics to derive the so-called apparent conductivity $\sigma_a(z)$, where z is the depth into the test material. By this method, 2D-profiles of the layered samples can be drawn. The pulse frequency was chosen to be a multiple of the power line frequency (50 Hz) to suppress the power line noise. The drawback of SQUID systems is that a cooling mechanism is required as the operating temperature of SQUID sensors is –193°C (Krause 2003). A portable dry cooler for SQUID has been developed at the University of Strathclyde (EPSRC 2003).

A Netherlands-based company called RTD, has manufactured a PEC tool called RTD-Incotest. The equipment has been successfully applied in corrosion detection (Robers and Scottini 2002), especially on insulated and coated objects. Problems in detection have been reported when the corrosions are so localised such as pitting. In this situation, the detection becomes unreliable due to the averaging effect of the sensor.

Some work on PEC systems has also been carried out at National Cheng Kung University, Taiwan (Yang, Liu et al. 1999; Tai, Yang et al. 2002; Yang and Tai 2002).

2.4 Signal Processing and Eddy Current NDT

As computing power becomes more powerful and the cost becomes cheaper, more and more digital signal processing algorithms have been developed and employed to help solve problems in various fields such as artificial intelligence, computer science and engineering. The new algorithms reduce signals' noise, analyse signals, transform signals into a more meaningful form, compress signal data etc. The role of signal processing is very crucial as all information coming from the real world is taking place in the form of electrical signals produced by transducers of various types. Some of the applications include image processing, pattern recognition, digital communications, control, biomedical applications, speech processing and radar signal processing.

In pattern recognition, Principal Component Analysis (PCA) is commonly used for pattern classification and identification. It involves a mathematical procedure that transforms a number of (possibly) correlated variables into a (smaller) number of uncorrelated variables called *principal components*. The first principal component accounts for as much of the variability in the data as possible, and each succeeding component accounts for as much of the remaining variability as possible. There are two steps for application PCA such as using model data for getting the principal components and determining the number of components, and the components for testing and interpreting the measurement signals. In the last decade, PCA has developed for complex signal understanding and interpretation such as medical applications ECG, image understanding, content-based image retrieval and object recognition. PCA has been proved a popular approach for facial recognition (Turk and Pentland 1991), where the face has a similar pattern with different details.

In contrast to FFT, Wavelet analysis is useful in decomposing a time series into time-frequency space simultaneously. The analysis provides information about both the amplitude of any "periodic" signals within the series, and how this amplitude varies with time. Recently, Wavelet analysis has been used in various applications thanks to its functionality (Chen, Yoshida et al. 1995; Graps 1995; Dokur, Olmez et al. 1999; Pittner and Kamarthi 1999; Yen and Lin 2000; Tico, Kuosmanen et al. 2001; Verlinde, Beckers et al. 2001; Goumas, Zervakis et al. 2002; Ionescu and Llobet 2002).

In Eddy Current NDT, digital signal processing has also played increasingly versatile and important roles. More and more researchers use the advanced signal processing techniques for NDT, particularly signal interpretation (Shyamsunder, Rajagopalan et al. 1999; Li, Tso

et al. 2000; Morabito 2000; Kojima, Kubota et al. 2001; Brence and Brown 2002; Golovkin, Mancini et al. 2002; Rao, Raj et al. 2002; Staszewski 2002; Mijarez, Gaydecki et al. 2003). A large number of research work has investigated the incorporation of advanced signal processing techniques into Eddy Current NDT systems for various purposes, among others:

- To suppress or reduce unwanted electrical, material and structural noise and improve signal-to-noise ratio of the systems (Kreutzbruck and Allweins 2002; Rao, Raj et al. 2002)

- To analyse and interpret the signals and gain information for classification and quantification of flaws (Chen, Yoshida et al. 1995; Wu and Upadhyaya 1996; Chen, Yamaguchi et al. 1997; Gros, Bousigue et al. 1999; Shyamsunder, Rajagopalan et al. 1999; Katragadda, Lewis et al. 2000; Khandetsky and Antonyuk 2002; Rao, Raj et al. 2002)

- To implement data mining. An example of this is finding relationships between NDT data and flaws (Brence and Brown 2002)

- To implement a data fusion that makes a synergistic use of data from multiple sources (Gros, Bousigue et al. 1999). NDT techniques with better reliability are, then, achievable.

With the introduction of advanced signal processing techniques into NDT techniques, the performance has generally improved in terms of reliability, probability of detection, quantitative NDT information, and ease of use of NDT systems. Despite the more significant use of advanced signal processing techniques in ECT, their use in PEC is still limited as reported in the previous section. Based on research achievements in the use of advanced signal processing techniques in other applications, this project will investigate and expand advanced signal processing techniques such as PCA and Wavelet analysis for interpretation of PEC signals and classification of flaws.

2.5 Electromagnetic NDT Techniques for Steel Inspection

One of the objectives of the research is to investigate the use of PEC in ferromagnetic steel inspection. In this section, various electromagnetic NDT techniques that have been applied

for steel inspection are reported. One of the most economical NDT in steel inspection is magnetic flux leakage (MFL) (Mandal, Cramer et al. 2000). MFL has been intensively used in monitoring corrosion in buried pipelines. This technique requires magnetisation of the specimen. The magnetisation generates magnetic flux flowing in the specimen in a certain direction. The presence of flaws will implement as an abrupt change of magnetic permeability to the flux in the specimen. This permeability is lower than flawless parts, provides high resistance to the flux and forces it to take a different route. In cases where the other routes are magnetically saturated, some flux has to leave the specimen before re-entering and causing flux 'leakage'. This leakage is readily detectable by magnetic sensors located in the proximity of the specimen surface. The parameters of a defect that affect the distribution of leakage flux are the ratio of depth of the defect to the thickness of the pipe wall, length, width, sharpness at the edges and sharpness at the maximum depth (Mukhopadhyay and Srivastava 2000). In practice, the magnetisation agent can be a permanent DC magnet or an AC electromagnet (Atherton 1997; Mandal, Cramer et al. 2000; Goktepe 2001). For DC inspection, hall device, magnetoresistive and SQUID (Krause and Kreutzbruck 2002) can be used to measure the leakage field. For AC measurement a pick-up coil is another alternative.

Another reported technique is Pulsed Magnetic Saturation (Dodd, Deeds et al. 1998). This technique is useful when space is at a premium, e.g. for pipe inspection that has to be carried out from the interior. Permanent magnets will not fit into the bore, and electromagnets will generate extensive heat rapidly. Using the pulsed magnetic technique, the saturating magnetic field is only generated for short periods of time. Tube walls of up to 5mm thick have been tested, and the power required was 500kW. Using a technique called multiple-property technique, the defect characteristics are derived. In the technique, a number of values at particular times along the base signal are used. The relations between the defect characteristics and the reading functions are derived using linear least-square fits of the polynomial.

AC field measurement (ACFM) is a relatively new technique in NDT although it has developed into one of the established NDT techniques. This technique is particularly suited for crack sizing (Dover, Collins et al. 1991) and can also be used for crack detection. Some of the advantages of these techniques are that in many situations it requires no calibration and that it is relatively insensitive to permeability changes and lift-off (Raine and Lugg 1999). On carbon steels, its use is limited to the detection of surface-breaking flaws (Raine

and Lugg 1999). The technique induces a uniform electric current into the specimen. The magnetic component that is perpendicular to the current and parallel to the surface, B_x and the component that is normal to the specimen's surface, B_z are measured. The length and depth of a surface-breaking defect are derived from a set of B_x and B_z readings. A butterfly plot of the readings is used to give some visualised indication to the user (LeTessier, Coade et al. 2002; Raine and Cameron 2002).

Alternating Current Potential Drop (ACPD) is the only established magnetic technique for measuring crack depth in welds, and it is not used for crack detection (Ditchburn, Burke et al. 1996). It is generally only applicable for surface-breaking cracks and requires electrical contact with the specimen. The use of AC, in oppose to DC, allows low current and thin layer inspection due to the skin effect. The specimen must be homogeneous and isotropic (σ, μ and k are constant) to allow accurate results. An AC field is applied to the specimen so that the current is perpendicular to the crack. A pair of contacts with fixed distance is used to measure the potential difference between two points. When a crack exists, the reading will be affected. The change in reading is used to estimate the crack depth. The technique requires no calibration (Dover, Collins et al. 1991).

A technique for inspection of steel-reinforcing bars embedded within concretes has been investigated and developed at the University of Manchester (Gaydecki, Silva et al. 2000; Quek, Gaydecki et al. 2002; Miller, Gaydecki et al. 2003). The technique uses inductive sensors and achieves 3D imaging of corrosion on the steels.

2.6 Summary

A review has been presented on various NDT techniques and the use of advanced signal processing in NDT. More attention was given to Eddy current NDT and, particularly, pulsed eddy current NDT research work and systems for industrial applications around the globe.

PEC is an emerging technique in NDT. This technique has potential for quantitative NDT as it has a wide band of frequency components, as opposed to conventional or multi-frequency eddy current techniques that only have one or few frequencies. It has been acknowledged that the signal interpretation is still in its infancy, especially when compared to other ECT techniques. For the signal interpretation, the choice of signal features used

depends on the type of the sensing device. When a magnetic sensor is used, mainly the peak values and times of the PEC differential signals are used as features for making qualitative and quantitative judgements. This means that there are still vast areas for improvement, as the amount of information can be gained also depend on the number of uncorrelated features used. The innovations such as LOI have also supported that peak value and peak time are not sufficient to function alone effectively. It is, therefore, a challenge to apply advanced signal processing techniques for signal feature extraction that will yield new features that are sensitive to flaws and insensitive to interference noise. Many other NDT techniques have already enjoyed the benefits of recently established signal processing techniques.

The investigation of the performance of the PEC system and the feature extraction technique will be carried out on both non-ferromagnetic and ferromagnetic materials. The literature survey shows that when electromagnetic NDT techniques are used for ferromagnetic material inspection, some sort of magnetisation of the sample is generally applied. The magnetisation is implemented either locally or globally. This practice will also be considered when ferromagnetic materials are dealt with.

Chapter 3. PEC System Design and Implementation

3.1 Background

The comprehensive literature survey suggests that research work on PEC systems and their signal analysis are still required for NDT applications. In order to carry out the research work, it is proposed to design and implement a PEC system as the basis for the experimentation. It is not expected that the system built within this project will be exhaustive. Continual efforts for improvement will be made to achieve industrial requirement after the completion of the PhD project.

3.2 Overall System Design

All the PEC research groups reported in Chapter 2 have had their own system designs. Figure 3-1 shows the features of the system of the research groups. In general, there are three main features that distinguish the systems developed by each group. These features include:

- Sensing device

  Two different approaches are available to measure the magnetic field induced by the eddy current flowing in the sample. The first approach is by measuring the rate of change of the magnetic field, and this is achieved by using a pick-up coil. The second approach is by sensing magnetic field intensity that can be achieved by using magnetic sensors. The advantage of using magnetic sensors is that it is more sensitive measuring

low frequency magnetic field components, and this becomes vital when sensitivity to flaws located deep down in the sample is of interest. Another advantage of the second approach is that the spatial resolution can be better, as generally these sensors have small sizes and small cross sections. Therefore, the second approach is chosen.

- Excitation mode

  Considering how the transmitter coil is driven the PEC systems can be classified into two groups, namely current driven and voltage driven. With current driven, the driver is basically a constant current source, and with voltage driven, the driver drops a given voltage across the excitation coil. The current driven is more consistent as it drives approximately the same current regardless the inductance of the coil used, so long as the inductance is within a specified range. The voltage driven is generally less complicated in electronics design, and needs manual adjustment to set the current. It should be noted that the magnetic field generated by the coil is proportional to the coil current, and not the voltage. The design reported in this thesis is voltage driven.

- Signal pre-processing

  As discussed in Chapter 2, the signal analysis of PEC is mainly done in time domain. In this project it is attempted to use both temporal and spectral analysis of the signals. A signal pre-processing is applied for further process.

Table 3-1 also shows the current status of the research and development work by each group and the applications targeted for the developed systems. The research group iat Huddersfield University aims to extend the use of PEC into inspection of rail tracks and manufacturing processes.

To anticipate the necessity in the research work, the specifications of the design have been outlined as follows:

- The system will be interfaced to a PC for processing and presentation

- The excitation frequency must be adjustable over the range of 100 Hz up to 2 kHz.

- The duty cycle of the excitation must be adjustable. The duty cycle ranges from 5%-50%. The PEC technique has the advantage of allowing higher coil current to

be driven without overheating the probe windings by reducing the duty cycle if necessary. This is not achievable with single frequency systems.

- The coil current should be adjustable from 100 mA up to 2 A approximately

	Sensing Device	Excitation Mode	Signal Analysis	Status	Applications
QinetiQ (UK)	Hall device	Current driven	Time domain	Product: TRECSCAN	Aircraft
Iowa State University (USA)	Hall device	Current driven	Time domain	Ready for Commercialisation	Aircraft
Canada	Coil	Voltage driven	Time domain	Research	Aircraft
France	Hall devices / Magneto-resistives	Voltage driven	Time-Frequency	Research	Aircraft
Hudders-field	Hall device	Voltage driven	Time-Frequency	Research	Aircraft, Rail tracks, Manufacturing

Table 3-1 PEC System Comparison

The block diagram of the new system design is shown in Figure 3-1. The new PEC system consists of a rectangular waveform generator, a coil driver, a probe consisting of a Hall device and an excitation coil, a data acquisition (DAQ) card and a PC with signal processing and result presentation software and a mechanical housing to contain the electronic hardware.

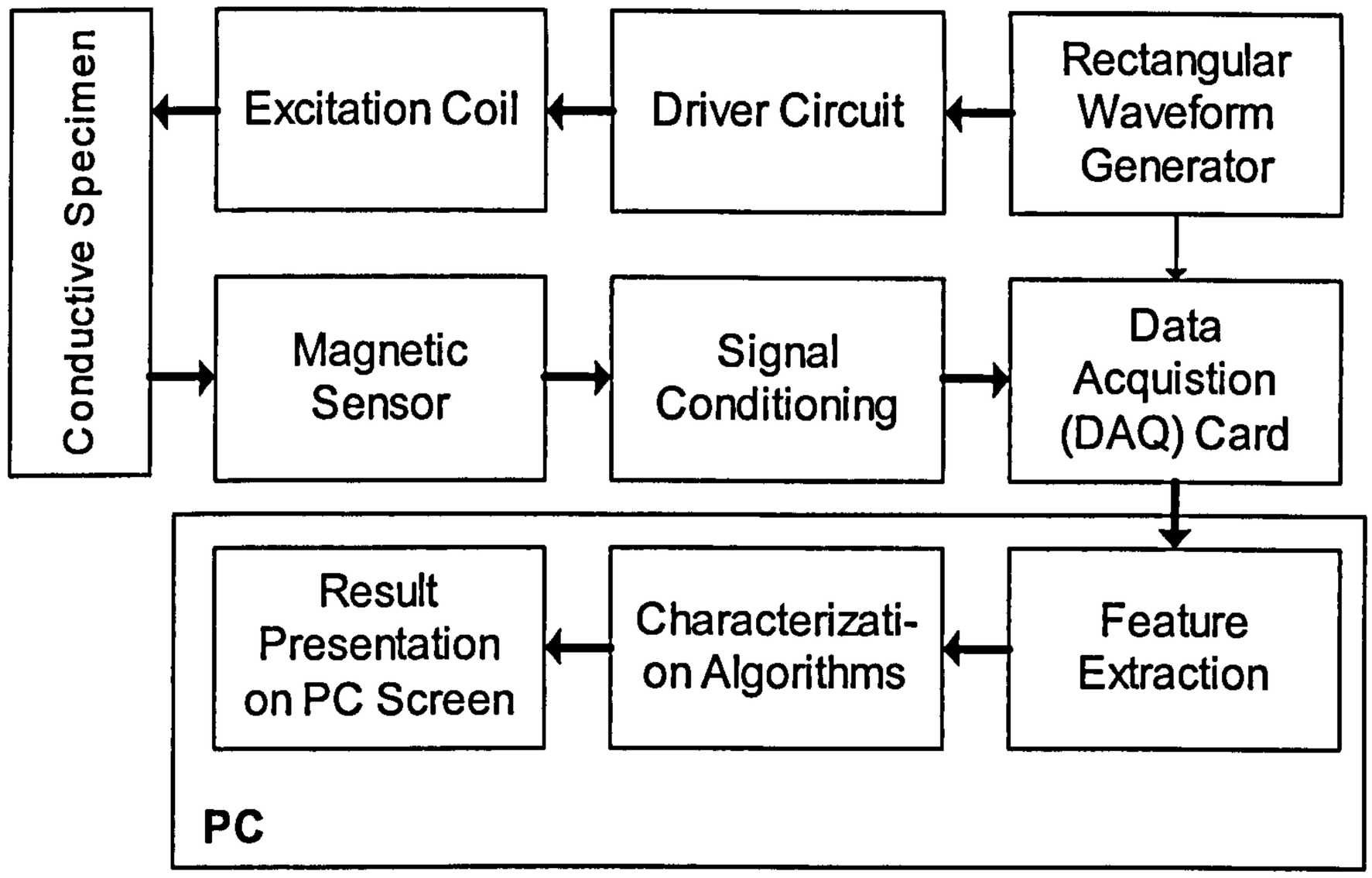

Figure 3-1 The System Design

Briefly, the system works as follows; the waveform generator produces a rectangular waveform with variable frequency and duty cycle. The waveform is fed to a coil driver circuit, which excites the induction coil in the probe with pulsed current. The pick-up sensor will measure the vertical resultant magnetic field, which is the sum of the one generated by the excitation coil and the opposing one generated by the induced eddy current in the sample. A voltage amplifier with variable gain then amplifies the signal so that the dynamic input range of the data acquisition card (or analogue-to-digital converter card) is used effectively. The A/D card will convert the input signal into digital data ready to be processed by written software in the PC. The software performs communication with the data acquisition card, the control of the data transfer from DAQ card buffer to the PC RAM, signal pre-processing, feature extraction, defect categorisation, and the presentation of the results are on the PC monitor. Figure 3-2 shows the photographic view of the developed PEC system.

Figure 3-2 The Photographic View of the PEC System Box

3.3 Electronics Design

The block diagram of the electronics is shown in Figure 3-3. A brief overview of how the system works has been explained in the previous section. In addition, the signal splitter is basically an inverting buffer with two identical outputs. One of the outputs is used for data acquisition synchronisation trigger and the other is used for coil excitation. The voltage divider is used to scale down the trigger signal to lend itself to the DAQ channel's maximum input voltage.

A better solution can be achieved by using a microcontroller-based circuit so that all the settings can be done via software, which would be more convenient for the users, as all the control will be centralised and accessible from the software-based graphical user interface (GUI). However, the current approach has been chosen to save development time and it is sufficient for research purposes. The electronic design schematic can be seen in Appendix 1.

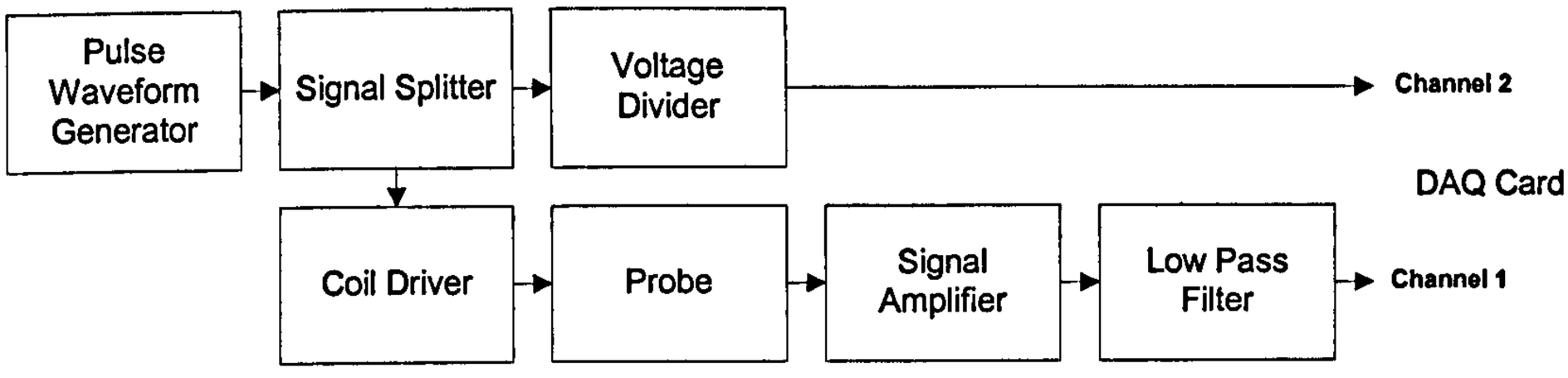

Figure 3-3 The Block diagram of the Electronic Design

The following sub-sections give more detailed description of the design and implementation of the pulse waveform generator, the coil driver, the signal amplifier, the low pass filter and the probe. Relevant information about the DAQ card is also included.

3.3.1 Rectangular Waveform Generator

The rectangular waveform generator is required to produce the waveform to drive the coil with pulsed excitation. The core component in the waveform generator sub-circuit is ICL8038 chip. As introduced in Section 3.2, the waveform generator is designed to have predefined frequencies and duty cycles. This is achieved by using a set of capacitors and resistors of different appropriate values. The waveform generator sub-circuit is shown in Figure 3-4. The only output pins used for our purpose is pin 9.

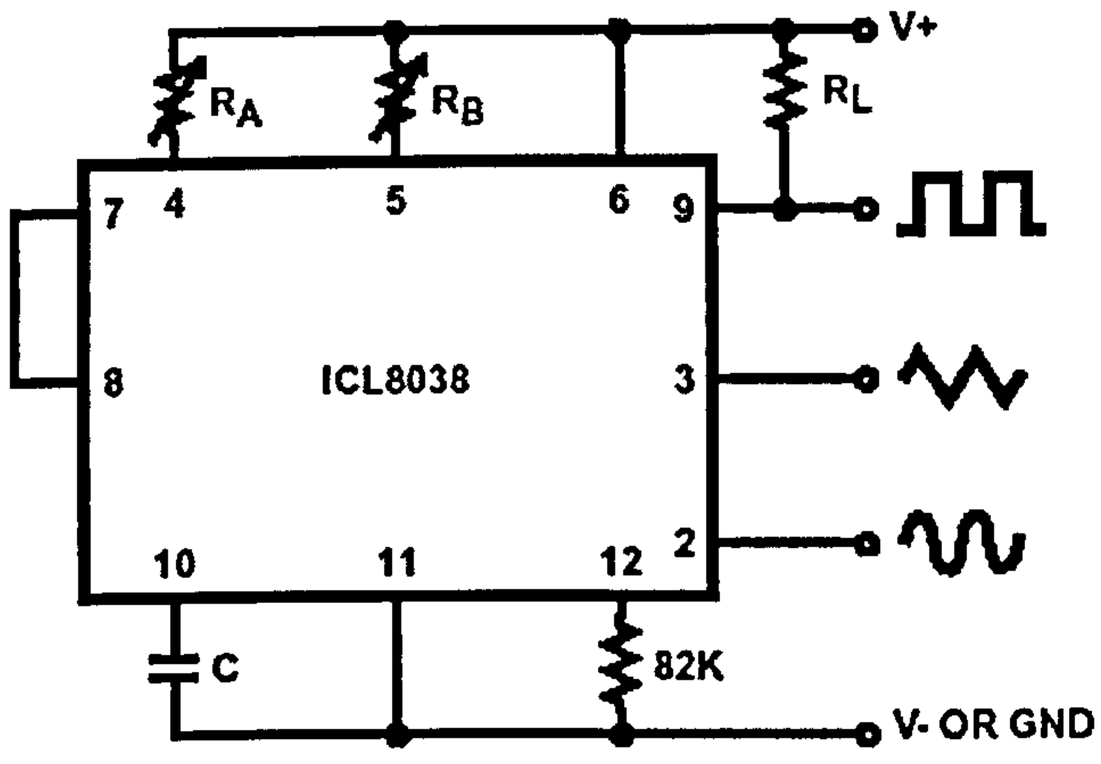

Figure 3-4 The Variable Frequency and Duty Cycle Rectangular Waveform Generator

The rectangular waveform characteristics are set by a capacitor C and two timing resistors R_A and R_B (Semiconductor 1996). It is assumed that the rectangular waveform period $T = t_1 + t_2$, where t_1 is the pulse width or the high state width and t_2 is low state width. The following equations are used to calculate the values of C, R_A and R_B

$$t_1 = \frac{R_A \times C}{0.66} \tag{3-1}$$

$$t_2 = \frac{R_A \times R_B \times C}{0.66(2R_A - R_B)} \tag{3-2}$$

When the frequency and duty cycle of interest are specified, T, t_1, and t_2 can be derived. Then the resistors and capacitor values can be determined using the above equations. Three different values of C are chosen to allow three different excitation frequencies: 100 Hz, 300 Hz and 1 kHz. Three sets of different R_A and R_B values are chosen to allow three different duty cycles: 10%, 20% and 50%. The various predefined values are necessary mainly for experimental purposes, but they could also be useful when the design is used in real applications.

With this variation range, the setting of frequency and duty cycle is achieved by turning rotary switches that are incorporated in the implementation.

3.3.2 Coil Driver

The essential parameters in the excitation are the peak current value and the transient characteristics of the current pulse rising edge. The higher the peak current, the higher the generated varying magnetic field strength will be, and in turn, the resulting eddy current energy increases in the specimen. Consequently, this will increase the signal to noise ratio of the system. However, too high current can easily introduce significant temperature variations and overheat the coil. This needs to be considered in choosing the excitation current.

The rate of change of the rising edge of the current pulse is also crucial as it determines the highest frequency components contained in the excitation. The higher the rate of change, the more high frequency components will be generated and hence more diagnostic depth information can be expected. This is especially beneficial when surface flaws are of the interest.

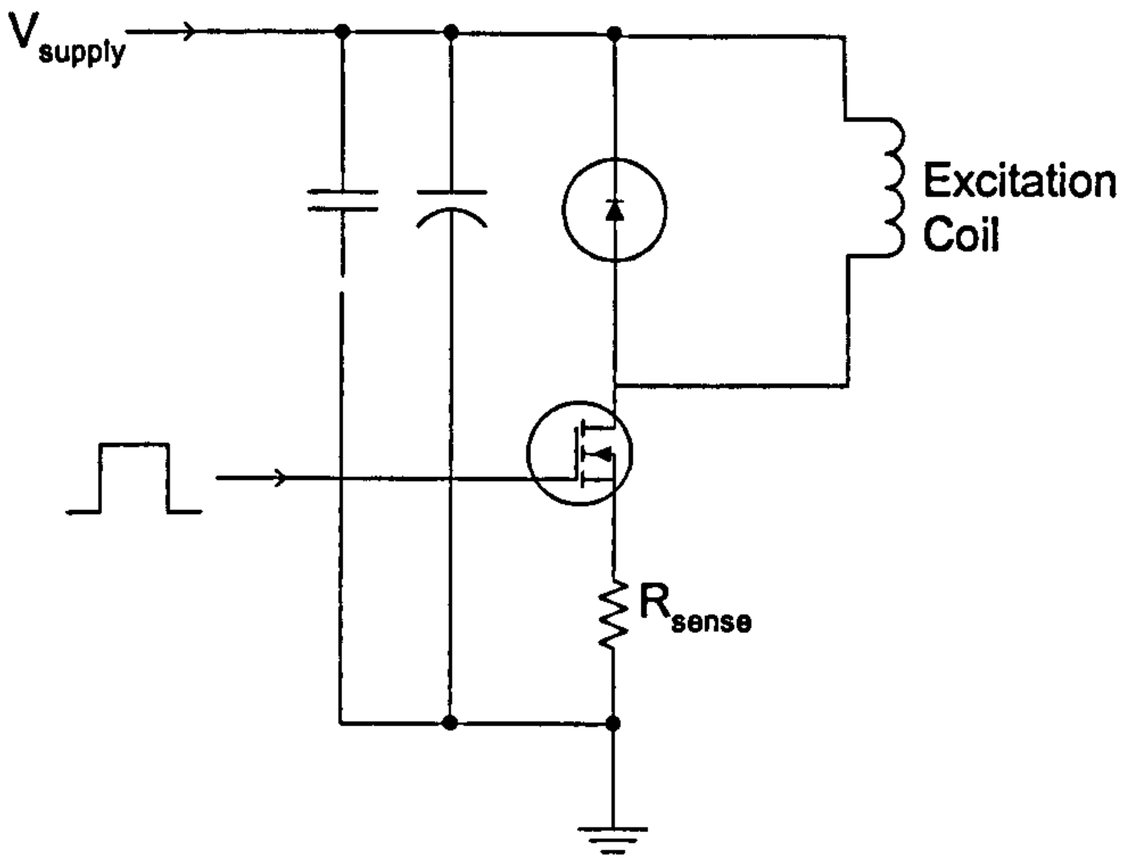

Figure 3-5 The Coil Driver Circuit

The excitation circuit schematic design is shown in Figure 3-5. The circuit uses a Metal Oxide Semiconductor Field Effect Transistor (MOSFET) as a switch that is switched on and off by signal coming from the rectangular waveform generator. MOSFETs have some advantages over bipolar junction transistors (BJTs) when used as a switch. MOSFETs have fast switching speeds. MOSFET's gate driver circuits are simpler than BJT's base driver circuits. To switch on a MOSFET, the voltage across gate and source must be higher than a threshold voltage V_T that varies from one device to another.

A high power MOSFET was chosen to anticipate high excitation current. The MOSFET should have a low RDS-on to allow major proportion of the supply voltage dropped across the coil and also to obtain high efficiency. RDS is the resistance of drain-source channel in the MOSFET, through which the coil current will also flow.

Variable voltage supply is used for the driver circuit to allow the adjustment of the magnitude of the excitation current. The excitation current can be monitored by measuring the voltage across the sense resistor R_{sense} whose value is 0.1 ohm. The low value is chosen to minimise its effect in limiting the current and dissipating extra power unnecessarily. The voltage is read through an oscilloscope. In the future, this should be measured by the use of an ADC port in a microcontroller, which will allow a centralised control panel through a PC.

3.3.3 Magnetic Sensors

There are different types of magnetic sensors available, namely Hall devices, magnetoresistives, giant magneto resistances (GMRs) and SQUIDs. Each of these has their own advantages and disadvantages. A Hall device utilises the Lorentz force on charge carriers. The charge carriers will be deflected into one direction and build up to create a Hall voltage across the device.

Magnetoresistive sensors make use magnetoresistive effect, i.e. the property of a current-carrying magnetic material to change its resistivity in the presence of external magnetic field.

SQUIDs are currently the most sensitive magnetic sensors, however, as mentioned in Chapter 2, commercial SQUIDs need cooling to operate, even the High Temperature versions of SQUIDs. In addition, the price of SQUID sensor is still relatively high. These are the reasons SQUIDs are not the option for this research and development, although it would be interesting to investigate their performance with PEC.

	SS495A1 (Hall Device)	**HMC1001** (Magnetoresistive)	**AA005-02** (GMR)
Magnetic Field Range (Gauss)	-670 to +670	-6 to +6	-100 to +100
Operation Frequency Range	0 - 100 kHz	0 - 5 MHz	0 - >1 MHz
Sensitivity (mV/V/Gauss)	0.625	3.2	0.55
Linearity (%)	1	2	1
Circuitry Requirements	Requires a simple supply voltage circuit	Requires additional high current set/reset pulse waveform generator	Requires a simple supply voltage circuit

Table 3-2 Comparison between magnetic sensors

Some magnetic sensors, whose part numbers are SS495A1 (Hall device) (Honeywell 1998), HMC1001 (magnetoresistive) (Honeywell 1999) and AA005-02 (GMR) (Rhopoint 2001), were available for testing. The process of making the selection of the representative

of each magnetic sensor family was limited by their availability. Table 3-2 provides some comparisons between these devices.

The Hall device was chosen for several reasons. Based on some experimental measurements, the magnetic field intensity close to the end of the coil can reach more than 150 Gauss when current of 1.5 A is used. Both the magnetoresistive and GMR cannot cover this range, only the Hall device would be able to do so. Another advantage of the Hall device is the absence of Hysteresis. The other two devices have some Hysteresis effect and need some compensation mechanism. From the data in Table 3-2, only the operation frequency range constitutes the weakness of the Hall device, however, in this application the operation frequency range required is 0 to around 20 kHz.

The schematic diagram of the Hall sensor circuit is shown in Figure 3-6. A voltage regulator is used to generate a 5 V supply required by the Hall device from the main +15 V supply. When no magnetic field is present, the Hall device output is at 2.5 V, which is equal to 0.5 x (V_+ - V_-). The transfer characteristics of the device are shown in Figure 3-7. Therefore, to obtain a proper reading for the measurement, a reference voltage of 2.5V is required, and this is implemented by using a voltage divider comprising of two resistors with the same value and one variable resistor to adjust the voltage output level. The output of this circuit will be differential outputs. R_{16} is added to function as signal return for the Hall device output signal and reduce the noise. Coupling capacitors are used to reduce the noise at the supply rails.

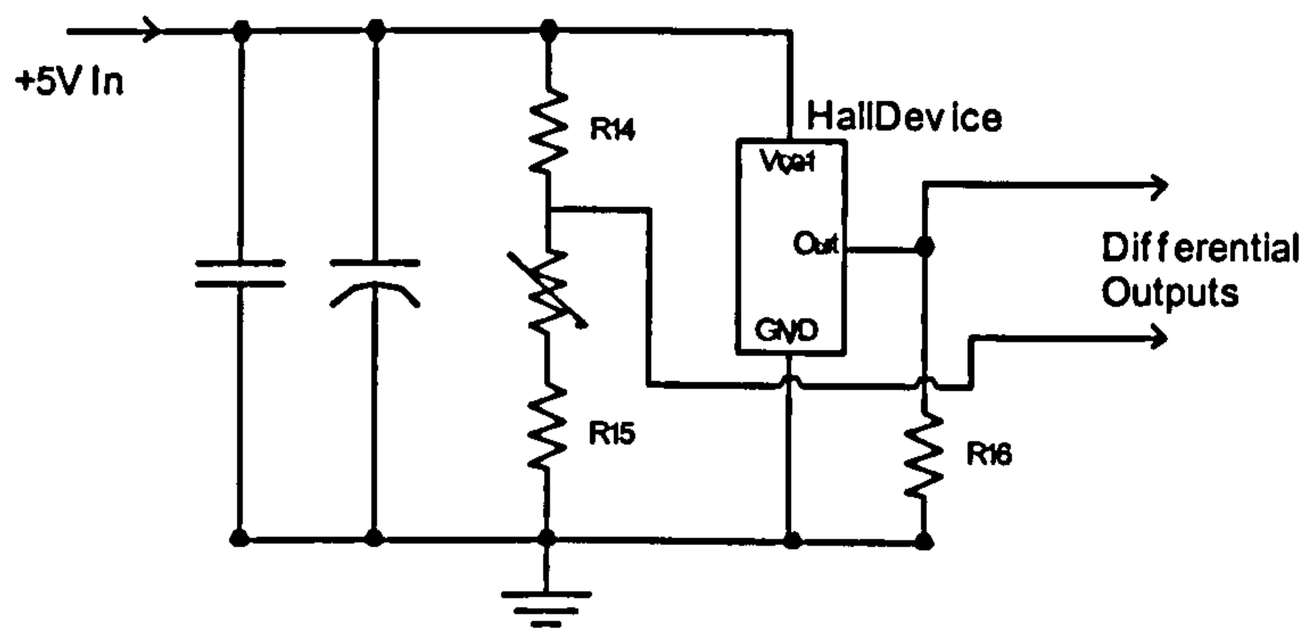

Figure 3-6 The Sensor Circuitry

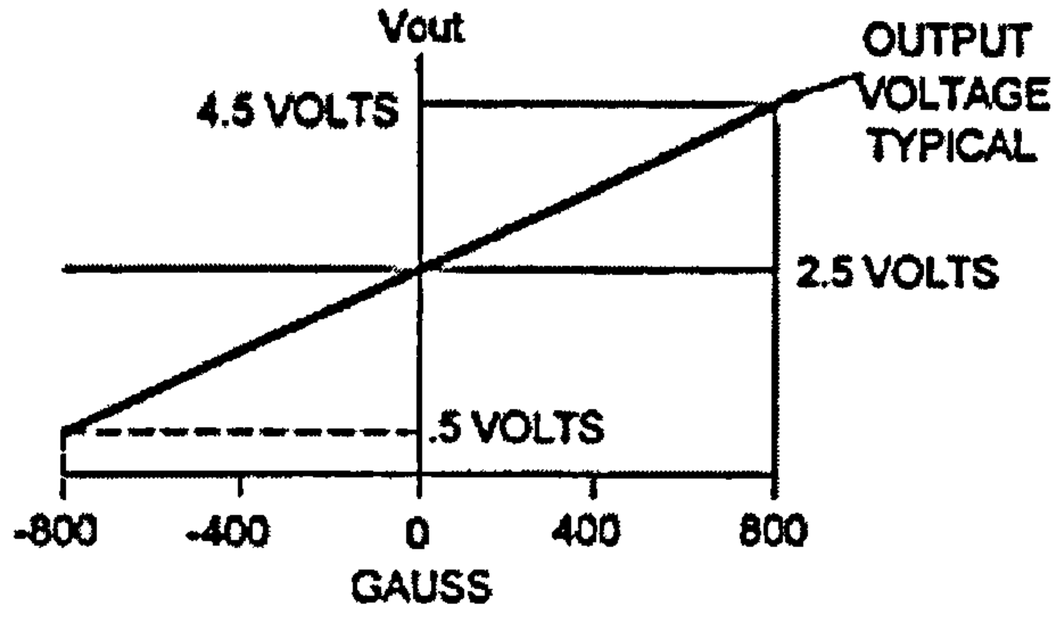

Figure 3-7 The Hall device transfer characteristic at *Vs* = 5V

3.3.4 Signal Conditioning

Signal conditioning is generally required for reliable and accurate data acquisition by the use of filters and amplifiers or attenuators. Filters are used to reduce the noise intensity and amplifiers are used to amply the signal level to allow optimum use of the input dynamic range of the ADC card. Without conditioning, the signal level can be too small for the input dynamic range of the ADC card, which gives rise to a non-optimum data acquisition with low signal-to-noise ratio. In the PEC system, the signal conditioning involves signal low pass filtering with a cut-off frequency of 20 kHz and signal amplification with a variable gain.

3.3.4.1 Instrumentation Amplifier

To amplify the signal so that the input dynamic range of the DAQ card can be utilised optimally, an instrumentation amplifier is added to the circuit. This stage is part of signal conditioning before the analogue signal is converted into digitised form. Instrumentation amplifiers have high precision in amplification and reject large values of common mode noise. They generally have wide bandwidth. These features are crucial for our sensor system. The adopted circuit for the instrumentation amplifier in this project is commonly used and shown in Figure 3-8. The gain of the amplifier can be computed as

$$V_{out} = \left(1 + \frac{2R}{R1}\right) V_{in} \tag{3-3}$$

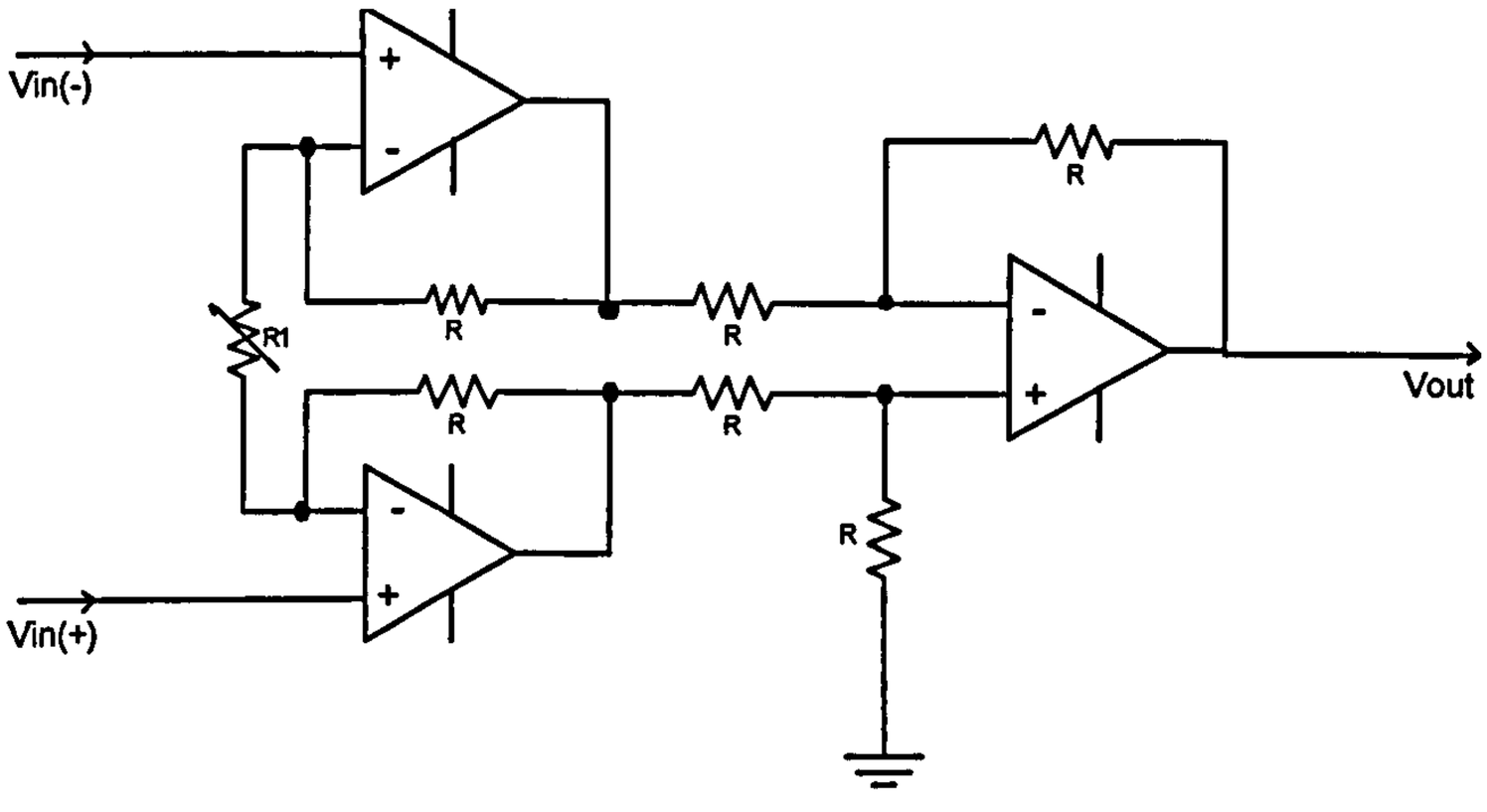

Figure 3-8 The Schematic Layout of the Instrumentation Amplifier

A variable resistor is used to enable adjustment of the gain of the amplifier. This is necessary as the magnetic field intensity may vary significantly depending on the magnetic permeability of the sample. Non-ferromagnetic materials with low magnetic permeability produce low resultant magnetic field intensity, while ferromagnetic materials give out high resultant magnetic field intensity and hence higher output voltage levels. Therefore, the adjustment is required to amplify the output voltage levels appropriately to allow optimum use of ADC dynamic range.

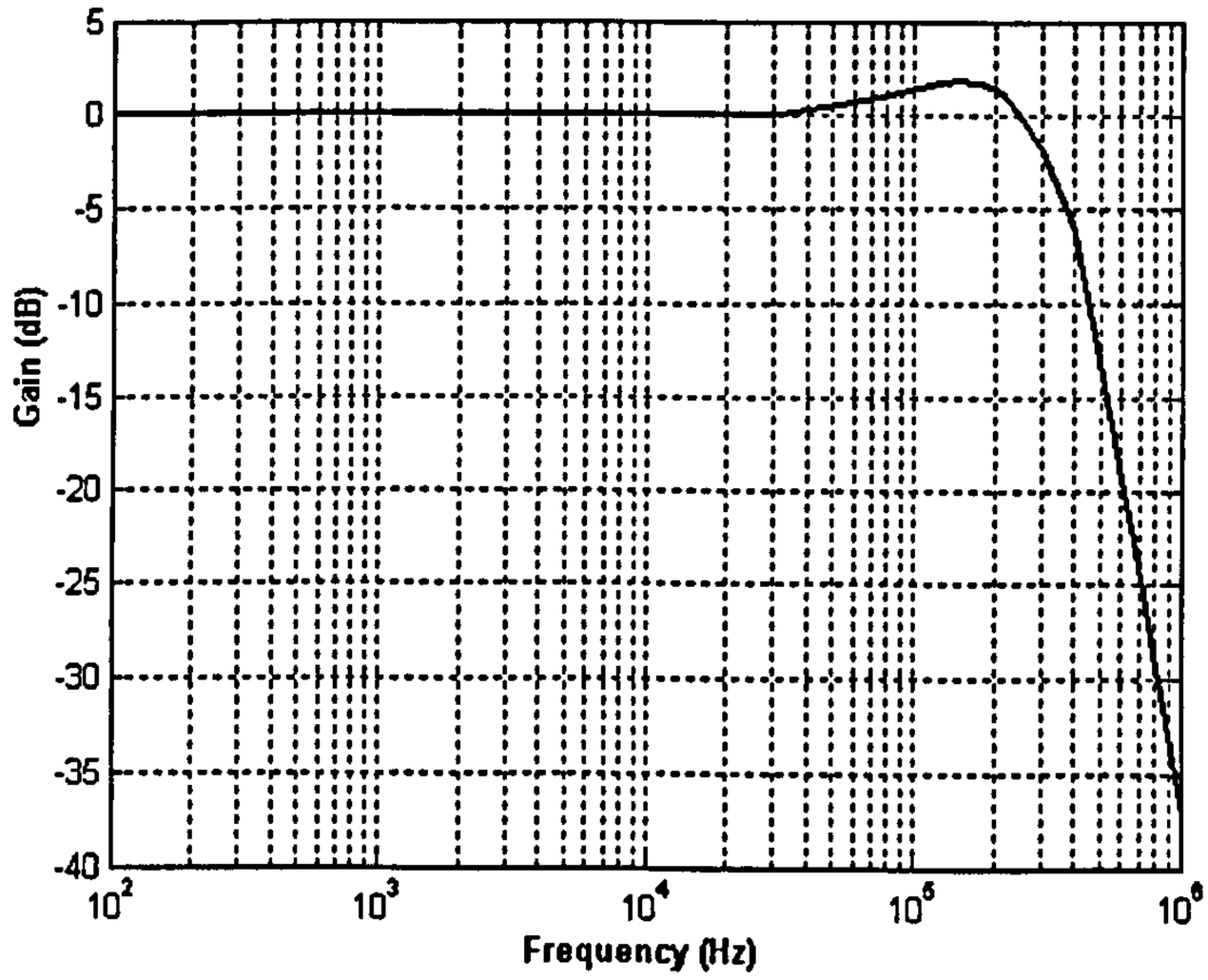

Figure 3-9 The Measured Instrumentation Amplifier Frequency Response

The measured frequency response of the instrumentation amplifier is shown in Figure 3-9. It shows that the gain starts to roll off at frequency of 200 kHz approximately, which is more than adequate to meet our requirements.

3.3.4.2 Low Pass Filter

The low pass filter is used to filter out high frequency noises and also serves as anti-aliasing filter. A second order filter is chosen, as they have a fast roll-off and can be implemented in a simple circuit. A well-known Sallen and Key 2nd order low pass filter (Niewiadomski 1989) was selected and implemented. The circuit schematic can be seen in Figure 3-10.

Resistors R_1, R_2 and R_3 should have the same resistance value equal to R. Then the resistance of R_4 can be determined using the following equation

$$R_4 = (2 - d)R \tag{3-4}$$

where d is the damping factor of the filter that determines the roll-off of the filter response. The values of d was chosen to be 1.414 to have the maximally flat response. This response has an attenuation of 3 dB at the selected cut-off frequency f_o, after which the roll-off gets steeper and eventually reaches 12 dB/octave, which is common for all 2nd order filters.

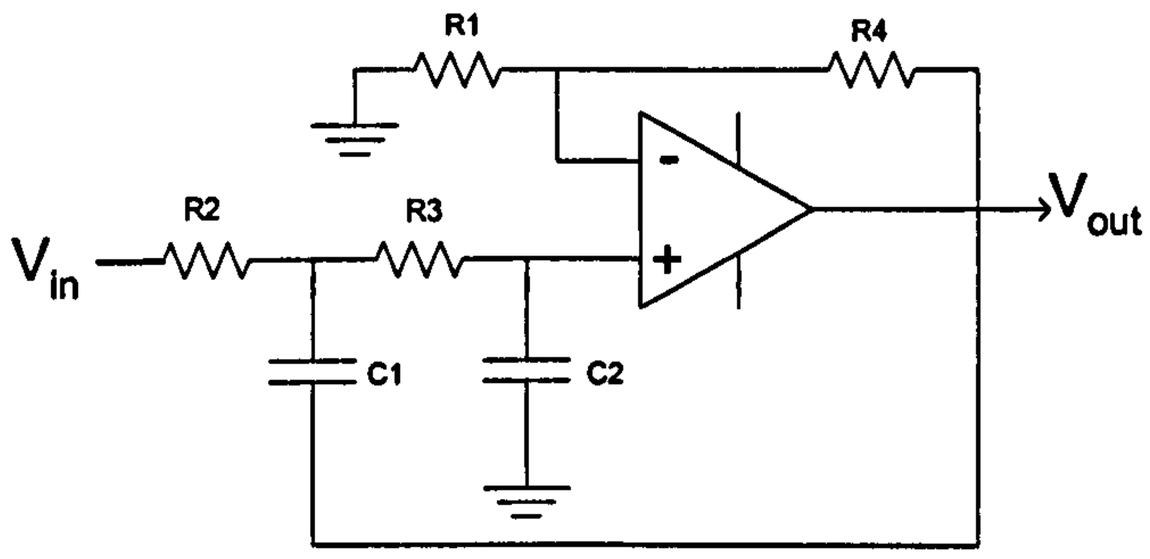

Figure 3-10 The Schematic Layout of the 2nd Order Low Pass Filter

The values of C_1 and C_2 are always the same, say C, and can be calculated using the following equation:

$$C = \frac{1}{2\pi f_o R} \tag{3-5}$$

The frequency response of the filter can be seen in Figure 3-11, which shows that the cut-off frequency of the filter is around 20 kHz.

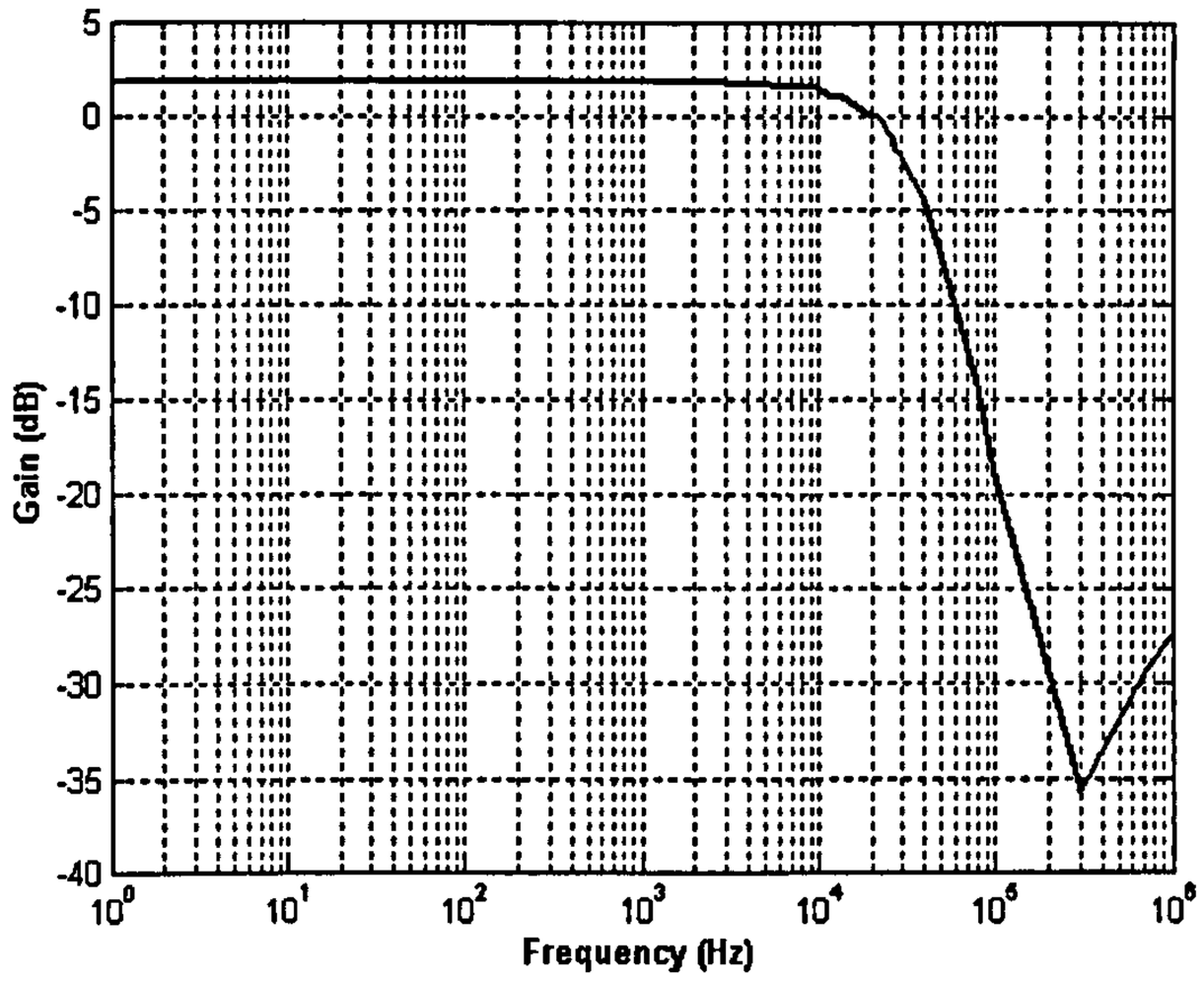

Figure 3-11 The Measured Frequency Response of the 2nd Order Low Pass Filter

3.4 Data Acquisition

Data acquisition system is required to acquire data by converting signals into digitised form that can be processed by a PC or any other processor-based system. In our system, the core of the data acquisition is a 12-bit PCI9812 data acquisition card that is interfaced to the PC via a PCI bus. The card is able to sample data at a rate of up to 20 MHz. The block diagram of the data acquisition card is shown in Figure 3-12. The card has four analog-to-digital conversion channels, which are designated as channels 0, 1, 2 and 3. It incorporates two FIFO buffers that can store up to 32K samples in total. The FIFO buffers are used to hold the data temporarily as the flow of data from the ADCs can be too fast for the PCI bus. The hardware support 1-, 2- or 4-channel data acquisition, but not 3-channel. The presence of the tristate latches allow this to happen. The tristate latches can have three different output states: high, low and no connection. The buffers are shared by active channels, for example when 2 channels are active, the FIFO size is 16K samples per channel. When one data acquisition cycle is accomplished, the hardware returns the control to the software program. Then an instruction can be sent to the hardware to transfer

the data to user-defined PC memory address using Direct Memory Access (DMA) via the PCI bus. DMA transfer is very fast and does not burden the host CPU unnecessarily.

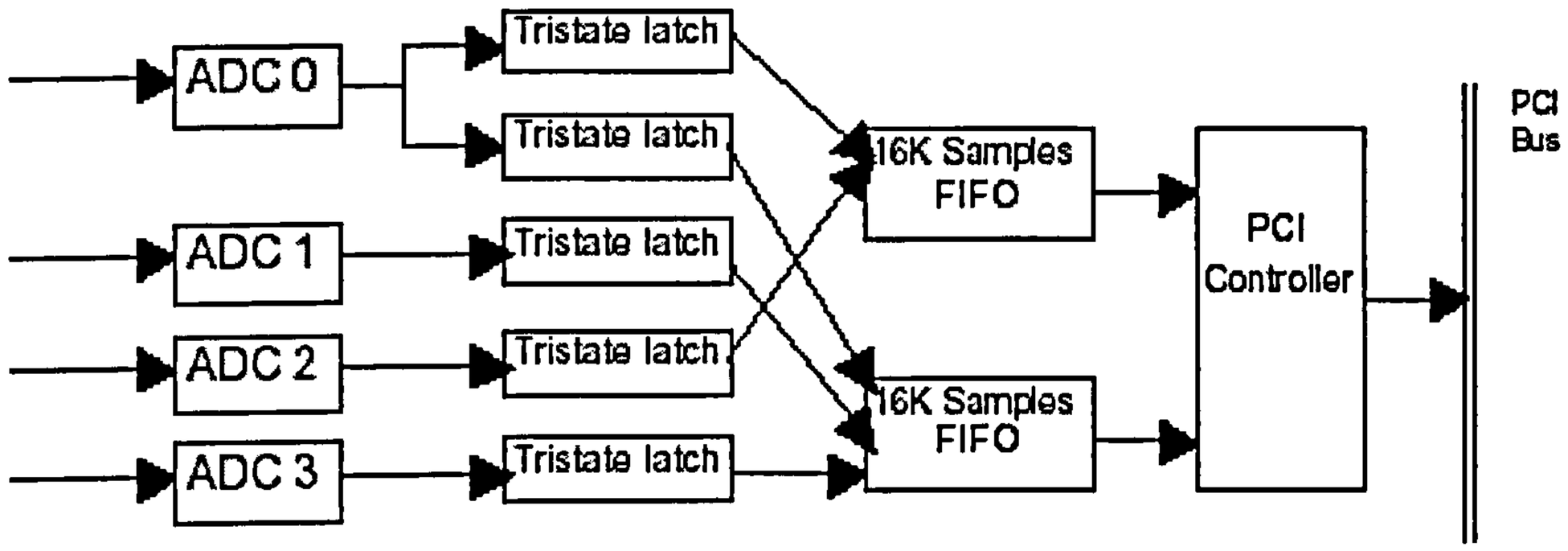

Figure 3-12 The PCI9812 Block Diagram

For 5V input range, the input impedance can be configured at 1.25kΩ or 50Ω. To keep the circuit design simple, the high impedance of 1.25 kΩ was chosen (Adlink-Technology 2000). The input voltage range and impedance is set by soldering or desoldering to close or open corresponding gap switches on the card.

For the acquisition to start, the card has to be triggered. The card has five trigger modes, one of them is a software trigger. For our application, it is desired to start the acquisition ***m*** data prior to the pulse, where ***m*** >0. This is necessary to prevent the distorting effect that may happen due to further signal processing on the important part of the signal. For example a digital Gaussian filter generally has an edge effect, where the beginning and last part of a signal that it is applied to will become distorted. Therefore, to be able to capture the preceding part, Middle-Trigger acquisition mode is chosen. This trigger mode is illustrated in Figure 3-13. In this mode, the acquisition is started ***m*** data prior to the trigger event.

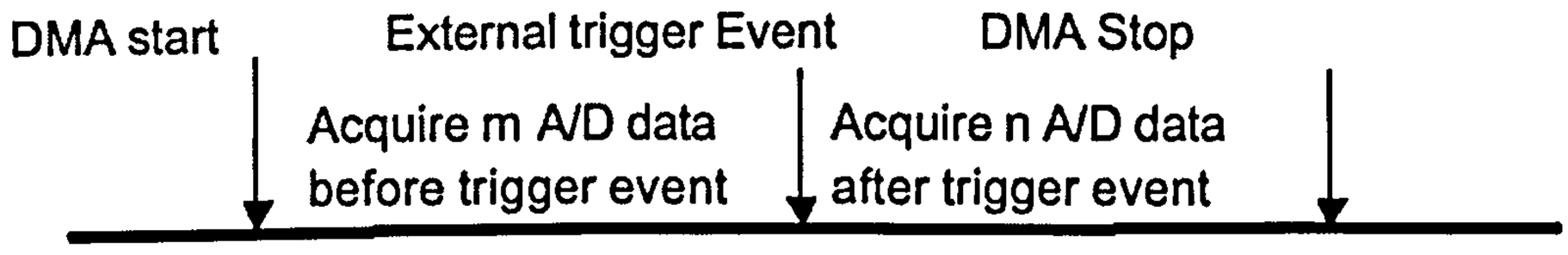

Figure 3-13 The Middle-Trigger Acquisition Mode

The PCI-9812 has a supporting dynamic link library that contains high-level functions to configure the card and transfer digitised data from the card buffer to PC memory. The

software development is carried out in the Visual C++ environment and is discussed in section 3.6. More information about the acquisition card can be found in (Adlink-Technology 2000).

3.5 Probe Design

The probe consists of four main parts, namely excitation coil, Hall sensor, coil former and probe sleeve, as shown in Figure 3-14. The hall device measures magnetic field strength perpendicular to the surface of the sample, B_z. The coil former is what the coil is wound upon. The sleeve holds the coil former, protects the PCB from undesired contacts, and serves as a handler in the measurement. The material for these mechanical parts is chosen so that the design will have a low temperature change. Therefore, material with a low temperature coefficient is chosen. The material must also be rugged enough to be used in the field, as the probe scan over a metal surface.

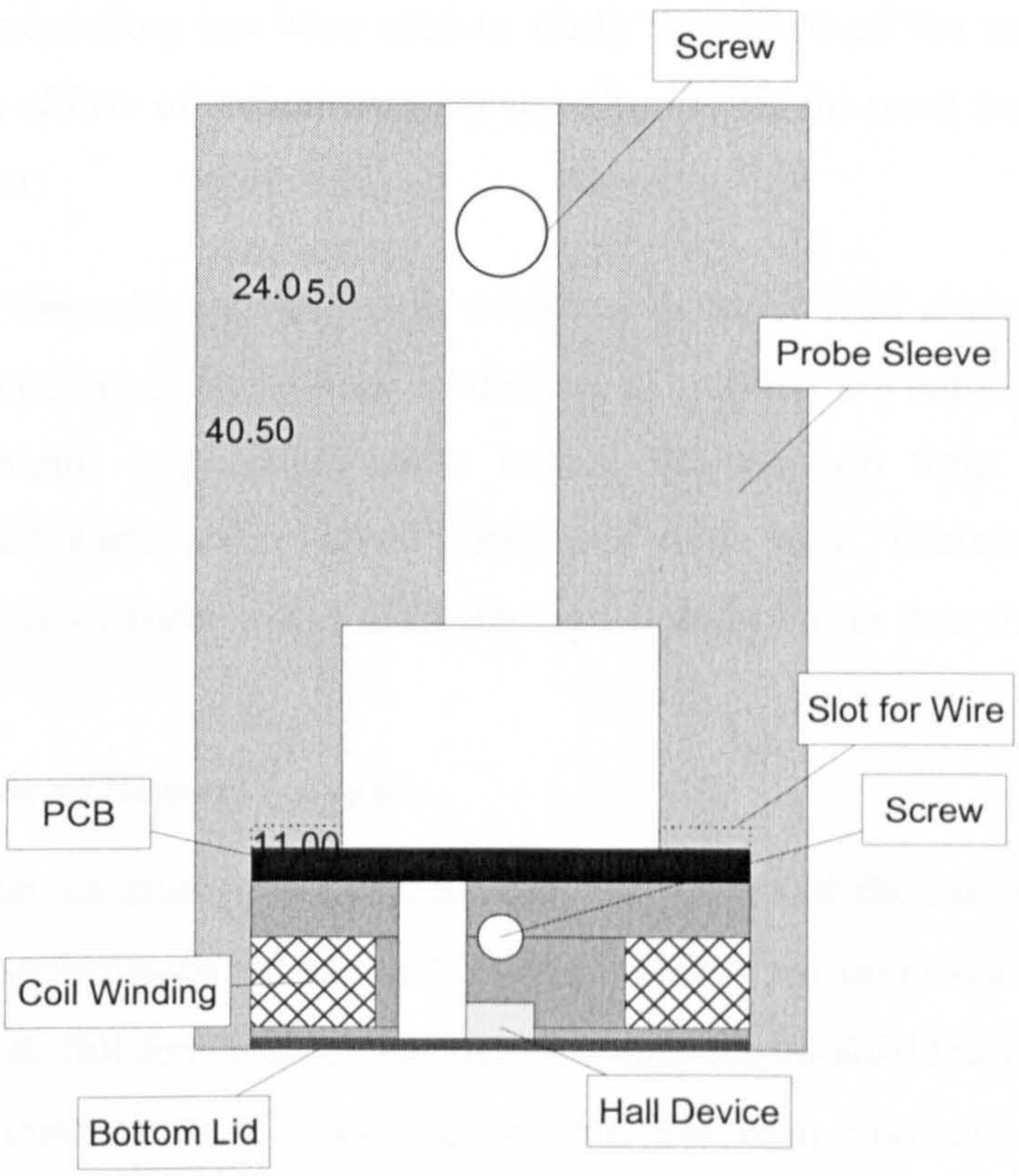

Figure 3-14 The layout of new probe

The coil design determines the sensitivity of the probe. Some main parameters that should be considered include the wire diameter, coil diameter and coil height. There is no exact

analytical technique to determine the most effective values for these parameters. In this study, parameter values are determined by considering general principles:

- the bigger the diameter, the deeper the penetration
- the closer the coil to the sample, the better the coupling of the field
- the minimum length of the detectable defect is proportional to the coil diameter

To aid design and familiarity with the relevant issues, Finite Element modelling (FEM) has been used. The use of mathematical modelling such as FEM is beneficial to save development time and costs as different designs can be tested without the need to build the real objects. It has been reported that FEM has been used by researchers and developers in eddy current probe design (Rao, Kalyanasundaram et al. 2000; Morozov and Novotny 2002; Wilde and Lai 2003). This modelling can generate indicative pictures about the effects of changing parameters such as probe structure layout and coil dimensions. In this design work, the modelling has been used to study the effects of the use of shielding and cores, to study the effects of coil parameters and also to find the most sensitive position for the magnetic sensor.

In the modelling, the coil is modelled as a hollow cylinder with a given wall thickness. Axisymmetric modelling is used. In the modelling, 3D models are reduced to 2D models to simplify the problems and consequently reduce the solution time. The approach is applicable when all parts are revolved about one same axis. Therefore, the sample is assumed to be a solid cylinder with a diameter significantly larger than that of the coil.

3.5.1 Simulation of Sensor Layout

In this investigation, an attempt is made to study the effects of the use of ferrite cores and shielding on the performance of the coil. Five structures are investigated, which include side ferrite-shielded, full ferrite-shielded, ferrite-cored, ferrite-shielded-and-cored, and air-cored by using finite element modelling. Ferrite has high magnetic permeability but virtually non-conductive, hence no energy loss due to induced current takes place. The coil parameters are as follows:

- inner radius r_i: 2.5 mm

- outer radius r_o = 7.5 mm
- height h = 5.0 mm
- lift-off d = 0.1 mm

Figure 3-15 illustrates the coil parameters and their notations. Figure 3-16 shows the layouts of the different probe coil structures for simulation.

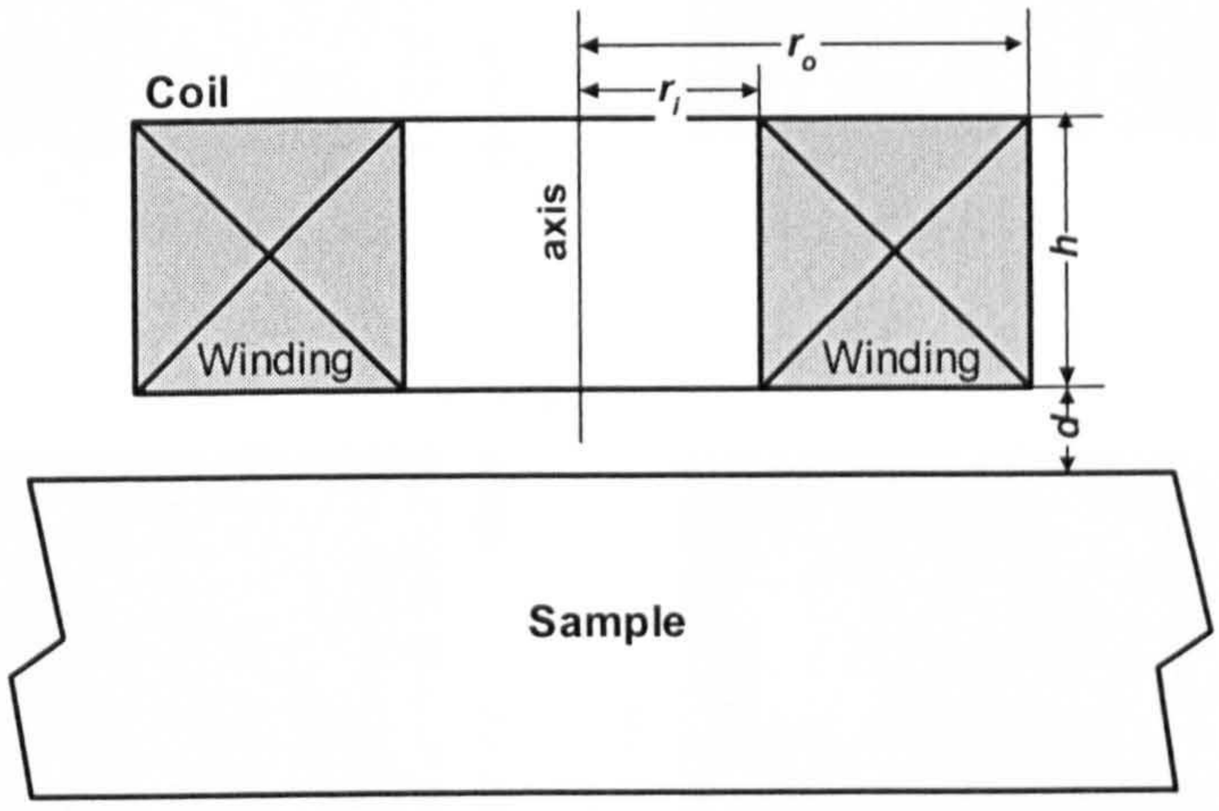

Figure 3-15 Coil Dimensions

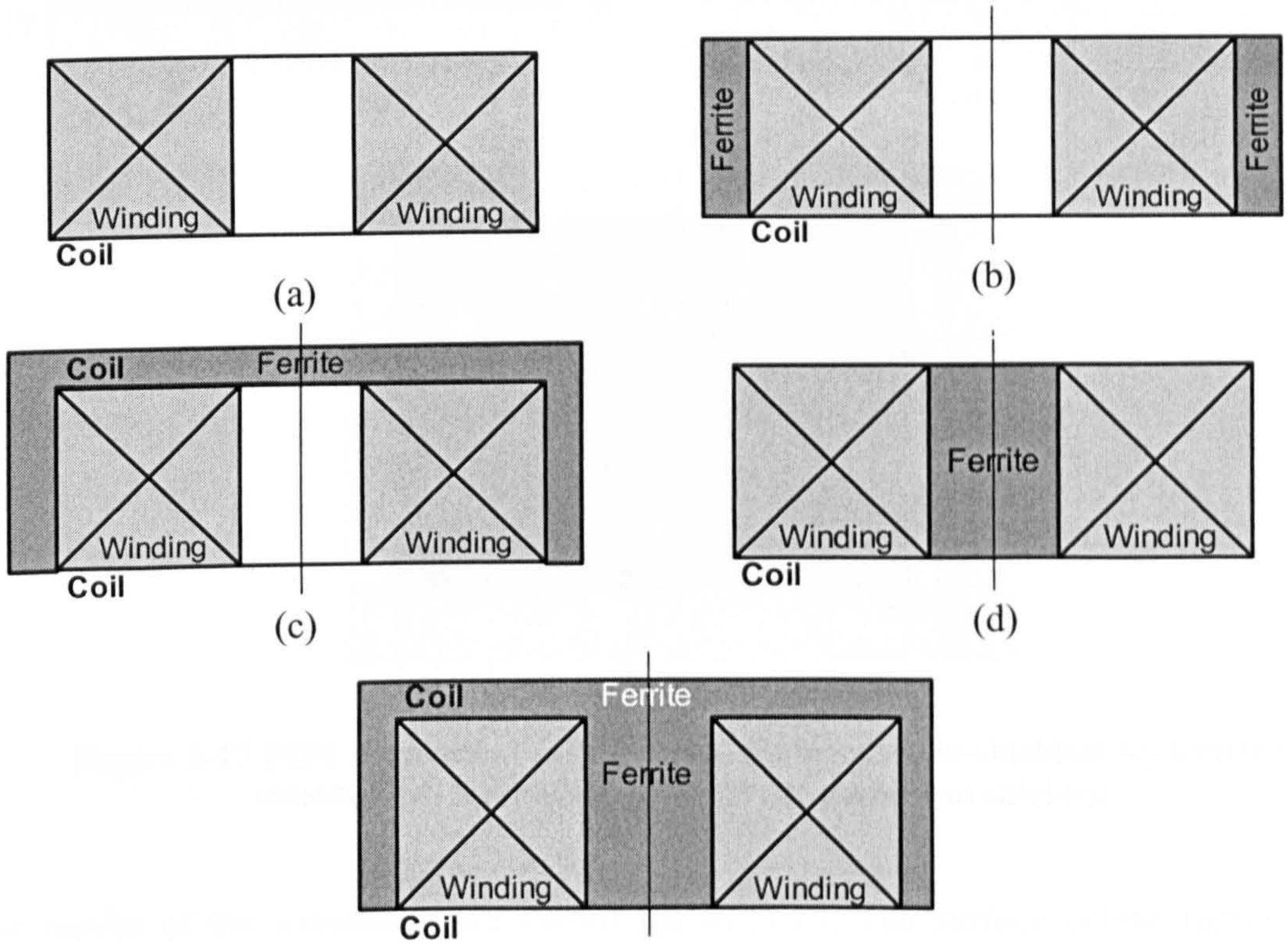

Figure 3-16 Probes' layouts: (a) air cored, (b) ferrite side-shielded, (c) ferrite full-shielded, (d) ferrite cored, (e) ferrite cored and shielded

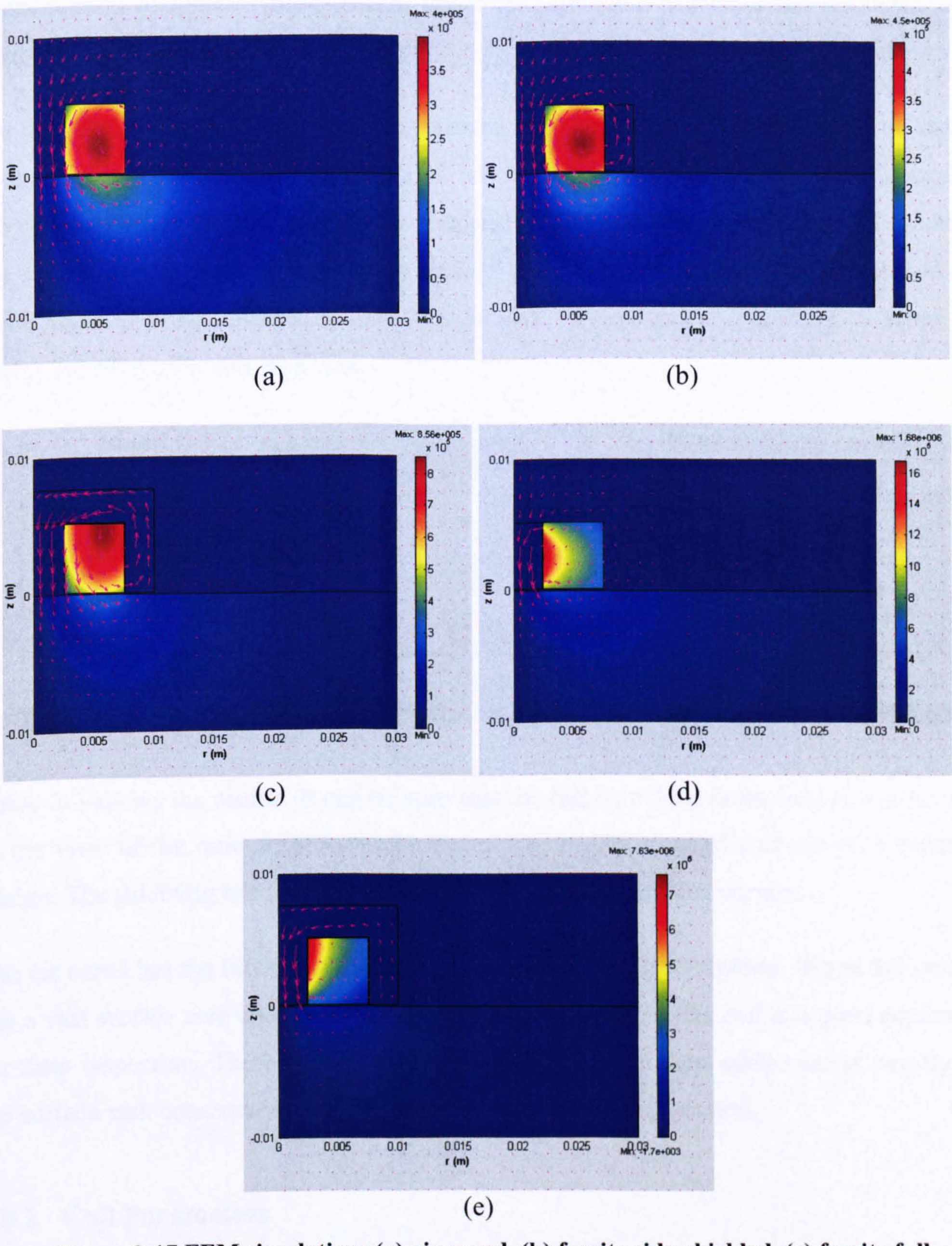

Figure 3-17 FEM simulation: (a) air cored, (b) ferrite side-shielded, (c) ferrite full-shielded, (d) ferrite cored, (e) ferrite cored and shielded

The results of the simulation are shown Figure 3-17. The surface colour represents the intensity of the induced current, and the arrows correspond to the direction and magnitude of the magnetic flux density. To evaluate the performance of each probe, the penetration

depth and the lateral spread of the induced current are looked into. Logically deep penetration and low lateral spread is desirable. Low lateral spread means high concentration of induced eddy current under the probe and minimise the interference of surrounding structural discontinuities.

For penetration depth, the decay of the induced eddy current J underneath the inner radius of the coil is examined. The depth $z_{0.5}$ at which the induced eddy current has reduced to 0.5 of its value on the surface is to be obtained. For lateral spread, the radius $r_{0.2}$ close to the surface at which the induced eddy current has reduced to 0.2 of its peak value at the same depth is to be obtained. Finally, the ratio R of $z_{0.5}$ / $r_{0.2}$ is calculated to score the performance of each coil structure.

Mode	$r_{0.2}$ (mm)	$z_{0.5}$ (mm)	R	Peak induced current
Side-shielded	17 .0	4.0	.0.24	2.2×10^5
Top and side shielded	13.5	3.4	0.25	3.15×10^5
Cored	17.5	2.0	0.11	4.75×10^5
Cored and shielded	10.0	1.5	0.15	14.0×10^5
None	22.0	4.2	0.19	2.15×10^5

Table 3-3 Evaluation of the Use of Ferrite Shielding and Cores Based on the FEM Results

Table 3-3 shows the results. It can be seen that the fully-shielded is the best coil structures in the view of the ratio R. Side-shielded performs nearly as good and can be simpler in design. The shielding has reduced the lateral spread of the induced current.

The air cored has the highest lateral spread but also the best penetration. When the sample has a vast surface area and when the resolution is not critical, this coil is a good contender for deep inspection. The both shielded and cored has the highest eddy current density on the surface and, consequently, could be the best for surface inspection.

3.5.2 Coil Parameters

In this investigation, how the coil parameters: inner radius r_i, outer radius r_o and height h of the coil affect the performance of the coil is examined. The investigation is carried out by comparing the performance when one of the parameters is varied. Tables 3-4, 3-5 and 3-6 show the performance of each configuration based on the results of FEM.

Internal Radius (mm)	$r_{0.2}$ (mm)	$z_{0.5}$ (mm)	R
1.0	0.0207	0.0035	0.1691
2.5	0.0208	0.0043	0.2067
3.0	0.0213	0.0045	0.2113
3.5	0.0214	0.0047	0.2196
4.0	0.0220	0.0051	0.2318

Table 3-4 Performance vs. Coil Inner Radius

Outer Radius (mm)	$r_{0.2}$ (mm)	$z_{0.5}$ (mm)	R
6.0	0.0208	0.0040	0.1923
7.5	0.0208	0.0043	0.2067
9.0	0.0220	0.0047	0.2136

Table 3-5 Performance vs. Coil Outer Radius

Height (mm)	$r_{0.2}$ (mm)	$z_{0.5}$ (mm)	R
3.0	0.0208	0.0049	0.2356
5.0	0.0208	0.0043	0.2067
7.0	0.0214	0.0041	0.1916

Table 3-6 Performance vs. Coil Height

From the above table, it can be concluded that

- The larger the internal radius, the deeper the penetration and the larger the lateral spread, the higher the ratio R
- The larger the outer radius, the deeper the penetration and the larger the lateral spread, the higher the ratio R
- The smaller the height h, the deeper the penetration and the larger the lateral spread, the higher the ratio R

3.5.3 Lateral Location of Magnetic Sensor

To determine the most sensitive radial position of magnetic sensor, FEM is also used. The radial distribution of the vertical magnetic flux density halfway between the coil and the sample is examined. This examination is carried out in two different situations, i.e. when no samples are present and when an aluminium sample is present underneath the coil.

These two conditions correspond to two extreme situations and therefore should give the maximum difference that can be observed.

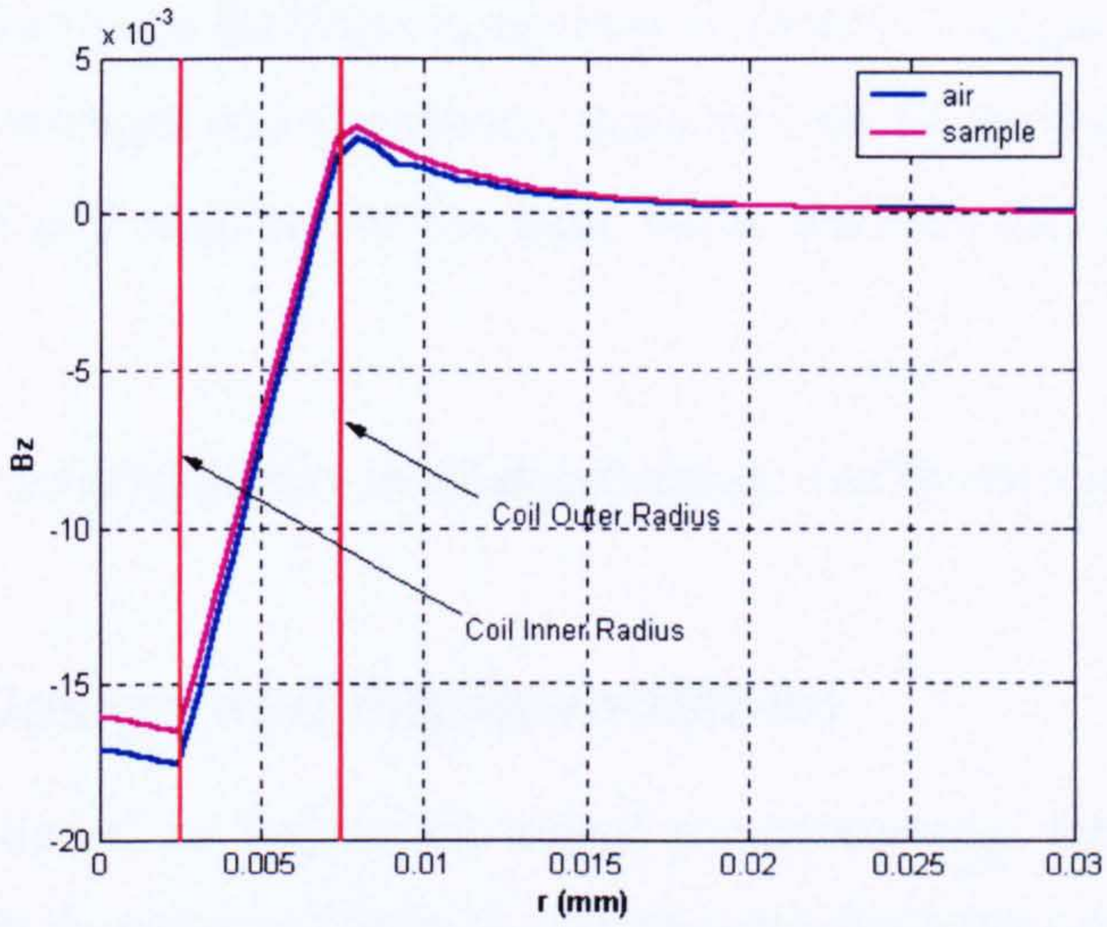

(a)

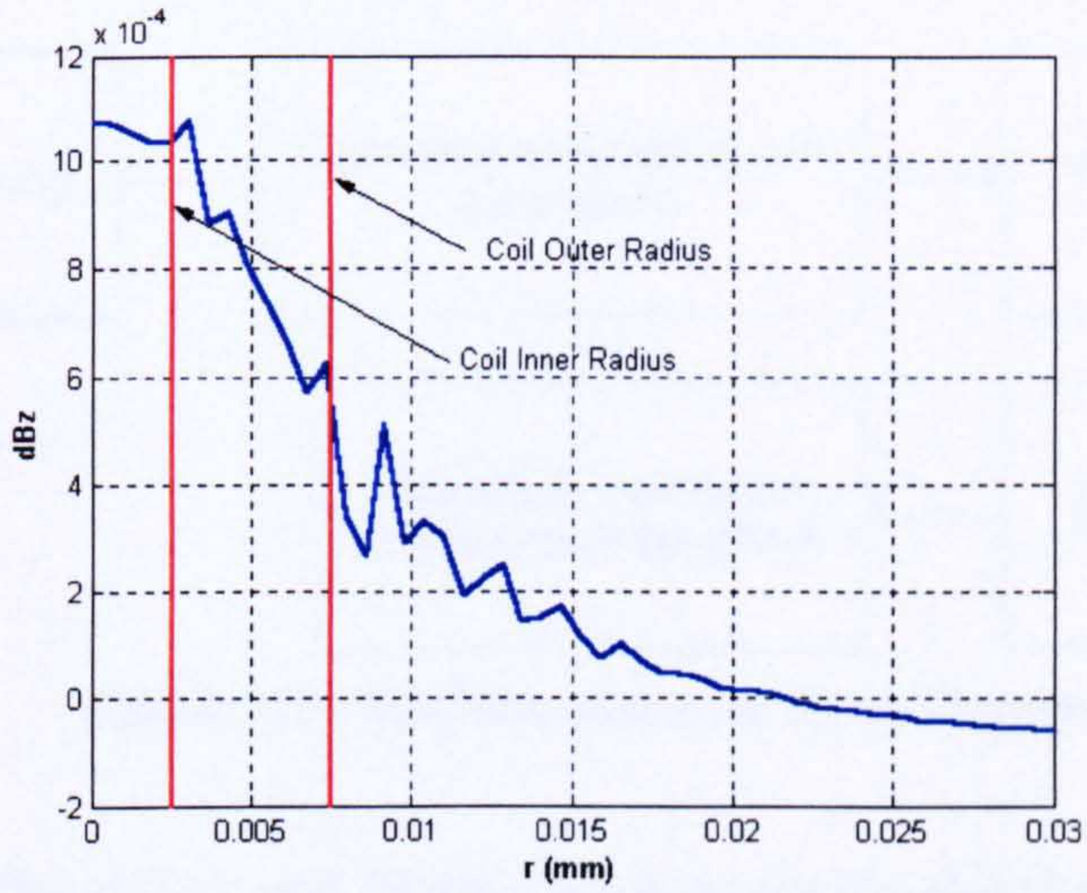

(b)

Figure 3-18 The Magnetic Flux *Bz* Distribution Just above the Sample along the Radius *r* (a) Both when the sample is present and absent (b) The difference

Graph in Figure 3-18(a) show the vertical magnetic flux density when no sample is present, B_{z_air} (blue line) and when sample is present, B_{z_sample} (purple line). Figure 3-18(b) shows the difference, $B_{z\_air} - B_{z\_sample}$. The graph indicates that the maximum difference, which should correspond to the most sensitive point is taking place at the central axis of the coil, i.e. $r = 0$.

As the simulation results indicate, the optimum probe parameters vary for different purposes. The simulation results can be used for guiding the design of probes including the selection of parameters. Several coils were built and tried, and the one considered as having the best performance for deep inspection is chosen. The performance is evaluated based on the signal strength and sensitivity. Sensors with larger diameters, coil windings closer to the sample and smaller heights have better performance for sub-surface defect detection.

The diagrams of the detailed probes mechanical design can be seen in Appendix 2.

3.6 Software Design and Implementation

The software is designed to implement signal pre-processing, data analysis and result presentation. A block diagram in Figure 3-19 illustrates the software framework. The data analysis comprises of feature extraction, defect classification and defect quantification.

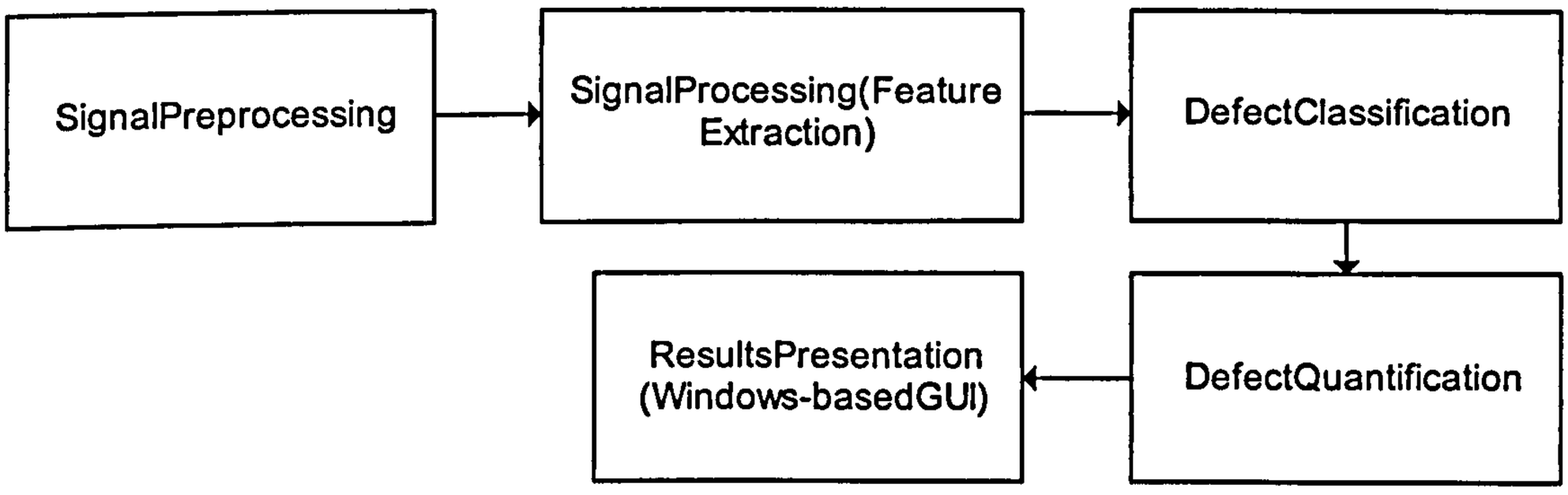

Figure 3-19 The New Software Block Diagram

At this stage, both Visual C++ and Matlab are used for the development of the software. Visual C++ is used mainly for data acquisition and some simple signal processing, while Matlab is used for signal conditioning, data analysis and presentation. Matlab is used because it has such a good library of useful functions so that the development and investigation time can be shortened. However, it is expected that in the future development, only Visual C++ will be used to enable optimised processing speed.

3.6.1 Windows-based GUI

Figure 3-20, Figure 3-21 and Figure 3-22 show snapshots of both GUIs created using Visual C++ and Matlab. Figure 3-23 and Figure 3-24 show simplified flow charts for data

acquisition and analysis coded in C++ and Matlab respectively. Some of the menu items have not been developed. The Visual C++ graphical user interface allows the user to configure the data acquisition, such as sampling frequency and data size. The interface also allows the displays of both base and differential signals acquired through the DAQ card. The Matlab user interface allows the user to choose the signals to be displayed and the features to be calculated and displayed. In general, the functionalities of the software include:

- Flexible data acquisition
  - Variable sampling frequencies
  - Variable data lengths
  - Automatic saving and loading the acquisition configuration
  - Single shot for single measurement
  - Continuous measurements
- Signal pre-processing
  - Signal averaging
  - Mean filtering
  - Spike filtering
  - Gaussian filtering
  - Normalisation of signals, can be useful for ferromagnetic inspection
- Signal synchronisation
- Display of signals: reference, base and differential signals
- Feature extraction and presentation
  - Peak value and peak time
  - Wavelet-based PCA

- Save acquired data into a file

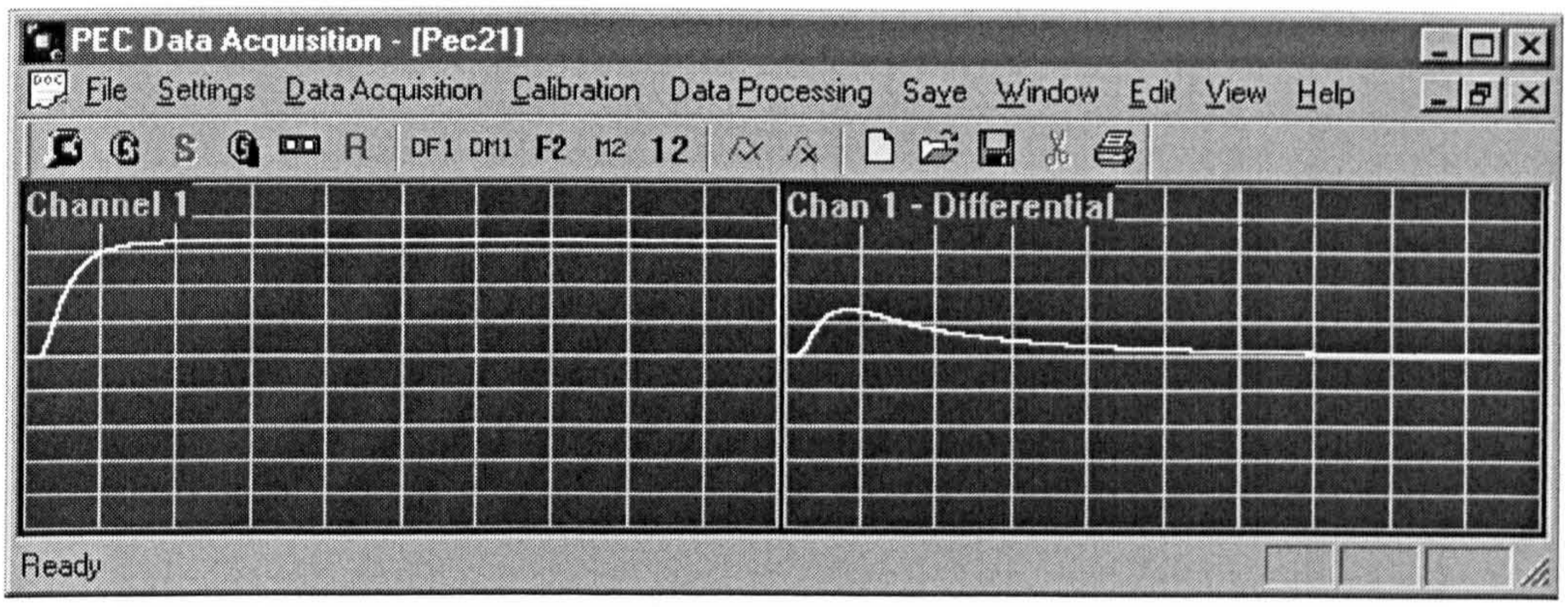

Figure 3-20 The Developed Windows-based Graphical User Interface

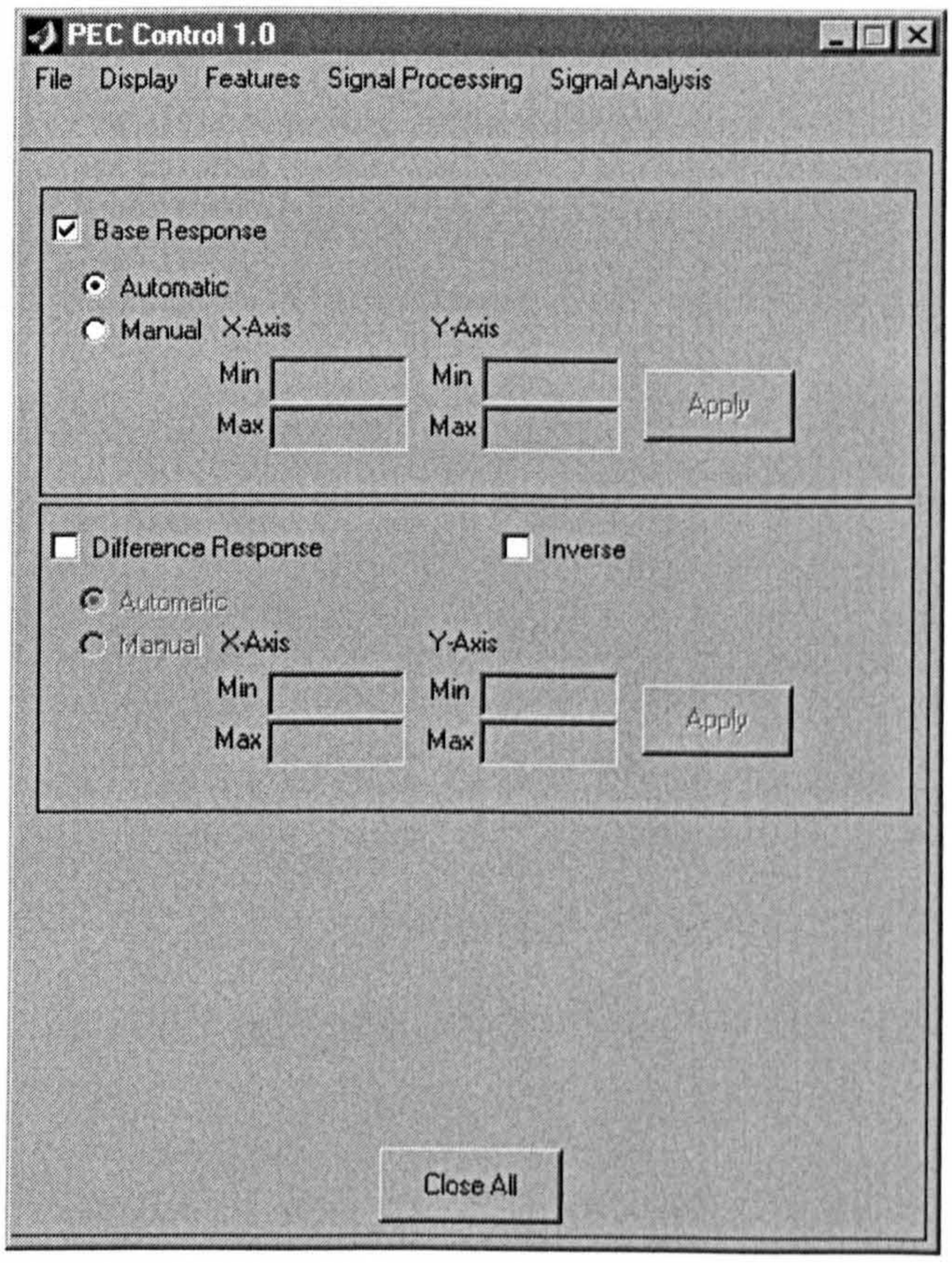

Figure 3-21 The Developed Matlab-based GUI

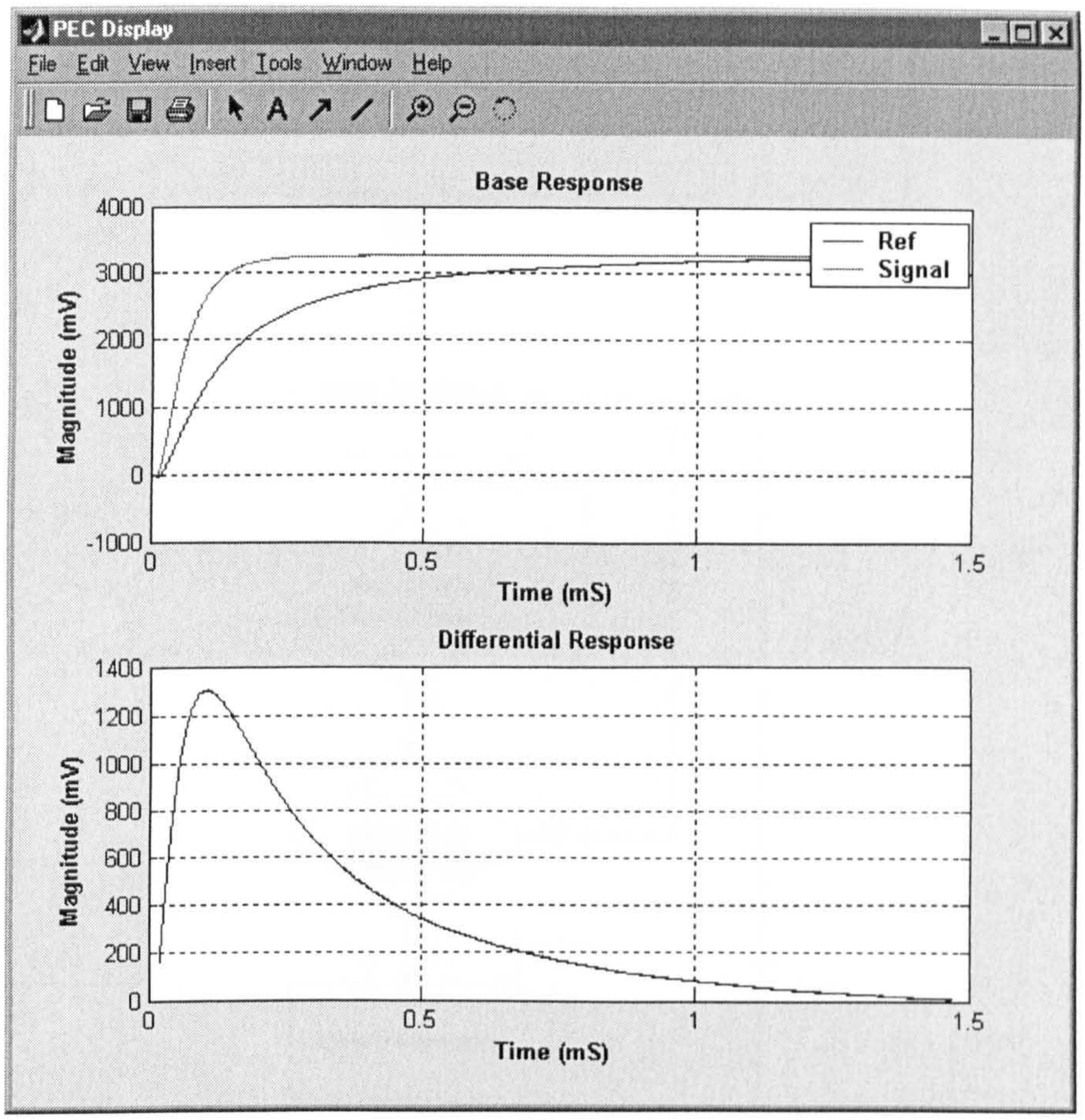

Figure 3-22 Displays of Signals

Figure 3-23 and Figure 3-24 show the core sequence inside the programs written using VC++ and Matlab.

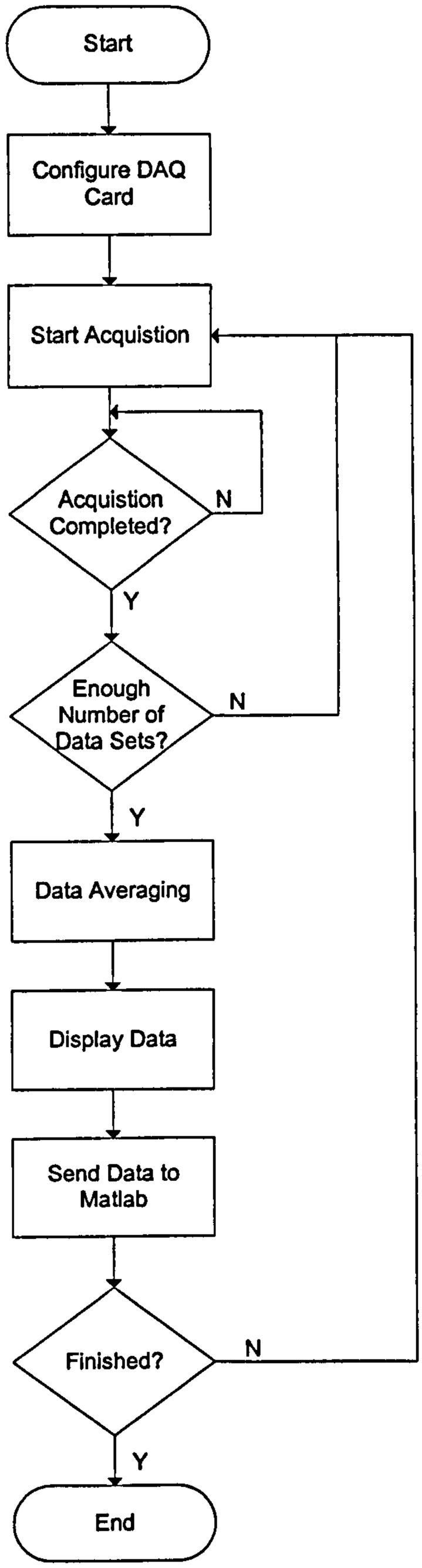

Figure 3-23 Simplified VC++ Program Flow Chart

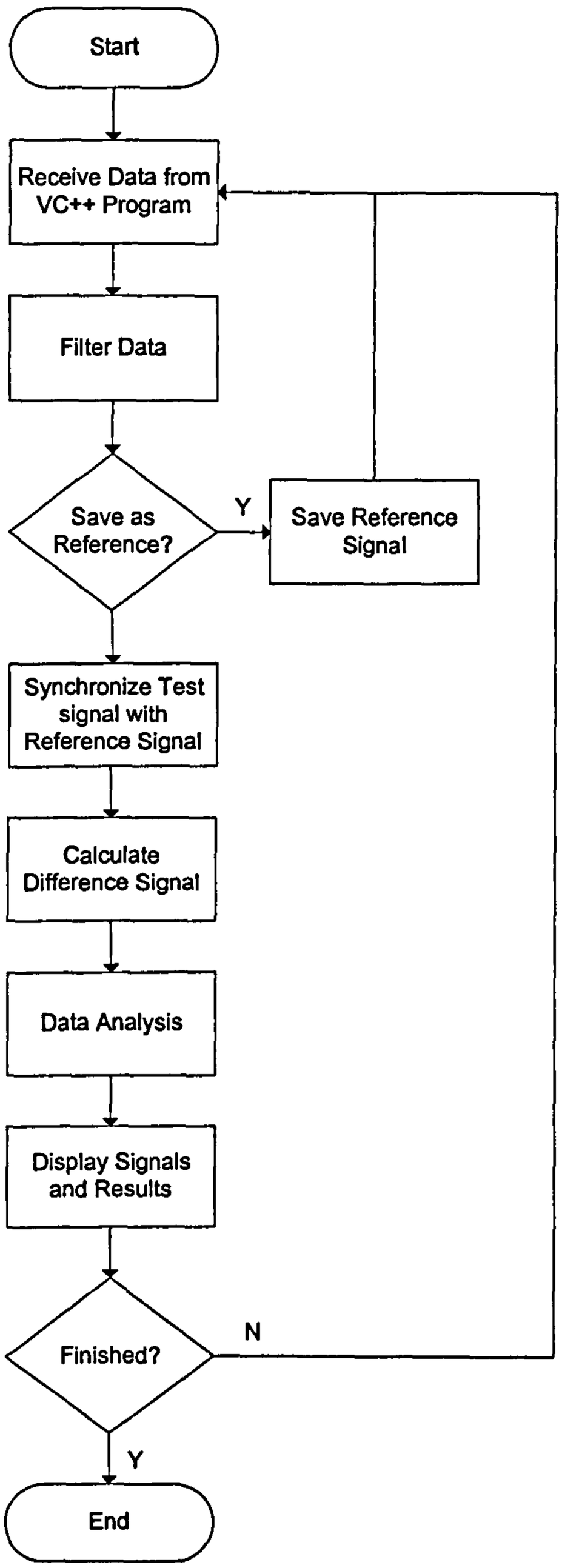

Figure 3-24 Simplified Matlab Program Flow Chart

3.6.2 Signal Pre-processing

Signal pre-processing is used to improve the signal-to-noise ratio of the PEC signals. After the pre-processing, the signals can be used for analysis for defect classification and quantification in both time and frequency domains.

3.6.2.1 Electrical Noise Reduction

All electrical systems have electrical noise, and the PEC system is no exception. This electrical noise is also called instrument noise. It is necessary to eliminate or minimise the noise and improve the signal-to-noise ratio (SNR) to allow measurements that are more effective. Large noise level can mask defect signals out. The SNR is defined as

$$SNR = \frac{V_{signal}}{V_{noise}} \tag{3-6}$$

The signals become weaker when the flaw characteristics are very close to a flawless condition. Therefore, noise reduction plays an important role in improving the sensitivity of a sensor system.

It has been identified that two main sources of noise are present in the system, namely the Hall device and the data acquisition card. The Hall device noise is reduced by electronic hardware low pass filter, and the noise of the data acquisition card must be resolved using software noise reduction.

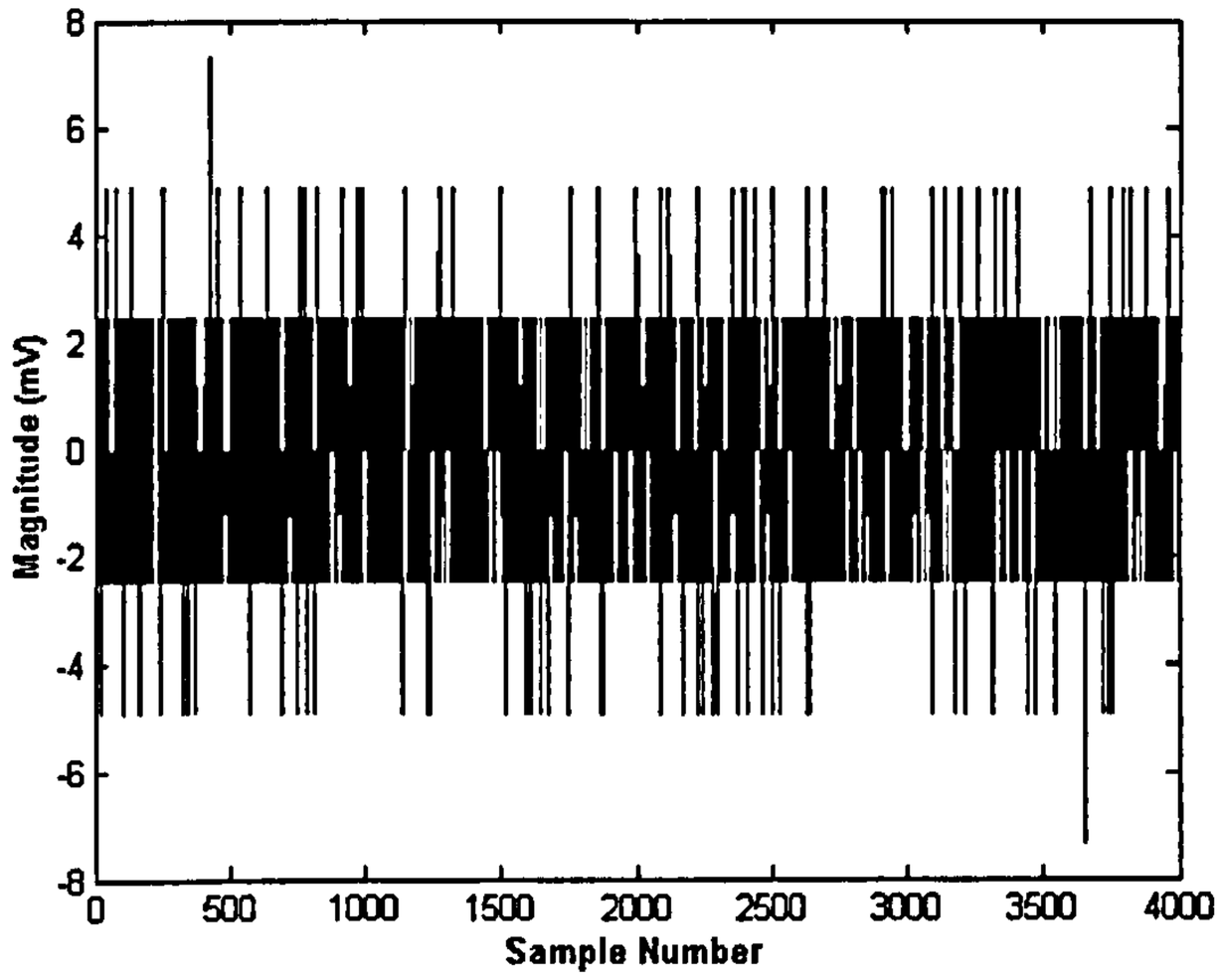

Figure 3-25 A/D card noise

The noise of the ADC card is measured by measuring the voltage across the terminals of a 1.2V battery. Then the median of the measured signal is subtracted from the signal. The resulting signal is shown in Figure 3-25. It can be seen from the signal, that the card has a maximum ±3 bit error or equivalent to ±7.32 mV. It can also be seen that the nature of the noise is random. Figure 3-26 shows the frequency spectrum of the noise that is distributed across all frequencies, which means it is a white noise.

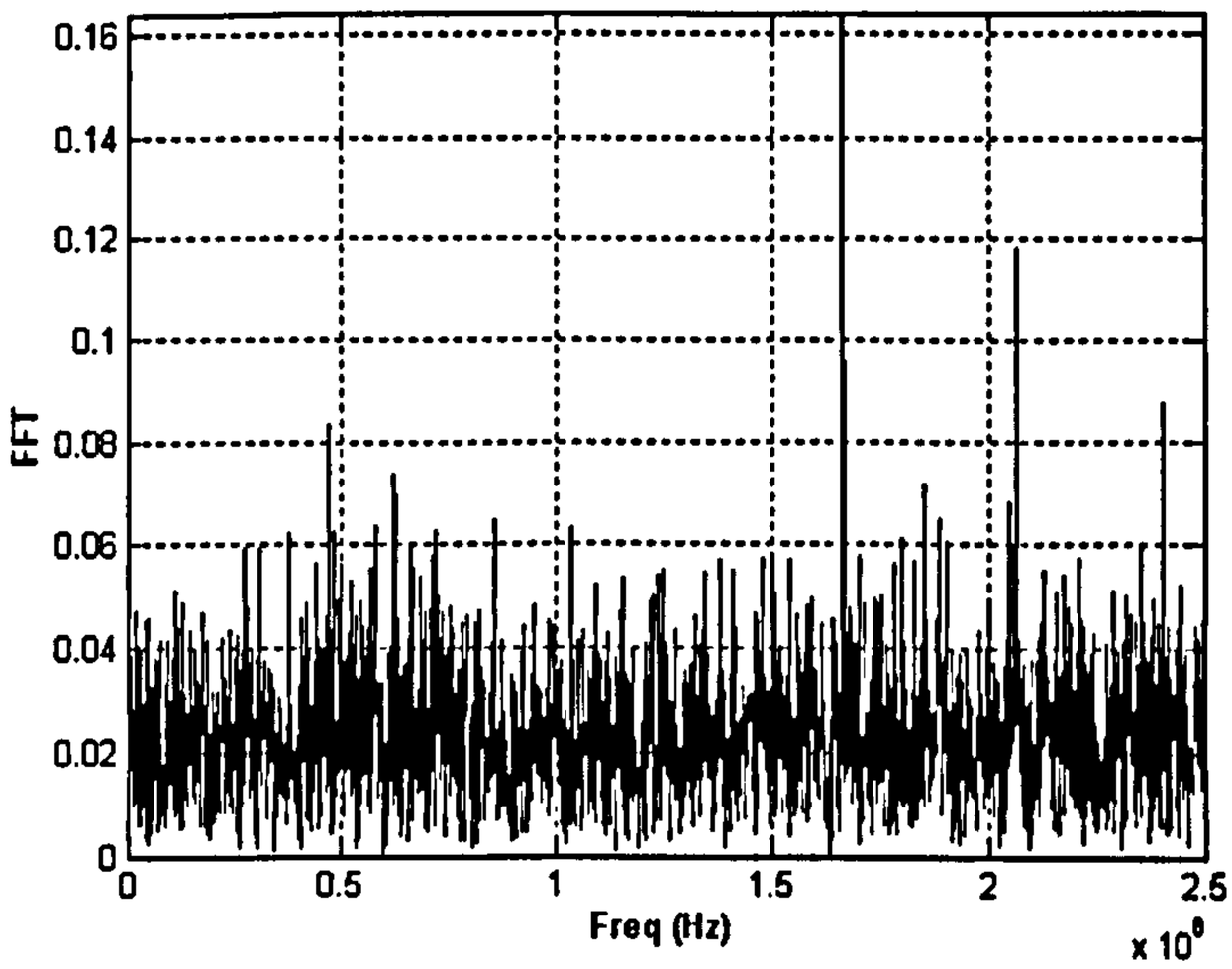

Figure 3-26 The Frequency Spectrum of the A/D Noise

Electrical noise is caused by various factors and fall into different categories. White noise that spreads across the spectrum is detected on the acquired signals. Therefore, a noise reduction mechanism must be introduced. Techniques widely used for noise reduction and signal smoothing include signal averaging, mean filters and Gaussian filters. Apart from signal averaging, all these techniques will change both the time and frequency characteristics of the signals. Significant noise reduction is possible but accompanied with loss of high frequencies that is undesired for our PEC system.

Signal averaging requires acquisition of N signals and then averages the sum of these signals. Mathematically it is defined as

$$y[i] = \frac{1}{N}\sum_{n=0}^{N-1} x_n[i] \tag{3-7}$$

The more signals to be averaged, the higher the attenuation of the noise, as shown in Figure 3-27 that is derived by experiments. It can be seen that there is a linear relationship between the number of the averaged signals N and the square of the noise attenuation figure. The drawback of this noise reduction technique is that it can be slow and very time-consuming. Furthermore, the reduction level is not as good as other techniques. In order to obtain the optimum solution, the two techniques, signal averaging and one of the filters, will be combined.

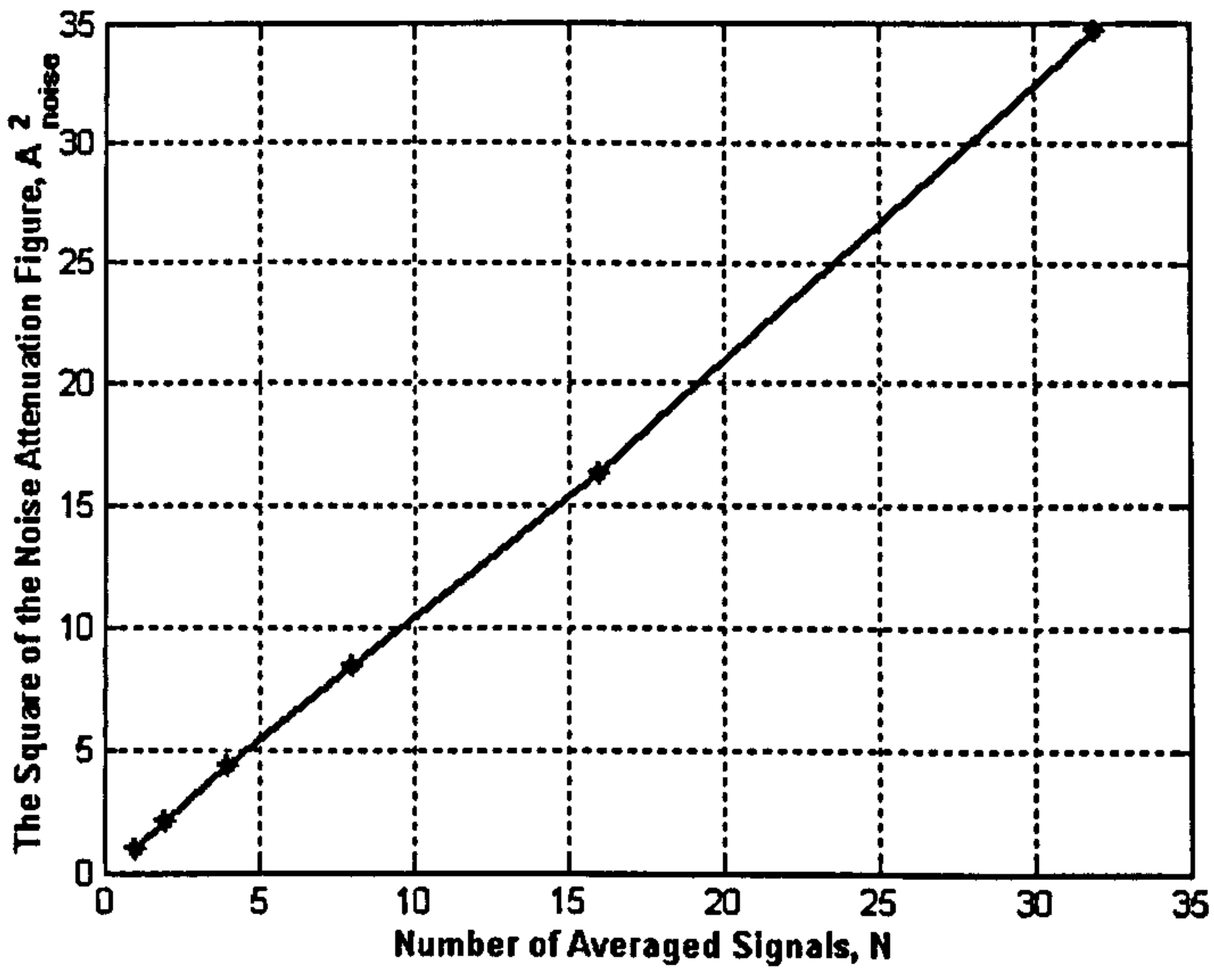

Figure 3-27 Measured Noise Attenuation with Signal Averaging

Mean filter is a linear filter that is very commonly used in DSP. It operates by averaging a number of points from the input signal to produce each point in the output signal (Smith 1999). The operation is defined as:

$$y[i] = \frac{1}{M} \sum_{j=0}^{M-1} x[i+j] \tag{3-8}$$

where M is the number of points to be averaged to produce one output point. A larger M will give smoother output with the expense that the pass bandwidth gets narrower. Figure 3-29 and Figure 3-30 demonstrates this phenomenon, when different values of M are used. Figure 3-28 shows how the noise attenuation figure changes with M.

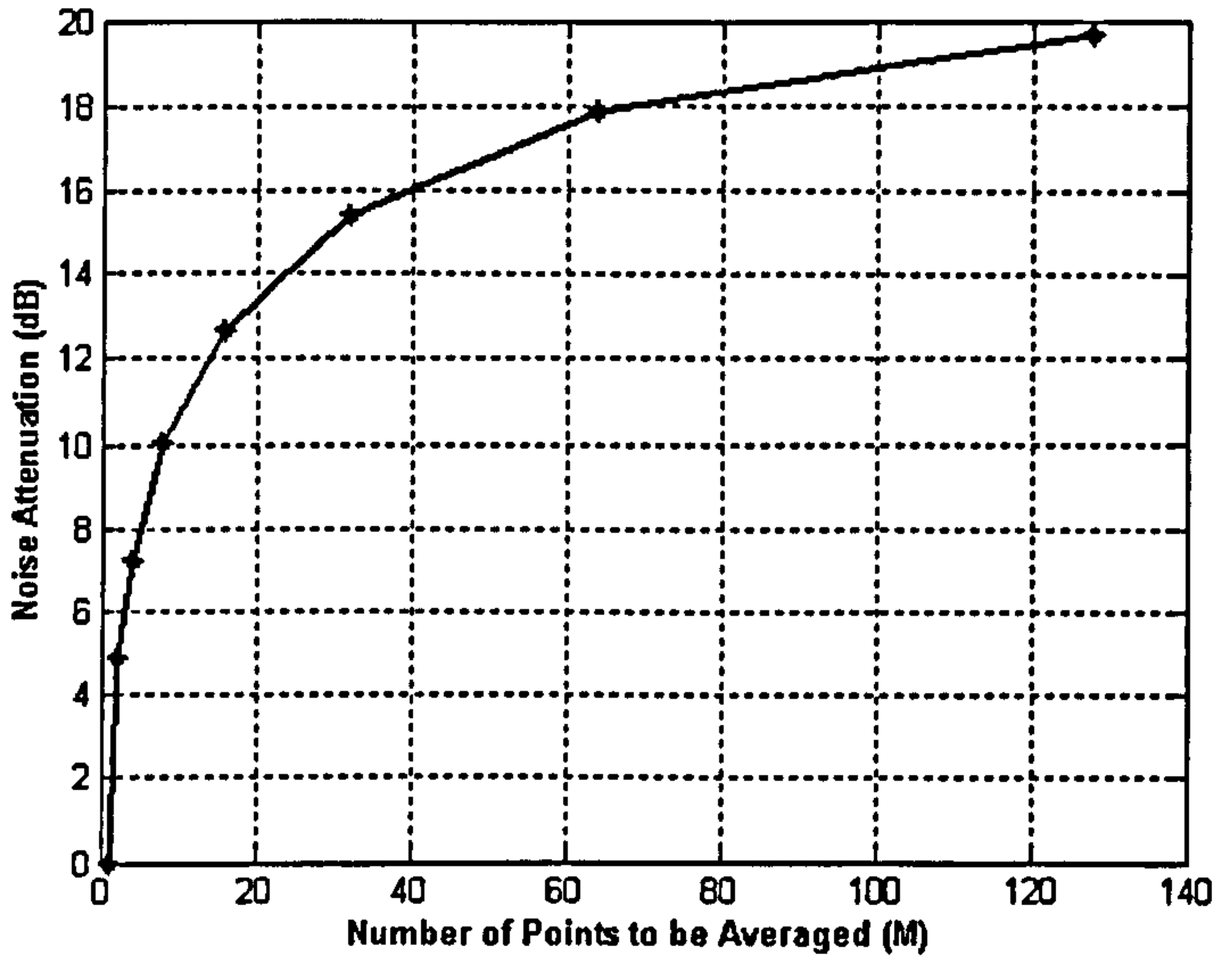

Figure 3-28 Noise Attenuation against Number of Averaged Points

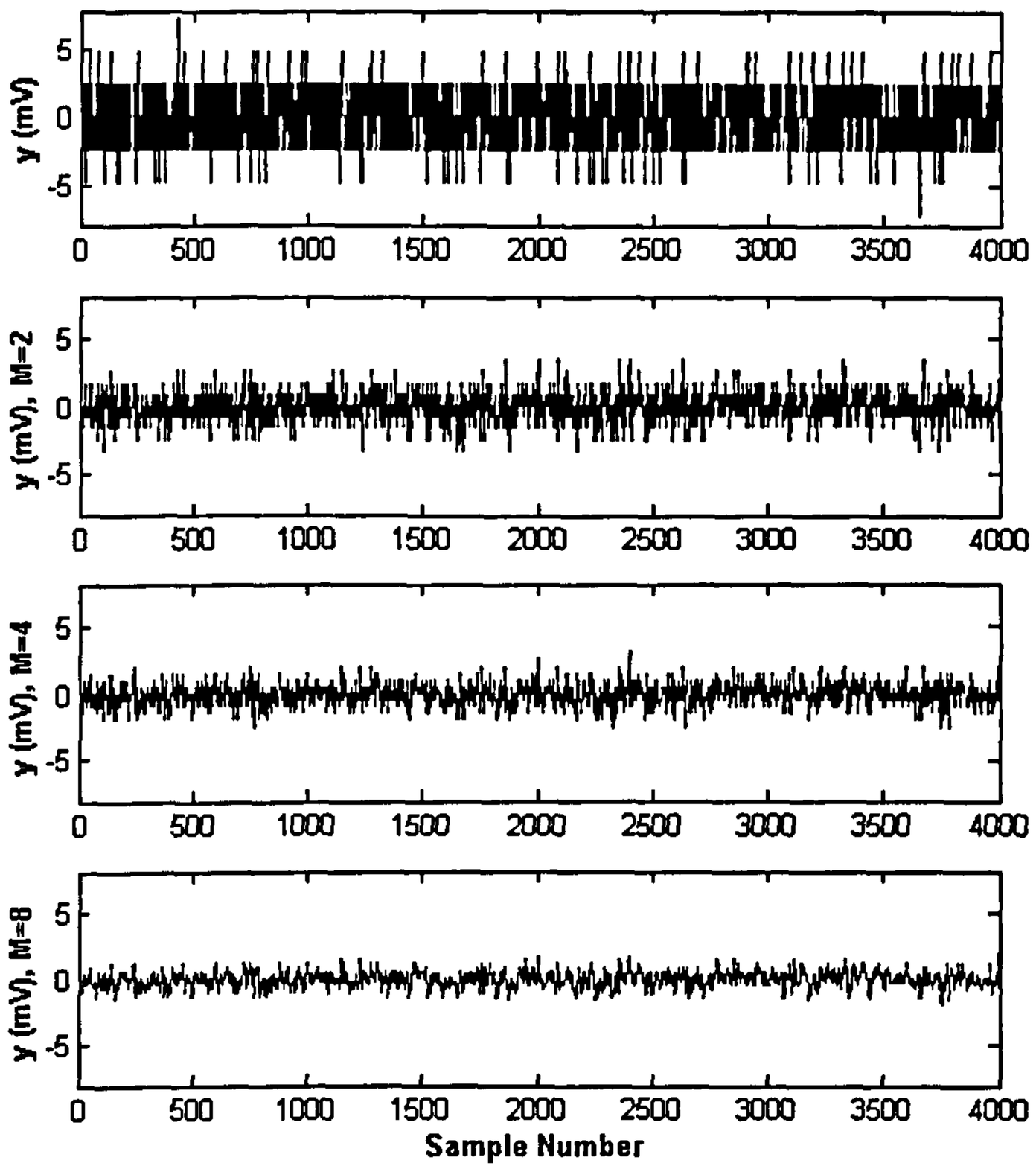

Figure 3-29 Noise Reduction using Mean filters with different *M* values

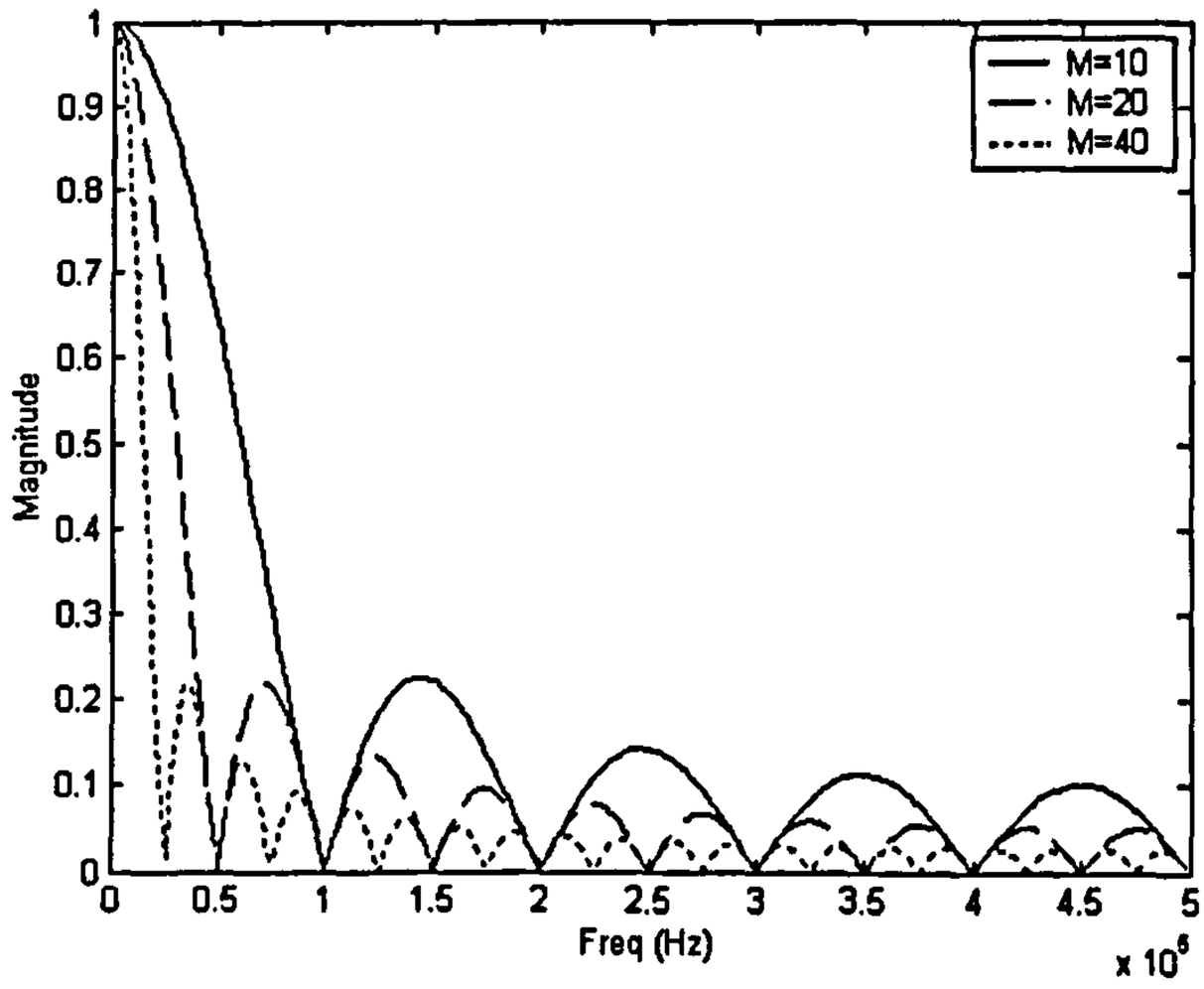

Figure 3-30 The Frequency Responses of Mean Filters with different *M* values

Gaussian filters work in a similar way as the mean filters. However, with Gaussian filters, the points are given different weightings with the middle point given the highest weighting. The weightings distribution follows Gaussian function, defined as:

$$y[i] = \frac{1}{M} \sum_{j=-M/2}^{M/2} x[i+j].\exp\left(-\frac{j^2}{2\sigma^2}\right) \tag{3-9}$$

The frequency response of Gaussian filters is affected by the value of σ chosen. The higher the σ is, the narrower the pass band will be and smoother signals are achieved. Figure 3-31 and Figure 3-32 show how σ affects the performance of Gaussian filters. Three different σ values - 2, 4, and 8 - are used for comparison, the noise attenuation are 7.71, 9.27 and 11.12 respectively.

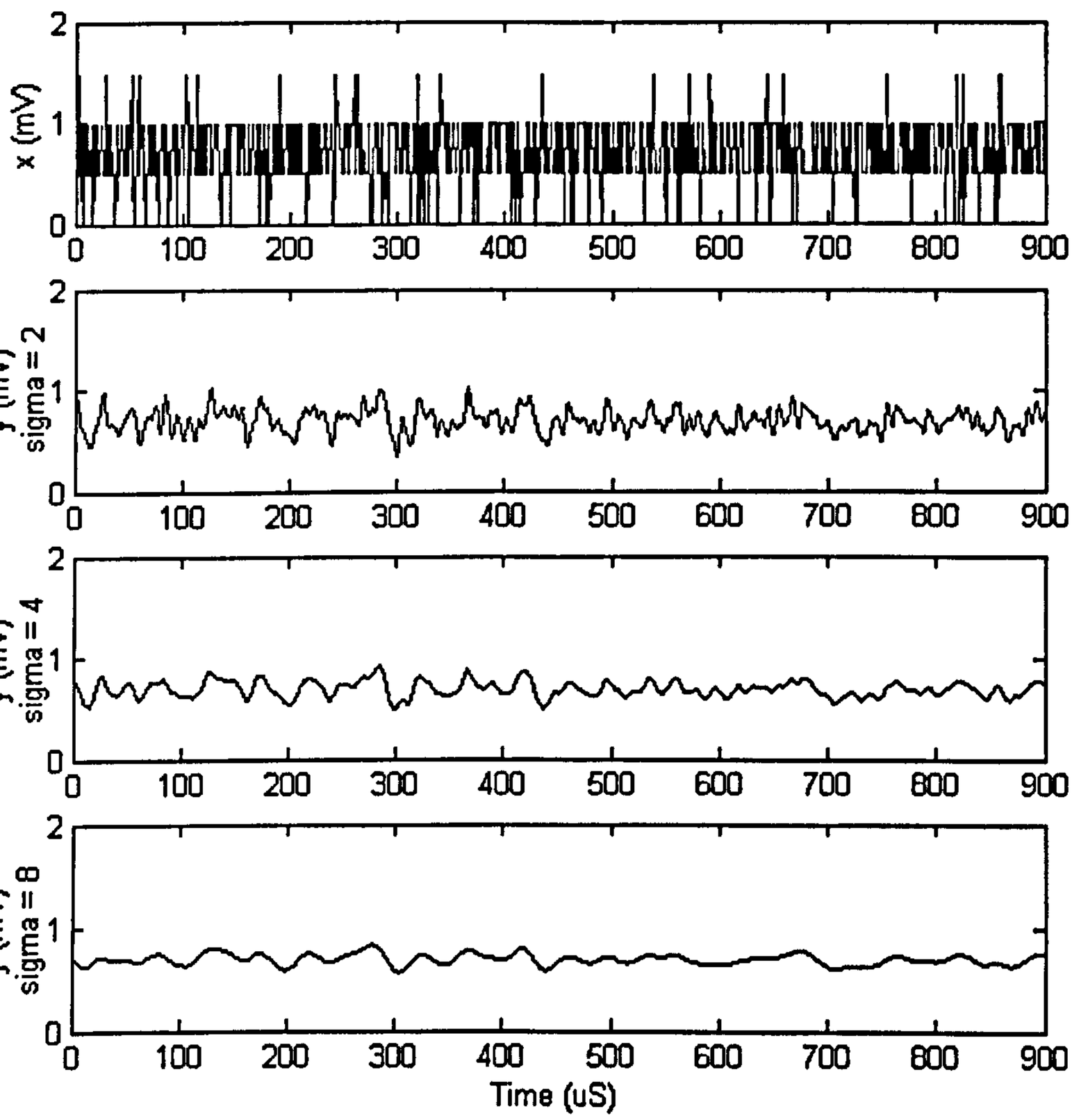

Figure 3-31 Noise Reduction using Gaussian filters with different Sigma Values

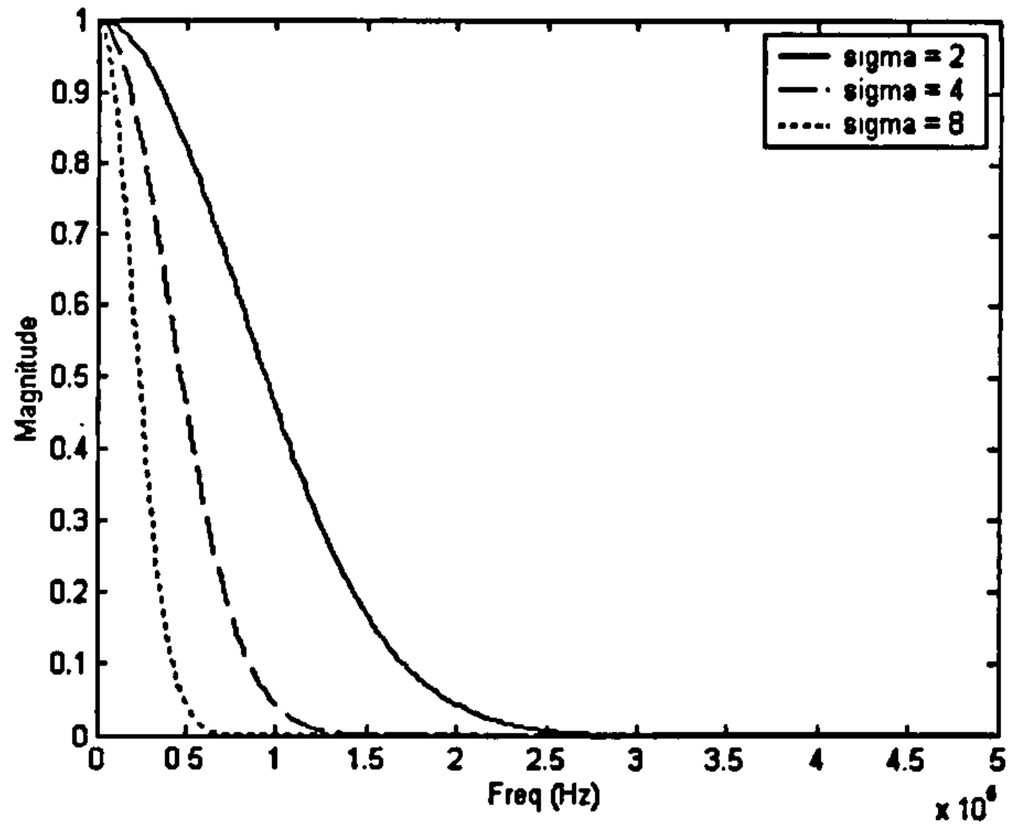

Figure 3-32 The Frequency Responses of Gaussian Filters

To serve our purpose and to balance the noise and frequency components, a low-pass-band of 20 kHz is chosen. To achieve this, experimentally it is suggested that for the mean filter, the value of M should be 12 and the value of σ should be 4 if Gaussian filter is used. A high value of σ reduces the measurement resolution besides the noise. Between these two configurations, the Gaussian filter performs slightly better than the mean filter on the noise attenuation. Therefore, a Gaussian filter with $\sigma = 4$ is chosen.

For the signal averaging, $N = 5$ is chosen to balance the noise attenuation and processing speed. As a result, the total noise attenuation using the signal averaging and Gaussian filter in combination is 12.58 dB. Figure 3-33 demonstrates how the noise reduction technique effectively reduces the noise.

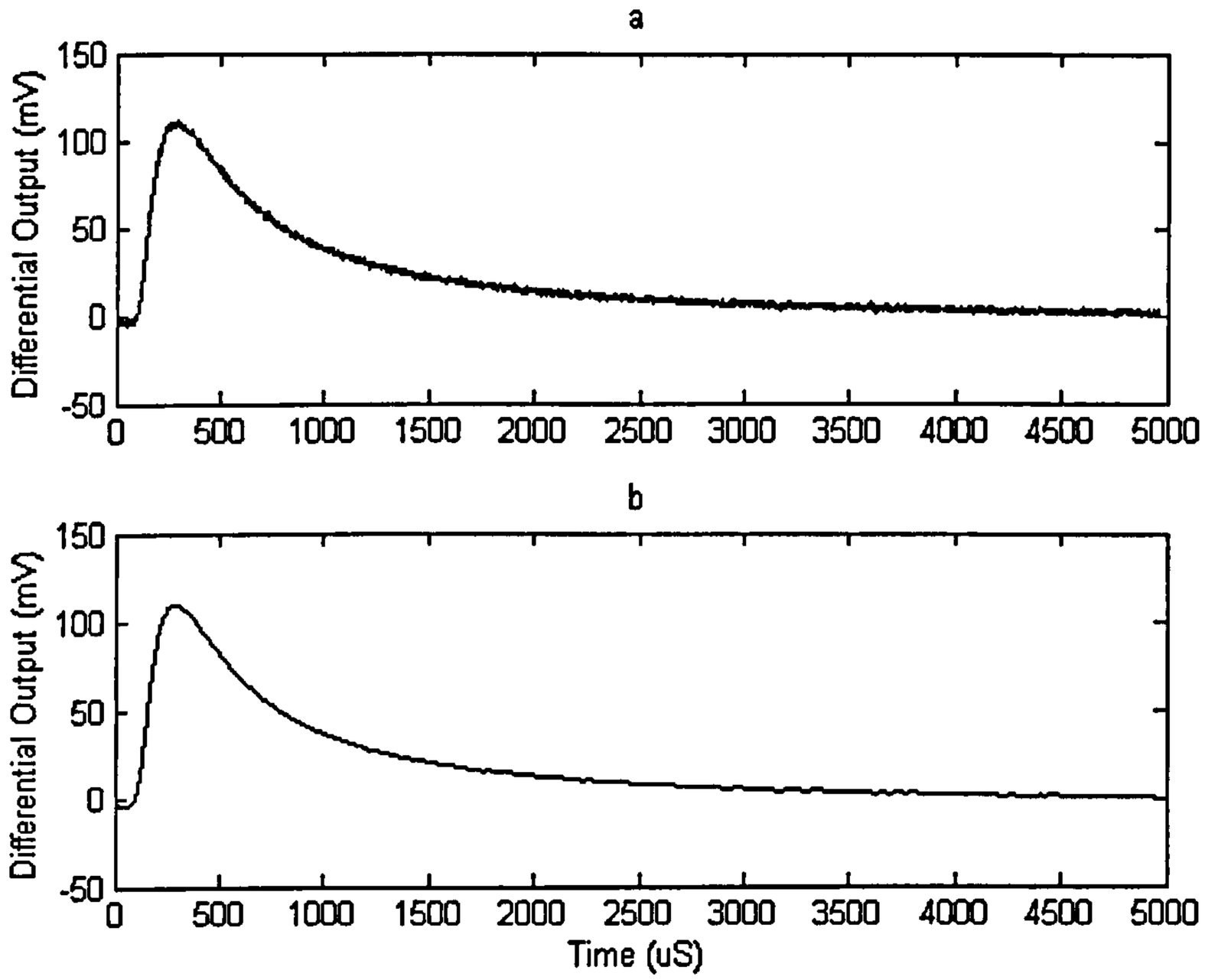

Figure 3-33 Differential Signals: (a) Raw Signal (b) Gaussian-filtered Signal

3.6.2.2 Synchronisation

In order to attain the correct differential signals, the test signal must be synchronised with the reference signal. Figure 3-34 shows the effects when signals are not properly synchronised. A sharp spike takes place at the beginning of the rising edge of the differential signal.

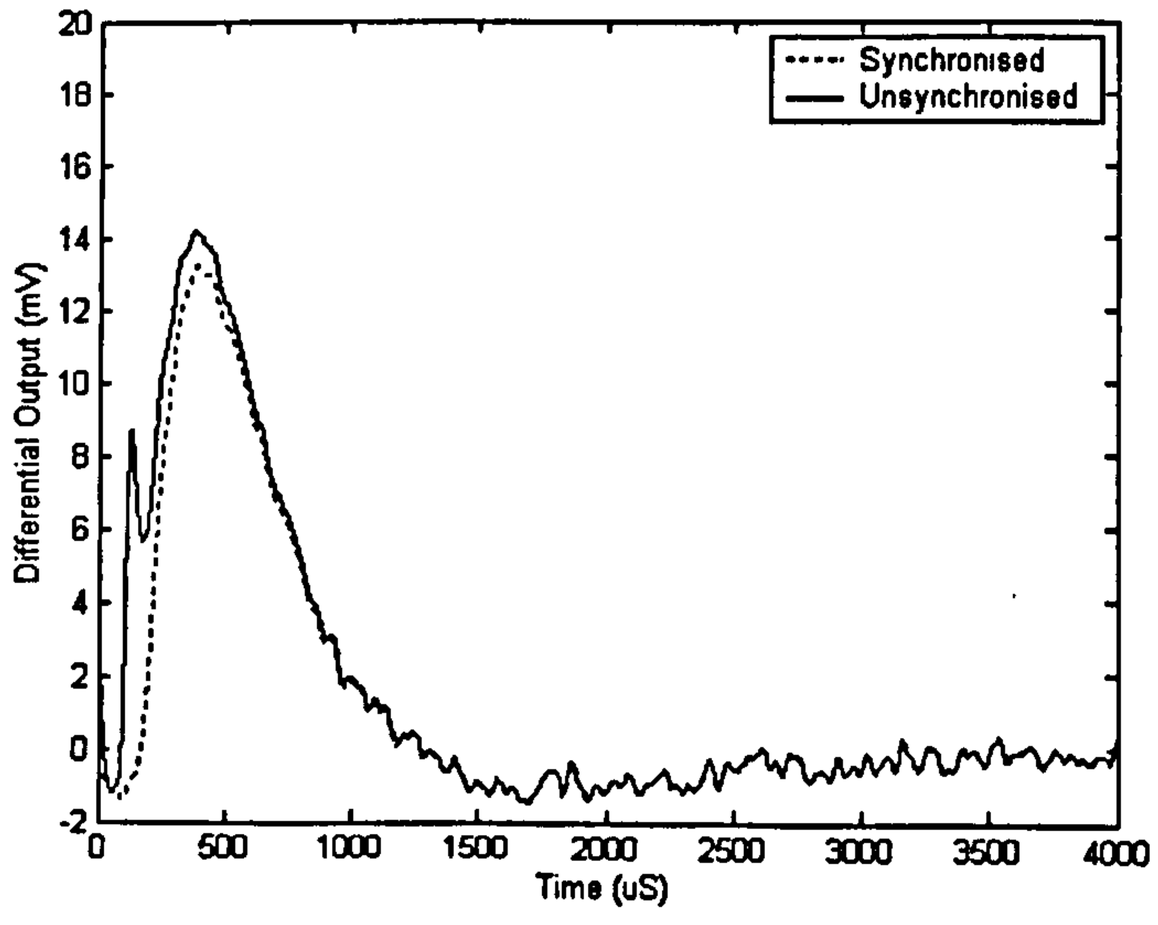

Figure 3-34 Synchronised and unsynchronised differential signals

It was found that the time shift variation occurred due to limitation of the AD card used. Figure 3-35 illustrates the phenomenon, the green signal is triggered at the right set timing, i.e. n=1500, but the blue signal is acquired late by 2 samples. Figure 3-36 shows how the triggering time delay varies when 1000 measurements are taken. The effect is especially apparent and most destructive when the differential signals are small. Small differential signals are very common, especially, in ferromagnetic material inspection.

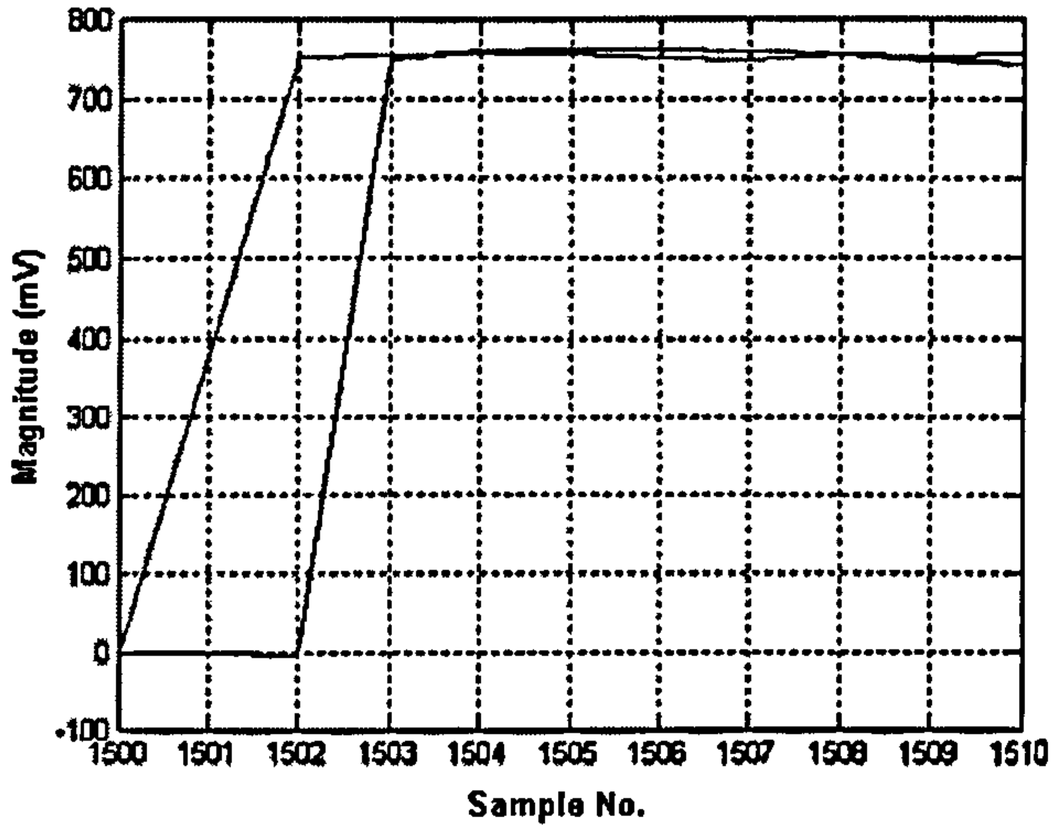

Figure 3-35 Examples of Variation in Rising Points

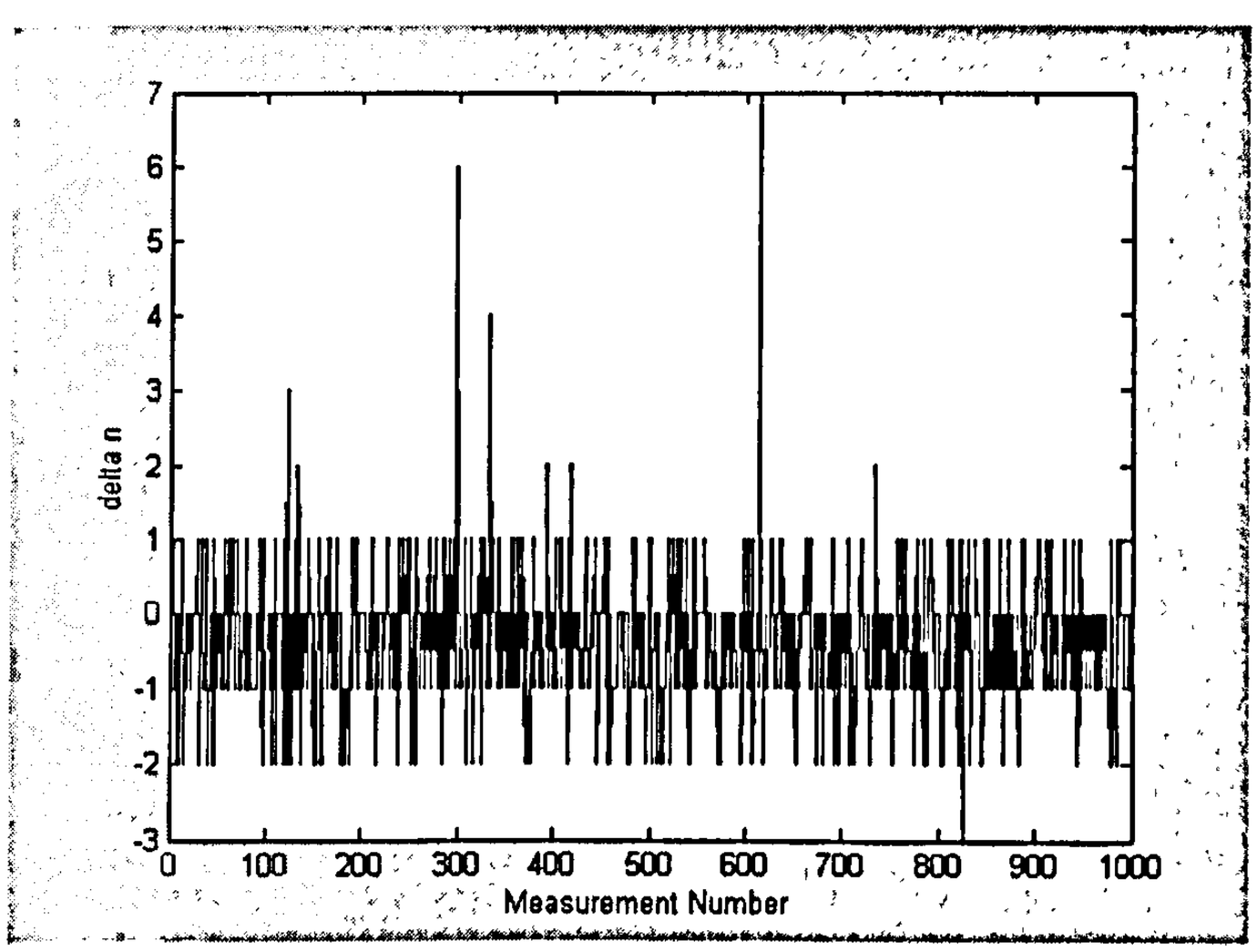

Figure 3-36 Variation in Triggering Time

To overcome this problem, two measures were taken. Firstly, the sampling rate is increased up to 5 MHz when necessary. In this way, the time slice between samples gets

smaller, and this readily reduces the time delay variations. Secondly, a synchronisation mechanism is introduced in the software. The synchronisation detects the start of rising, calculates the delay (or advance) and shifts it in time if necessary so that all signals share the same start time of the rising edge. The shift time is taken into account when the differential signal is calculated, i.e.

$$f_{diff}(n) = f_{ref}(n) - f_{test}(n + \Delta n) \tag{3-10}$$

3.7 Summary

A new PEC system has been designed and implemented and serves as the basis for further research and development work. The systems includes both hardware and software aspects. The hardware has basically been implemented fully and ready to use, although some iterations still need to be carried out to improve the performance of the system, such as stability and repeatability. Having investigated different magnetic sensing devices, Hall device sensors have been chosen to be used in our probe design.

Finite element modelling has been used to aid familiarise with the characteristics of coil parameters and structures. The information can be used in the design work of eddy current probes for different applications.

The main sources of electrical noise that potentially reduces the performance of the system have been identified, and a solution by both hardware and software has been provided. The significant error of the data acquisition card now dominates the remaining noise. The problem with synchronisation due to the triggering problem of the card has been identified and the solution has been presented and implemented.

For digital signal processing, feature extraction and user interface, a windows-based software has been written. The data acquisition and some signal conditioning is done using Visual C++ programming, and the rest of the software is written using Matlab. Matlab codes are suitable for experiments as Matlab library has a very good collection of functions for signal processing and other purposes.

Chapter 4. Feature Extraction for Flaw Classification and Quantification

4.1 Background

As discussed in Chapter 2, the conventional PEC technique generally uses the differential signal's peak value and peak arrival time to infer information regarding the size, location, and type of flaws. It is difficult to classify and quantify a wide variety of defects by using the two parameters. Moreover, the peak-based features are relatively prone to noise and sample frequencies. This may lead to loss of accuracy or, even worse, misdetection of flaws. As an alternative, a new feature extraction technique is proposed and its performance will be evaluated against that of the conventional technique. The proposed technique will utilise both temporal and spectral information of the PEC signals by applying Principal Component Analysis (PCA) and Wavelet Transforms. This will allow more features to be generated, which potentially lead to more information being gained for defect classification and quantification. Specifically, PCA is used for improving discriminability of different defect signals from PEC systems. It is aimed to develop a model for feature extraction and combination for better defect classification and quantification.

A feature can be defined as a minimal unit that distinguishes samples. Feature extraction is a transformation process of original measured data to a data set with a reduced number of variables that contain the most discriminatory information. Through this process, the data

dimension is reduced, removing redundant or irrelevant information, and the data is transformed to a form more appropriate for subsequent classification processes (Webb 2002). Improved classification performance through the transformed data representation should be gained. Advanced techniques generally lead to pattern or vectorial representations for better discriminability (Staszewski 2002).

4.2 Feature Extraction

Feature extraction techniques are commonly applied in the pattern recognition field. Part of the idea to be presented is taken from this field. Pattern recognition is a technique that studies a given pattern and determines the class membership of the pattern. A pattern is generally comprised of a vector of measurement results, $x=(x_1, \ldots, x_n)^T$. A given vector will be associated with one of C classes, therefore it can be said that the main theme is *classification*.

A classifier is built by training. Based on the training approach used, classifications fall into two categories, namely supervised and unsupervised. In supervised classification, the possible classes have been known and defined by the investigator, while in the unsupervised the classifier will create the possible classes from the given training data sets. The former is generally called *discrimination* and the latter is referred as simply *classification* or *clustering* (Webb 2002).

Part of the classification is a stage where features that are considered to be significant are selected from the data vector $\boldsymbol{x}$. The dimension of the selected features is generally significantly smaller than the dimension of the original data vector. This step is commonly referred to as feature extraction and is vital for a successful classification. By putting less relevant features aside, further processing can be performed more effectively and faster without losing information important for classification of a pattern.

Ideally, the resulting features extracted should possess the following properties:

- Vary widely from class to class.

- Stable over a long period of time.
- Easily computed from the input samples.
- Small in dimension.
- Insensitive to the irrelevant variation or noise.
- Uncorrelated with other features.

4.3 PCA

PCA is a statistical tool, which is useful to identify new uncorrelated variables from a set of multi-dimensional data that might have high correlation. The new variables that are obtained by linear transforms that project the data into orthonormal sub-spaces explain the maximum amount of variance possible. The new variables are generally significantly smaller in number than the original variables. Therefore, PCA will enable us to reduce the number of the data dimensions and the extracted features should contain the most relevant discriminating information. This can be used to classify or recognise a testing condition that is represented by the input signal. In our case, the multi-dimensional data can be the time-domain measurement data obtained by the system or their transformed values.

To give a clearer picture, an example is given here. A set of data has a distribution as shown in Figure 4-1(a). Each data sample is represented with two variables or axes, x and y. If we have to choose only one variable to represent the data, then y will be chosen as it explains the bigger variation. The error of the new presentation will also be smaller than if x was chosen. However, if we have an option to create a new variable or axis to represent the data, we could choose this new variable, say v, which is represented by the thick black line in Figure 4-1 (b). The variable v through this line axis will obviously be better than y in representing the data, as larger variation is covered and smaller errors are achieved. If, now, a second variable is desired, then this variable, say w, should be defined by the dotted line in Figure 4-1 (c). This new variable is characterised by being perpendicular to the first variable. Functions are required to transform x and y into v and w. The functions are called the transformation

functions. This simple example shows how a situation where PCA can be helpful. PCA will define the new variables, which are referred to as Principal Components, and will generate the transformation functions, which are referred to as eigensignals. In this way, multidimensional data with so many variables can be reduced to a few representing variables while the variation is explained maximally and the error is kept minimised.

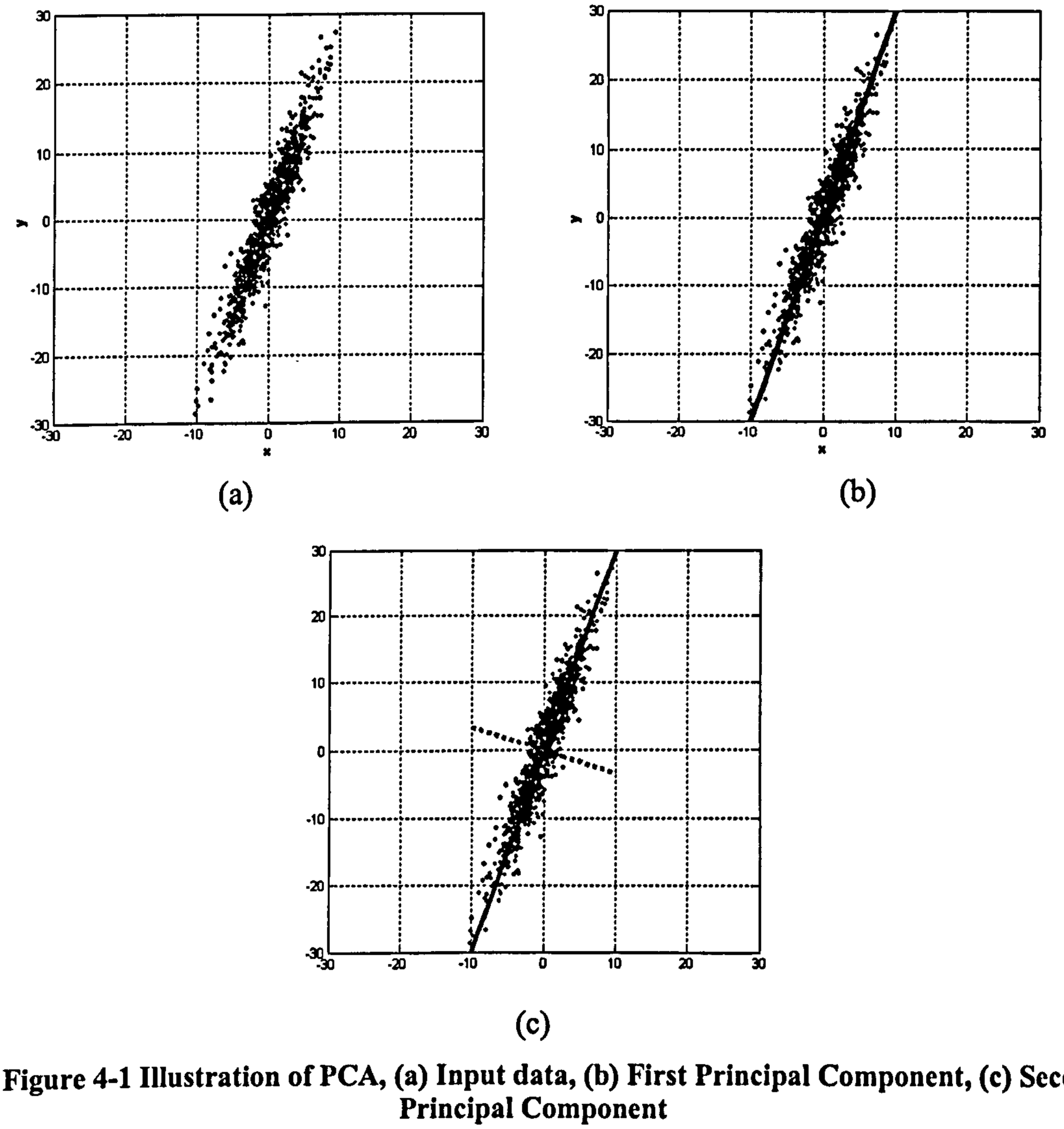

Figure 4-1 Illustration of PCA, (a) Input data, (b) First Principal Component, (c) Second Principal Component

The PCA approach requires training where many data sets from various testing conditions are required as inputs. The first stage is to obtain eigensignals, which in essence are sets of weightings for transformation. Here, each data set from an observation is formed into a

column vector, Γ_n, whose length N depends on the number of variables used. For M observations, we will have an array matrix Γ with the size of $M \times N$. Therefore, we have

$$\Gamma = [\Gamma_1, \Gamma_2, \Gamma_3, \ldots, \Gamma_M] \tag{4-1}$$

The average signal Ψ is defined by:

$$\Psi = \frac{1}{M} \cdot \sum_{n=1}^{M} \Gamma_n \tag{4-2}$$

Difference signals are computed by subtracting the average signal from each training signal:

$$\Phi_i = \Gamma_i - \Psi \tag{4-3}$$

These vectors are now subjected to principal components analysis. To find the orthogonal eigenvectors the covariance matrix C should be worked out:

$$C = \frac{1}{M} \sum_{n=1}^{M} \Phi_n \cdot \Phi_n^T = \frac{1}{M} A \cdot A^T \tag{4-4}$$

where $A = [\Phi_1, \Phi_2, \ldots, \Phi_M]$ and Φ^T is the transpose of the matrix Φ.

However, the determination of the eigenvectors for the covariance matrix C will require excessive computation as the matrix C will have the size of $N \times N$. A better way is considered. If v_i are the eigenvectors of $A^T * A$ and μ are the eigenvalues:

$$A^T A v_i = \mu_i v_i \tag{4-5}$$

then the eigenvectors of C can be computed by:

$$u_i = A v_i \tag{4-6}$$

where $C = A^* A^T$.

The u_l are referred to as eigensignals. Having obtained the eigensignals, the most significant M eigensignals are chosen according to the largest corresponding eigenvalues. The magnitudes of the eigenvalues represent the variations explained by the corresponding principal components. Any signal can be identified as a linear combination of the eigensignals. The principal components for any signal Γ are defined by:

$$w_k = u_k^T(\Gamma - \Psi) \tag{4-7}$$

The value w_k represents the data mapped into the axis represented by the eigenvector. These values are the new features that can be used for classification and recognition purposes, and in our case they might correlate with quantities to be measured. Two eigenvectors which correspond to the two largest eigenvalues are chosen for investigation.

Figure 4-2 illustrates examples of eigensignals obtained when applying PCA on PEC signals of defects of different types and sizes, where the defects were obtained from the manufactured Aluminium samples detailed in Chapter 5. Some of the differential signals are shown in Figure 4-3 for illustration. The two eigensignals are clearly unrelated. The first eigensignal highlights the importance of the peak points of signals from surface slots for discrimination. This means that, for surface slots the first principal component will be highly correlated to the peak time. The PCA based feature extraction uses eigensignals as different weightings for signal signatures. The area around peak values from the PEC differential signals has a much higher weighting. The second eigensignal reflects the peaks of defects of other types. These peaks reflect the propagation time of the field in the sample. As discussed, the first two eigensignals have correlation with the peak time and peak values, which are related to eddy current intensity and electromagnetic field propagation. The new features are calculated by using signal signature not specific feature points, which is robust to data acquisition condition and noise. More importantly, more feature may be generated by using different eigensignals, e.g. using Wavelet analysis for different time-frequency data.

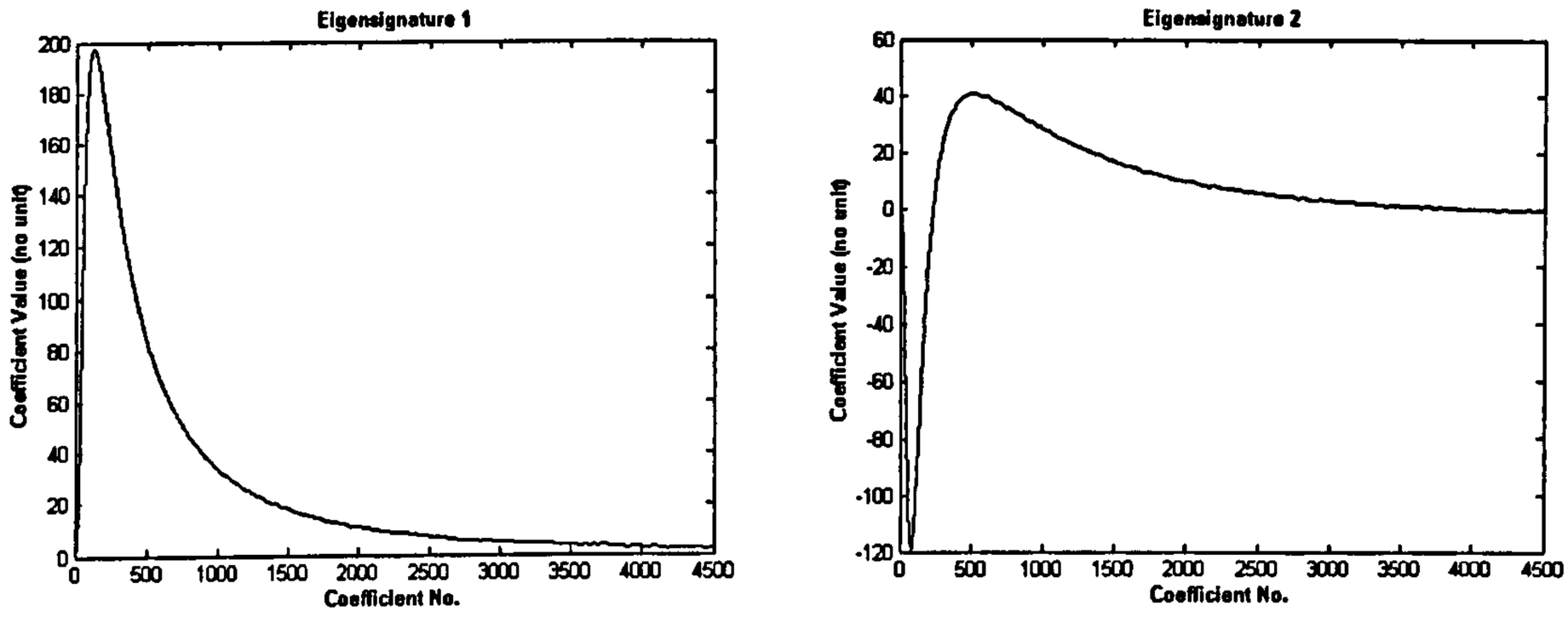

Figure 4-2 Examples of Eigensignals

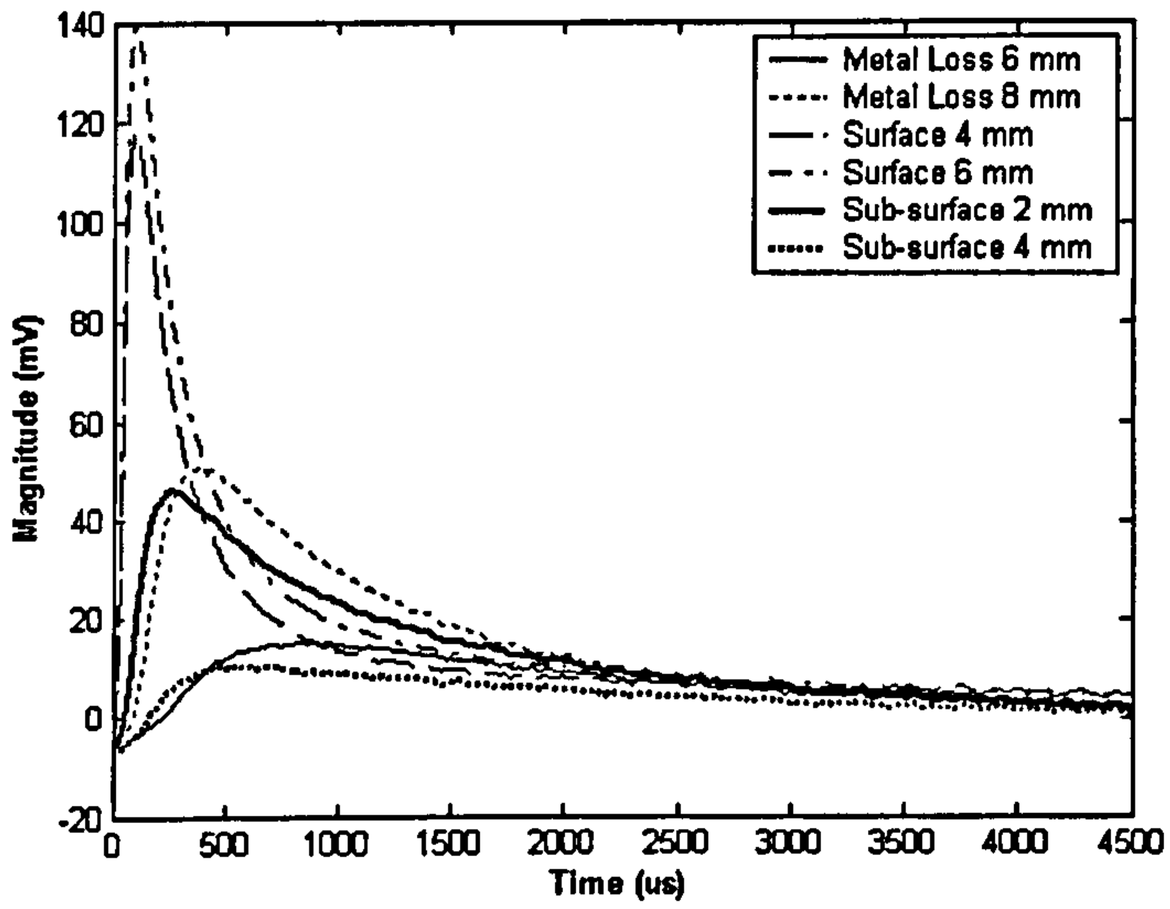

Figure 4-3 Examples of the signals in the training data set

4.4 Wavelet Transforms

The Wavelet Transform is a relatively new technique in signal processing and has gained a widespread use in numerous applications including condition monitoring (Li, Tso et al. 2000; Yen and Lin 2000), speech recognition (Sarikaya and Hansen 2000; Farooq and Datta 2001), classification of washing machine vibration signals (Goumas, Zervakis et al. 2002), finger print recognition (Tico, Kuosmanen et al. 2001), engine diagnosis (Guo, Crossman et al.

2000), medical applications (Dokur, Olmez et al. 1999; Pittner and Kamarthi 1999), and astronomy (Graps 1995), among others.

The fundamental idea behind the Wavelet Transform is to analyse signals according to scale, therefore, both gross and fine features of a data signal can be probed into (Graps 1995). The analysis exploits both time and scale (or frequency) aspects simultaneously, while the similar and widely used Fourier analysis provides only frequency aspect and loses the time information. The lack of temporal capability of Fourier Transform can be overcome by windowed Fourier Transform. However, windowed Fourier Transform does not have the flexibility that the Wavelet Transform has, i.e. the Wavelet Transform uses compressed form to extract the higher frequency components and uses an expanded form for lower frequency components. This results in more localised frequency observation.

The Wavelet Transform performs the decomposition of a signal onto the family of wavelet functions generated from a prototype function called mother wavelet - $\psi(t)$ by dilation and translation operations (Mallat 1989). The Wavelet Transform of a signal $f(t)$ can be computed by using the following equation:

$$c_{m,n} = \int_{-\infty}^{\infty} f(t)\Psi_{m,n}(t)dt \tag{4-8}$$

The transform generates wavelet coefficient $\boldsymbol{C}$ that subsequently will be passed to the next stage in the feature extraction.

The mother wavelet is constructed from the scaling function $\phi(t)$ in the following way:

$$\phi(t)=\sqrt{2}\sum_{k=-\infty}^{\infty} h(k)\phi(2t-k), \tag{4-9}$$

$$\Psi(t) = \sqrt{2}\sum_{k=-\infty}^{\infty} g(k)\phi(2t-k), \tag{4-10}$$

where $g(k) = (-1)^k h(1-k)$. Different sets of coefficients $h(k)$ will produce mother Wavelets with different properties.

In contrast to FFT where the basic function is only sinusoids, in Wavelet analysis various basic functions or mother Wavelets exist. These mother Wavelets perform differently in different applications. For the feature extraction, the Morlet wavelet is chosen. Based on our initial experiments, results are affected by the choice of mother wavelet. However, the Morlet gives among the best results. The shape of the Morlet wavelet can be seen in Figure 4-4. Matlab's Morlet wavelet equation is given by

$$\Psi(t) = e^{-t^2/2} \cos(5t), \tag{4-11}$$

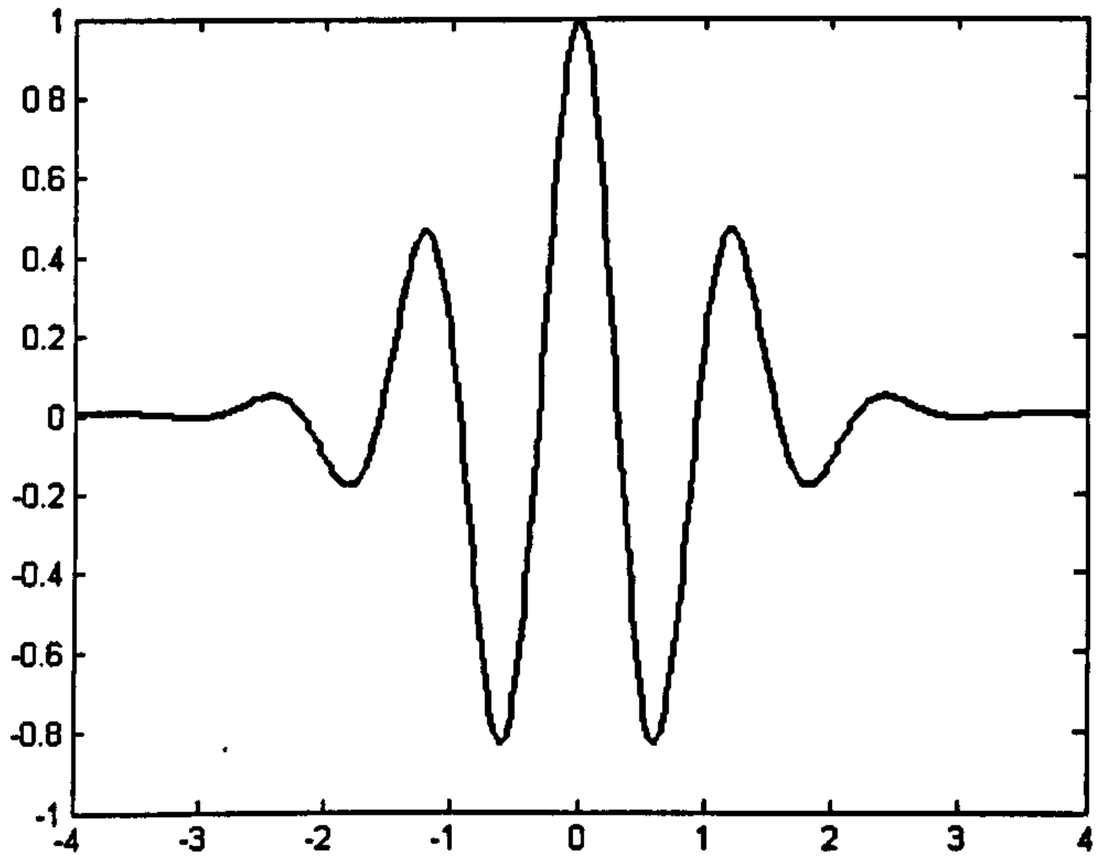

Figure 4-4 The Morlet Wavelet

With the aid of the Wavelet Transform, the scales or frequencies at which the analysis is carried out can be chosen. This will also reduce the interference of some electrical noise.

4.5 The New PEC Feature Extraction Technique

In the new proposed approach, in order to be able to provide both the defect type and size, hierarchical PCAs are used in analysing the PEC signals as illustrated in the block diagram shown in Figure 4-5. As shown in the diagram, in general the whole process is divided into two stages, firstly, to define the class of flaw and secondly, to define the size of the flaw. Each stage will comprise of similar steps, which include Wavelet Transforms and PCA.

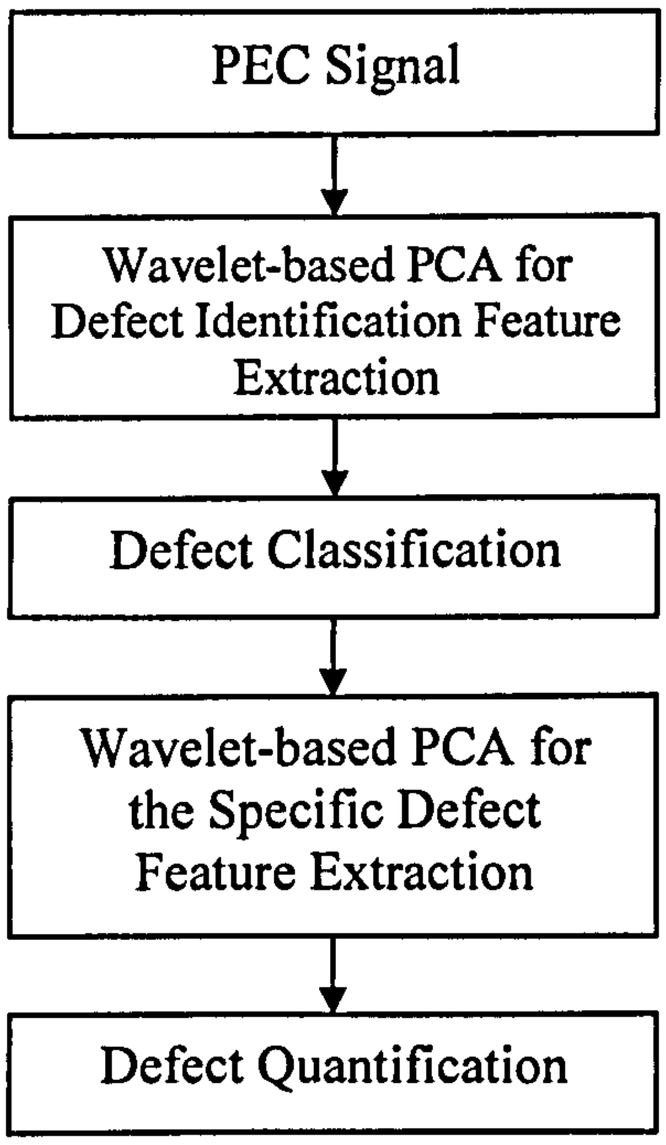

Figure 4-5 The Flow Diagram of the New Approach

The steps in each stage is shown in the block diagram in Figure 4-6. The processes in boxes with broken lines are performed off-line, while those in boxes with solid lines are performed on-line. Off-line processes refer to the processes undertaken before the actual inspection is carried out. On-line processes refer to the processes during the actual inspection of a given sample.

The off-line processes include calculating the principal components and determining the number of components (eigensignals) to be used for feature extraction by calibrated samples. The off-line processes include setting up a training data set by recording signals representing

relevant flaws and a flawless part. Then, following the steps described in section 4.3, the eigensignals are generated and ready to be used in the online processes.

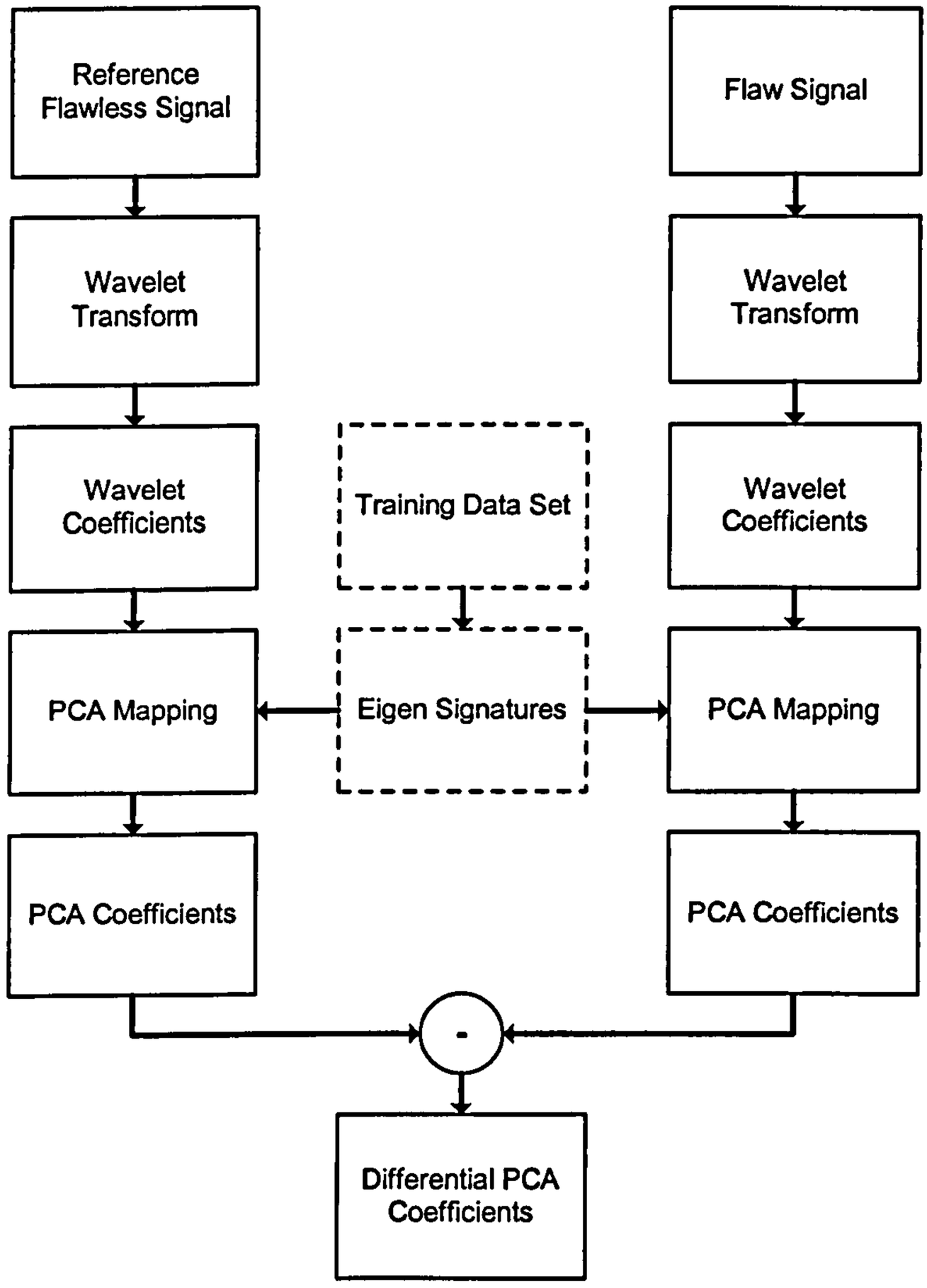

Figure 4-6 The Flow Diagram of the Wavelet-based PCA for Defect Classification/Quantification

The on-line stage starts with recording a reference signal from a flawless part of the sample. The Wavelet Transform is then applied on the signal generating Wavelet coefficients at appropriate levels which are discussed in the next two chapters. Subsequently, PCA mapping is carried out by basically summing the weighted wavelet coefficients, while the weightings are given by the pre-recorded eigensignals. This results in PCA coefficients representing the

reference signal. Then, the same steps apply to the flaw signal resulting in PCA coefficients representing the flaw signal. Finally, differential PCA coefficients are worked out by finding the difference between the two sets of PCA coefficients representing the reference and flaw signals.

In the following sections, the differences between the Wavelet-based PCA for flaw classification and that for flaw quantification are described.

4.5.1 Wavelet-based PCA for Flaw Classification

In this stage, it is attempted to assign a flaw to a class. The training data set is comprising signals representing flaws of different types, which may include, for example, surface defects, sub surface defects, and metal losses from calibration samples described in Chapter 5. Figure 4-7 illustrates the first two eigensignals for flaw classification. The mother wavelet chosen is the Morlet wavelet. The two eigensignals are clearly unrelated. The first eigensignal's local maxima and minima points highlight the points in time where the major differences are taking place among the training signals' wavelet coefficients. From the point of Wavelet analysis, it is noticed that good discrimination is achieved when high levels are used. This is as expected as these levels correspond to low frequencies that are required to achieve deep penetration.

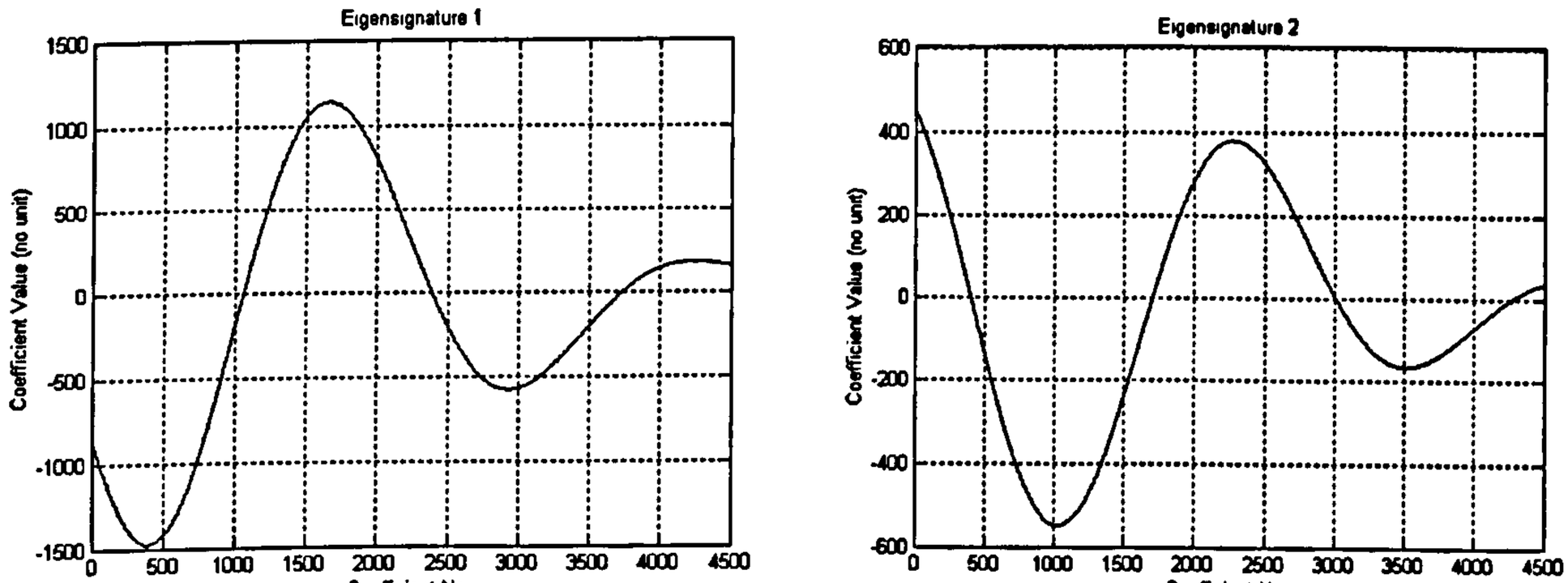

(a) (b)

Figure 4-7 Examples of Eigensignal for Flaw Classification

4.5.2 Wavelet-based PCA for Flaw Quantification

In contrast to the Wavelet-based PCA for flaw classification, the training data set is comprised of signals representing flaws of the same type and of various sizes. Figure 4-8 illustrates eigensignals for flaw quantification. This stage is carried out once the type of the flaw is already identified from the defect classification. For example, this should produce estimation of the depth of the flaw for sub-surface defects or the sizes of surface defects. The levels of Wavelet Transform are variable depending on the flaw type and its expected range of sizes.

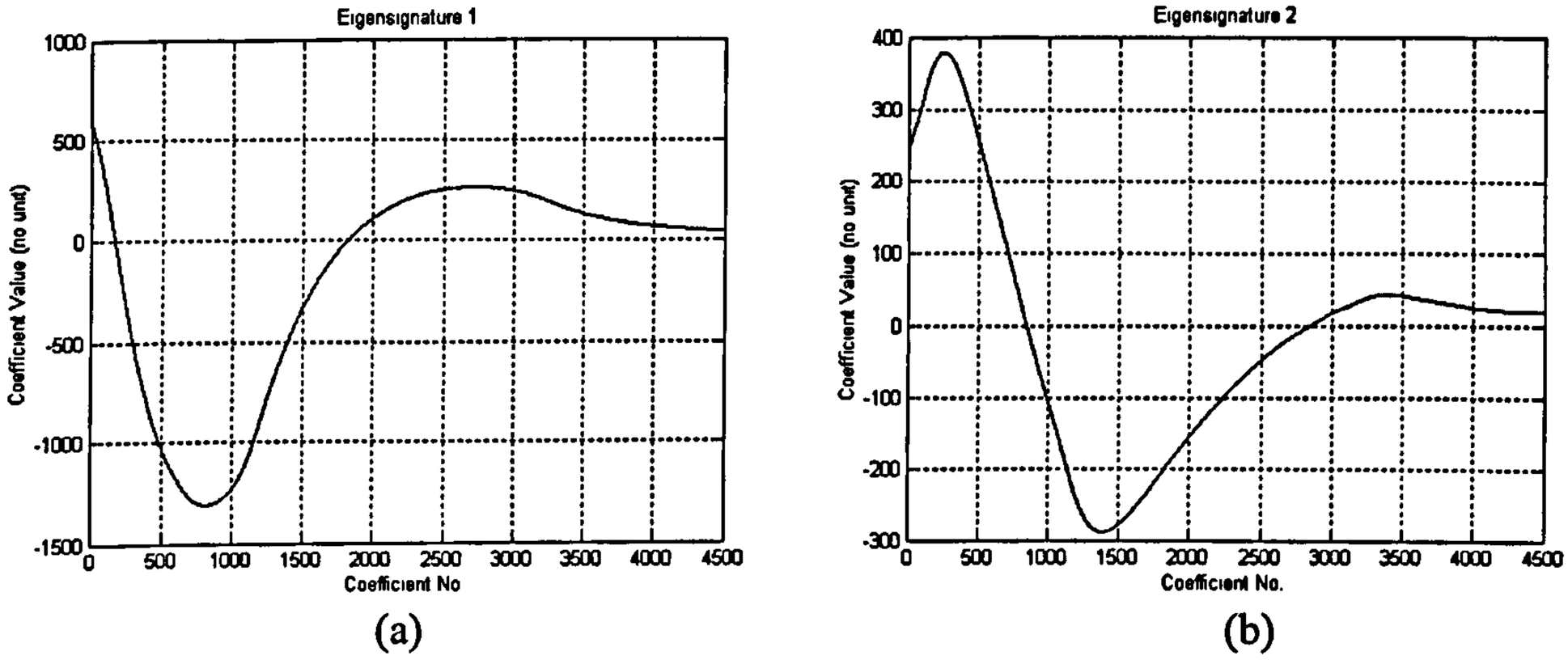

(a) (b)

Figure 4-8 Examples of Eigensignal for Flaw Quantification

When comparing the eigensignals in Figures 4-7 and 4-8, the characteristics of weighting for time-domain can be seen to be clearly different. The features obtained using this technique for maximising the discriminability or sensitivity for quantification may be combined with the conventional time-domain features of peak time and peak values from differential signals. Experimental work will be undertaken in the following chapters.

4.6 Summary

A new feature extraction using Wavelet-based PCA for pulsed Eddy current NDT and a model for defect classification and quantification have been proposed and presented. A hierarchical structure of Wavelet-based PCAs for flaw classification and quantification has been discussed. The orthogonal eigensignals for different purposes have been illustrated and discussed. The

PCA has been designed to improve the discriminability of defects and additionally, it has been noted that their eigensignals have also reflected some physical characters such as propagation time and attenuation in the time-domain.

Based on the characteristics of the new technique, a number of advantages can be expected. Firstly, the analysis is done on both time and frequency domain simultaneously by the use of Wavelet Transforms. Secondly, more features can be generated. This may lead to more information, such as better classification and sizing of defects. Thirdly, the use of PCA optimises the range explained by the resulting feature values; therefore, measurement resolution is optimised. Fourthly, the resulting features are potentially more robust to electrical noise in the signals as the features are derived using all samples in the signal in contrast to just one sample value in the peak point.

It is expected that the technique can give additional information to that given by peak values and times. The experimental tests will be discussed in the next few chapters. The optimisation of wavelet base functions will be left for further investigation.

Chapter 5. Testing on Aluminium Samples

5.1 Background

Eddy current testing is sensitive to the conductivities and the magnetic permeabilities of the metal samples. Non-ferromagnetic materials, such as aluminium, have relative permeability close to unity, but ferromagnetic materials can have relative permeability higher than $1x10^6$. As a consequence, ECTs including the PEC technique have more challenges dealing with ferromagnetic materials as such high permeabilities significantly prevent the eddy current from penetrating the sample further. This is due to skin effect as discussed previously. Based on this fact, the performance of our PEC system will be evaluated on these two classes of materials.

This chapter investigates aluminium testing and the next chapter will be on ferromagnetic steel testing. The investigation looks at how PEC signals respond to different types and sizes of flaws and how the newly proposed feature extraction technique performs on these signals.

5.2 Sub-surface Metal Loss and Thickness Variation

In this experiment, the sample shown in Figure 5-1 is used. The sample contains steps with thickness varying from 1 mm up to 10 mm with an increment of 1 mm. This experiment can be seen as both thickness variation and sub-surface metal loss tests. When being perceived as

the latter, it is assumed that the flawless part had a thickness of 10 mm and the only surface exposed to the investigator is the top surface, and due to corrosion on the opposite surface, the thickness of the sample is reduced.

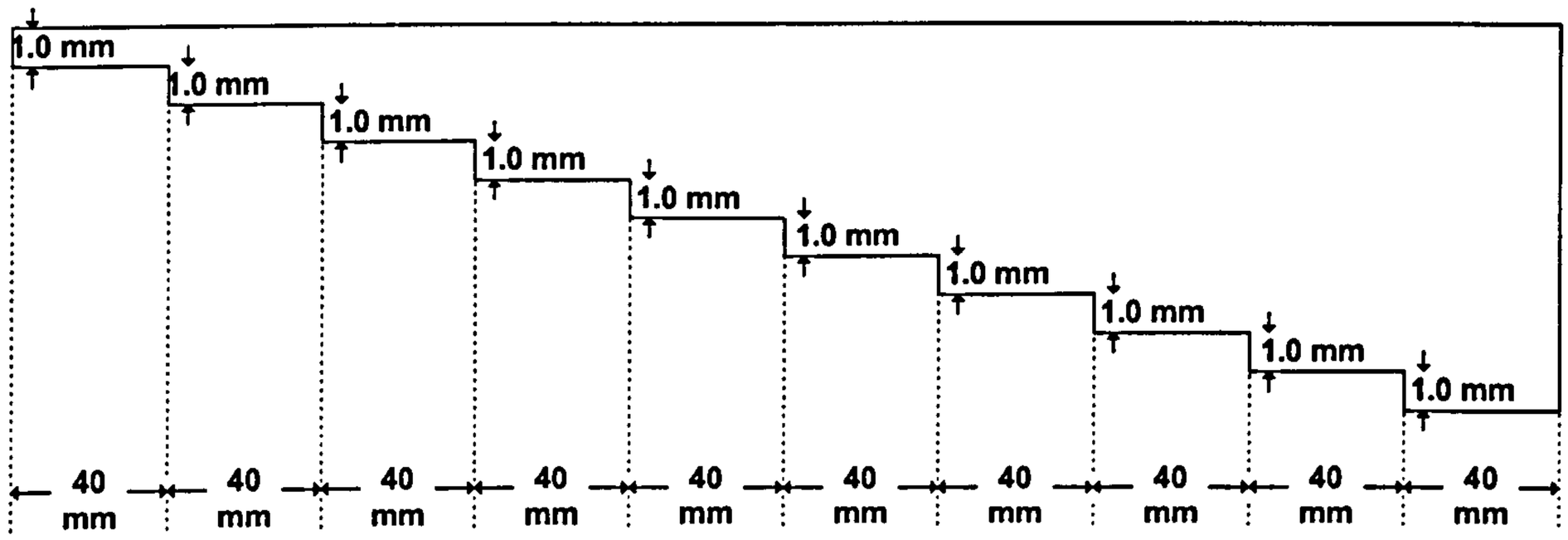

Figure 5-1 Specimen 1: Metal Loss Detection (Thickness Variation)

The measured response signals are shown in Figure 5-2. The results show that the thickness variation in the metal sample affects both the peak heights and the time-to-peak. Figure 5-3 indicates that the relation between the peak heights and the thickness is exponential. While Figure 5-4 suggests that, the relation between the time-to-peak and the thickness is more linear. Figure 5-4 also shows the proneness of the approach to noise, when the signal gets very small, i.e. when depth is more than 6 mm.

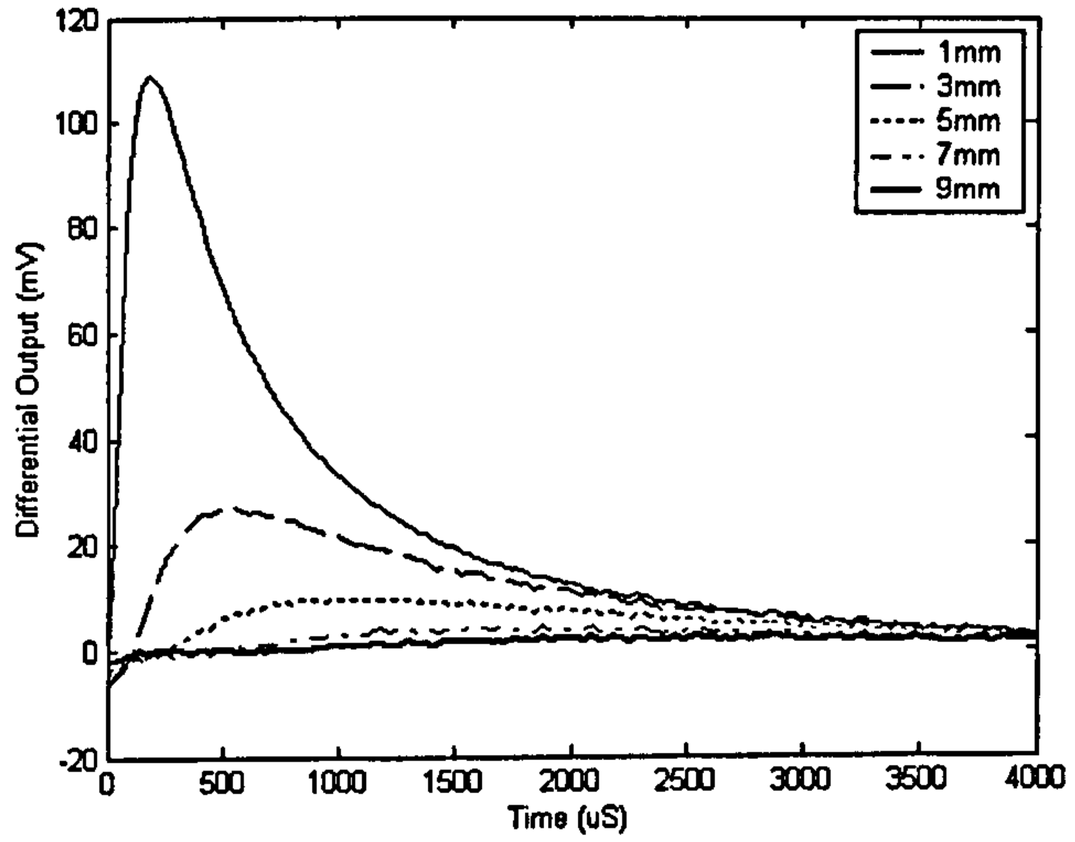

Figure 5-2 The Signals with Thickness Variation

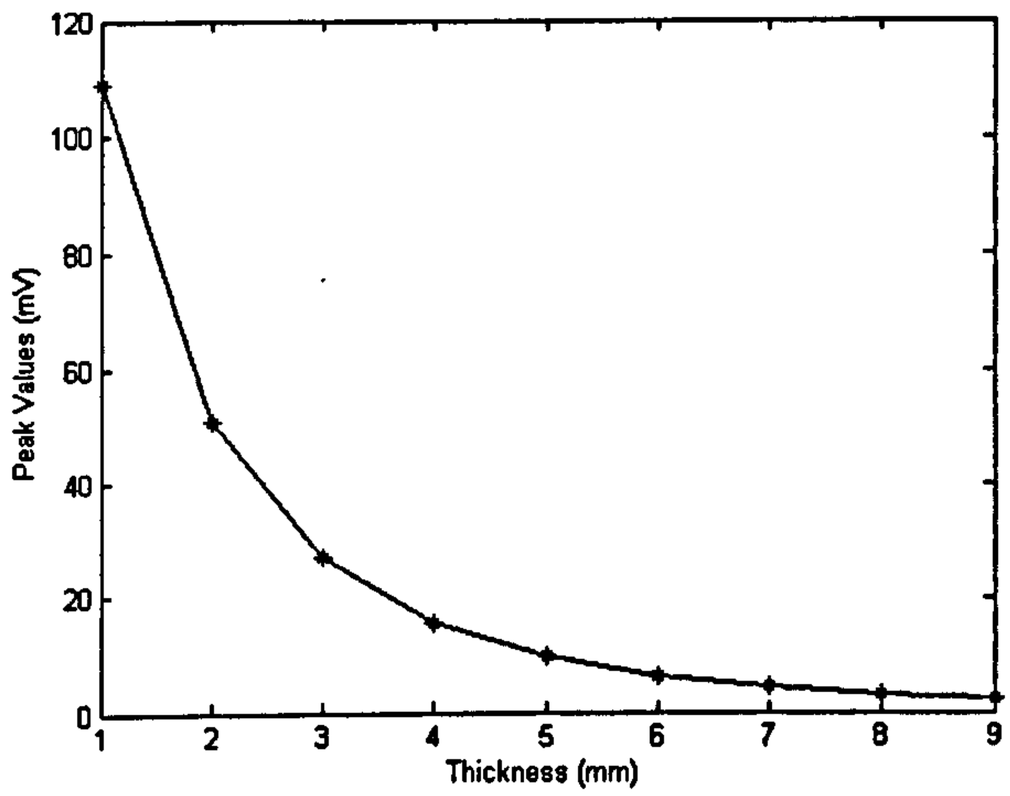

Figure 5-3 The Peak Values for Various Thickness

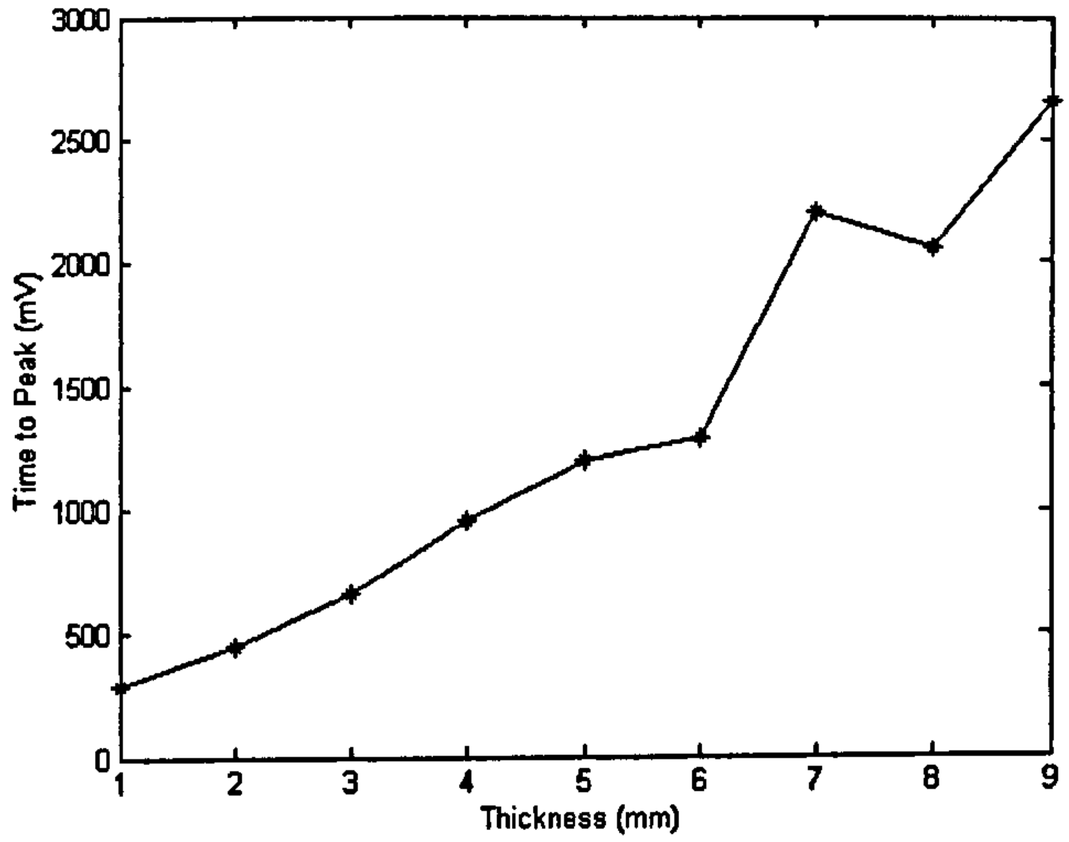

Figure 5-4 The Time to Peak for Various Thickness

5.3 Surface Discontinuities

The sample shown in Figure 5-5 is used for this experiment. The sample is turned upside down so that the slots are facing upwards. Then the probe is positioned above each slot for measurement. The slots simulated discontinuities in the real situation.

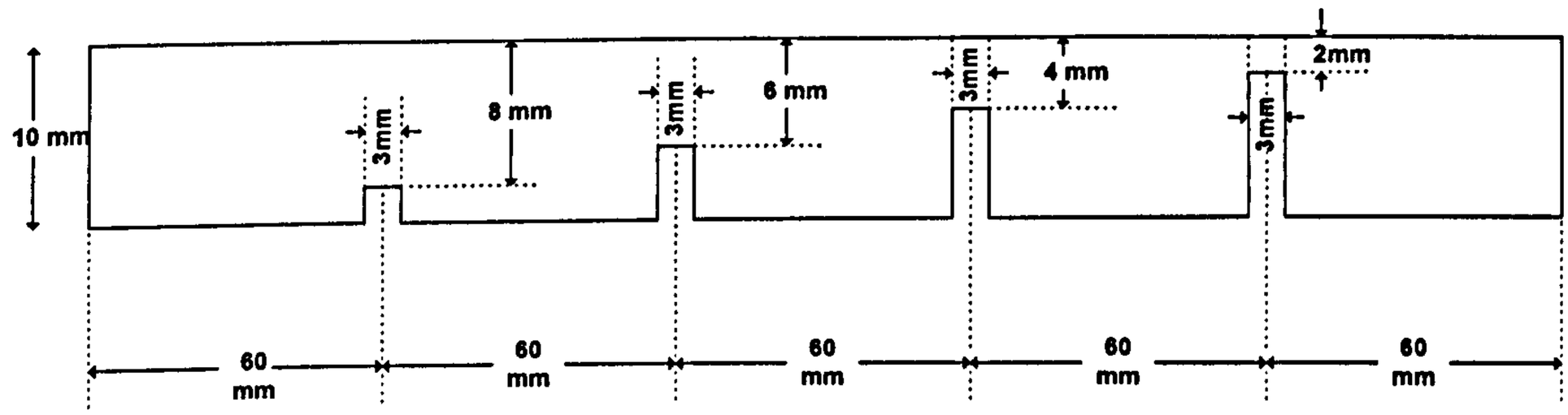

Figure 5-5 Specimen 2: Discontinuity Detection

Before each measurement is taken, the probe is maintained for about 20 seconds on the sample. This is to minimise the temperature variation due to the temperature difference of the air and the sample, which can be significant. The centring of the sensor above the slot is achieved by ensuring that the peak of the differential signal is reaching the maximum. The peak height will reduce when the sensor is off the centre of the slot.

The differential signals are shown in Figure 5-6 that demonstrates that the depths of surface slots do not affect the time-to-peak but they affect the peak heights significantly. Figure 5-7 suggests that the relation between the peak values and the depth is somewhat exponential.

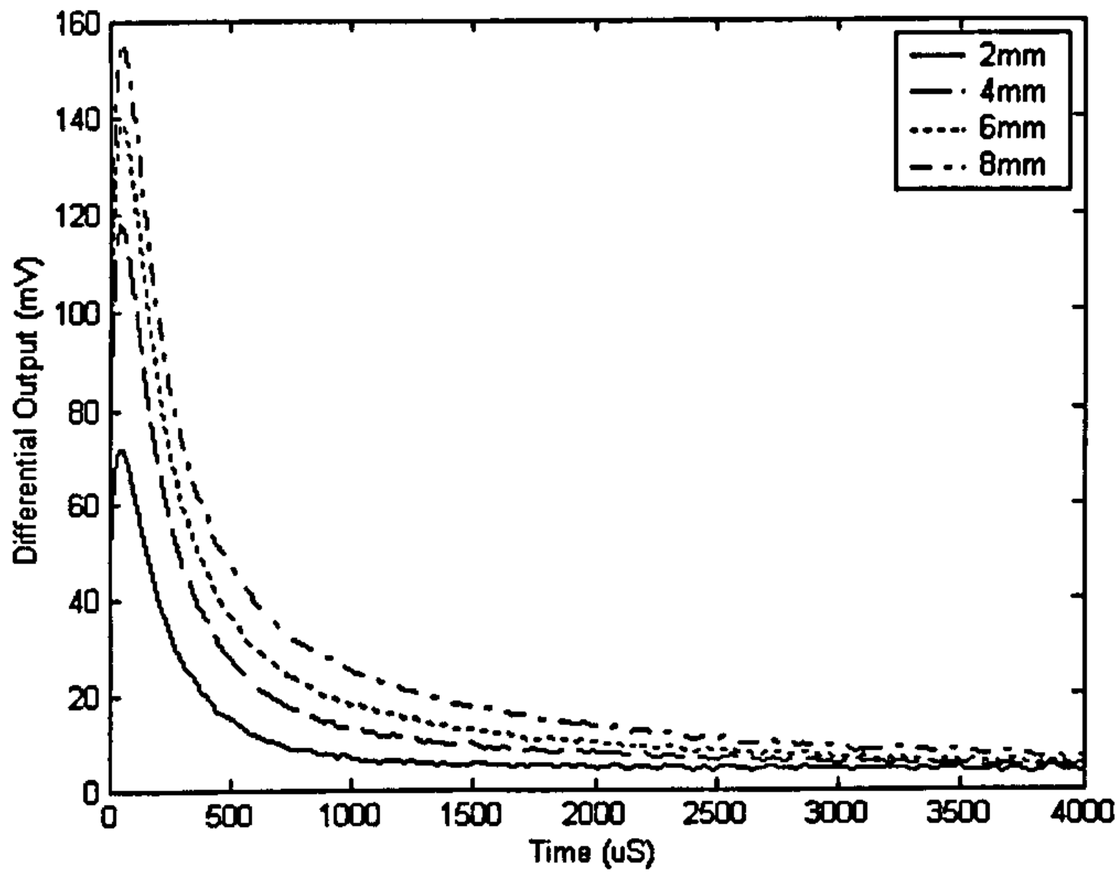

Figure 5-6 Surface Slot Differential Signals

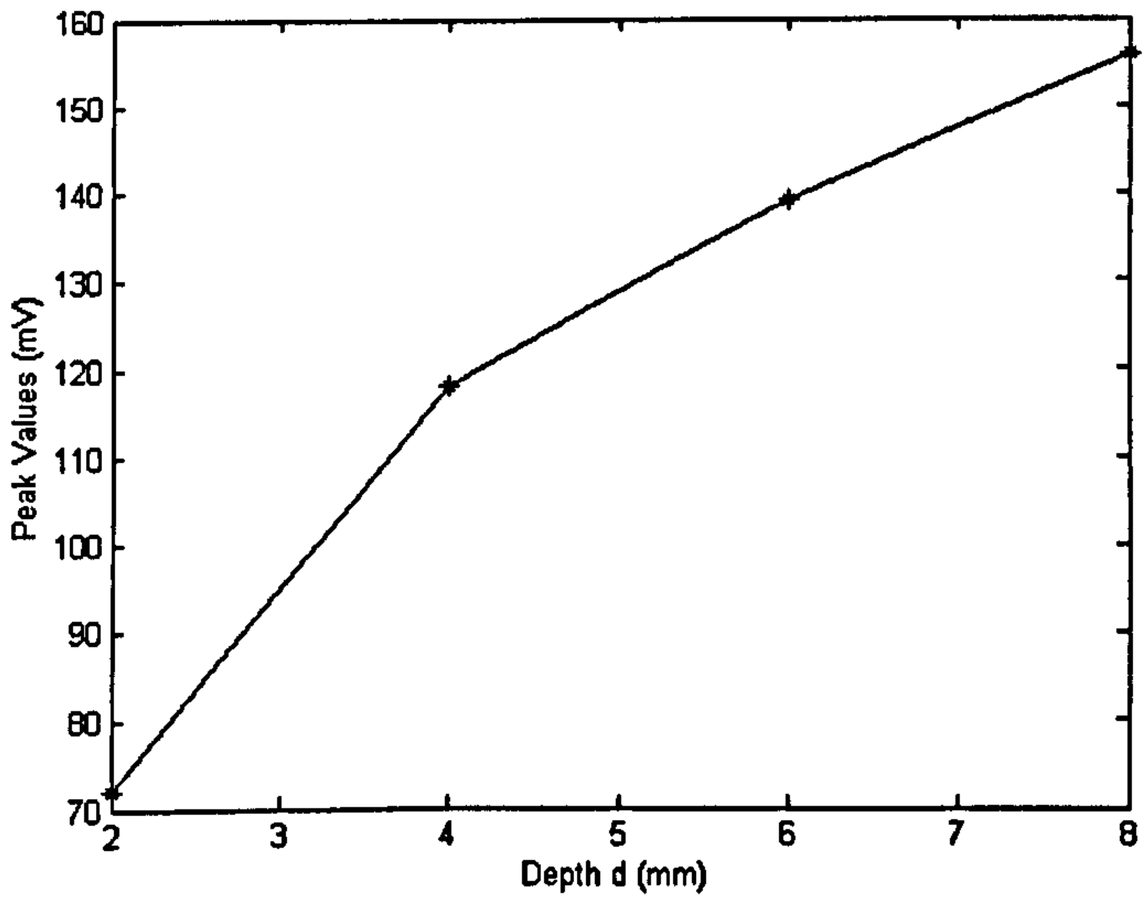

Figure 5-7 The Peak Values Against Surface-slot Depths

5.4 Sub-surface Discontinuities

For this experiment, again the sample shown in Figure 5-5 is used, although this time the probe is positioned on the surface opposite the one where the slots are.

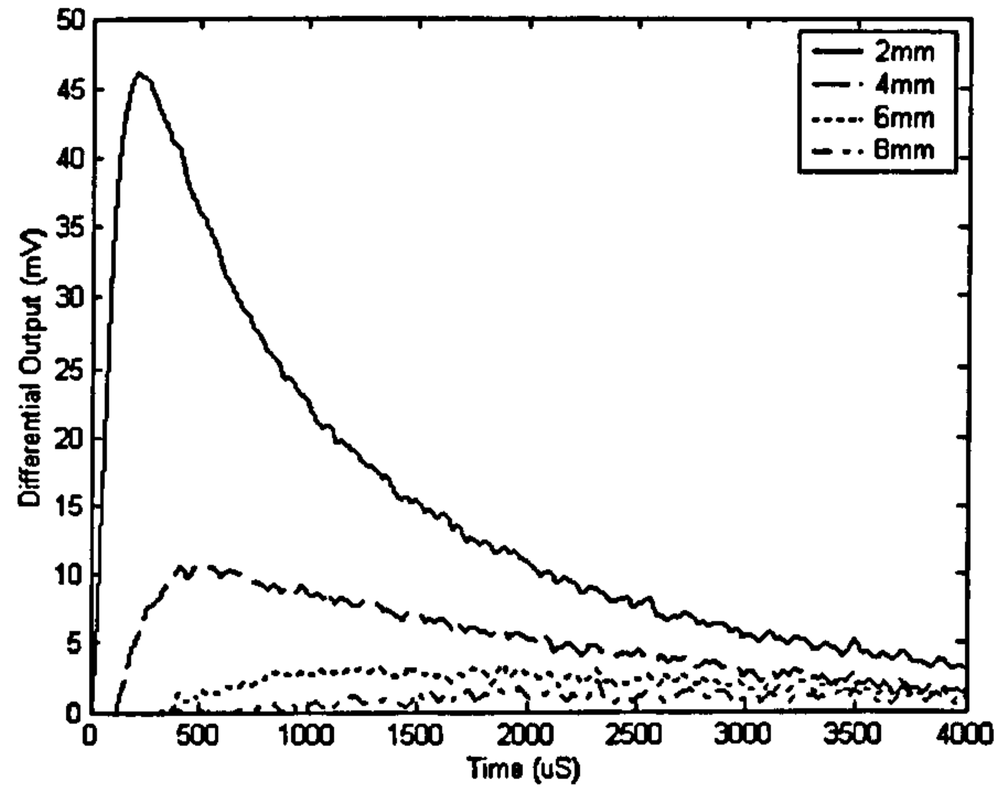

Figure 5-8 Sub-surface Slot Differential Signals

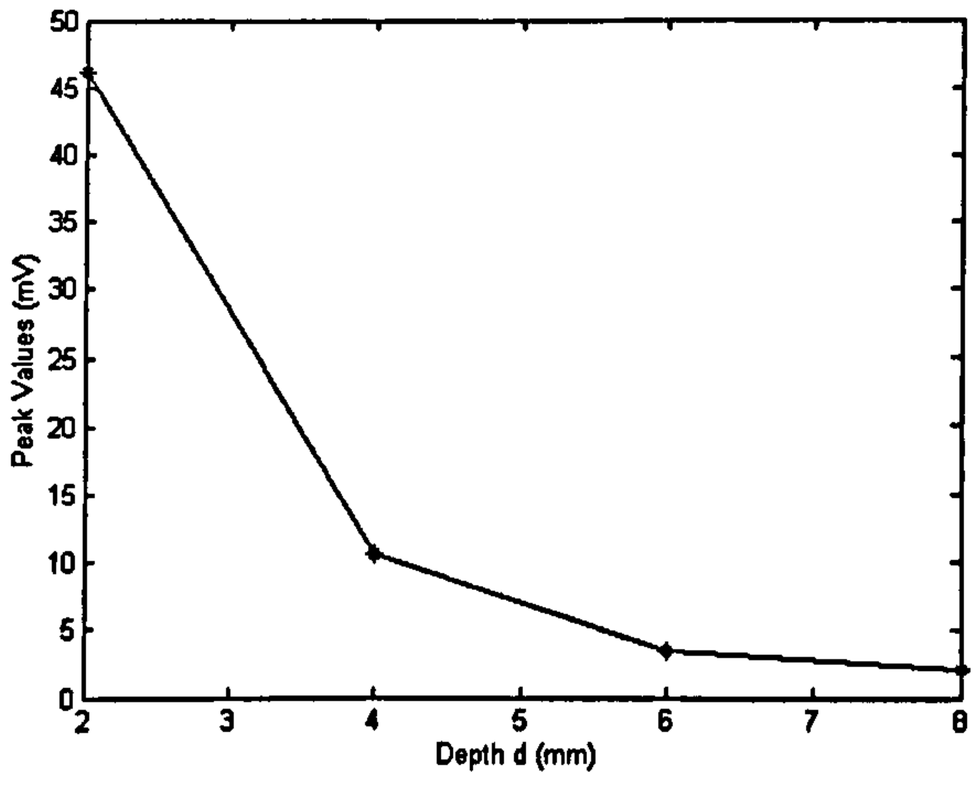

Figure 5-9 The Peak Values Against Sub-surface Slot Depths

Figure 5-8 shows that the sub-surface defects affect both the peak height and time-to-peak. Slots with higher depths generate smaller signals with lower peak heights and higher peak arrival times. The relationship between the peak values and the depths is somewhat exponential.

5.5 Width Variation

The experiment was carried out with sub-surface slots of 2mm depths. The widths of the slots are 0.5mm, 1.0mm and 1.6 mm. The sample layout is shown in Figure 5-10. The resulting signals are shown in Figure 5-11.

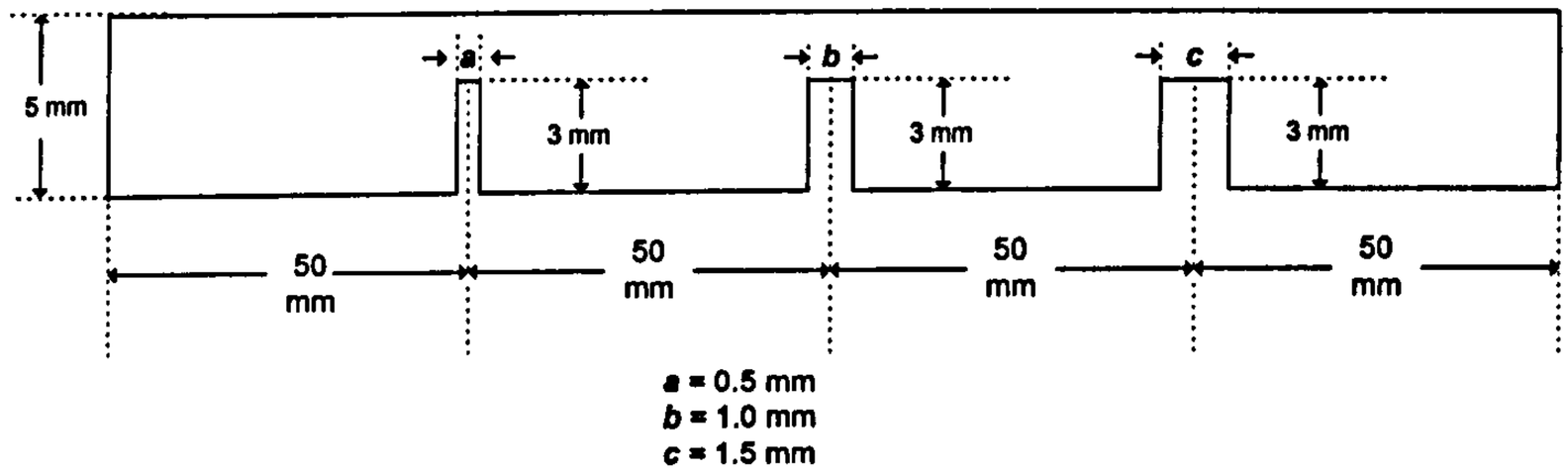

Figure 5-10 Sample Test for Slot Width Variation

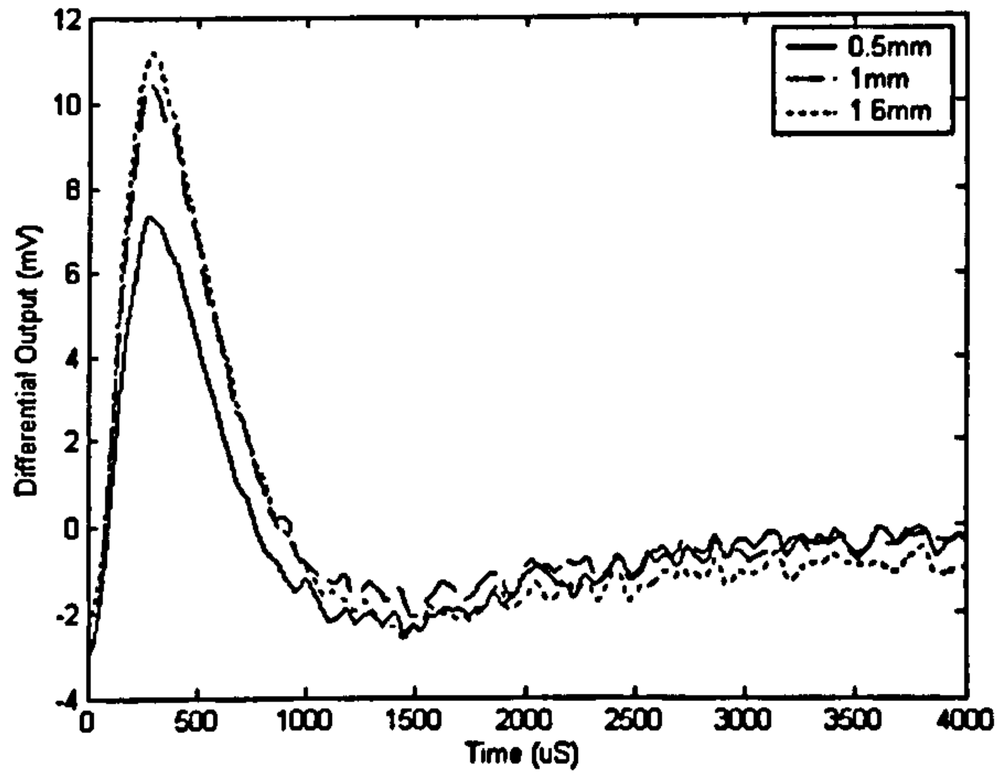

Figure 5-11 Differential Signals with Slot Width Variations

The results show that the time-to-peak is relatively constant for the same depth regardless of the widths of the slots. This means that the propagation time of the wave is insensitive to the width but sensitive to the depth of the slots.

5.6 Flaw Classification

In this test, we are evaluating the performance of both feature extraction techniques, Wavelet-based PCA and peak point in the time domain. The samples shown in Figure 5-1 and Figure 5-5 are used. The samples provide three classes of defects, namely surface discontinuities (4 different sizes), sub-surface discontinuities (4 different sizes) and sub-surface metal loss (9 different sizes), with assumption that the normal, defect-free aluminium slab has a depth of 10 mm. Table 5-1 list the type and size of defects used in the experiment. A unique number is given for each class of defect. For each defect, five measurements are taken. The position of the probe might vary slightly with respect to each defect from one measurement to another. All the responses are sampled by 1MHz sampling rate and recorded. Both feature extraction techniques are used to classify their defects according to the responses.

Condition	Description	Defect Class No.	Size (mm)
1	Metal Loss	1	9
2	Metal Loss	1	8
3	Metal Loss	1	7
4	Metal Loss	1	6
5	Metal Loss	1	5
6	Metal Loss	1	4
7	Metal Loss	1	3
8	Metal Loss	1	2
9	Metal Loss	1	1
10	No Defect	0	-
11	Surface Slot	2	2
12	Surface Slot	2	4
13	Surface Slot	2	6
14	Surface Slot	2	8
15	Sub-surface Slot	3	2
16	Sub-surface Slot	3	4
17	Sub-surface Slot	3	6
18	Sub-surface Slot	3	8

Table 5-1 List of Defetcs

The classification is carried out by finding the smallest distance between measured features to each feature curve. The feature curves are created by interpolating average feature points recorded previously. The interpolation is performed using Matlab's function ***interp1***. This populates the gaps between recorded measured feature points. Figure 5-12 shows graphically

the feature curve. The curve has been verified by deliberately removing one or two measured points for predicting the interpolated curve. There generally is a good match between the removed measured point and the predicted point though the interpolation. A poor match is encountered if metal loss of 8 mm (circled in the graph) is removed. This shows that more measured points are required to fill the gaps between two neighbouring measured points that are relatively far apart when reliable fitting is desired. This means that new flaws with the required depths to fill the gaps are required

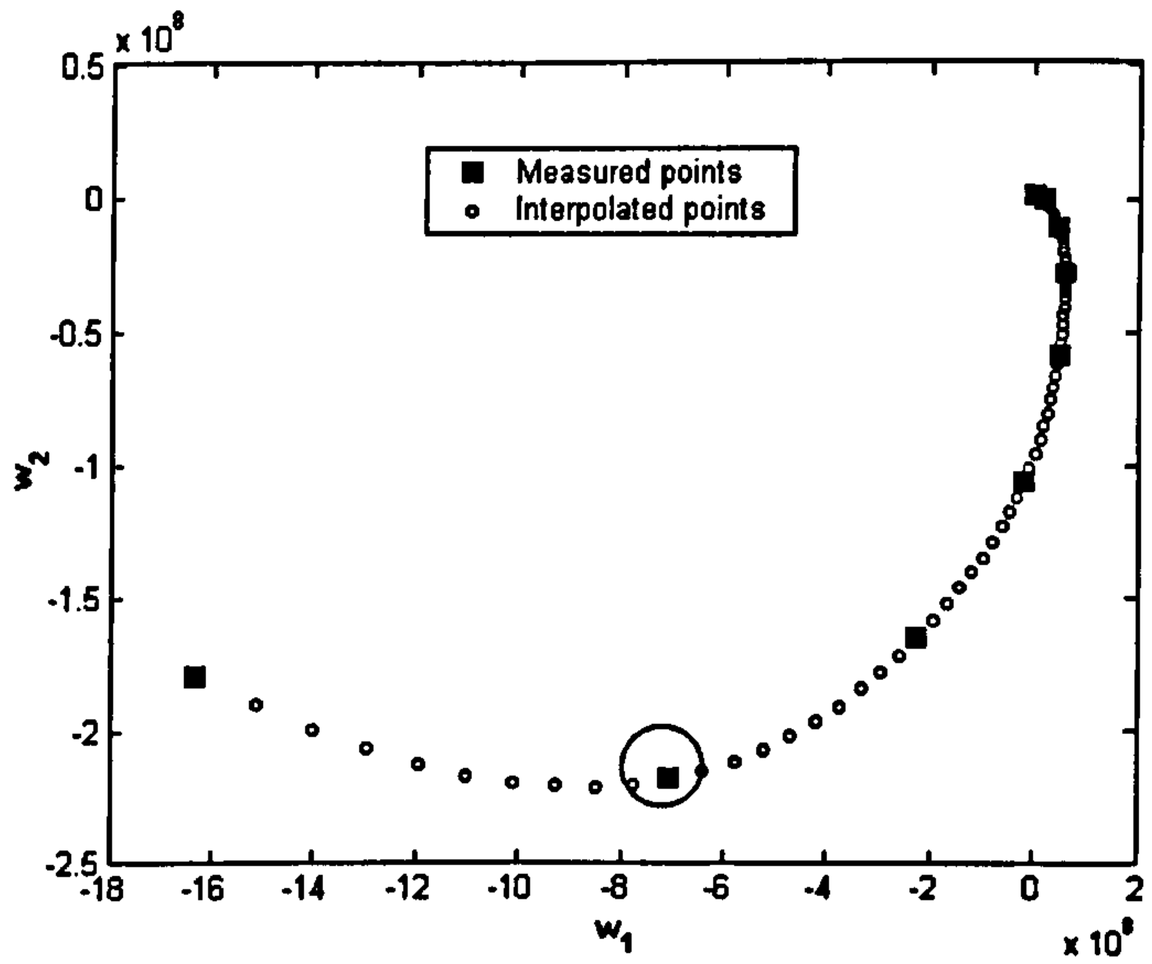

Figure 5-12 Interpolation of Measured Points

For a classification, each feature is considered to have the same weighting, therefore one of the two features must be scaled up or down to match the other. The Euclidean distance between measurement point and interpolated recorded points is calculated by:

$$d = \sqrt{(f_1 - f_{1\_0})^2 + (A*(f_2 - f_{2\_0}))^2} \tag{5-1}$$

where d is the Euclidean distance between two points, f_{1_0} and f_{2_0} are the recorded average feature scores and f_1 and f_2 are the current measurement feature scores. A is the scaling factor to equalise the orders of both features. It is obtained using the following equation:

$$A = \frac{f_{1\_0}\max - f_{1\_0}\min}{f_{2\_0}\max - f_{2\_0}\min} \tag{5-2}$$

5.6.1 The Conventional Approach

The flaw classification using the conventional approach using peak value and time is shown in Figure 5-13. The surface defects are easily distinguished from other defects as they have low peak arrival times that are relatively constant. However, for sub-surface slots and metal loss that are deeply buried, the discrimination gets vaguer. This is supported by the figures in Table 5-2.

Condition	Observation Output					Class Identification Rate (%)
	1	2	3	4	5	
1	1	1	1	1	1	100
2	1	1	1	1	1	100
3	1	1	1	1	1	100
4	1	1	1	1	1	100
5	1	1	1	1	1	100
6	1	1	3	1	1	80
7	1	1	3	1	1	80
8	1	1	1	1	3	80
9	0	3	1	1	0	40
10	0	1	1	1	0	40
11	2	2	2	2	2	100
12	2	2	2	2	2	100
13	2	2	2	2	2	100
14	2	2	2	2	2	100
15	3	3	3	3	3	100
16	3	3	3	3	3	100
17	3	3	3	3	3	100
18	1	3	3	1	0	40

Table 5-2 Classification using Peak Value and Peak Time

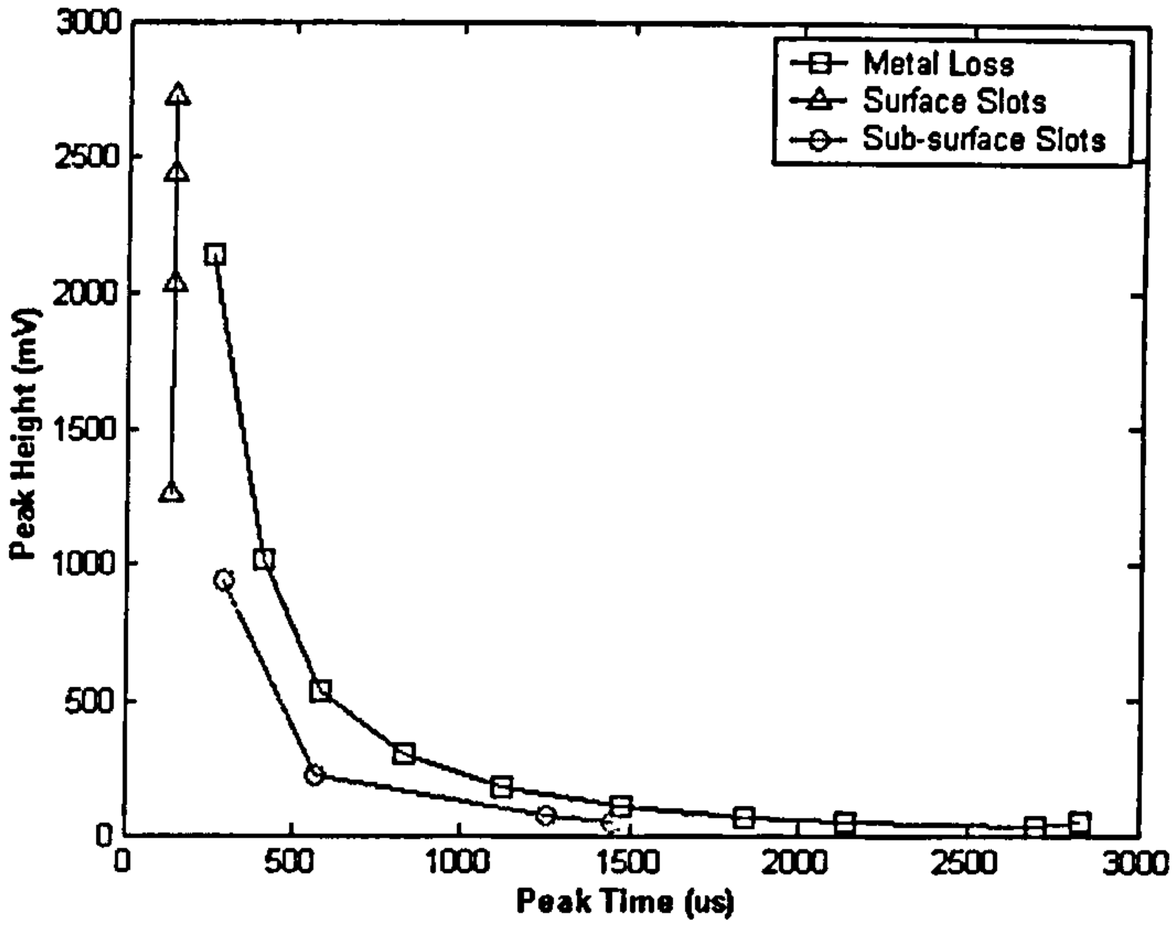

Figure 5-13 Classification using Peak Value and Peak Time

5.6.2 The Wavelet-based PCA

The technique details are as described in the previous chapter. The classification using this technique is shown below in Figure 5-14.

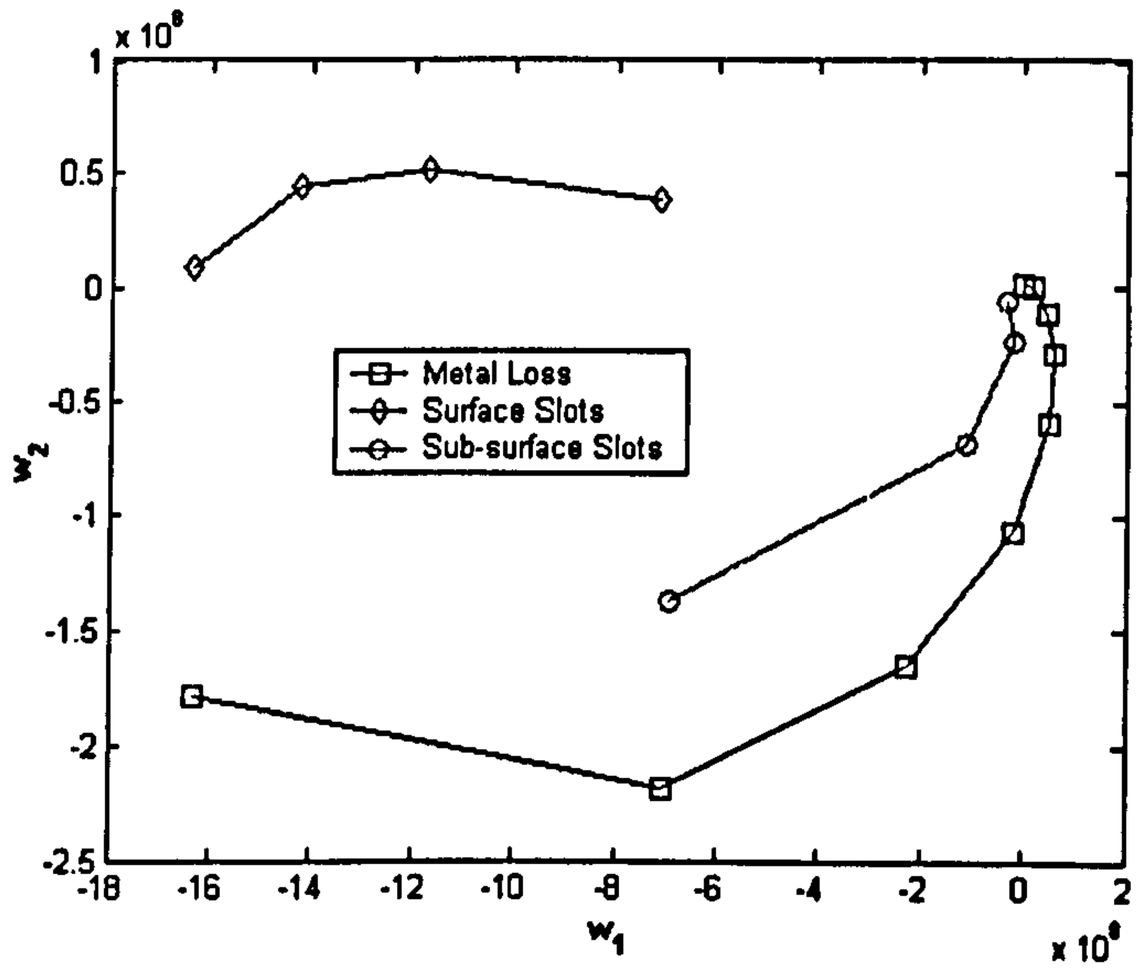

Figure 5-14 Classification using Features from Wavelet-based PCA

Condition	Observation Output					Class Identification Rate (%)
	1	2	3	4	5	
1	1	1	1	1	1	100
2	1	1	1	1	1	100
3	1	1	1	1	1	100
4	1	1	1	1	1	100
5	1	1	1	1	1	100
6	1	1	1	1	1	100
7	1	1	1	1	1	100
8	1	1	1	1	1	100
9	1	0	1	1	1	80
10	0	0	0	0	0	100
11	2	2	2	2	2	100
12	2	2	2	2	2	100
13	2	2	2	2	2	100
14	2	2	2	2	2	100
15	3	3	3	3	3	100
16	3	3	3	3	3	100
17	3	3	3	3	3	100
18	0	3	3	3	0	60

Table 5-3 Classification using Wavelet-PCA technique

5.6.3 Discussion

Both methods are shown to be able to identify and discriminate the surface discontinuities easily. Although Figure 5-13 seems to show that peak values and peak times can discriminate sub-surface slots from metal loss easily, Table 5-2 shows that it has problem with identification of deeply buried slots and metal loss. It has confusion in discriminating metal loss with size shallower than or equal to 4 mm, sub-surface slots with depths more than 6 mm and parts with no defects. This is signified by the recognition rate of just 40% with conditions numbered 9 and 18.

Figure 5-14 shows the classification results with the Wavelet-based PCA approach described previously. Table 5-3 shows how this technique performs in classification of defects. It is apparent that improvement from the technique using peak time and peak value has been achieved. The Wavelet-based PCA technique will detect and correctly identify all metal losses deeper or equal to 2 mm and sub-surface slots with depths up to 6 mm. The flawless parts are

all correctly identified. This also constitutes a significant improvement. Table 5-4 summarises the defect classification performances of both techniques.

	Correct Identification Rate (%)			
	Surface Slot	Sub-surface Slot	Sub-surface Metal Loss	No Defect
Wavelet-PCA	100	95.0	97.7	100
Peak Value and Peak Time	100	90.0	88.9	40.0

Table 5-4 Comparative Test Results

5.7 Flaw Depth Sizing

The flaw quantification results using the conventional technique can be seen in sections 5.2, 5.3 and 5.4. Good quantitative capabilities are shown by the results obtained using the technique. The quantitative capability can be explained, as the flaw size is bigger, the difference between the flaw and reference signals is also bigger. Therefore, it can be expected that the peak of the differential signal is also bigger, i.e. it correlates to the depth size of the flaw. It should be noted that in this experiment, flaws of the same type have the same width.

The flaw quantification using the Wavelet-PCA technique can be achieved by using two differential PCA coefficients as shown in Figure 5-15. The Figure shows how sizing depths of metal loss can be achieved. The steps in getting the coefficients are described in Section 4.5.2, with signals from metal loss and flawless parts are used as training data. A look-up table can be created which lists the values of the PCA feature points and their corresponding defect sizes. Feature values future measurements will be compared against the values in the table to find the closest values and the estimated size of the defect can subsequently be produced. The certainty of the estimations depends highly on the number of calibrated samples with different flaw depths and sizes and their range.

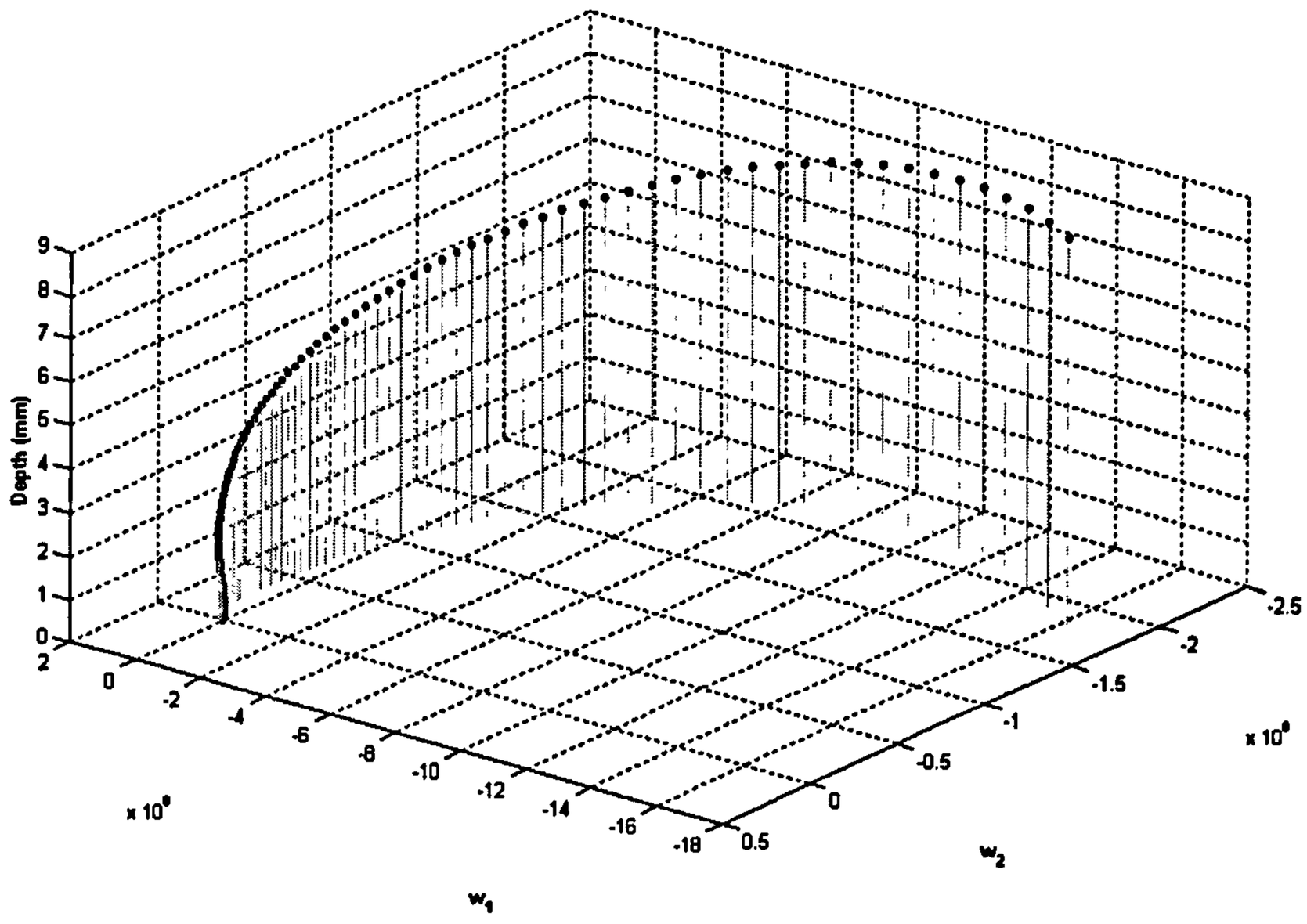

Figure 5-15 Quantification of Metal Loss using w1 and w2

5.8 Summary

The experiment results have shown that the designed PEC system has the capabilities of thickness measurement and artificial discontinuities detection on the manufactured aluminium samples. In addition, it is also able to classify and quantify the discontinuities detected under controlled conditions.

The new approach using hierarchical Wavelet-based PCA has been investigated. The results show that the approach using a combination of Wavelet and PCA provides better results in classification of defect types than the conventional approach. More deeply buried flaws are correctly identified using the proposed technique. This also shows that the new technique is more robust than the technique using peak value and peak time. The results also demonstrate that the new Wavelet-based PCA approach has a quantitative capability. In this case, it provides the depths of the defects.

Chapter 6. Testing on Ferromagnetic Steel Samples

6.1 Background

As opposed to aluminium, many carbon steels are ferromagnetic. Carbon steel is chosen in this investigation to represent ferromagnetic metals. In flaw detection, ferromagnetic carbon steels are generally more challenging for ECTs, including PEC, than non-ferromagnetic metals. The additional problems arise mainly due to the material property of the steels, namely high relative magnetic permeability and the variation of magnetic properties in steel materials. Due to these problems, and mainly the former one, ECTs are generally limited to surface breaking defects in steel inspection.

The high magnetic permeability limits the penetration of eddy current, as implied by the skin depth equation. The penetration is affected by the conductivity and the permeability of the sample material. The higher the permeability is, the smaller the effective penetration depth will be.

The variation of the magnetic property across a steel sample causes material noise appearing in the measurement signals. It can easily mask defect signals or give an indication that could lead to a false alarm. To minimise or reduce the affects of these two phenomena, the use of magnetisation will be considered.

The ability to detect and characterise flaws in steel is highly beneficial due to the wide use of carbon steels in various industries and numerous structures.

6.2 Saturating Magnetisation

As discussed in (Tian, Zhao et al. 1998), Z or L $=f(x,\sigma,\mu,f)$, the Eddy current magnetic field intensity is a function of the gap between the sensor coil and the target (x), the electrical conductivity of the target (σ), the permeability of the target (μ) and the frequency of current in the excitation coil (f). To use the sensor for flaw detection and quantification of steel materials, it is important to simplify the function by controlling the variables x, σ, μ and f. In PEC, theoretically, the frequency f has a wide spectrum, ranging from DC to infinite AC. To control the permeability μ and keep it relatively constant in the sensor signals, magnetisation is applied to eliminate or reduce the variation of permeability over different parts of the specimen.

From the skin depth equation, it can be seen that an increase in penetration can be achieved by reducing the magnetic permeability μ of the sample. Magnetisation can also be helpful to bring the sample into magnetic saturation. In saturation, the relative permeability of the material reduces towards unity, and hence, the eddy current penetration improves significantly.

Two magnetisation approaches are available, namely AC and DC magnetisation. It is known that AC magnetisation is very much limited to surface or near surface flaws detection. The field is confined to the area close to the surface due to the skin effect. On the other hand, DC magnetisation can penetrate deeper into the material inspected (Hull and John 1988; Halmshaw 1996; Bray and Stanley 1997).

Magnetisation of a specimen could be accomplished by different ways, among others (Hull and John 1988): using permanent magnets, passing a heavy current through the component (locally or overall), placing a coil around or close the component under test and making the component part of a magnetic circuit (e.g. by means of a hand yoke). The selection of

magnetisation technique depends on various factors, for example the working space and the geometry of the sample.

There are no universal rules regarding magnetisation levels for MFL inspection (Bray and Stanley 1997). In general practice, the strength of field required to magnetise industrial steel is about three times the value of the coercion H_c. At this level, the steels will be magnetically saturated.

Figure 6-1 shows how the magnetic flux distribution will appear around the sample and particularly the slot as simulated using finite element modelling software called FEMM (Meeker 2001). The simulation is a simplified model for the experimental setup illustrated in Figure 6-5. The simulation shows how flux leakage occurs above the sub-surface slot. Figure 6-2 shows the normal magnetic flux density just above the surface of the specimen. It demonstrates that the magnitude of the magnetic density peaks above the edges of the opening, and both edges have the opposite polarity of magnetic field density. Based on the simulation as illustrated in Figure 2, the magnetic field distribution across defects is enhanced. In other words, DC magnetisation could improve the detection depth of subsurface flaws and detection sensitivity. This DC magnetic flux density is readily detectable by the PEC sensor, and the leakage phenomena can be used to detect an existing crack.

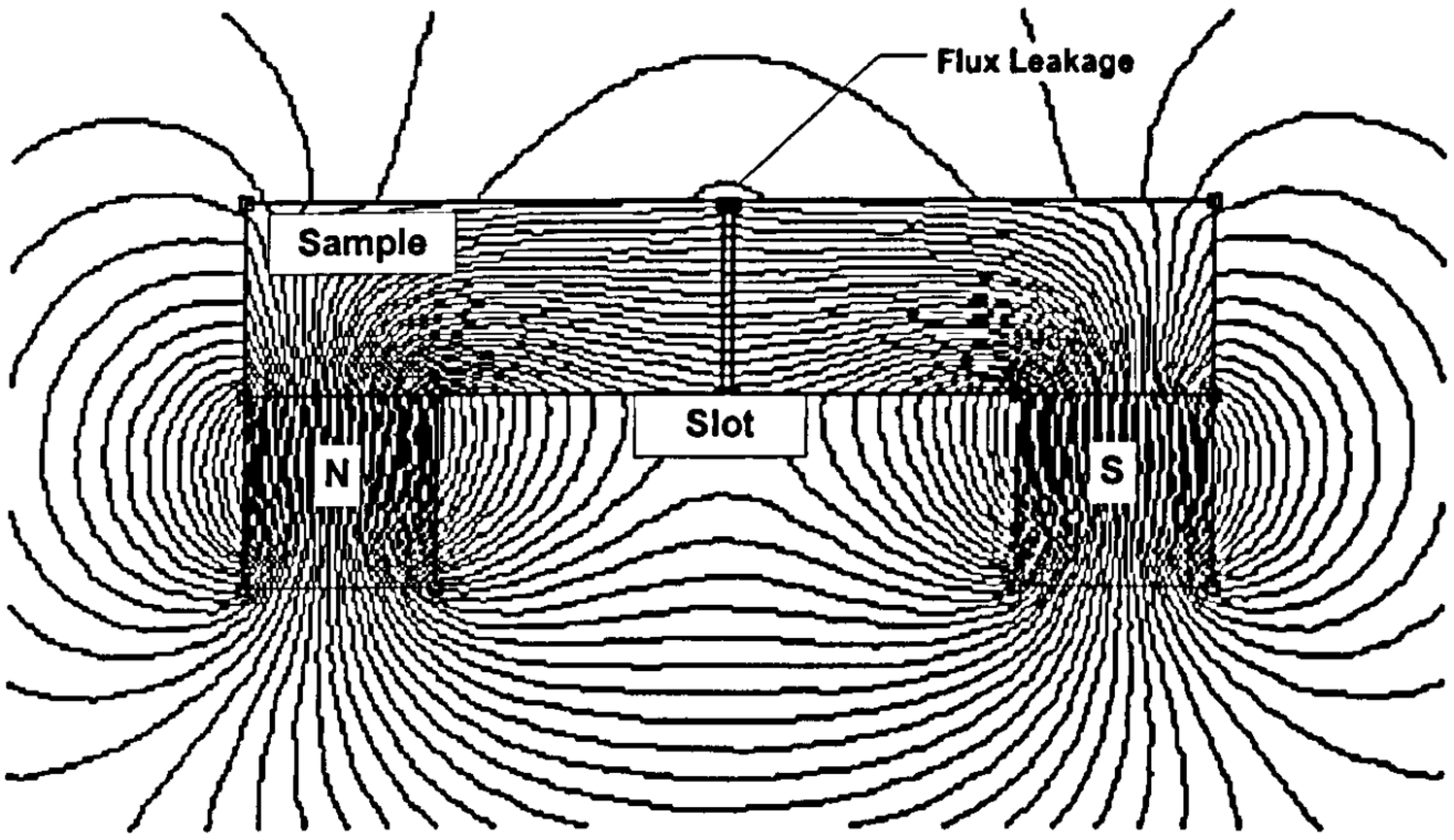

Figure 6-1 The Simulated Contour of Magnetic Flux

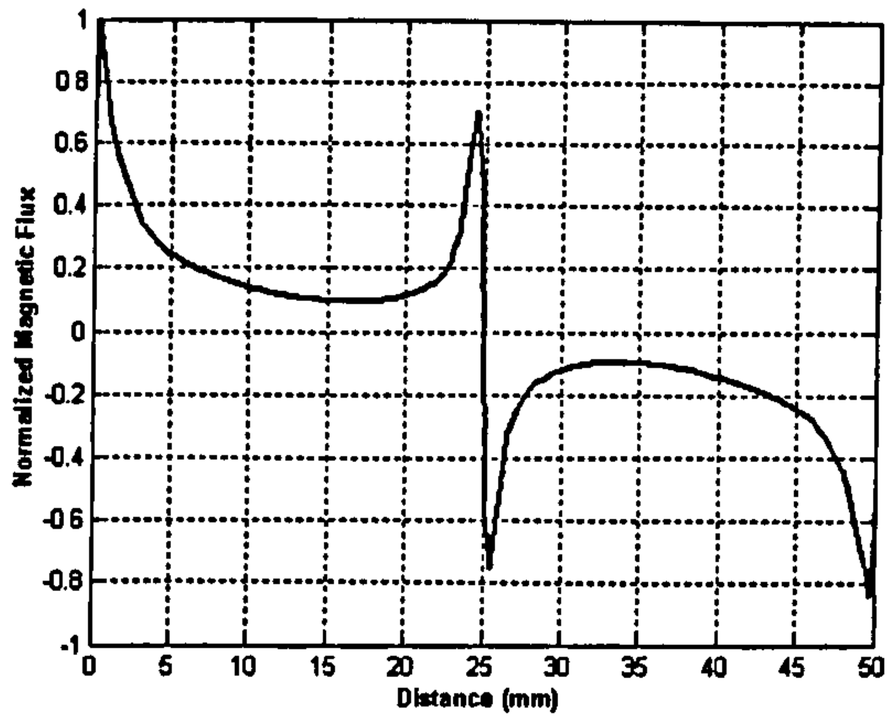

Figure 6-2 The Normal Magnetic Flux Density Above the Surface of the Specimen

6.3 Penetration Depth Test

This experiment will investigate the improvement of the penetration depth of the PEC when the steel specimen is magnetically saturated. A step steel block is used in this experiment. The step thickness ranges from 2mm to 10mm with a 2mm increment. In the experiment, the probe will be fixed on the surface of a step with thickness ***d***. The base response signal is then recorded as a reference signal. Then a written software works out the differential signal y_d by finding the difference between the reference signal y_{ref} and the current base response signal y_t. When there is no change in the configuration of the experimental setup, the differential signal y_d should be relatively flat and small, or ideally zero. Then an aluminium block is brought to the proximity underneath the sample. When change is present in the differential signal y_d, in terms of both shape and magnitude, a conclusion can be drawn that the system's field can penetrate through the depth of ***d***, and the experiment is repeated with larger ***d***'s until no change is detected in the differential signal y_d. The experiment will be carried out both with and without magnetisation for comparison. Figure 6-3 illustrates the two stages where the response signals, y_{ref} and y_t are measured. The illustration only shows the experiment without magnetisation. For the experiment with magnetisation, a magnetic yoke is used and located under the steel sample, as shown in Figure 6-5.

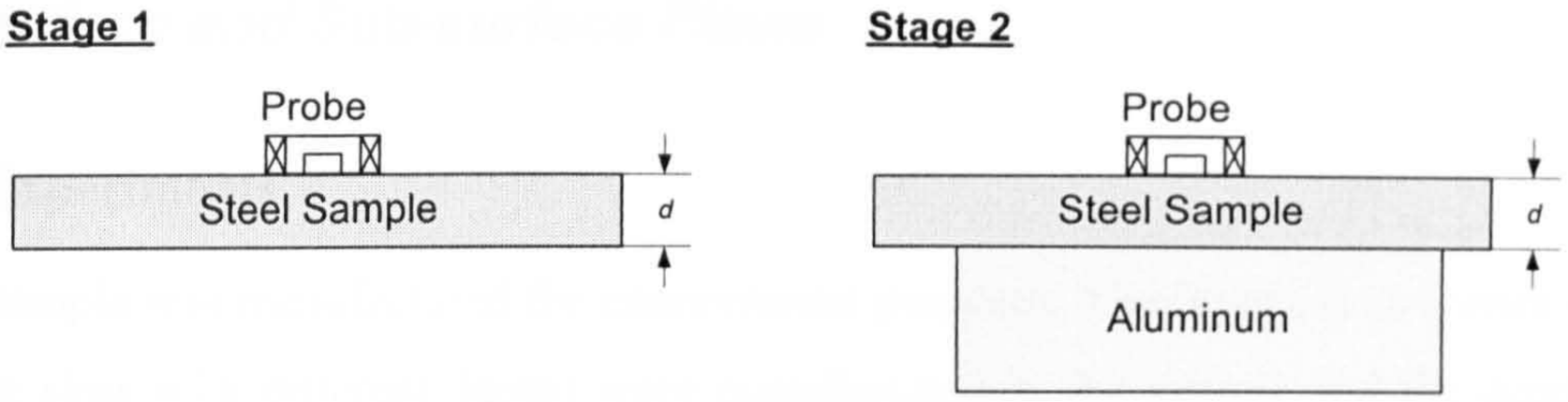

Figure 6-3 Penetration Depth Test

The results of the penetration depth are tabulated in Table 6-1. The table shows if the change due to the presence and absence of the aluminium is detectable or not at increasing depths. Standard deviation (STD) of the differential signal is used to measure the level of the signal. The STD should be around 0.3 when there is no change in the measurement condition, and this indicates the signal noise. When a change is present, the STD will also change. The figures in the table show that without magnetisation, there is hardly any change in the signal at depth of 6 mm. However, with magnetisation, even at a depth of 10 mm, a significant change is evident. Therefore, it can be concluded that the magnetic saturation has improved the penetration depth of the PEC system from about 5 mm to beyond 10 mm.

	Steel Thickness (mm)	Mean STD of Differential Signal		Change (%)
		No Aluminium	Aluminium Present	
Without Magnetisation	2.0	0.33	0.61	84.9
	4.0	0.35	0.38	8.6
	6.0	0.36	0.36	0.0
With Magnetisation	6.0	0.32	3.27	921.9
	10.0	0.35	0.45	28.6

Table 6-1 Penetration Depth Test Results

6.4 Surface and Sub-surface Flaws

6.4.1 Experiments

A steel sample was manufactured for experimental purposes. The layout is as shown in Figure 6-4. Four slots with different depths were manufactured in the sample and the depths of the slots were chosen to accommodate the fact that the sub-surface slots are more difficult to detect.

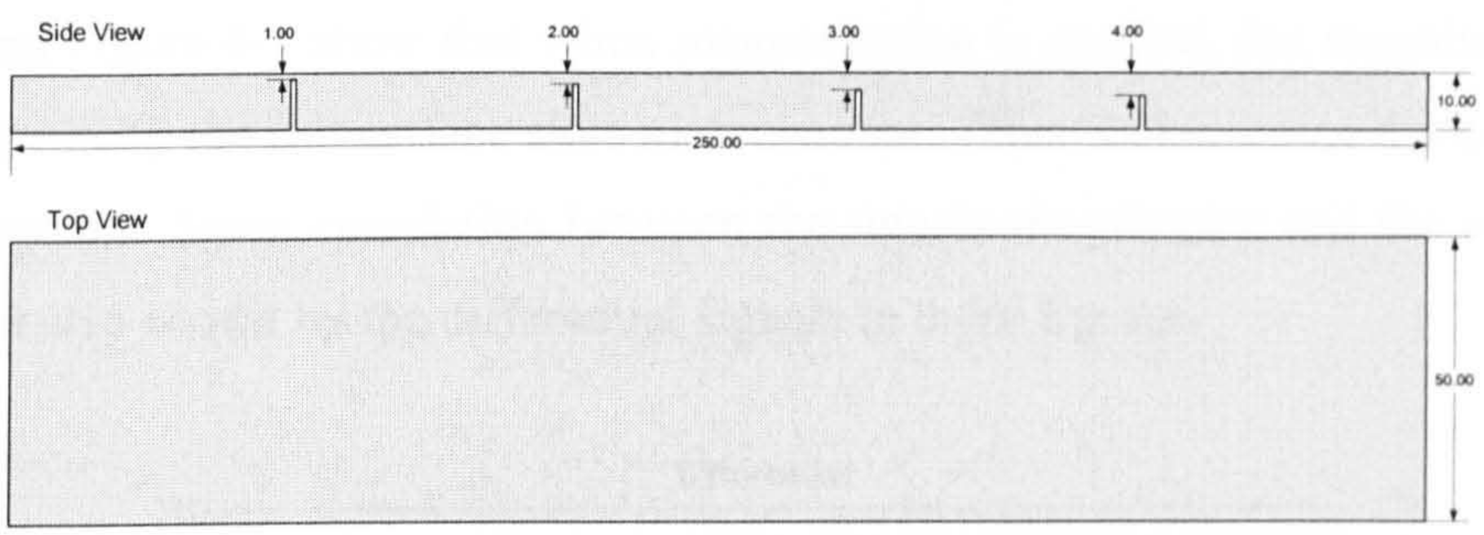

Figure 6-4 The Steel Sample

A strong DC magnet is used to saturate the sample, as shown in Figure 6-5. The position of the permanent magnet was supposed to be on the same side as the probe, however due to no magnetic yokes with suitable dimensions available during the experiment, the positioning of the yoke is as illustrated by Figure 6-5. The magnetic flux flows perpendicularly to the slot's main axis.

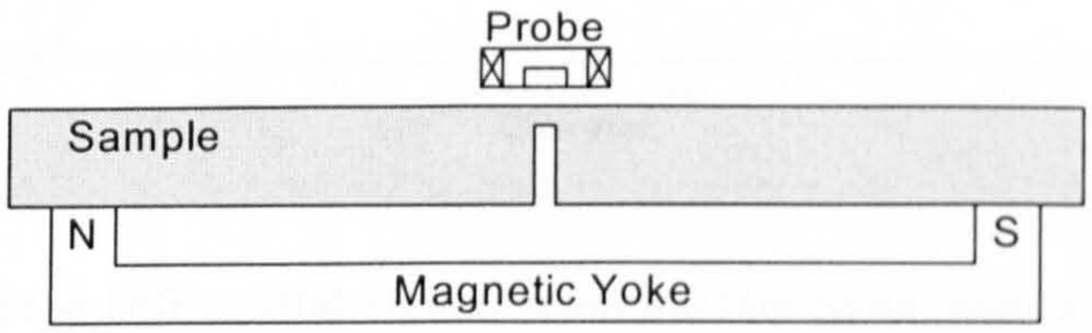

Figure 6-5 The Experimental Setup

In the experiment, the effects of magnetisation will be investigated by comparing inspection results using magnetisation against those without magnetisation. Measurement of both surface

and sub-surface slots will be investigated. The surface slots measurements will be carried out by positioning the probe on the same side as the slot.

6.4.2 Results and Discussion

Figure 6-6 and Figure 6-7 show the experimental results for measurement of surface and sub-surface slots respectively without magnetisation applied. It can be seen that there is no apparent pattern of magnitudes or anything that correlate with the depth of the slot.

Figure 6-8 and Figure 6-9 show that when magnetisation is applied, the magnitude levels are amplified, especially the sub-surface slots measurements. This will increase the signal-to-noise ratio of the system. Some correlation between the signals magnitudes and the corresponding slots depths is also shown by the differential signals in these figures.

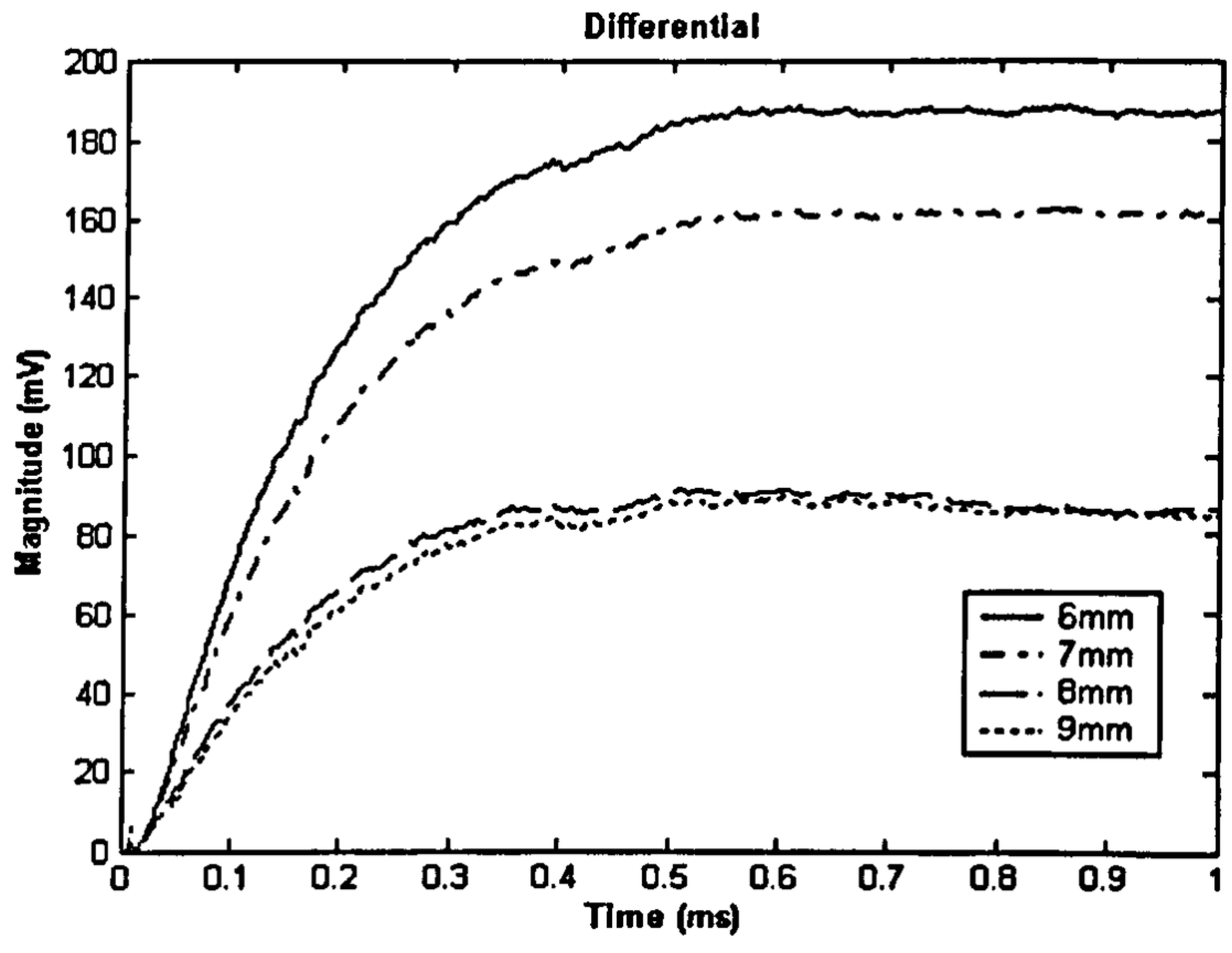

Figure 6-6 Differential Signals from Surface Slots (non-magnetised)

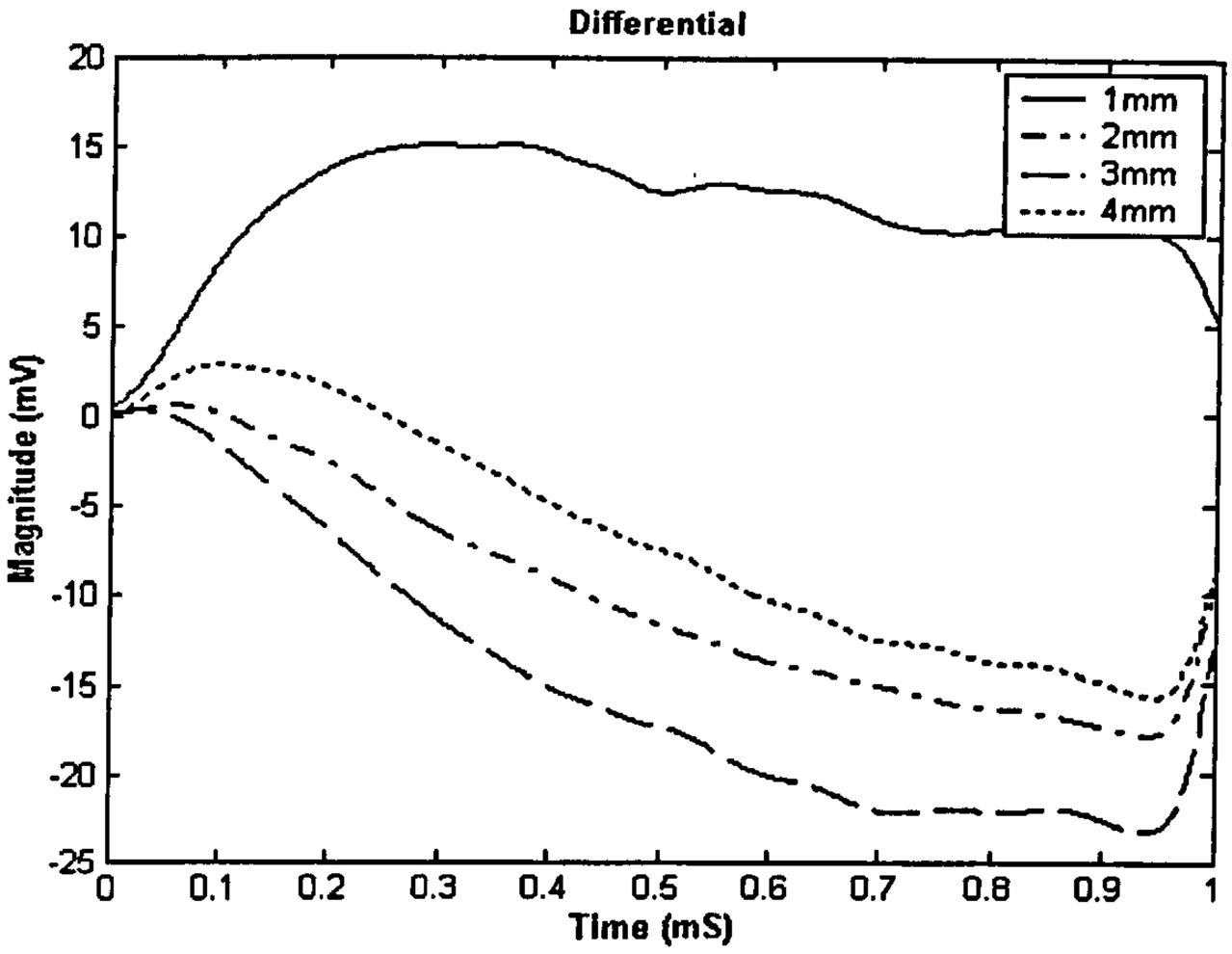

Figure 6-7 Differential Signals from Sub-surface Slots (non-magnetised)

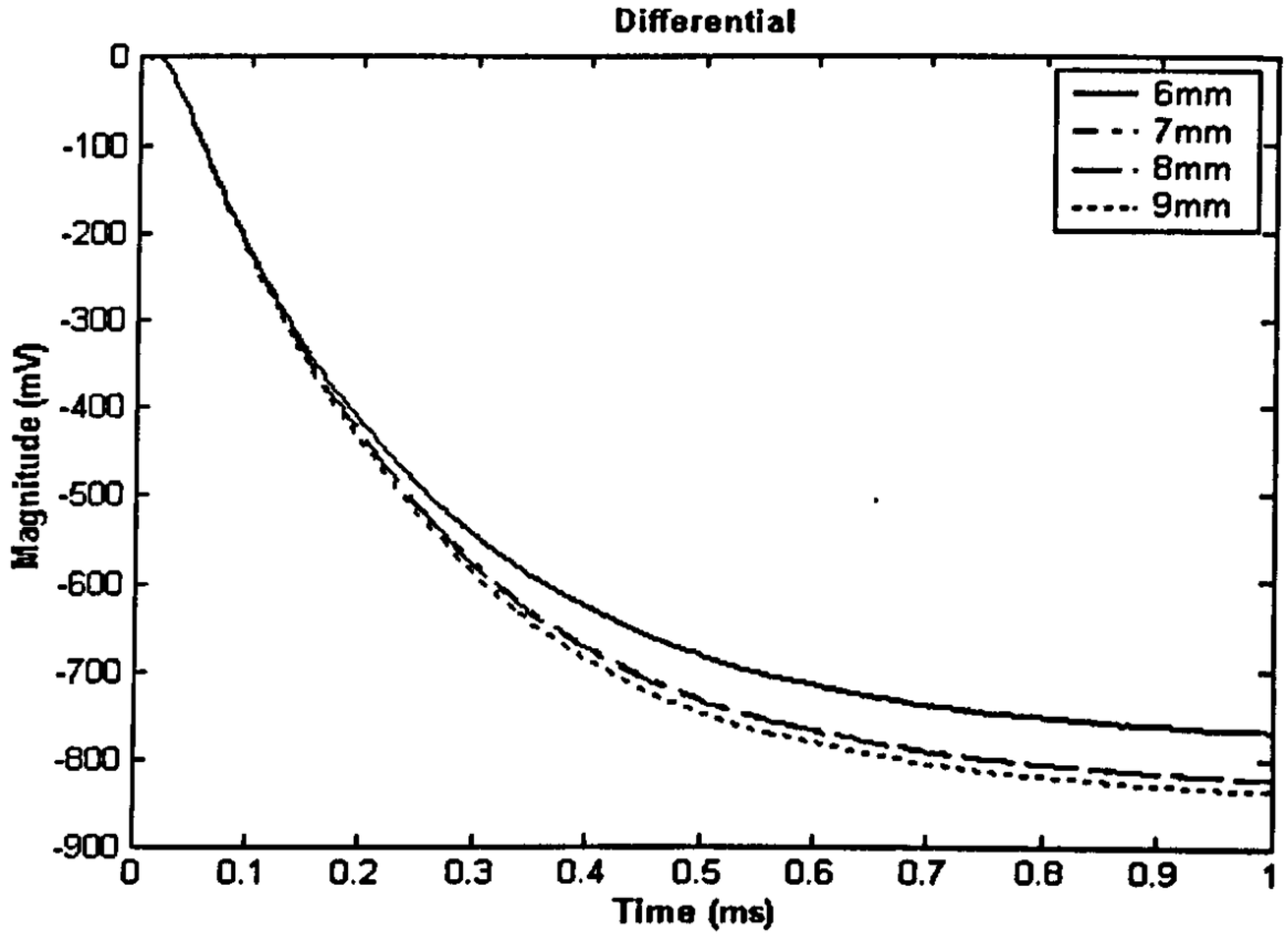

Figure 6-8 Differential Signals from Surface Slots (magnetised)

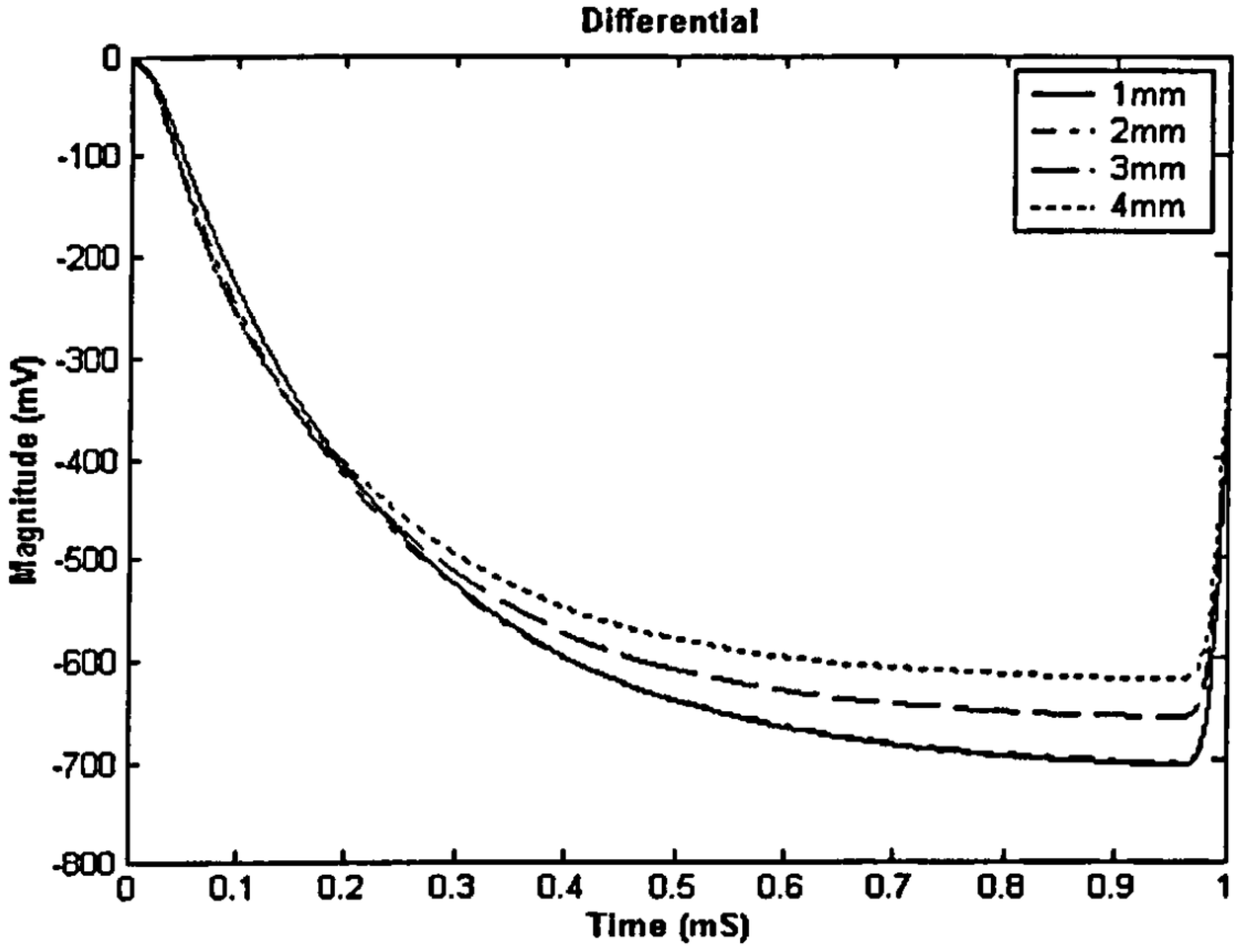

Figure 6-9 Sub-surface Slots (magnetised)

To improve the discrimination further, normalisation of signals is carried out before differential signals are derived. It is thought that this will also help reduce magnetic property and magnetisation level variations. The results are shown in Figure 6-10 and Figure 6-11. The time and magnitude of the peaks and the troughs clearly have some correlation with the corresponding slots depths, especially the sub-surface signals. The discrimination of depth of the surface slots is not very good. It is suspected that the depths of the slots are beyond the sensitive range of the sensor used in the experiment. Different shapes between the surface and sub-surface signals can be used to discriminate location of the detected slot.

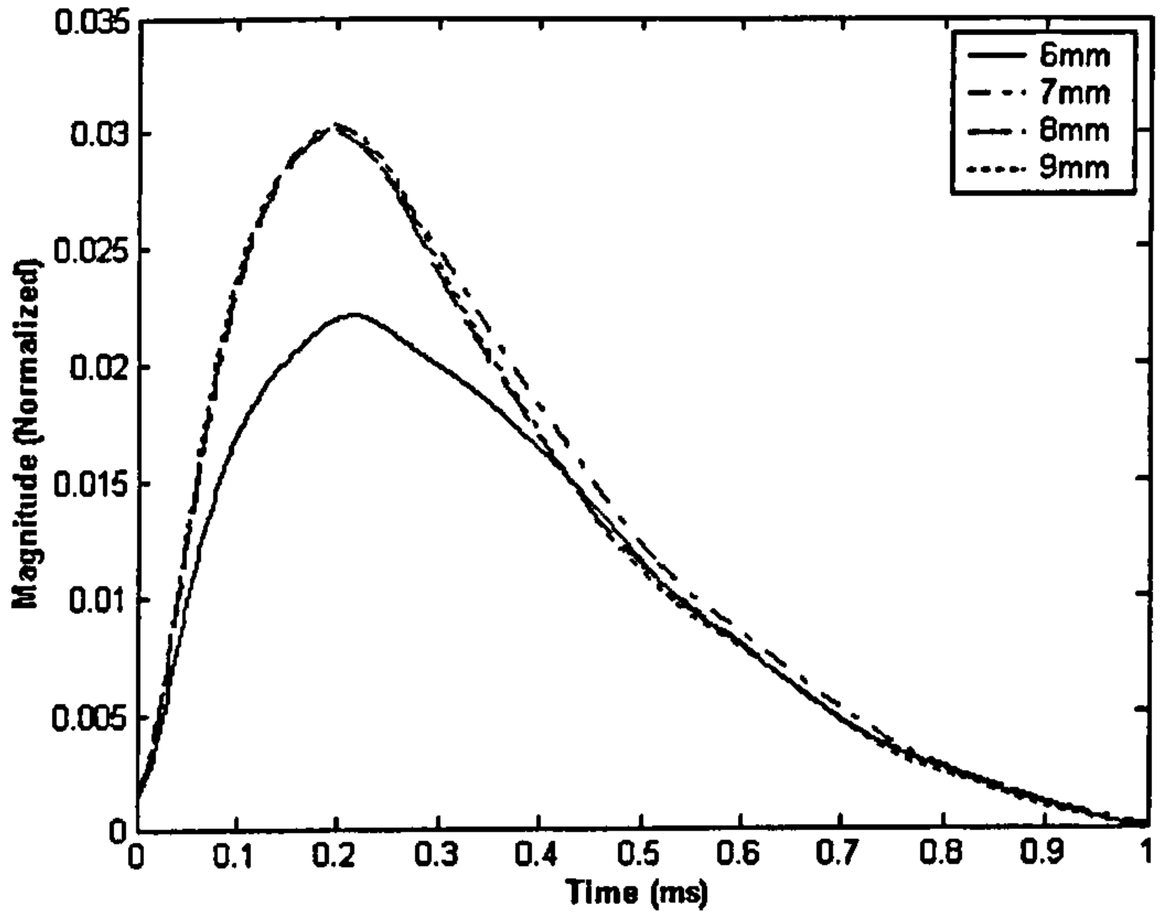

Figure 6-10 Surface Slots (magnetised)

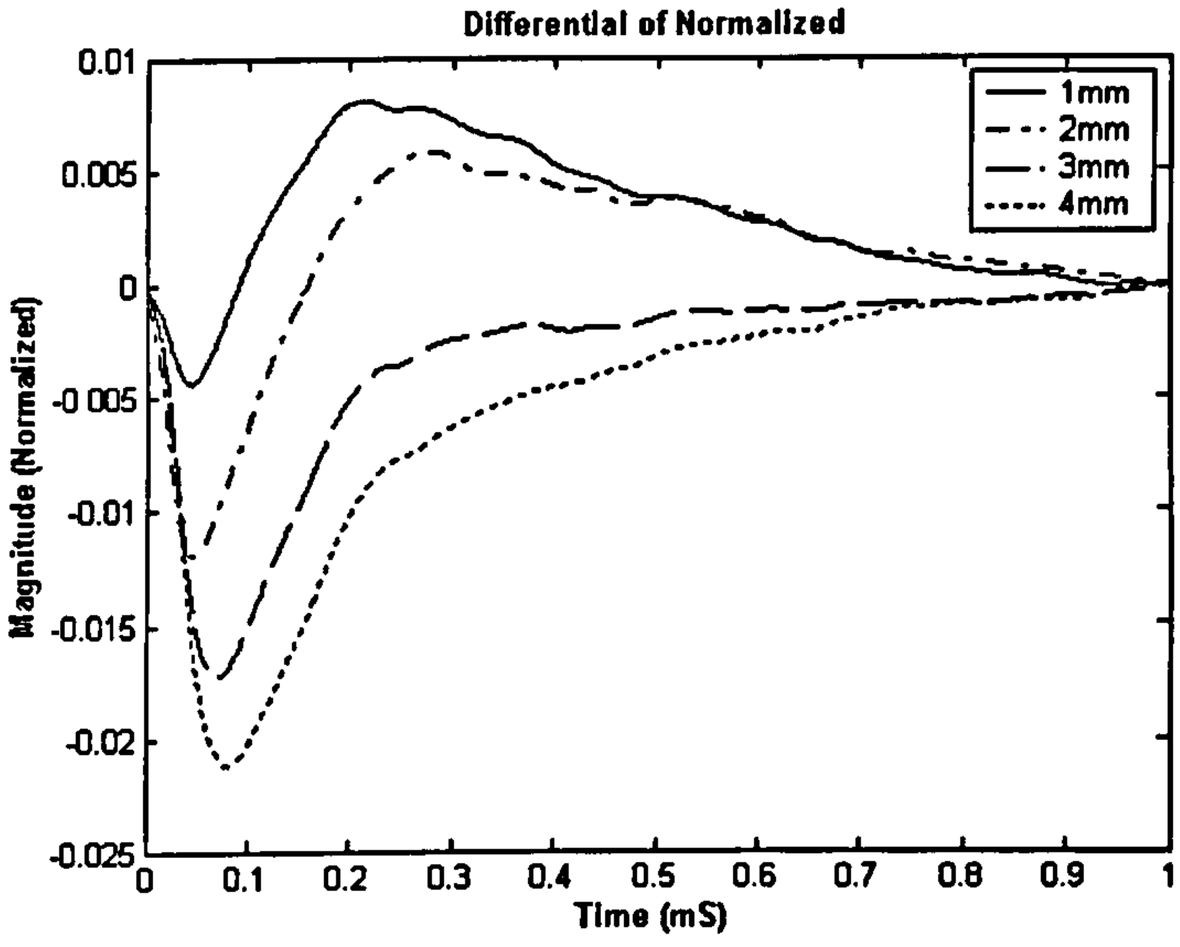

Figure 6-11 Sub-surface Slots (magnetised)

Figure 6-12 displays that the good classification is not achieved by the PCA-Wavelet technique. The graph in the Figure is a plot of differential PCA coefficients w_2 against differential PCA coefficients w_1. The graph in Figure 6-13 show how flaw classification is successfully achieved by using the newly proposed PCA-based feature extraction when the steel is magnetised during measurements.

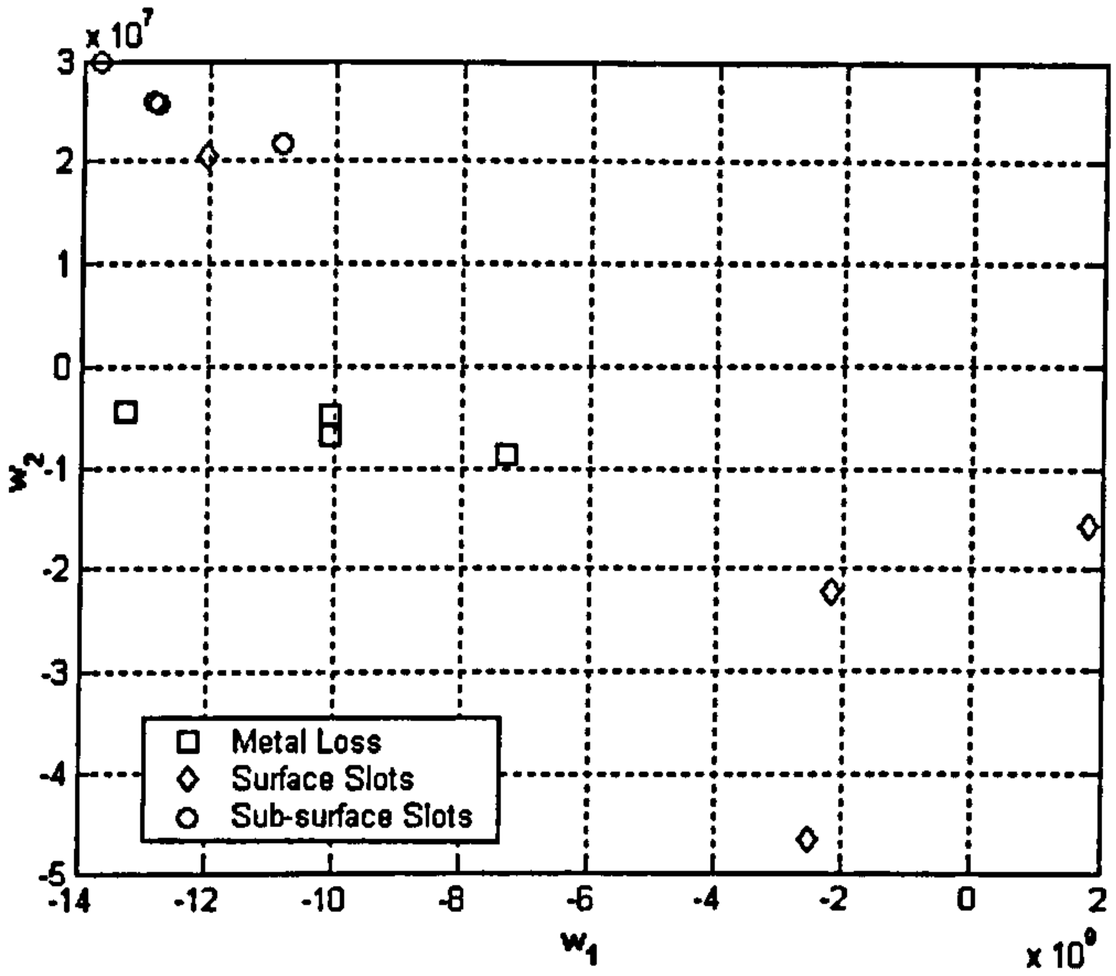

Figure 6-12 Unsuccessful Defect Classification without Magnetisation

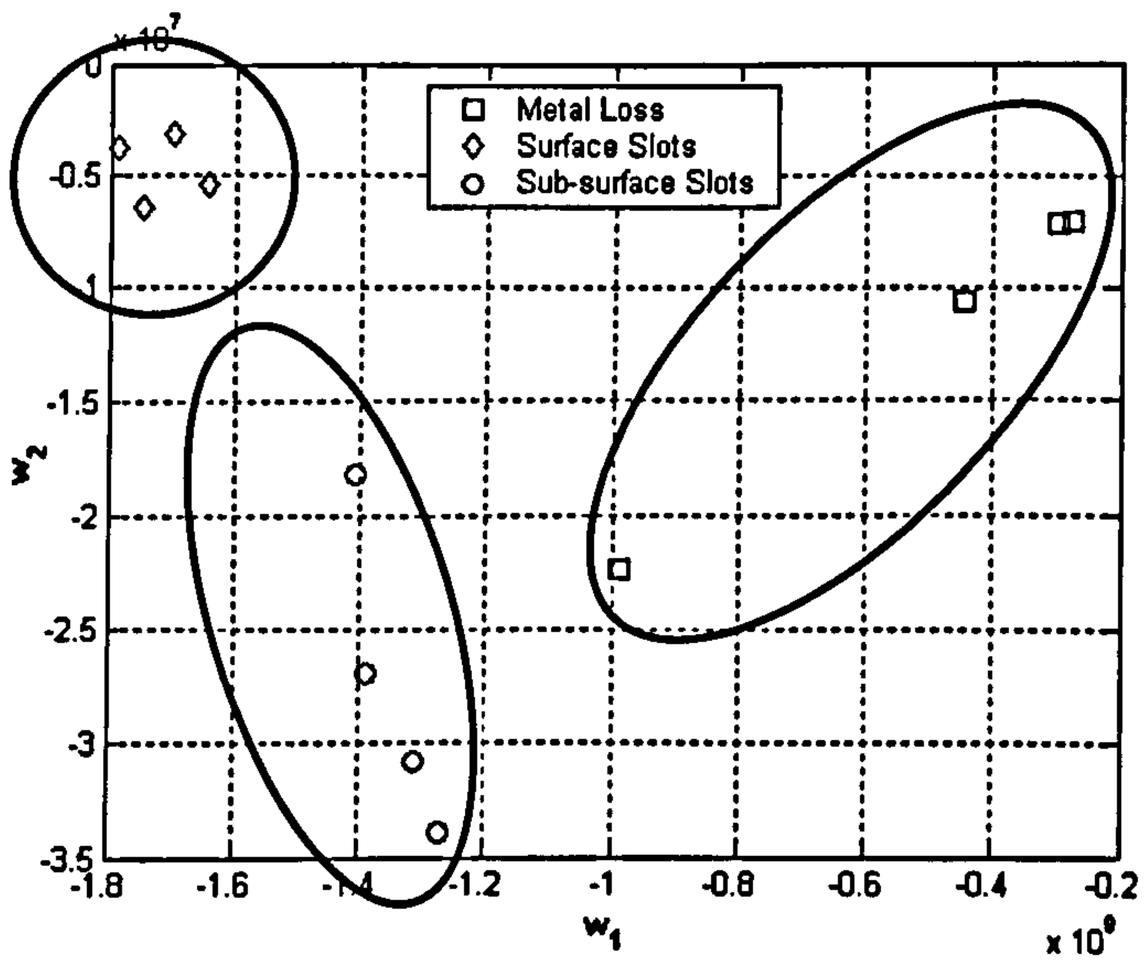

Figure 6-13 Defect Classification with Magnetisation

6.5 Summary

In this chapter, following a common practice in electromagnetic NDT steel inspection the use of magnetisation with PEC has been suggested for flaw detection in ferromagnetic steels. The magnetisation is used to magnetically saturate the sample to suppress the relative permeability of the sample and its variation across the sample.

The results show that the magnetisation has improved the signal strengths and has made deeper inspection into steel possible. It has also been shown that the magnetisation based PEC technique is able to quantitatively characterise sub-surface defects with good resolution using the differential normalised signals. The discrimination between surface and sub-surface defects is also shown by the shape of the differential signals, mainly the differential of the normalised signals. The same technique can be expected to gain similar benefits when applied on other conductive ferromagnetic materials.

The results also show the robustness of the developed feature extraction technique that successfully performs the classification of flaws in the ferromagnetic samples.

Chapter 7. Testing on An Aircraft Lap Joint Sample

7.1 Background

The proposed technique has shown promising results in the previous two chapters. In this chapter, a sample aircraft lap joint is used as a case study for testing purposes. This case study will investigate how the new feature extraction technique can be used with samples that are more practical from industry.

Most research on PEC has been undertaken for aircraft inspection. Parts of aircraft that consist of multi layers present a difficult task to other NDT techniques such as ultrasonic NDT techniques, the most widely used NDT techniques after the visual inspection. This is why PEC, which has an ability to scan through different depths simultaneously and a relatively deep penetration capability, is considered as a suitable technique.

7.2 Experimental Setup

The sample used in this experiment was provided by an industry. Two plates of aluminium are joined together by using rivets. Slots were manufactured on the top and bottom plates. The lengths of the slots fall into three different sizes, namely 6.35 mm, 12.7 mm and 25.4 mm. The location and the size of the slots are illustrated in Figure 7-1. The thick lines inside the illustration represent top or surface defects and the thin lines represent bottom or sub-surface

defects. The details of the surface and sub-surface defects under the rivets can be seen in Figure 7-2. One of the main challenges of the classification of flaws in the sample comes from the lift-off variation due to protruding rivets. The protruding parts of the rivets prevent the sensor maintaining a close contact with the surface of the lap joint sample.

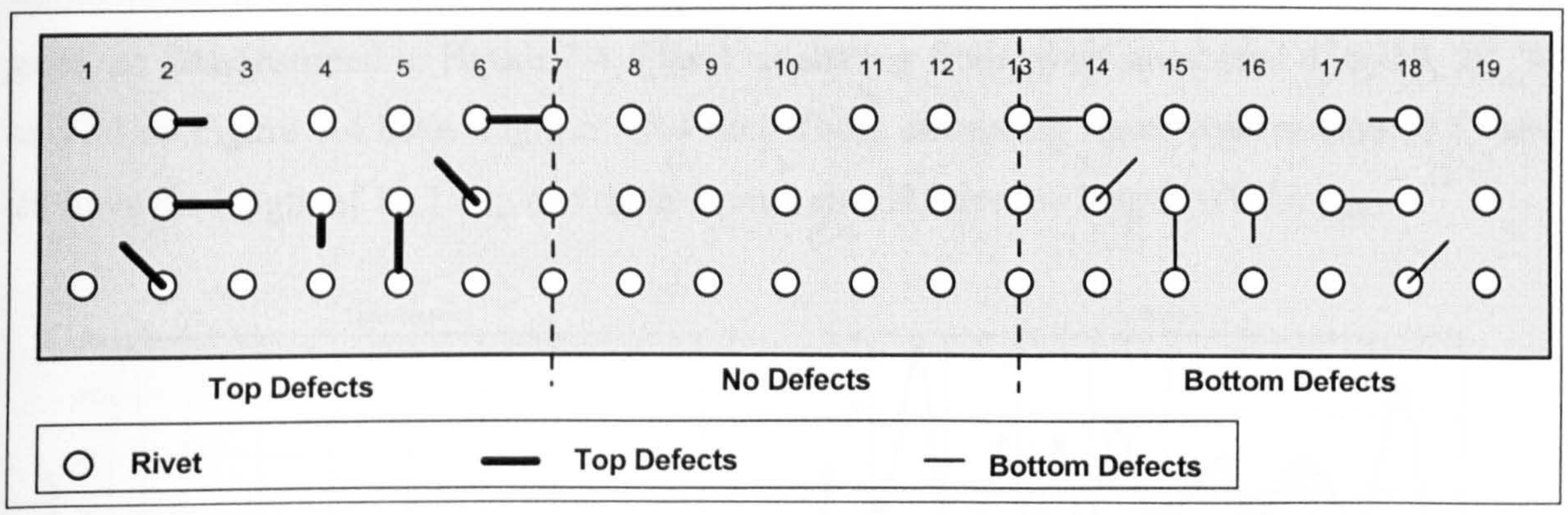

Figure 7-1 Lap Joint Defect Sample Layout

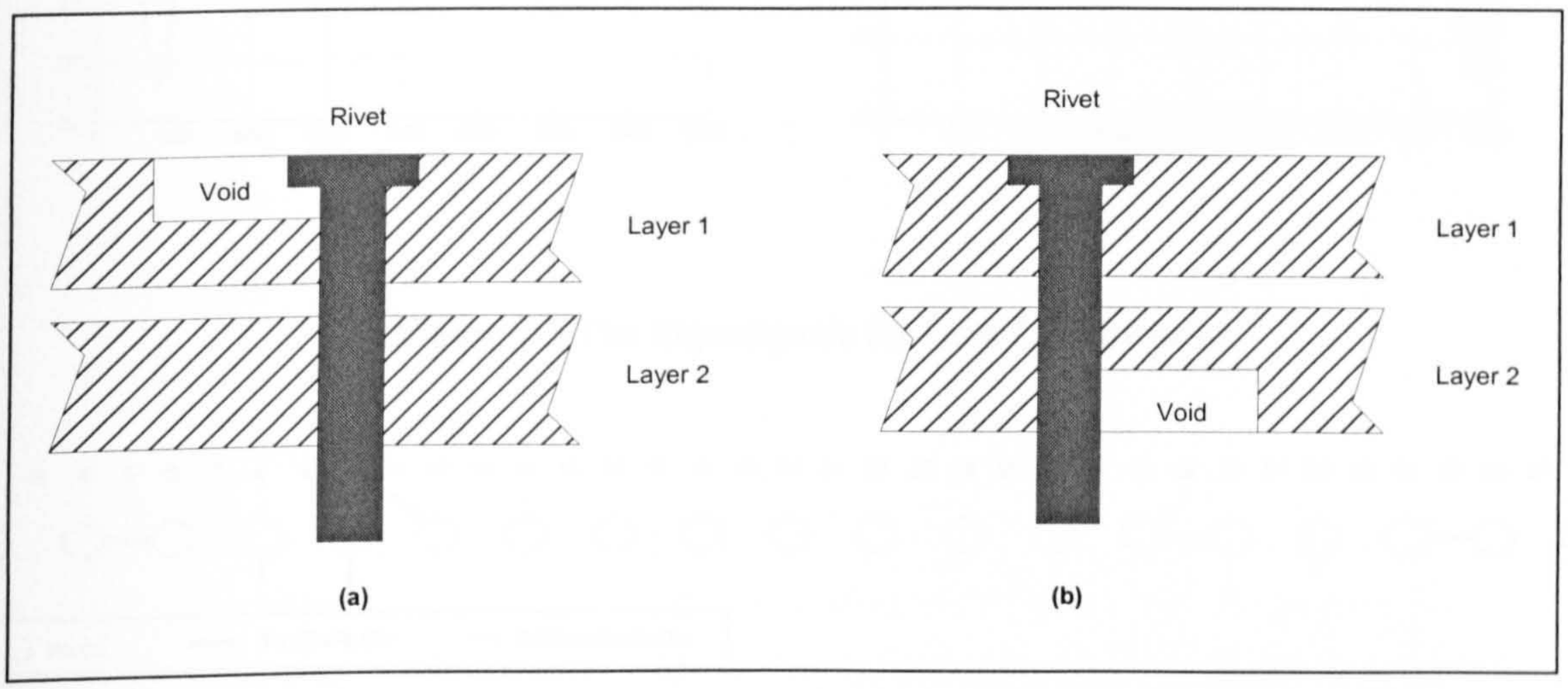

Figure 7-2 Rivet and Flaw Structures: (a) Top defect; (b) Bottom defect

Wavelet-PCA technique performance is investigated in the detection and classification of flaws in the sample and will be compared against that of peak-characteristic based technique. For training, both top and bottom flaws and some healthy parts on the top row are used. Based on the signals obtained, eigensignals are generated, which are shown in Figure 7-3. To test the application of the technique based on the training, the middle row that has the most flaws is

used. The probe will be 'scanned' from rivet 1 on the left hand side to rivet 19 on the right hand side on the middle row. Readings are taken when the probe is on the rivet and in the middle of gaps between rivets and also the outer sides of the rightmost and leftmost rivets, so there will be 39 measurements in total. The observations are numbered 1 to 39 with even numbers for measurements on the top of rivets and odd numbers for those on the in-between gaps, as demonstrated in Figure 7-4. Flaws emanating from rivets numbered 4, 6, 10, 30, 34 and 36 on Figure 7-4 have length of 25.4 mm. Those emanating from rivets numbered 11 and 29 have the length of 12.7 mm and those from 8 and 32 have the length of 6.35 mm.

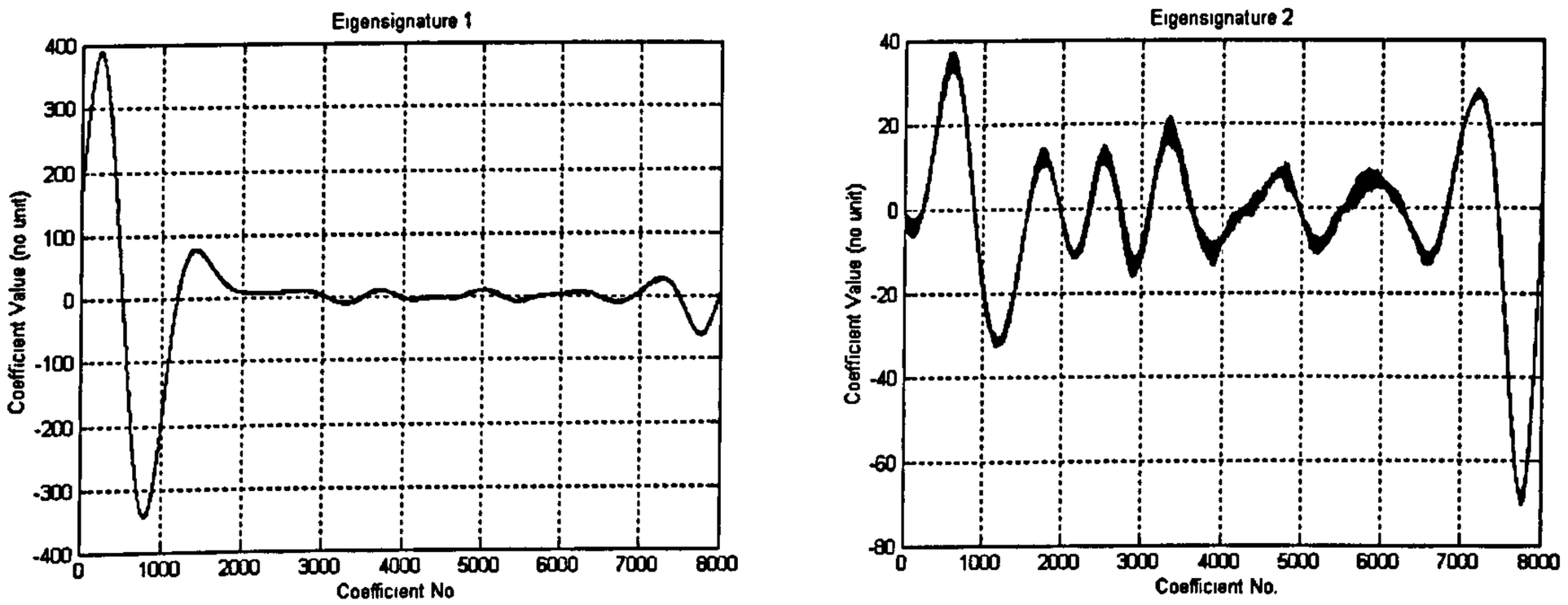

(a) (b)

Figure 7-3 The Eigensignals for Flaw Classification

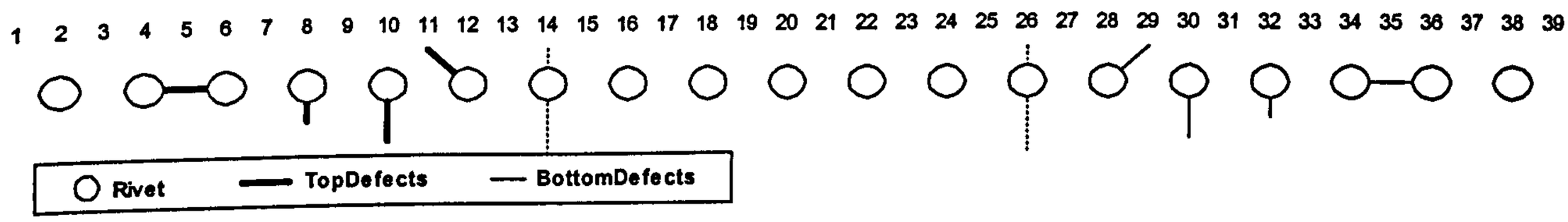

Figure 7-4 Row 2 and Location Numbering for Experiment

7.3 Results and Discussion

Using the data set described in the previous section, eigensignals are derived. The Wavelet-based PCA technique is used to generate the differential PCA coefficients w_1 and w_2 using the eigensignals. Figure 7-5 shows the plot of PCA coefficients w_1 and w_2 for classification using the proposed PCA-Wavelet technique. It shows that for this application, linear discrimination is possible. The majority of flaws have been grouped together according to their type successfully. However, there are 2 flaws that have not been detected or identified correctly, which are flaws with numbers 8 and 32. These are flaws with length of 6.35 mm, the shortest among the available flaws. The inability to correctly identify the two flaws could be due to the sensitivity of the sensor used as the sensor was not optimised for the aircraft sample.

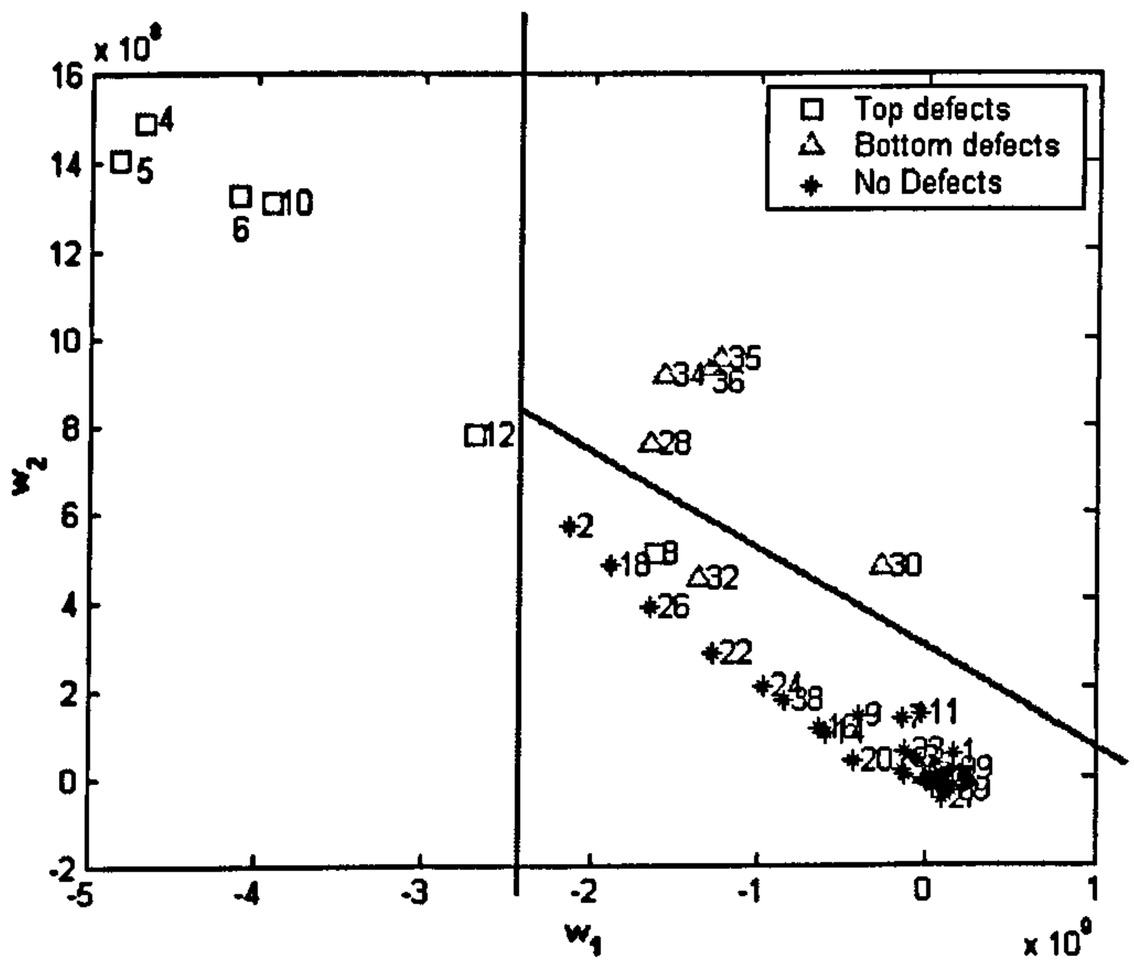

Figure 7-5 Classification of Flaws using the PCA-Wavelet Technique

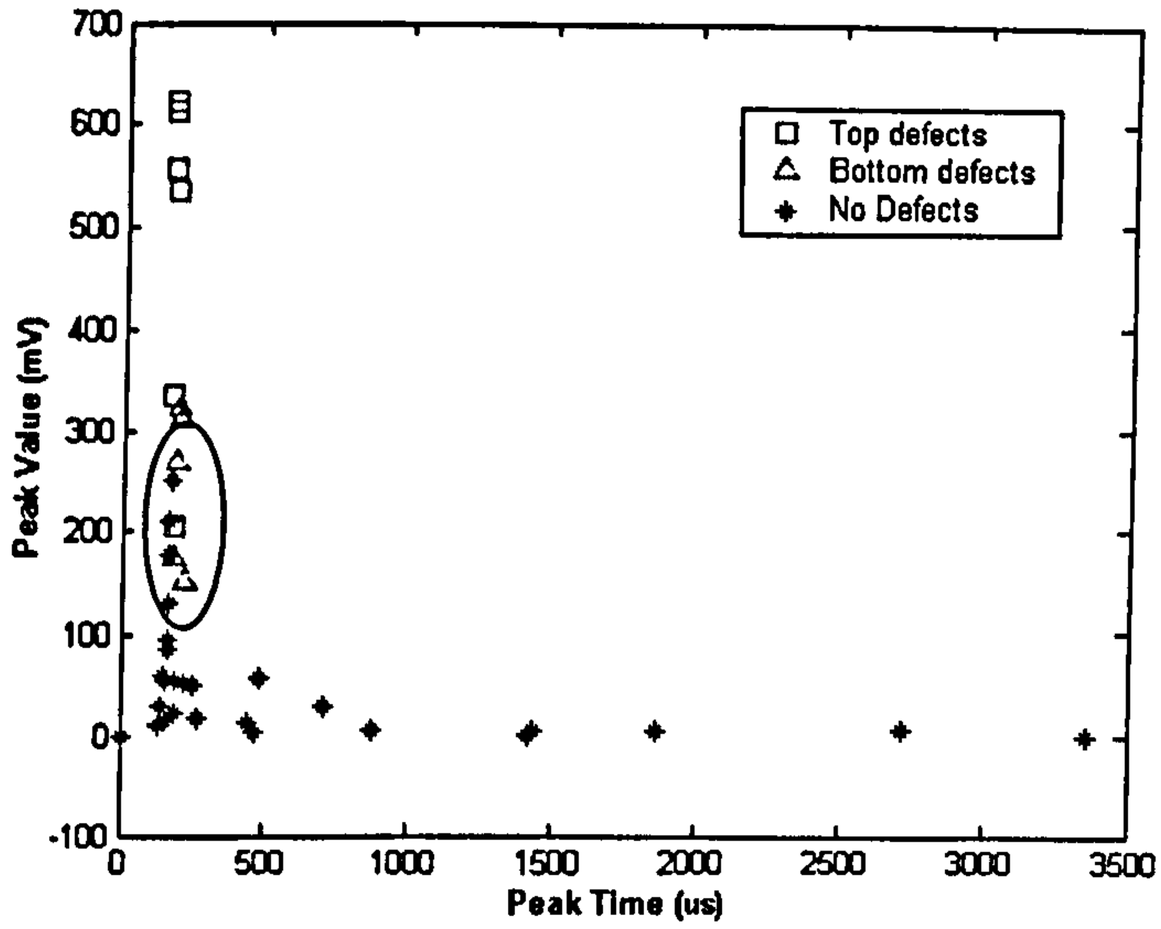

Figure 7-6 Classification using Peak Times and Values

Figure 7-6 shows the classification achieved using peak times and values. As illustrated in Figure 7-6, all the points in the circle represent signals from protruding parts. The no-defect and bottom defect signals are mixed in this area. Based on the comparison of Figure 7-5 and Figure 7-6, it can be seen that the performance of Wavelet-based PCA technique is better than that of conventional signal-peak-based approach. The performance of the traditional approach is degraded when dealing with the protruding parts.

7.4 Summary

In this chapter, a more practical sample from industry is used to evaluate the system and the proposed feature extraction technique. The sample is multi-layered and it has been shown that the system using the proposed feature extraction technique based on PCA and Wavelet transform is able to detect all the flaws but the shortest ones, and classify them according to their type, namely surface and sub-surface. It has also been shown that the performance is better than that of signal-peak-based technique.

The results also demonstrate that adaptability of the proposed technique to an industrial sample. In the experiment, it has performed the classification in a multi-layered sample, in contrast to the single-layered samples in the previous experiments.

It should be pointed out that such results are obtained despite the conditions that the probe is not specifically designed for the application and the lift-off variations due to protruding rivet heads. Better results might be achieved by using probes designed to maintain constant distant to the plate surface despite the rivet heads.

Chapter 8. Dynamic Behaviour Investigation and Evaluation

8.1 Background

The Wavelet-based PCA is a signal shape-based approach, whose sample is captured over a period of time, and may have a problem for dynamic measurement. Many industrial applications, such as a railway track manufacture, require on-line dynamic defect inspection for effectiveness. Ideally, such a dynamic defect monitoring can inspect and feed forward signals to control manufacturing processes. This capability will enable time and cost saving. To this end, the speed of data acquisition and processing must be optimised, and this speed or response frequency is an important parameter of dynamic behaviour of the chosen NDT system. One way of achieving this could be by minimising the length of the signal to be processed so long the output is still acceptable.

In PEC, the coil is excited by repeated pulses of a specified width. For every pulse, a set of response signal points are sampled. To optimise the dynamic response of PEC systems, the frequency of excitation pulses should ideally be as high as possible and/or the sample data of signals for each pulse should be reduced while the sampling frequency may be same. This means that the excitation pulse width should be made as small as technically possible, without reducing the overall performance of the system in achieving the desired targets. However, there are restrictions that need to be observed when determining the minimum effective pulse width.

When using the conventional technique, the maximum arrival time of the peak will determine the narrowest or minimum effective pulse width. The maximum arrival time depends on the target material and anticipated defect location in the target. The peak arrival times are relatively small for surface cracks, while for sub-surface cracks, they are directly proportional to the depth of the crack.

The proposed feature-based technique observes the transient signature of the signals rather than specific sample values, therefore it could be expected that the technique remains effective with smaller pulse widths. In this chapter, we will investigate and evaluate the dynamic behaviour of our PEC systems and conventional PEC systems. To evaluate the dynamic response, the minimum effective pulse widths will be searched. Effective pulse widths are the ones that allow effective defect classification and quantification.

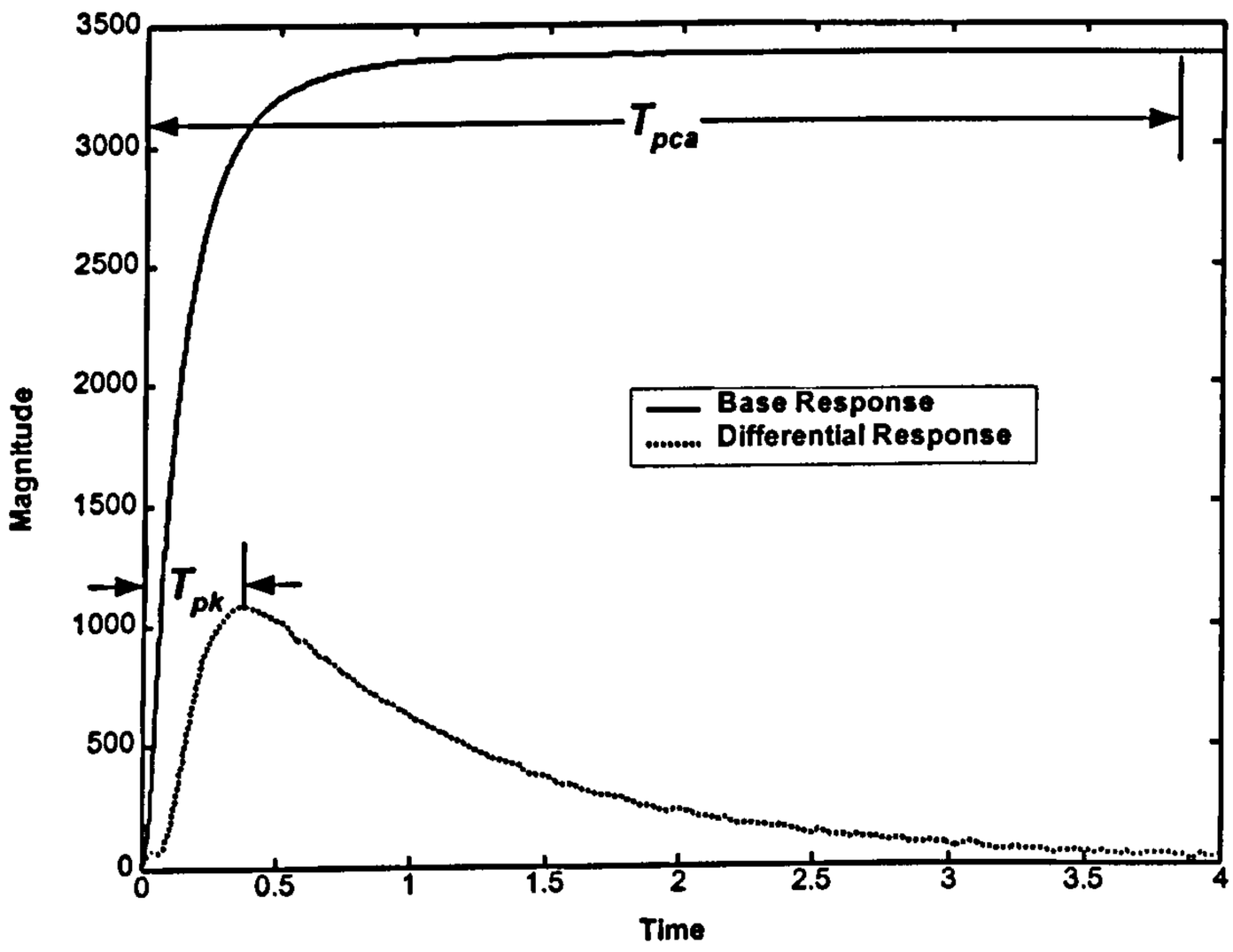

Figure 8-1 Signals and Notations

For the PCA feature extraction, a base response signal segment from t=0 to t=T_{pca} is used for each analysis, Figure 8-1 clarifies the notations. The smaller the signal segment used (i.e. T_{pca}), the more efficient the processing and the higher the response frequency will be. The experiment will establish the minimum effective pulse width using the conventional and the

Wavelet-based PCA feature extraction techniques, hence a conclusion as to the expected maximum inspection speed can be drawn. The value of T_{pca} corresponds to the pulse width in the real implementation of the PCA-based technique. For the conventional technique, the chosen pulse width should not be smaller than the anticipated peak arrival times T_{pk}. The experiment will show if T_{pca} can be smaller than T_{pk}.

8.2 Experimental Setup

The experiment is designed to investigate dynamic behaviours of different PEC signal processing techniques and the maximum possible processing speed of PEC signals using the Wavelet based feature extraction for the PEC inspection. During the experiment, the value of T_{pca} will gradually be reduced and both defect classification and quantification results be analysed. Samples of different materials, namely aluminium and carbon steel, are used in the experiment.

For this testing purpose, two aluminium samples as described in Chapter 4 are used. The samples can be seen in Figure 8-2.

Figure 8-2 Aluminium Samples: (a) Metal Loss, (b) Surface and Sub-surface Slots

For the sake of readable result presentation, only some of the discontinuities will be used. Table 8-1 lists the chosen discontinuities.

Defect No.	Defect Type	Depth
1	Metal Loss	20% (2mm)
2	Metal Loss	40% (4mm)
3	Metal Loss	60% (6mm)
4	Metal Loss	80% (8mm)
5	Surface slot	2mm
6	Surface slot	4mm
7	Surface slot	6mm
8	Surface slot	8mm
9	Sub-surface slot	2mm
10	Sub-surface slot	4mm
11	Sub-surface slot	6mm
12	Sub-surface slot	8mm

Table 8-1 Chosen Defects for Experiment

Two steel samples described in Chapter 6 are also used for a similar experiment to investigate the dynamic response with a different sample material and to investigate the applicability of the technique used with different materials. The layout of the samples is shown in Figure 8-3. To eliminate magnetic property variations and to allow deeper eddy current penetration, the steel samples are magnetised into saturation.

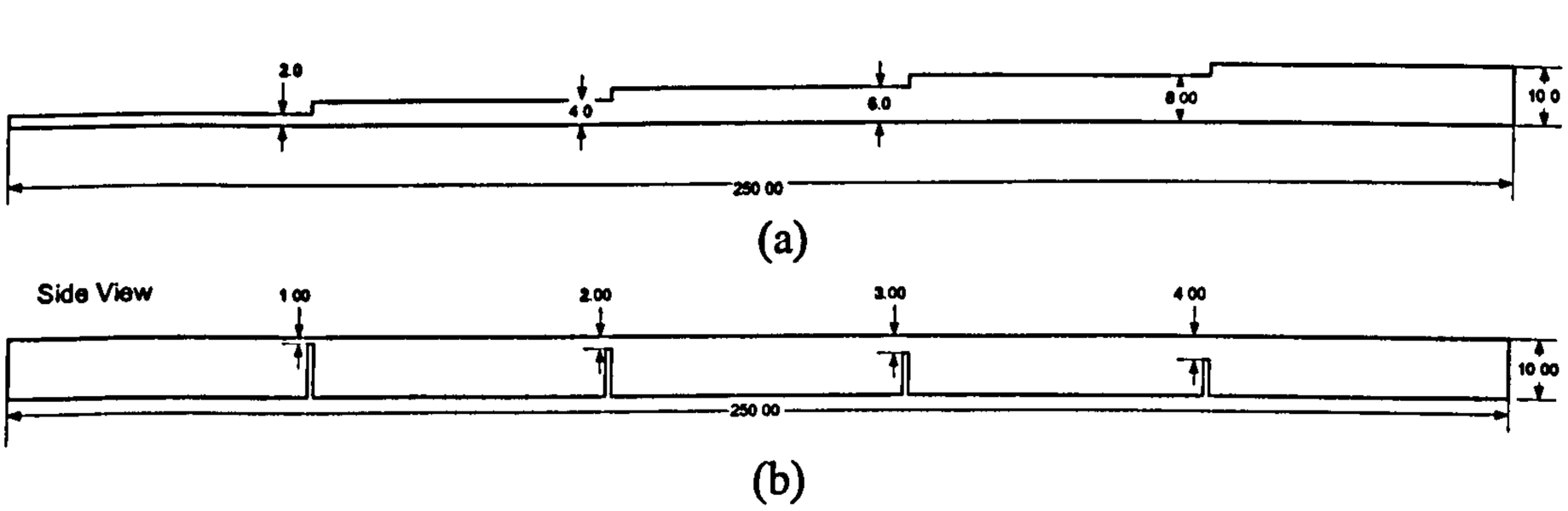

Figure 8-3 Steel Samples: (a) Metal Loss, (b)Surface and Sub-surface Slots

8.3 Experimental Results and Discussion

Table 8-2 below shows the measured time to peak for the chosen defects. The results show that for the chosen defect range, the maximum peak arrival time is 2.15 ms. This implies that the minimum effective pulse width is 2.15 ms.

Defect No.	Defect Type	Depth	t_{pk} (ms)
1	Metal Loss	20% (2mm)	2.15
2	Metal Loss	40% (4mm)	1.57
3	Metal Loss	60% (6mm)	0.86
4	Metal Loss	80% (8mm)	0.43
5	Surface slot	2mm	0.14
6	Surface slot	4mm	0.15
7	Surface slot	6mm	0.15
8	Surface slot	8mm	0.15
9	Sub-surface slot	2mm	0.31
10	Sub-surface slot	4mm	0.62
11	Sub-surface slot	6mm	1.46
12	Sub-surface slot	8mm	1.70

Table 8-2 Measured Time to Peak

For the Wavelet-based PCA feature extraction, initially T_{pca} was set to 4.0 ms and then reduced gradually. Table 8-3 and Table 8-4 show the comparison of flaw class and size identification rate using the conventional technique and Wavelet-based PCA. For the latter, results based on different sampling periods T_{pca} have been presented. The rates were computed using the same method as explained in Chapter 5.

It can be seen that the performance of Wavelet-based PCA can match the conventional even when the T_{pca} is reduced to 0.5 ms. This is a significant achievement when compared to the conventional technique that needs more than 2.0 ms to obtain the same performance. However, it can also be seen that the depth sensitivity has reduced significantly when the T_{pca} value is less than 0.9 ms is used. This is signified by the start of misidentification of defect no. 3, which is a metal loss of 4.0 mm. This misidentification did not happen when the T_{pca} was larger or equal to 0.9 ms. Therefore it can be said for the given system and sample conditions, T_{pca} of 0.9 ms is the optimal solution. Figure 8-4 shows the classification using T_{pca} of 4.0 ms and 0.9 ms. Here the plots of differential PCA coefficients w_1 against w_2 are shown. The graph in Figure 8-4(b) shows the resulting coefficients which are derived using reduced signal's T_{pca} of 0.9 ms.

Defect No.	Peak Time and Peak Value	Wavelet-based PCA					
		4 ms	1 ms	0.9 ms	0.7 ms	0.5 ms	0.25 ms
1	100	100	100	100	100	100	100
2	100	100	100	100	100	100	100
3	80	100	100	100	80	80	80
4	80	100	100	100	100	80	80
5	100	100	100	100	100	100	100
6	100	100	100	100	100	100	100
7	100	100	100	100	100	100	100
8	100	100	100	100	100	100	100
9	100	100	100	100	100	100	100
10	100	100	100	100	100	100	80
11	100	80	80	80	80	80	80
12	40	60	60	60	60	60	60
Overall	91.7	95.0	95.0	95.0	93.3	91.7	90.0

Table 8-3 Defect Class Identification Rate

Defect No.	Peak Time and Peak Value	Wavelet-based PCA					
		4 ms	1 ms	0.9 ms	0.7 ms	0.5 ms	0.25 ms
1	100	100	100	100	100	100	100
2	100	100	100	100	100	100	100
3	80	100	100	100	80	80	60
4	80	100	80	80	80	80	20
5	100	100	100	100	100	100	100
6	100	100	100	100	100	100	100
7	100	100	100	100	100	80	80
8	80	80	80	80	80	80	80
9	100	100	100	100	100	100	100
10	100	100	100	100	100	100	80
11	40	60	60	80	80	60	80
12	0	40	40	40	40	40	0
Overall	81.7	90.0	88.3	90.0	88.3	85.0	75.0

Table 8-4 Defect Size Identification Rate

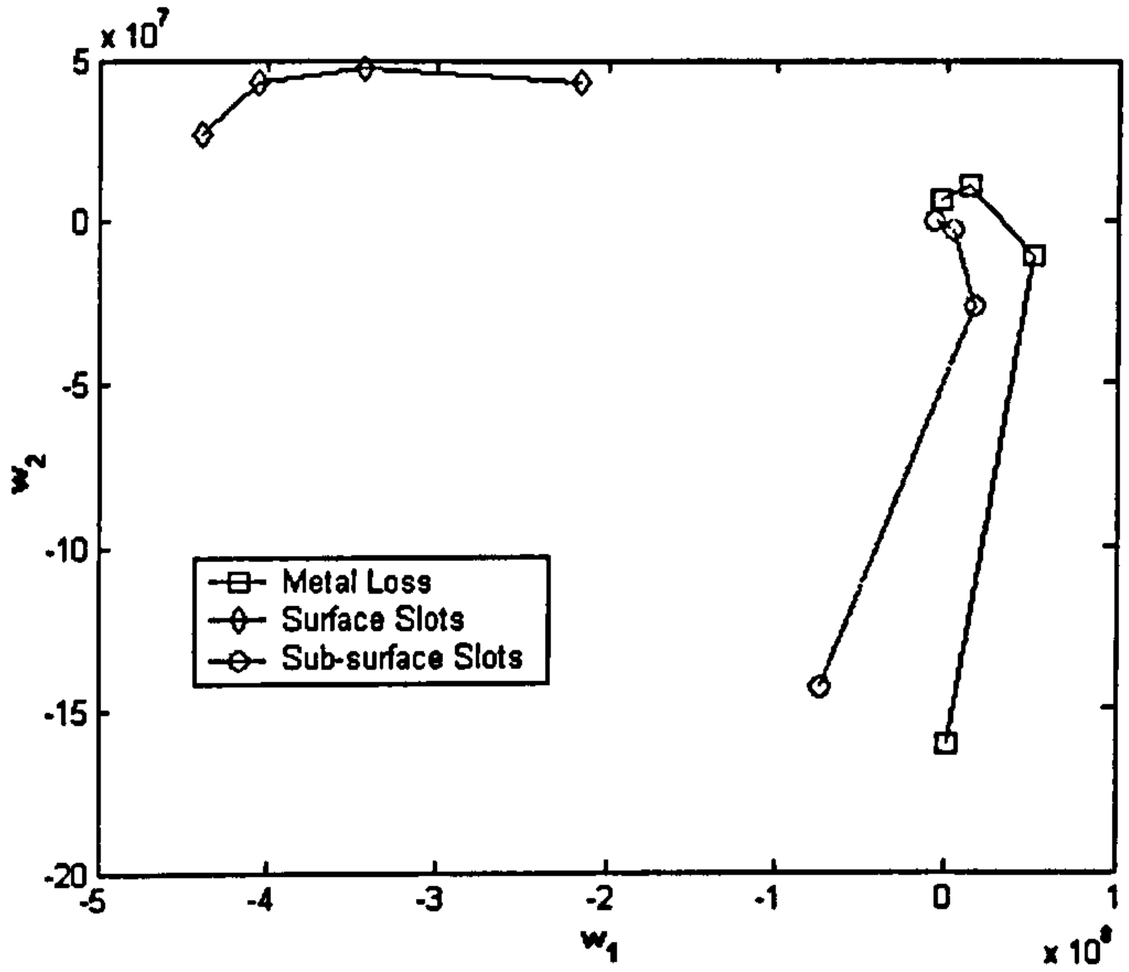

(a)

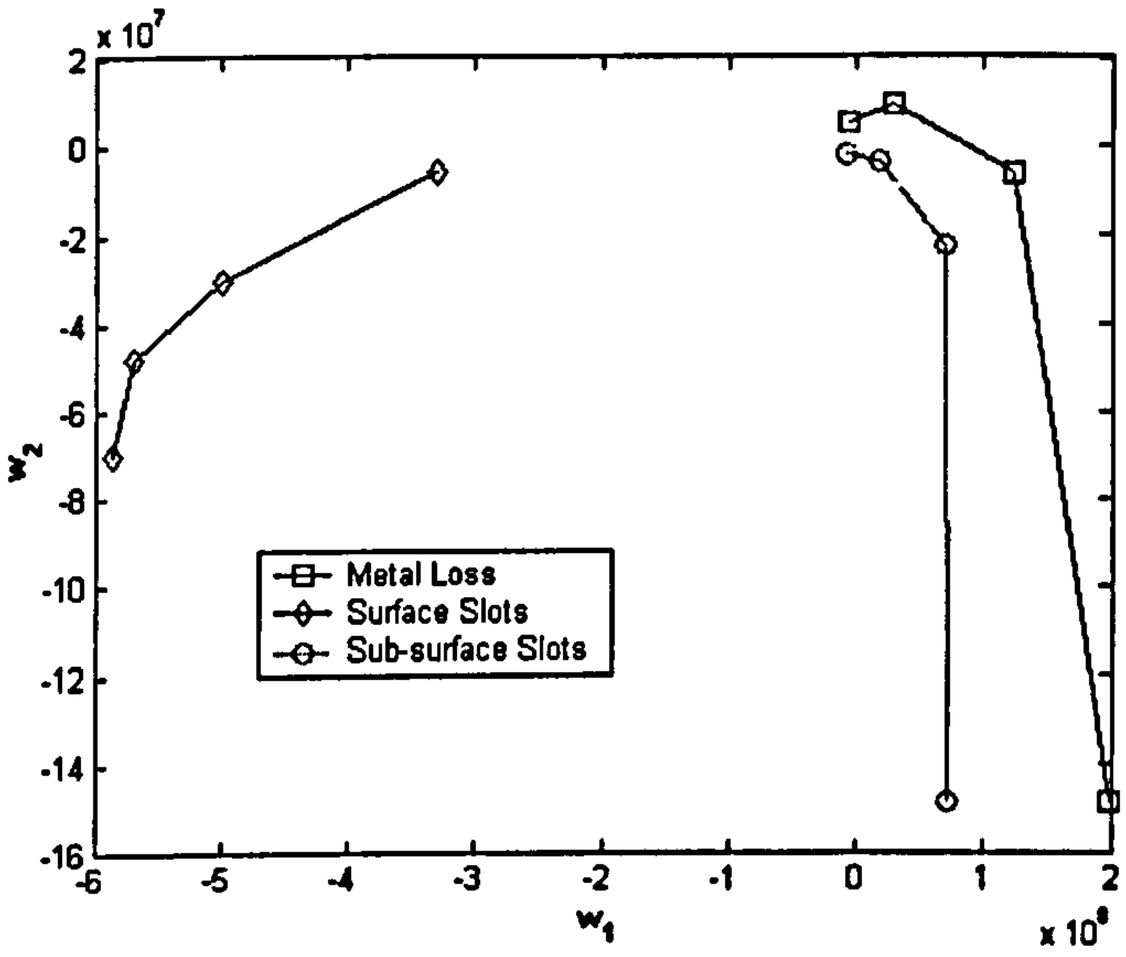

(b)

Figure 8-4 Classification of Defects using Wavelet-based PCA technique: (a) *Tpca* = 4.0 ms, (b) *Tpca* = 0.9 ms

From the experiments with steel samples under magnetisation, it is observed that most of the differential signals are exponential-like and do not have turning peak points, therefore the conventional PEC technique will be impractical without modification, particularly for inspection of ferromagnetic targets with magnetisation. On the other hand, the experiments

show that with the use of PCA-Wavelet based feature extraction, T_{pca} can be reduced down to 0.25 ms whilst still being capable of discriminating the defect types. The clustering of the defects under this condition is shown in Figure 8-5(b), while Figure 8-5(a) shows the classification when T_{pca} =2.0 ms. The figure shows that the defects are successfully clustered into defect type groups accordingly.

Table 8-5 summarises the minimum pulse widths or the smallest sampling periods for different PEC techniques. The new T_{pca} for steel is sufficiently fast for many on-line dynamic inspection systems, including the ones used in a rail track manufacturing line that has a typical inspection movement speed of 0.6-1.6 m/sec. In this particular case, the target will move 0.18-0.48 mm during each sampling period. The identified defects will be the average effect from the span of 0.18-0.48 mm long. This average effect from the motion will be acceptable when considering the diameters of the excitation coil range between 7-15 mm. In conclusion, the PEC system and its PCA based feature extraction have very good potential to be used in dynamic defect monitoring systems.

Technique	Test Material	Minimum Pulse Width (ms)
Peak Value and Peak Time	Aluminium	2.15
	Steel	N/A
PCA	Aluminium	0.9
	Steel	0.25

Table 8-5 List of Minimum Pulse Width

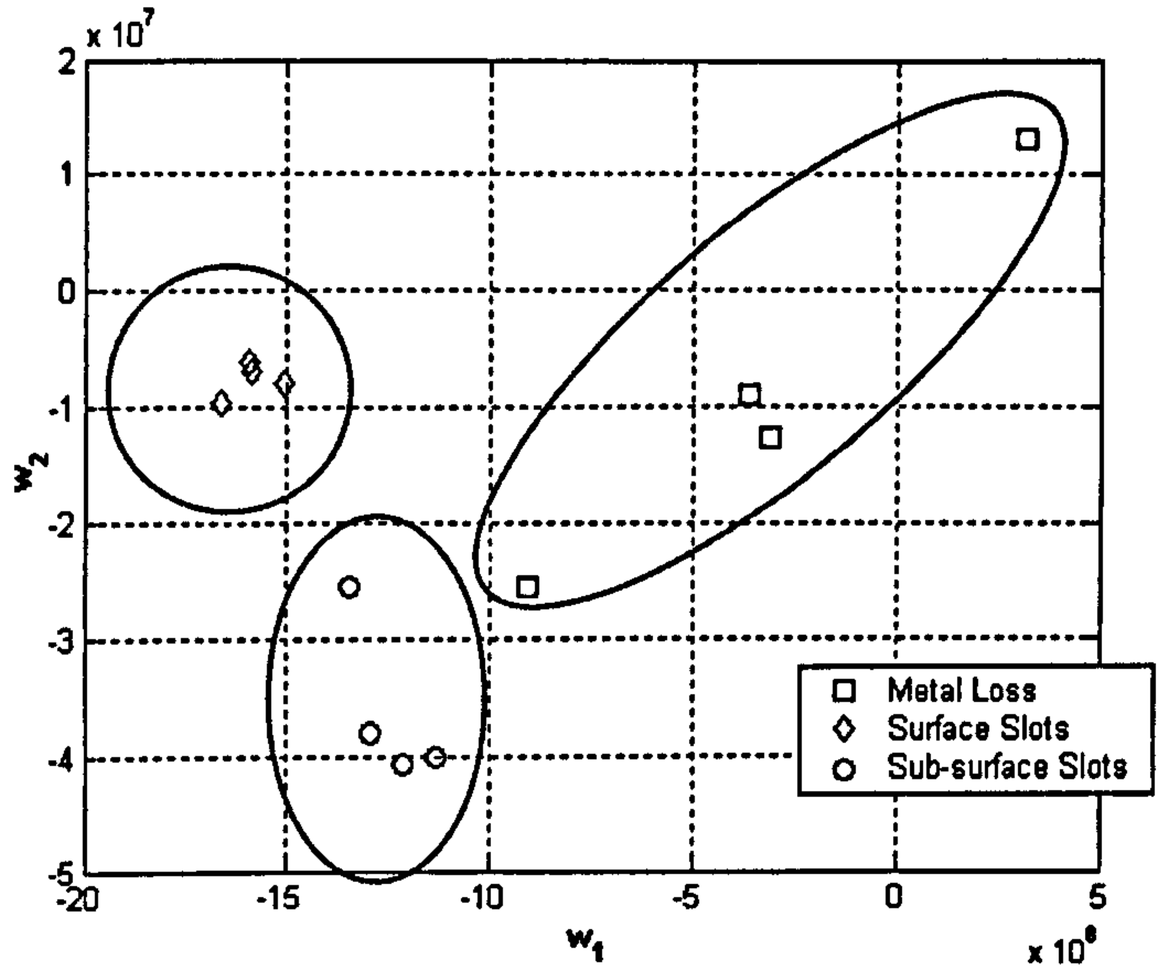

(a)

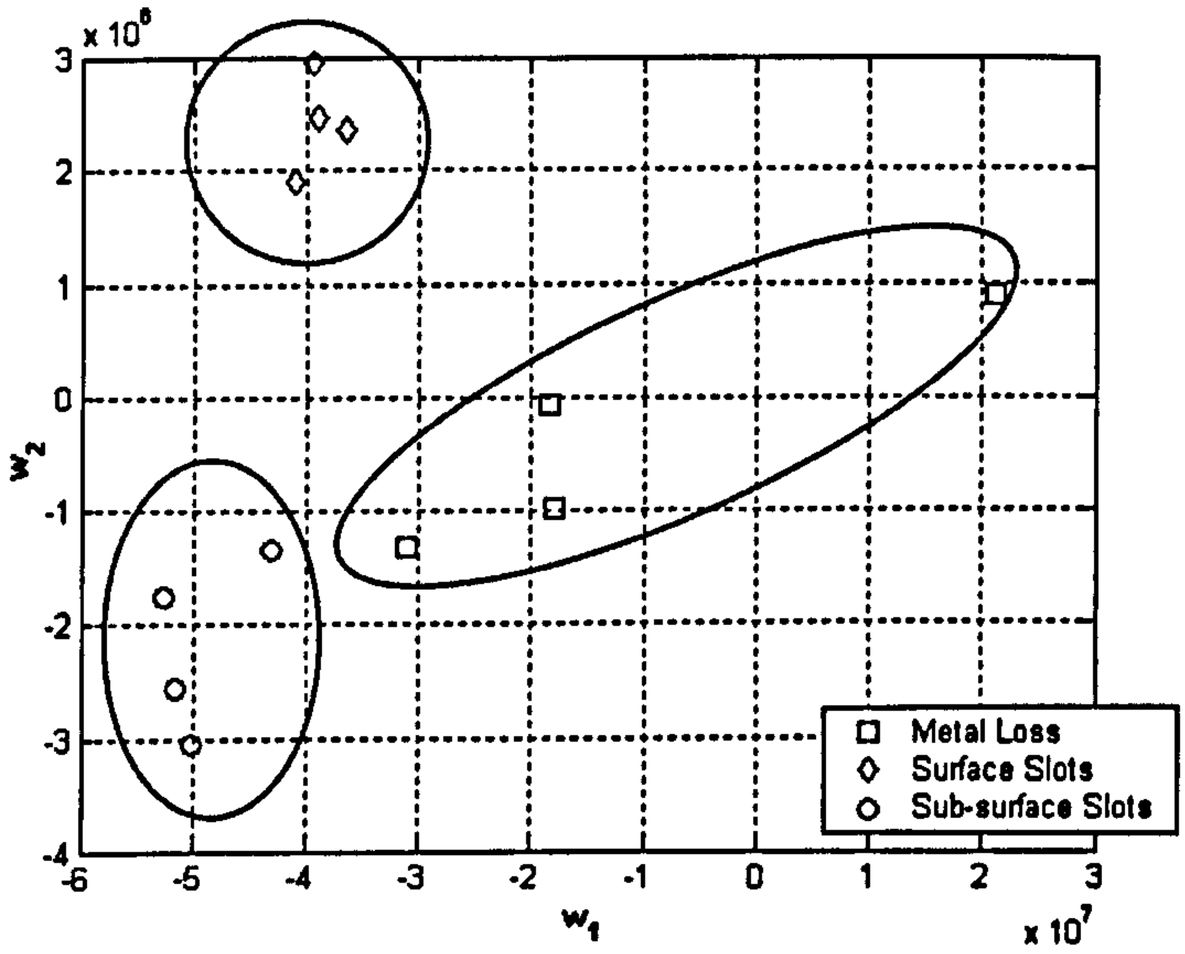

(b)

Figure 8-5 Classification of Flaws in Steel Samples using Wavelet-based PCA technique: (a) *Tpca* = 2.0 ms, (b) *Tpca* = 2.5 ms

8.4 Summary

In this chapter, the dynamic behaviour of the PEC system using both the signal peak parameters and the newly proposed technique is investigated. In the experiments, the signal's length in time is gradually reduced and the ability of the new technique in flaw classification is monitored. The dynamic response including data processing is much faster than conventional PEC technique using peak time and peak value features. The PCA feature-based technique is able to produce indication of the defect type with smaller pulse widths. Subsequently, this leads to faster information gathering. This work shows the potential of the developed PEC system to be used for dynamic on-line inspection at both manufacturing and in-service stages.

Chapter 9. Further Work

The results of the research work have paved the way for further research on PEC systems and signal analysis. Further research needs to be carried out to improve the performance of our system itself and also to expand its functionalities by integrating the system with other NDT techniques or systems.

9.1 Further Research on Feature Extraction and Optimisation

Like other artificial intelligence and statistical approaches, the accuracy of flaw classification and quantification depends on the calibration samples. Further investigation will be undertaken by using wide range of defect samples for calculating PCA components. The selection of Wavelet base function, Wavelet levels and integration of PCA components will be optimised for improving the discriminability of signals for defects. Subsequently, the algorithms of feature extraction and flaw classification will be used for evaluation of the design and development of our PEC system. Various calibrated industrial samples will be inspected for evaluation of the proposed system and feature extraction method.

9.2 Lift-off Compensation

In this project, the experiments were carried out with controlled lift-off. In the next stage, the problem of lift-off should be investigated. Eddy current techniques are sensitive to lift-off variations that can easily mask flaw signals. The strategy in the investigating and resolving

lift-off related problems is to find a technique that is able to detect that lift-off is occurring. It will be investigated if the Wavelet-based PCA feature extraction can be used to quantify the lift-off and overcome the problem by separating the distance between the probe and the test from different PCA components.

9.3 PEC Sensor Arrays

In order to enhance the information obtained from the sample and to improve the inspection efficiency, the use of multiple sensors could be investigated in the future. The NDT sensors involved could be both uniform and mixed in separate investigations. The research will also include the data fusion, how to use the data obtained by all sensors in an integrated manner to produce extra information both quantitatively and qualitatively. When more information can be retrieved by using multi sensors, accompanied with flaw analysis using fracture mechanics, more accurate decision can be made regarding the future use of the inspected samples. Potentially this will lead to longer use of the inspected system and reduced costs.

9.3.1 Multiple Uniform Sensors

When uniform sensors are involved, each sensor is used to sense the measurands with different focus and from different viewpoints in an integrated manner. In future investigation, an array of Hall devices can be incorporated in the PEC probe to measure the distribution of magnetic flux density across the area under the probe. A two-dimensional 'image' can then be produced. Correlation features between the image and the structure of the probed area will be extracted by extending the above new technique. It is expected that more information in terms of quality and/or quantity is obtainable as more data are now available. Qualitative gains might implement as more reliable and accurate information. Quantitative gains might implement as more information such as the orientation and shape of the flaw, the variation of lift-off, or even 3D profiles of the flaw. Investigation needs to be done in order to establish the benefits of PEC sensor arrays using appropriate signal processing techniques.

Another potential advantage is the increase of testing speed as bigger area can be covered simultaneously, i.e. without moving the probe. The study of how to compensate the signal variation due to off-the centre Hall Devices is required.

9.3.2 Mixed NDT Sensors

The new feature extraction and flaw classification can be used for interpretation of other NDT signals such as ultrasonic and thermal images. Different NDT techniques have different advantages and they are complementary to each other. More than one NDT technique is generally required to inspect a structure or material, particularly for safety critical systems. For example, in railway inspection, ultrasonic and eddy current techniques are used complementarily. The eddy current is sensitive to flaws on and very close to the surface, while the ultrasonic is sensitive to deeper flaws. The inspection time could be reduced if both techniques are combined in one single system. In addition, extra information could potentially be obtained when advanced data fusion techniques with the help of the above proposed feature extraction technique are applied to the output data of both techniques. The automation of data interpretation and intelligent data fusion systems need to be developed for future NDT.

Based on this hypothesis, a collaborative research work between University of Warwick and University of Huddersfield will be carried out on an NDT system using a combination of pulsed Eddy current and ultrasonic techniques for railway inspection or other NDT applications. The use of multi-sensors requires rigorous research and development of communication, calibration, synchronisation, data-flow control, and multi-feature classification (Xiong and Svensson 2002).

Chapter 10. Conclusions

This thesis has reported the achievements and findings obtained in the research project. The main achievements of the research work include:

- Literature survey that brought understanding and familiarity with electromagnetic NDT techniques, PEC research work and the use of signal processing in ECTs. Part of the review was published.
- The new design of a PEC system that allows research work to be carried out and also becomes a basis for further development. Probe layouts and coil dimensions have been investigated through simulation and the results have been discussed.
- Design and development of a PCA or Wavelet-based PCA as a feature extraction method, which effectively extracts features from PEC signals for flaw classification. The PCA based features, which might be integrated with conventional peak time and peak value, can also be used for quantification. A hierarchical structure for defect classification and quantification has been introduced.

- Investigation on the performance of the proposed Wavelet-based PCA technique for dynamic measurements compared to the technique using peak time and peak height features.
- Magnetisation that minimises the effective permeability and its variations to improve the ferromagnetic material inspection results using a PEC system.
- Publications of the work through refereed journals and conferences.
- Two prototype systems have been established in the University of Huddersfield and TWI in Cambridge for demonstration of NDE applications.

The main contributions are highlighted in the following paragraphs.

A full PEC system has been designed and implemented. It provides a platform for the research work to be carried out. It also serves as a preliminary platform for NDT inspection in industry. The design comprises of various aspects including mechanical, electronic and software elements. The probe housing design is also presented, which serves as a coil former and a holder. Inside the probe, a hall device is incorporated as a means to pick up the resultant magnetic field induced by the coil current and the eddy current. Hall devices are suitable for PEC applications.

The electronics mainly serves two functions, firstly to drive the excitation coil with pulsed current and secondly, to condition the hall device signal before being fed to the data acquisition card interfaced to the PC. The coil driver circuit supplies the coil with the required current to generate the pulsed magnetic field that induces pulsed eddy current in the sample. This is achieved by using a MOSFET as a switch connected to a variable power supply to allow the adjustment of the excitation current. The signal conditioning consists of an amplifier with an adjustable gain and a low pass filter.

Part of the system has been implemented in software using Microsoft Visual C++, Matlab and relevant Matlab toolboxes. The functions in the Windows based software include the configuration and control of the data acquisition, noise reduction, signal processing, feature

extraction and results presentation. Graphical user control interface is incorporated to allow the user to adjust data acquisition parameters easily and to choose and control the feature extraction. The use of Matlab is very useful for rapid development of signal processing techniques. However, the overall processing time of the software will be optimised if all software is implemented using Visual C++.

During implementation, techniques for improving signal-to-noise ratio and signal synchronisation were also investigated and developed. Typical techniques, such as signal averaging and Gaussian filter have also been incorporated into the design.

A comprehensive literature survey on eddy current NDT, with focus on PEC NDT, has been carried out. The survey brings out the current situation and problems currently associated with PEC NDT. The current parameters or features generally used with PEC are not adequate for PEC to be used in real applications, due to noise interferences. Another finding is that the interpretation of the PEC signals is still at infancy, and hence many areas are stil open to further research works.

A new feature extraction technique has been proposed through this research. The new feature extraction technique uses the Continuous Wavelet Transform to analyse PEC signals both in time and frequency domain simultaneously. The Wavelet Transform decomposes the signals into signal components with different frequencies and by this way, the frequencies to be analysed can be chosen. Experimentally, it has been shown that transient PEC signals have transient changes that vary depending on the location of defect. Some signals change faster than the others at the beginning of the pulse, but have slower rates of change at later stages. The frequency components and the time when the frequency changes can be extracted using Wavelet Transforms.

Principal Component Analysis is used to extract orthogonal features that optimally discriminate the input PEC signals leading to effective defect classification and quantification. This technique has self-learning capability when a set of pre-recorded signals representing a good range of potential flaw types and sizes are available for training.

The new technique generates features using the whole signal instead of using a signal sample value. This has allowed better robustness to noise. In this research, it has been shown that the technique achieves better performance in classification than the conventional counterpart does. The new technique provides a flexible approach for flaw classification and quantification by using different PCA components. Potentially, the technique can be used for signal separation of PEC signals and lift-off compensation.

Further experiments have also shown that the new feature extraction has a better dynamic behaviour, which is essential for online dynamic inspection system. The technique can use just a fraction of length of the signal that is required by the conventional technique. This leads to possibility of using higher excitation frequency.

Based on this new feature extraction technique, an algorithm for defect characterisation has also been proposed as shown below in Figure 10-1.

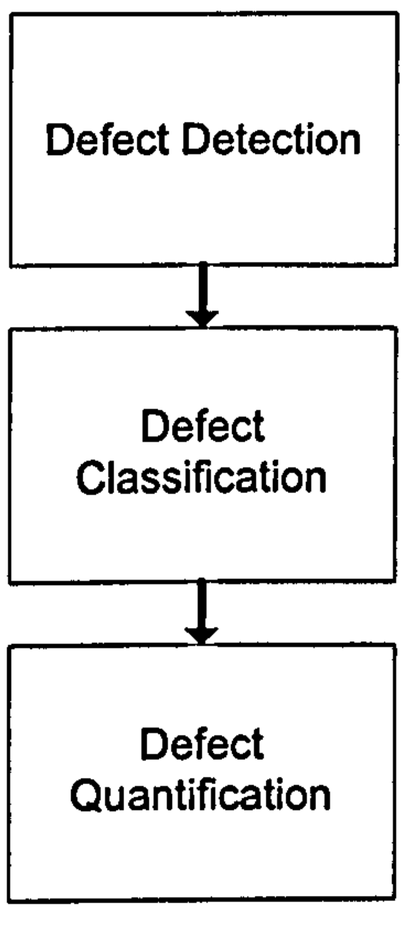

Figure 10-1 The Defect Detection, Classification and Quantification Algorithms

The experiments carried out have supported the reports by other researchers that the location and size of the defects are correlated to the height and arrival time of the PEC signals. However, it has been found that the signal-peak-based technique is not suitable for ferromagnetic materials. A proposed modified technique by normalisation of the base of

responses prior to finding the differential signals helps in producing perceptive signals that have parameters correlated to the flaw size and locations.

It has been found that the system is not able to carry out effective inspection on ferromagnetic steels with the standard configurations. Related to this issue, it is a common knowledge that magnetisation will improve the penetration of eddy current techniques on ferromagnetic samples. In our experiment, it has also been proven that the magnetisation improves the penetration and signal to noise ratio of the PEC system in ferromagnetic steel evaluation. The new feature extraction technique can also be effectively applied to the signals with magnetisation. This can expectedly be generalised for other ferromagnetic materials.

References

Achenbach, J. D. (2000). "Quantitative nondestructive evaluation." International Journal of Solids and Structures **37**(1-2): 13-27.

Adlink-Technology, I. (2000). NuDAQ PCI-9812 Users' Guide.

Atherton, D. L. (1997). "Magnetic inspection is key to ensuring safe pipelines." NDT & E International **30**(1): 40.

Attaar, M. and Davis, J. B. (1997). Ultrasonic and Eddy Current Inspection of a Reactor Vessel Drain. The 14th Int Conf on NDE in the Nuclear and Pressure Vessel Indutries.

Bar-Cohen, Y. (2000). "Emerging NDE Technologies and Challenges at the beginning of the 3rd Milennium Part II." Materials Evaluation **58**(2): 141-150.

Bar-Cohen, Y. (2000). "Emerging NDE Technologies and Challenges at the Beginning of the 3rd Millennium - Part I." Materials Evaluation **58**(1): 17-30.

Beamish, D. (2000). "Coating Thickness Measurement." Metal Finishing **98**(6): 559-560.

Bieber, J. A., Shaligram, S. K., Rose, J. H. and Moulder, J. C. (1997). "Time-gating of Pulsed Eddy Current Signals for Defect Characterisation and Discrimination in Aircraft Lap-Joints." Review of Progress in QNDE **16B**: 1915-21.

Blitz, J. and Peat, T. S. (1981). "The Application of Multi-frequency Eddy Currents to Testing Ferromagnetic Metals." NDT International 14(1): 15-17.

Bowler, J. (1997). "Pulsed Eddy Current Inversion for the Determination of Crack Shape." Electromagnetic Nondestructive Evaluation: 263-269.

Bowler, J. R. and Harrison, D. J. (1992). "Measurement and Calculation of Transient Eddy-Currents in Layered Structures." Review of Progress in Quantitative Nondestructive Evaluation 11(1): 241-248.

Bray, E. and Stanley, R. K. (1997). Nondestructive Evaluation - A tool in Design, Manufacturing, and Service, CRC Press Inc.

Brence, J. R. and Brown, D. E. (2002). "Data mining corrosion from eddy current non-destructive tests." Computers & Industrial Engineering 43(4): 821-840.

Buckley, J. M. and Calvert, J. H. (1995). "Improved Eddy Current Techniques for Aerospace Industry." The Air Transport Assocication Non-Destructive Testing Forum.

Burke, S. K., Hugo, G. R. and Harrison, D. J. (1997). "Transient Eddy-Current NDE for Hidden Corrosion in Multilayer Structures." Review of Progress in Quantitative Nondestructive Evaluation 17A: 307-315.

Chady, T. and Enokizono, M. (1999). "Crack Detection and Recognition Using An Eddy Current Differential Probe." IEEE Transactions on Magnetics 35(3): 1849-1852.

Chady, T. and Enokizono, M. (2000). "Multi-frequency Exciting and Spectrogram-based ECT Method." Journal of Magnetism and Magnetic Materials: 700-703.

Chen, G., Yamaguchi, A. and Miya, K. (1997). "Signal Processing for detection and Characterisation of Defects from Composite Eddy Current Signals." Insight 39(11): 785-789.

Chen, G., Yoshida, Y., Miya, K. and Uesaka, M. (1995). "Application of eddy current testing inspection to the first wall of fusion reactor with Wavelet analysis." Fusion Engineering and Design **29**: 309-316.

Clauzon, T., Thollon, F. and Nicolas, A. (1999). "Flaws Characterisation with pulsed eddy current N.D.T." IEEE Transactions on Magnetics **35**(3/1).

D'Annucci, F., Baro, G. and Assice, A. (1995). "Inspections of pressure vessel head penetrations." Nuclear Engineering and Design **159**(2-3): 177-182.

de Halleux, B., de Limburg Stirum, B. and Ptchelintsev, A. (1996). "Eddy current measurement of the wall thickness and conductivity of circular non-magnetic conductive tubes." NDT & E International **29**(2): 103-109.

Deutsch, V. (2000). History of NDT-Instrumentation. 15th World Conference on Nondestructive Testing, Roma, Italy, NDT.net.

Ditchburn, R. J., Burke, S. k. and Scala, C. M. (1996). "NDT of Welds: State of the Art." NDT&International **29**(2): 111-117.

Dixon, S., Edwards, C. and Palmer, S. B. (1999). "A laser-EMAT system for ultrasonic weld inspection." Ultrasonics **37**(4): 273-281.

Dodd, C. V., Deeds, W. E. and Chitwood, L. D. (1998). "Eddy Current Inspection of Ferromagnetic Materials Using Pulsed Magnetic Saturation." Material Evaluation **46**(11): 1592-1597.

Dokur, Z., Olmez, T. and Yazgan, E. (1999). "Comparison of discrete Wavelet and Fourier transforms for ECG beat classification." Electronics Letters **35**(18): 1502-1504.

Dover, W. D., Collins, R. and Michael, D. H. (1991). "Review of Developments in ACPD and ACFM." The British Journal of Non-destructive Testing **33**(3): 121-127.

EPSRC (2003). EPSRC's Website. **2003**.

Farooq, O. and Datta, S. (2001). "Robust features for speech recognition based on admissible Wavelet packets." Electronics Letters **37**(25): 1554-1556.

Finlayson, G. D. and Tian, G. Y. (1999). "Colour normalisation for colour object recognition." International J. of Pattern Recognition and Artifical Intelligence **13**(8): 1271-1285.

Gao, W., Glorieux, C. and Thoen, J. (2003). "Laser ultrasonic study of Lamb waves: determination of the thickness and velocities of a thin plate." International Journal of Engineering Science **41**(2): 219-228.

Gaydecki, P., Silva, I., Fernandes, B. T. and Yu, Z. Z. (2000). "A portable inductive scanning system for imaging steel-reinforcing bars embedded within concrete." Sensors and Actuators A: Physical **84**(1-2): 25-32.

Giguere, S. and Dubois, J. M. S. (2000). "Pulsed Eddy Current: Finding Corrosion Independently of Transducer Lift-off." Review of Progress in Quantitative Nondestructive Evaluation: 459-456.

Giguere, S., Lepine, B. A. and Dubois, J. M. S. (2001). "Pulsed Eddy Current Technology: Characterizing Material Loss with Gap and Lift-off Variations." Research in Nondestructive Evaluation **13**(3): 119-129.

Gledhill, D., Tian, G. Y., Taylor, D. and Clarke, D. (2003). "Panoramic imaging--a review." Computers & Graphics **27**(3): 435-445.

Goktepe, M. (2001). "Non-destructive crack detection by capturing local flux leakage field." Sensors and Actuators A: Physical **91**(1-2): 70-72.

Goldberg, L. O. (1998). "Eddy Current Testing an Emerging NDT Method for Ferritic Weld Inspection."

Golovkin, I. E., Mancini, R. C., Louis, S. J., Lee, R. W. and Klein, L. (2002). "Analysis of X-ray spectral data with genetic algorithms." Journal of Quantitative Spectroscopy and Radiative Transfer **75**(5): 625-636.

Goumas, S. K., Zervakis, M. E. and Stavrakakis, G. S. (2002). "Classification of washing machines vibration signals using discrete Wavelet analysis for feature extraction." IEEE Transactions on Instrumentation and Measurement **51**(3): 497-508.

Graps, A. (1995). "An introduction to Wavelets." IEEE Computational Science and Engineering **2**(2): 50-61.

Gros, X. E., Bousigue, J. and Takahashi, K. (1999). "NDT data fusion at pixel level." NDT & E International **32**(5): 283-292.

Guo, H., Crossman, J. A., Murphey, Y. L. and Coleman, M. (2000). "Automotive signal diagnostics using Wavelets and machine learning." Vehicular Technology, IEEE Transactions on **49**(5): 1650-1662.

Halmshaw, R. (1996). Introduction to the Non-destructive Testing of Welded Joints, Abington Publishing.

Honeywell (1998). Solid State Sensors, Honeywell: 20-23.

Honeywell (1999). 1- and 2-axis Magnetic Sensors. Data Sheets, Honeywell.

Hoshikawa, H. and Koyama, K. (1998). "A New Eddy Current Probe by Uniform Rotating Eddy Current." Materials Evaluation **56**(1): 85-89.

Hoshikawa, H. and Koyama, K. (1998). "Non-destructive Testing of Weld Zone with a Uniform Eddy Current Probe." Insight: Non-destructive Testing and Condition Monitoring **40**(4): 269-271.

Hoshikawa, H. and Koyama, K. (1998). "Uniform Eddy Current Probe with Little Disrupting Noise." Review of Progress in Quantitative Nondestructive Testing **17**: 1059-1066.

Hull, B. and John, V. (1988). Non-destructive Testing. London, MacMillan Education.

Hulsey, R. C. and Goolsby, A. D. (1996). "Nondestructive crack depth measurement in internally weld overlayed clad pressure vessels." NDT & E International **29**(2): 130.

Ionescu, R. and Llobet, E. (2002). "Wavelet transform-based fast feature extraction from temperature modulated semiconductor gas sensors." Sensors and Actuators B: Chemical **81**(2-3): 289-295.

Katragadda, G., Lewis, D., Wallace, J. and Si, J. (2000). "Swept Frequency Eddy Current Material Profiling Using Radial Basis Function Neural Networks for Inversion." Materials Evaluation **58**(1): 70-73.

Khandetsky, V. and Antonyuk, I. (2002). "Signal processing in defect detection using back-propagation neural networks." NDT & E International **35**(7): 483-488.

Kojima, F., Kubota, N. and Hashimoto, S. (2001). "Identification of Crack Profiles using Genetic Programming and Fuzzy Inference." Journal of Materials Processing Technology **108**: 263-267.

Koyama, K., Hiroshikawa, H. and Taniyama, N. (2000). Investigation of Eddy Current Testing of Weld Zone by Uniform Eddy Current Probe. 15th World Conference on NDT, Roma.

Krause, H.-J. (2003). Nondestructive Evaluation of Aircraft Wheels and Fuselage with SQUIDs, http://www.fz-juelich.de/isg/Krause/aircraft.htm.

Krause, H.-J. and Kreutzbruck, M. v. (2002). "Recent developments in SQUID NDE." Physica C: Superconductivity **368**(1-4): 70-79.

Kreutzbruck, M. v. and Allweins, K. (2002). "High field resolution for nondestructive testing using sensitive magnetometers." Sensors and Actuators A: Physical **101**(1-2): 85-91.

Kriezis, E., Tsiboukis, T., Panas, S. and Tegopoulos, J. (1992). "Eddy Currents: Theory and Applications." Proceedings of the IEEE **80**(10): 1559-1589.

Lebrun, B., Jayet, Y. and Baboux, J.-C. (1995). "Pulsed Eddy Current Application to the Detection of Deep Cracks." Materials Evaluation **53**(11): 1296-1300.

Lebrun, B., Jayet, Y. and Baboux, J.-C. (1997). "Pulsed eddy current signal analysis: application to the experimental detection and characterization of deep flaws in highly conductive materials." NDT & E International **30**(3): 163-170.

Lepine, B. A., Giguere, G., Forsyth, D. S., Chahbaz, A. and Dubois, J. M. S. (2002). "Interpretation of Pulsed Eddy Current Signals for Locating and Qualifying Metal Loss in Thin Skin Lap Splices." Review of Quantitative Nondestructive Evaluation **21**: 415-422.

Lepine, B. A., Giguere, J. S. R., Forsyth, D. S., Chahbaz, A. and Dubois, J. M. S. (2002). "Interpretation of Pulsed Eddy Current Signals for Locating and Quantifying Metal Loss in Thin Skin Lap Splices." Review of Quantitative Nondestructive Evaluation **21**: 415-422.

Lepine, B. A., Giguere, J. S. R., Forsyth, D. S., Dubois, J. M. S. and Chahbaz, A. (2001). Applying Pulsed Eddy Current NDI to the Aircraft Hidden Corrosion Problem. Aging Aircraft 2001, Orlando, Florida.

Lepine, B. A., Wallace, B. P., Forsyth, D. S. and Wyglinski, A. (1999). Pulsed Eddy Current Method Developments for Hidden Corrosion Detection in Aircraft Structures. PACNDT '98.

Lepine, B. A., Wallace, J., Forsyth, D. S. and Wyglinski, A. (1998). Pulsed Eddy Current Method Developments for Hidden Corrosion Detection in Aircraft Structures. PACNDT '98.

LeTessier, R., Coade, R. W. and Geneve, B. (2002). "Sizing of cracks using the alternating current field measurement technique." International Journal of Pressure Vessels and Piping 79(8-10): 549-554.

Li, X., Tso, S. K. and Wang, J. (2000). "Real-time tool condition monitoring using Wavelet transforms and fuzzy techniques." Systems, Man and Cybernetics, Part C, IEEE Transactions on 30(3): 352-357.

Libby, H. L. (1970). Multiparameter Eddy Current Concepts. Research Techniques in Nondestructive Testing. London, Academic Press Inc. Ltd.

Liu, Z., Tsukada, K. and Hanasaki, K. (1998). "One-dimensional Eddy Current Multi-frequency Data Fusion: A Multi-resolution Analysis Approach." Insight 40(4): 286-289.

Mallat, S. G. (1989). "A Theory for Multiresolution Signal Decomposition: The Wavelet Representation." IEEE Transactions on Pattern Analysis and Machine Intelligence 11(7): 674-693.

Mallat, S. and Zhong, S. (1992). "Characterization of signals from multiscale edges." IEEE Transactions on Pattern Analtsis and Machine Intelligence 14: 710-732.

Mandal, K., Cramer, T. and Atherton, D. L. (2000). "The study of a racetrack-shaped defect in ferromagnetic steel by magnetic Barkhausen noise and flux leakage measurements." Journal of Magnetism and Magnetic Materials 212(1-2): 231-239.

McNab, A. and Thomson, J. (1995). "An Eddy Current Array Instrument for Application on Ferritic Welds." NDT&E International 28(2): 103-112.

Meeker, D. (2001). Finite Element Method Magnetics Version 3.0, User's Manual, http://members.aol.com/dcm3c.

Mijarez, R., Gaydecki, P. and Burdekin, F. (2003). Continuous monitoring ultrasound lamb waves encoded sensor for flood detection of oil rig leg cross beams. BInstNDT 2003, Warwick, BINDT.

Miller, G., Gaydecki, P., Quek, S., Fernandes, B. T. and Zaid, M. A. M. (2003). "Detection and imaging of surface corrosion on steel reinforcing bars using a phase-sensitive inductive sensor intended for use with concrete." NDT & E International **36**(1): 19-26.

Morabito, C. F. (2000). "Independent Component Analysis and Feature Extraction Technique for NDT Data." Materials Evaluation **58**(1): 85-92.

Morozov, M. and Novotny, P. (2002). "Evaluation of eddy current probes based on local field excitation." NDT & E International **35**(3): 147-153.

Mottl, Z. (1990). "The Quantitative Relations Between True and Standard Depth of Penetration for Air-cored Probe Coils in Eddy-current Testing." NDT International **23**(1): 11-18.

Moulder, J. C. and Bieber, J. A. (1998). Pulsed Eddy Current Measurements of Corrosion and Cracking in Aging Aircraft. Materials Research Society Symposium.

Moulder, J. C., Shaligram, S. K., Bieber, J. A. and Rose, J. H. (2000). Pulsed Eddy Current Inspections and the Calibration and Display of Inspection Results. USA, Iowa State University Research Foundation, Inc.

Mukhopadhyay, S. and Srivastava, G. P. (2000). "Characterisation of metal loss defects from magnetic flux leakage signals with discrete Wavelet transform." NDT & E International **33**(1): 57-65.

NDTA (2002). NDT METHODS. **2002.**

Niewiadomski, S. (1989). Filter Handbook. Oxford, Heinemann Professional Publishing Ltd.

Oukhellou, L., Aknin, P. and Perrin, J.-P. (1999). "Dedicated sensor and classifier of rail head defects." Control Engineering Practice 7(1): 57-61.

Panaitov, G., Krause, H.-J. and Zhang, Y. (2002). "Pulsed eddy current transient technique with HTS SQUID magnetometer for non-destructive evaluation." Physica C: 278-281.

Patel, R. and Rudlin, J. R. (2000). "Analysis of corrosion/erosion incidents in offshore process plant and implications for non-destructive testing." INSIGHT 42(1): 17-21.

Patel, U. and Rodger, D. (1996). "Finite Element Modelling of Pulsed Eddy Currents for Nondestructive testing." IEEE transactions on Magnetics 32(3): 1593-1596.

Pittner, S. and Kamarthi, S. V. (1999). "Feature extraction from Wavelet coefficients for pattern recognition tasks." Pattern Analysis and Machine Intelligence, IEEE Transactions on 21(1): 83-88.

Quek, S., Gaydecki, P., Fernandes, B. and Miller, G. (2002). "Multiple layer separation and visualisation of inductively scanned images of reinforcing bars in concrete using a polynomial-based separation algorithm." NDT & E International 35(4): 233-240.

Raine, A. and Cameron, B. (2002). "Alternating current field measurement: Getting new technologies accepted by old industries." MATERIALS EVALUATION 60(3): 389-395.

Raine, A. and Lugg, M. (1999). "A review of the alternating current field measurement inspection technique." Sensor Review 19(3): 207-213.

Ramamoorthi, R. (2002). "Analytic PCA Construction for Theoretical Analysis of Lighting Variability in Images of a Lambertian Object." PAMI 24(10): 1322-1333.

Rao, B. P. C., Kalyanasundaram, P. and Raj, B. (2000). An Insight into Design and Development of Eddy Current Sensors for Non-destructive Evaluation of Materials. National Workshop on Sensors, Kalpakkam, India.

Rao, B. P. C., Raj, B., Jayakumar, T. and Kalyanasundaram, P. (2002). "An artificial neural network for eddy current testing of austenitic stainless steel welds." NDT & E International **35**(6): 393-398.

Rem, P. C., Leest, P. A. and van den Akker, A. J. (1997). "A model for eddy current separation." International Journal of Mineral Processing **49**(3-4): 193-200.

Rhopoint (2001). GMR Magnetic Field Sensors. AA002-AA006, Rhopoint Components.

Richardson, M. O. W., Zhang, Z. Y., Wisheart, M., Tyrer, J. R. and Petzing, J. (1998). "ESPI non-destructive testing of GRP composite materials containing impact damage." Composites Part A: Applied Science and Manufacturing **29**(7): 721-729.

Ricken, W., Liu, J. and Becker, W.-J. (2001). "GMR and eddy current sensor in use of stress measurement." Sensors and Actuators A: Physical **91**(1-2): 42-45.

Robers, M. A. and Scottini, R. (2002). Pulsed Eddy Current in Corrosion Detection. 8th ECNDT, Barcelona.

Rose, J. H., Uzal, E. and Moulder, J. C. (1999). "Pulsed eddy-current characterization of corrosion in aircraft lap splices: Quantitative modeling." Proc of the SPIE **2160**: 164-176.

Rudlin, J. R. (1996). Reliability of inspection for fatigue cracks in offshore structures. IEE Colloquium on Inspection Reliability: State-of-the Art, London, IEE.

Rudlin, J. R. (1997). "Review of existing and possible techniques for corrosion under insulation and wall thickness measurement in steel pressure containments." Insight **39**(6): 413-417.

Rudlin, J. R. and Wolstenholme, L. C. (1992). "Development of statistical probability of detection models using actual trial inspection data." British Journal of Non Destructive Testing **34**(12): 583-9.

Sadler, D. J. and Ahn, C. H. (2001). "On-chip eddy current sensor for proximity sensing and crack detection." Sensors and Actuators A: Physical **91**(3): 340-345.

Safizadeh, M. S., Lepine, B. A., Forsyth, D. S. and Fahr, A. (2001). "Time-Frequency Analysis of Pulsed Eddy Current Signals." Journal of Nondestruction Evaluation **20**(2): 73-86.

Sarikaya, R. and Hansen, J. H. L. (2000). "High resolution speech feature parametrization for monophone-based stressed speech recognition." IEEE Signal Processing Letters 7(7): 182-185.

Semiconductor, H. (1996). ICL8038 Data Sheet.

Shull, P. J. (2002). Nondestructive Evaluation - Theory, Techniques and Applications, Marcel Dekker.

Shyamsunder, M. T., Rajagopalan, C. and Raj, B. (1999). "Pattern Recognition Approaches for the Detection and Characterization of Discontinuities by Eddy Current Testing." Materials Evaluation **58**(1): 93-101.

Smith, R. A. and Hugo, G. R. (2001). Deep Corrosion and Crack Detection in Aging Aircraft using Transient Eddy-current NDE. Aging Aircraft 2001.

Smith, R. A. and Hugo, G. R. (2001). Detection of deep Corrosion and Cracks in Ageing Aircraft Using Transient Eddy-current NDE, QinetiQ Ltd.

Smith, R. A. and Hugo, G. R. (2001). "Transient eddy current NDE for ageing aircraft - capabilities and limitations." Insight: Non-Destructive Testing and Condition Monitoring **43**(1): 14-25.

Smith, S. W. (1999). The Scientist and Engineer's Guide to Digital Signal Processing, California Technical Publishing.

Sophian, A., Tian, G. Y., Taylor, D. and Rudlin, J. (2001). "Electromagnetic and Eddy Current NDT: A Review." INSIGHT **43**(5): 308-313.

Sophian, A., Tian, G. Y., Taylor, D. and Rudlin, J. (2002). "Design of a Pulsed Eddy Current Sensor for Detection of Defects in Aircraft Lap-Joints." Sensors and Actuators A.

Staszewski, W. J. (2002). "Intelligent signal processing for damage detection in composite materials." Composites Science and Technology **62**(7-8): 941-950.

Swets, D. L. and Weng, J. J. (1999). "Hierarchical discriminant analysis for image retrieval." IEEE Trans. Pattern Anal. and Machine Intell. **21**(5): 386-401.

Tai, C. C., Yang, H. C. and Liang, D. S. (2002). "Pulsed Eddy Current for Metal Surface Cracks Inspection: Theory and Experiment." Review of Quantitative Nondestructive Evaluation **21**: 388-395.

Tehodoulidis, T. P. and Kotouzas, M. K. (2000). "Application of the Eddy Current Method in Ferritic Weld Inspection." Emerging Technologies in NDT: 357-361.

Theodoulidis, T. P. and Kotouzas, M. K. (2000). "Application of the Eddy Current Method in Ferritic Weld Inspection." Emerging Technologies in NDT: 357-361.

Thollon, F. and Burais, N. (1994). Modelling and Characterisation of Pulsed Eddy Current. Application to NDT of Riveted Assemblies in Aeronautic Structures. 2nd International Workshop on Electric and Magnetic Fields, Leuven, Belgium.

Thollon, F. and Burais, N. (1995). "Geometrical Optimization of Sensors for Eddy Currents Non-Destructive Testing and Evaluation." IEEE Transactions on Magnetics **31**(3): 2026-2031.

Tian, G. Y. (2001). "Frequency output eddy current sensors for precision engineering." INSIGHT **43**(5): 315-318.

Tian, G. Y., Gledhill, D. and Taylor, D. (2003). "Comprehensive interest points based imaging mosaic." Pattern Recognition Letters **24**(9-10): 1171-1179.

Tian, G. Y., Zhao, Z. X. and Baines, R. W. (1996). Precision measurement using an eddy current sensor device. Proceedings of twelfth National Conference on Manufacturing Research, Bath, UK.

Tian, G. Y., Zhao, Z. X. and Baines, R. W. (1998). "The research of inhomogeniety in eddy current sensors." Sensors and Actuators A **58**: 153-156.

Tian, G. Y., Zhao, Z. X. and Baines, R. W. (1999). "A miniaturised displacement sensor for deep hole measurement." J. of precision engineering of Americian Society **23**: 236-242.

Tian, G. Y., Zhao, Z. X., Baines, R. W. and Corcoran, P. (1997). "Blind sensing." IEE Manufacturing Engineer **176**(4): 179-183.

Tian, G. Y., Zhao, Z. X., Baines, R. W. and Corcoran, P. (1999). "The design of miniaturised displacement transducers for deep hole diameter measurement." Mechatronics **9**(4): 317-327.

Tico, M., Kuosmanen, P. and Saarinen, J. (2001). "Wavelet domain features for fingerprint recognition." Electronics Letters **37**(1): 21-22.

Turk, M. A. and Pentland, A. P. (1991). "Face Recognition Using Eigenfaces." Journal of Cognitive Neuroscience(3): 71-86.

TWI (2003). TWI Ltd's Website. **2003**.

Udpa, L. (2000). "Scanning the Issue - Neural Networks for NDT Applications." Matcrials Evaluation **58**(1): 63-64.

Udpa, L. and Udpa, S. S. (1997). "Application of Signal Processing and Pattern Recognition Techniques to Inverse Problems in NDE." International J. of Applied Magnetics and Mechanics **8**: 99-117.

Verlinde, D., Beckers, F., Ramaekers, D. and Aubert, A. E. (2001). "Wavelet decomposition analysis of heart rate variability in aerobic athletes." Autonomic Neuroscience **90**(1-2): 138-141.

Webb, A. R. (2002). Statistical Pattern Recognition, John Wiley & Sons.

Wilde, J. and Lai, Y. (2003). "Design optimization of an eddy current sensor using the finite-elements method." Microelectronics Reliability **43**(3): 345-349.

Wu, Y. and Upadhyaya, B. R. (1996). "An integrated signal processing and neural networks system for steam generator tubing diagnostics using eddy current inspection." Annals of Nuclear Energy **23**(10): 813-825.

Xiong, N. and Svensson, P. (2002). "Multi-sensor management for information fusion: issues and approaches." Information Fusion **3**(2): 163-186.

Yang, H. C., Liu, Y. H. and Tai, C. C. (1999). Design and Implementation of A pulsed Eddy-current Testing System. Proc. Of the 5th Far-East Conference on Nondestructive Testing.

Yang, H. C. and Tai, C. C. (2002). "The Interaction of Pulsed Eddy current with Metal Surface Crack for Various Coils." Review of Quantitative Nondestructive Evaluation **21**: 409-414.

Yen, G. G. and Lin, K.-C. (2000). "Wavelet packet feature extraction for vibration monitoring." Industrial Electronics, IEEE Transactions on **47**(3): 650-667.

Zahran, O. S., Shihab, S. and Al-Nuaimy, W. (2002). Recent Developments in Ultrasonic Techniques for Rail-track Inspection. NDT 2002, Southport, The British Institute of NDT.

Appendices

Appendix 1 Excitation Circuit Schematic

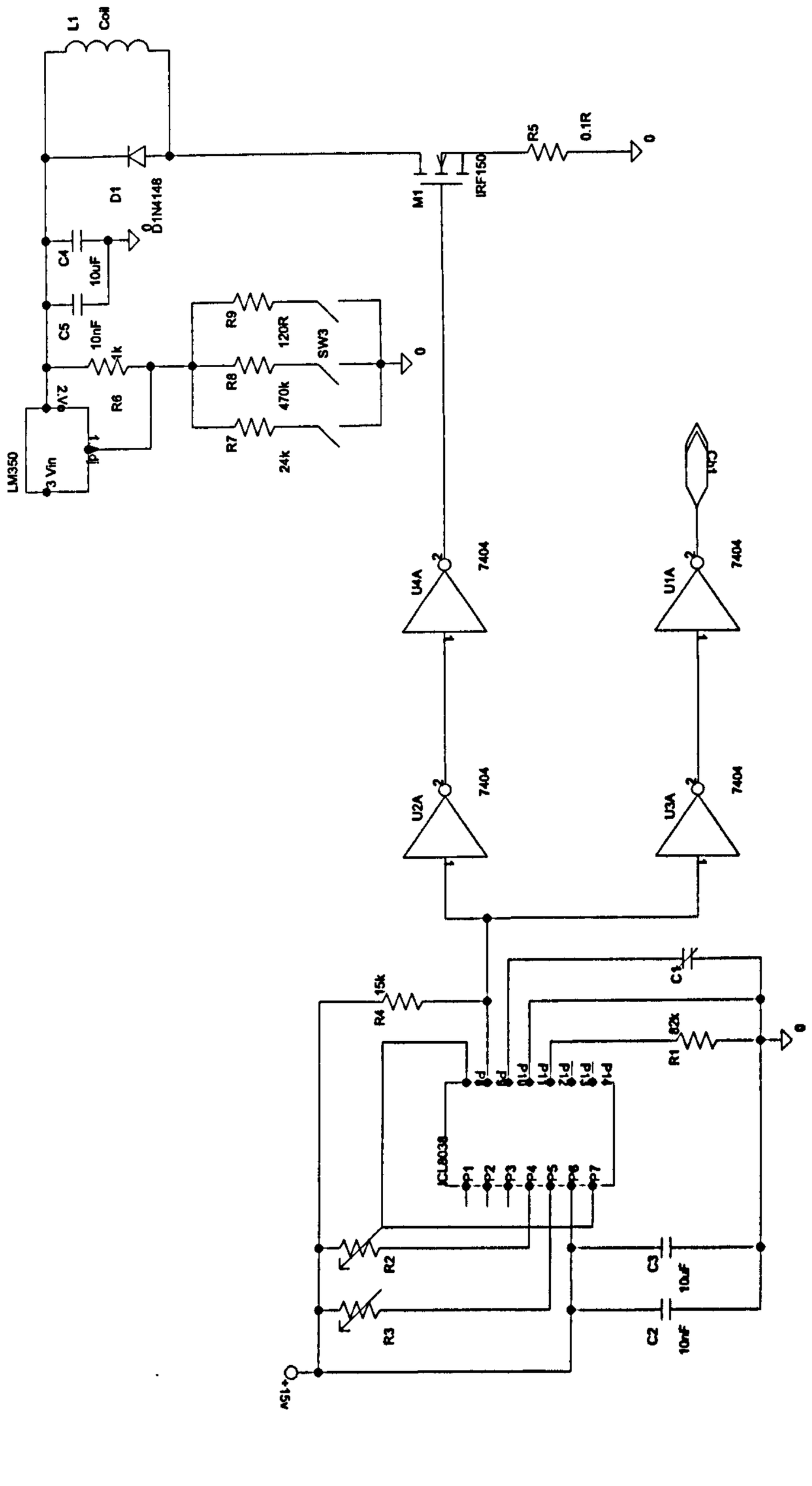

Appendix 2 Hall Device and Signal Conditioning Circuit Schematic

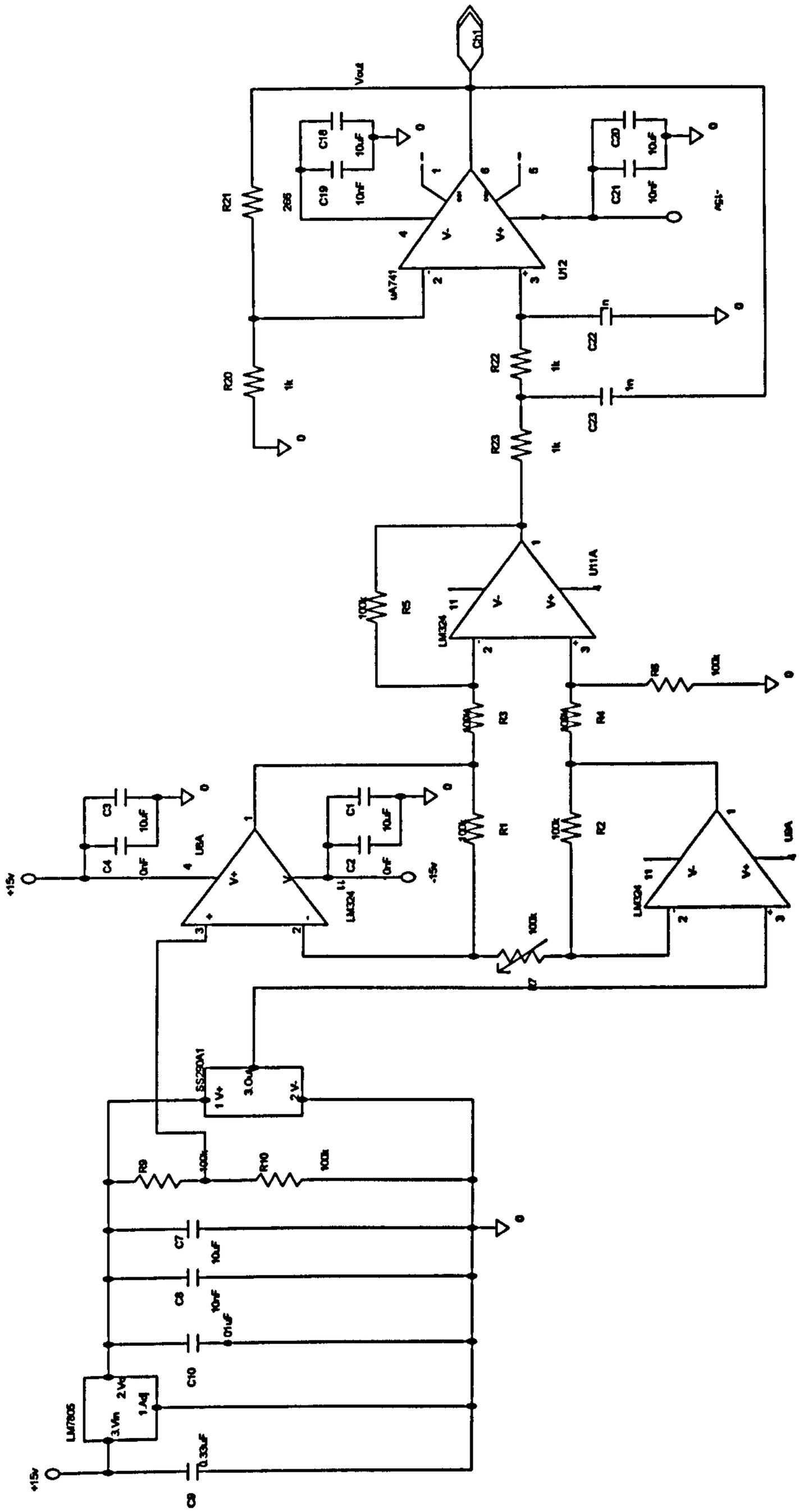

Appendix 3 Probe Design

Coil Former

TOP VIEW

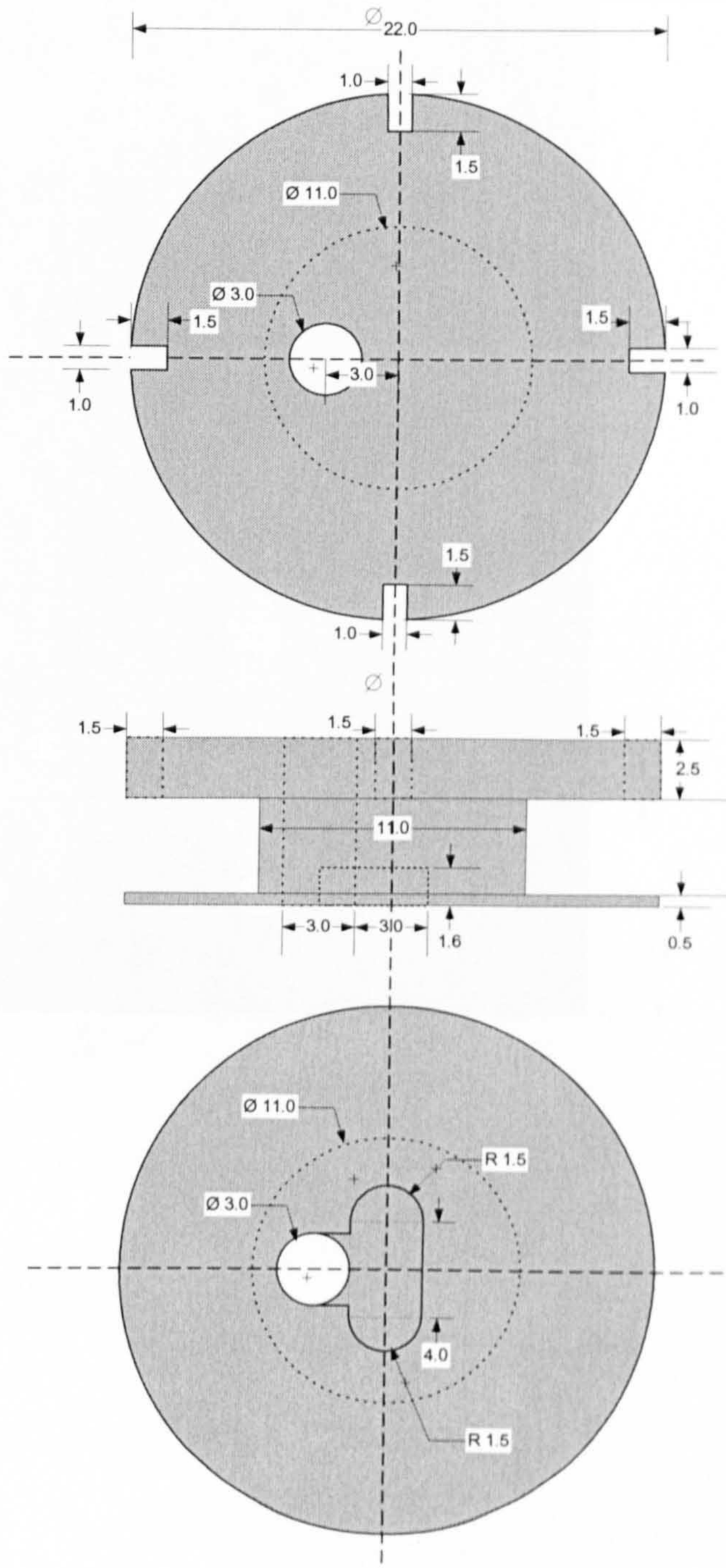

SIDE VIEW

BOTTOM VIEW

Probe Sleeve

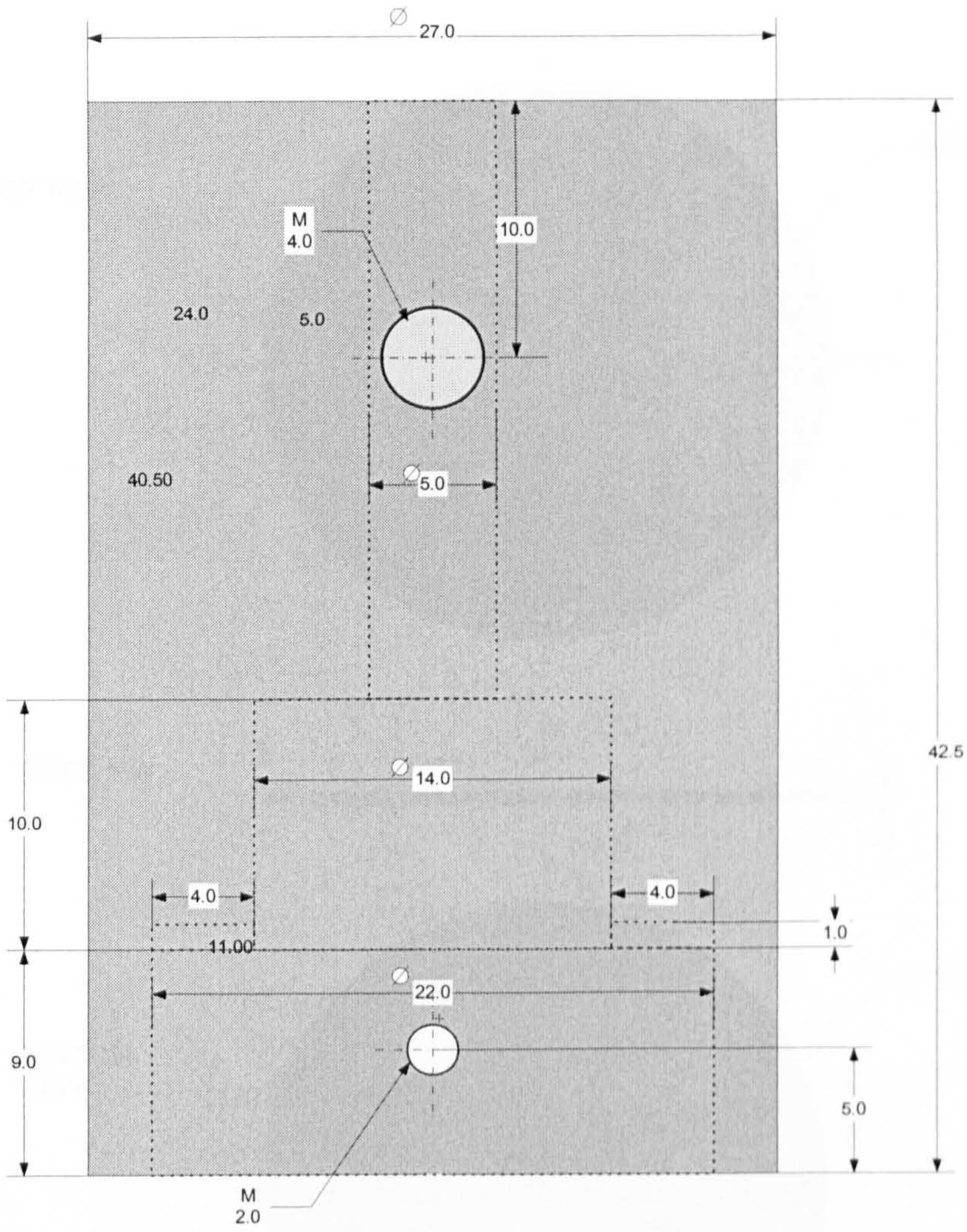

Probe Bottom Lid

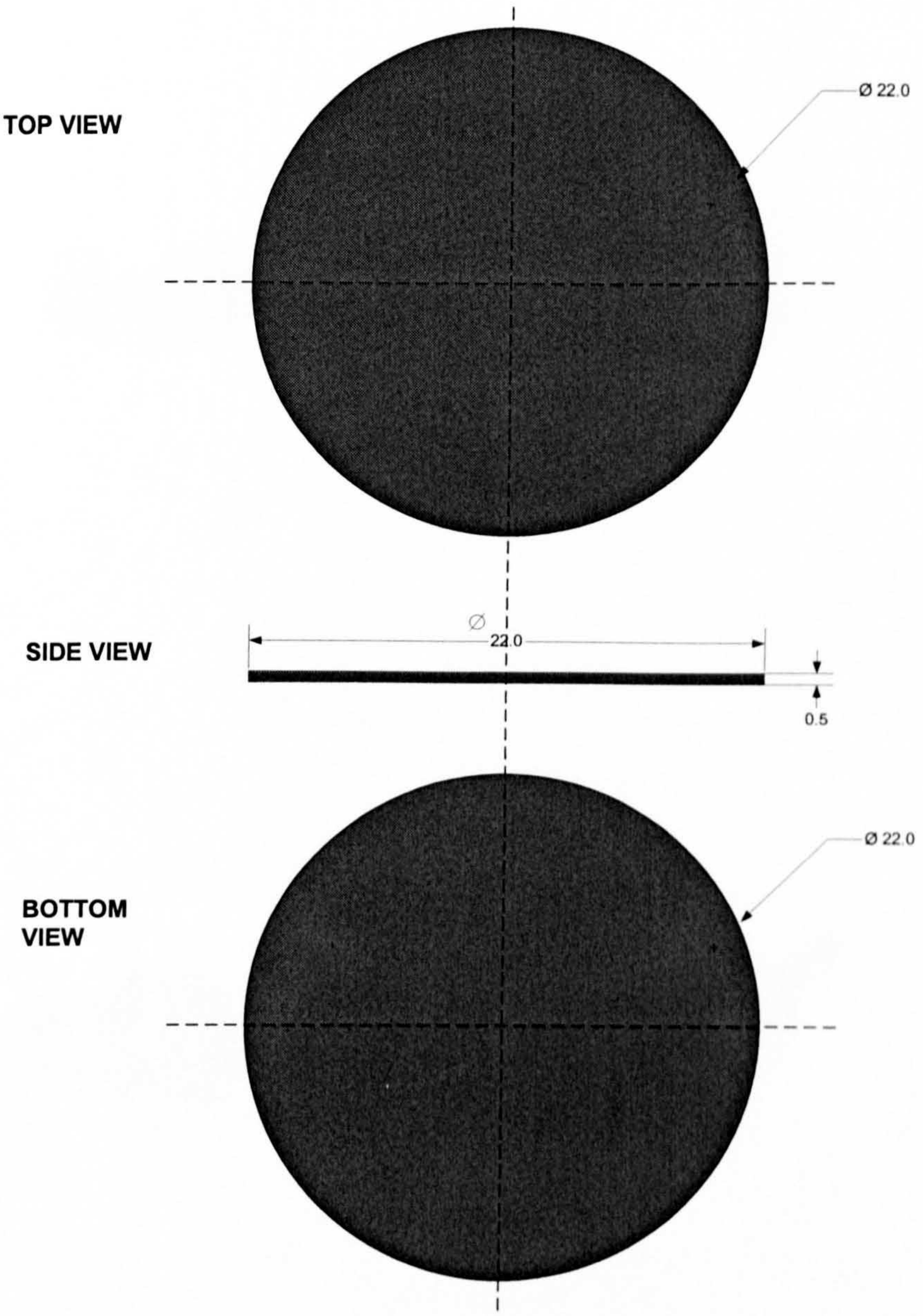

Appendix 4 CD-ROM containing Visual C++ and Matlab Codes